US Army Corps
of Engineers®
Engineer Research and
Development Center

The Chameleon Concept: Modeling Quaternary Geomorphic Surfaces Using Laboratory, Field, and Imaging Spectrometry in the Lower Colorado Sonoran Desert

J. David Lashlee   November 2005

The Chameleon Concept: Modeling Quaternary Geomorphic Surfaces Using Laboratory, Field, and Imaging Spectrometry in the Lower Colorado Sonoran Desert

J. David Lashlee

Topographic Engineering Center
U.S. Army Engineer Research and Development Center
7701 Telegraph Road
Alexandria, VA 22315-3864

ABSTRACT: Chameleon is a physics-based landscape modeling software system designed for modeling and simulations. Hyperspectral laboratory, field, and imaging spectrometer measurements are collected as empirical foundation data. Linear spectral unmixing decomposes each image pixel into spectral endmembers. Spectral editing tools allow mathematical manipulation of these fractional abundances and introduction of new spectral information. Image spectra are modified on a sub-pixel, per-pixel, or neighborhood basis, or the entire hypercube can be customized at once. Chameleon then regenerates synthetic, but spectrally accurate, terrain models using linear spectral remixing algorithms. By incorporating elevation, sun angle, and weather data, the landscape becomes a "Chameleon"—able to change hyperspectral properties based on multitemporal spectral measurements, requirements for developmental tests and operational training, or as required by specific simulation scenarios. Advanced knowledge of natural environments to be modeled is prerequisite to generating useful synthetic terrains. Our spectral research on arid Quaternary geomorphic surfaces suggests that deserts (often assumed to be less difficult to study remotely than humid, temperate, and cold environments) are more complex than is generally accepted. A variety of rock coatings can significantly alter reflectance in the solar reflected spectrum. Weathering rinds and carbonate deposits inhibit lithologic reflectance altogether. However, manganese-rich rock varnish obscures rock reflectance in the visible and near infrared wavelengths, but transmits lithologic information in the 2000 to 2500 nanometer wavelengths. Surface soils on desert pavements consist of a layer of eolian dust that overlies an accreting vesicular (Av) horizon. These soils have same structure and chemistry, and, therefore, the same hyperspectral signature, regardless of landform age, geomorphic process, or parent material. From a remote sensing perspective, this has a normalizing effect on reflectance across the landscape. Spectral Mixture Analysis is a proven hyperspectral technique for mapping composition and abundance of surface materials characteristic of volcanic landforms that exhibit diagnostic absorption features. We found that desert pavement spectra are featureless in that they exhibit few distinct spectral features related to rock varnish, clast lithology, or soil. Image spectra of these surfaces are the result of intimate mixtures of heterogeneous materials, requiring non-linear spectral unmixing solutions.

AN ABSTRACT OF THE DISSERTATION OF

J. David Lashlee for the degree of Doctor of Philosophy in Geography presented on June 2, 2005.

Title: The Chameleon Concept: Modeling Quaternary Geomorphic Surfaces Using Laboratory, Field, and Imaging Spectrometry in the Lower Colorado Sonoran Desert.

Abstract Approved:

_____

Charles L. Rosenfeld

Chameleon is a physics-based landscape modeling software system designed for modeling and simulations applications. Hyperspectral laboratory, field, and imaging spectrometer measurements are collected as empirical foundation data. Linear spectral unmixing is performed to decompose each image pixel into spectral endmembers. Mathematical manipulation of these fractional abundances and introduction of new spectral information is accomplished with spectral editing tools. Image spectra are modified on a sub-pixel, per-pixel, or neighborhood basis, or the entire hypercube can be customized at once. Chameleon then regenerates synthetic, but spectrally accurate, terrain models using linear spectral remixing algorithms. By incorporating elevation, sun angle, and weather data, the landscape becomes a "Chameleon"—able to change hyperspectral properties based on multitemporal spectral measurements, requirements for developmental tests and operational training, or as required by specific simulation scenarios.

Advanced knowledge of natural environments to be modeled is prerequisite to generating useful synthetic terrains. Our spectral research on arid Quaternary geomorphic surfaces suggests that deserts (often assumed to be less difficult to study remotely than humid, temperate, and cold environments) are more complex than is generally accepted. A variety of rock coatings can significantly alter reflectance in the solar reflected spectrum. Weathering rinds and carbonate deposits inhibit lithologic reflectance altogether. However, manganese-rich rock varnish obscures rock reflectance in the visible and near infrared wavelengths, but transmits lithologic information in the 2000 to 2500 nanometer wavelengths. Surface soils on desert pavements consist of a layer of eolian dust that overlies an accreting vesicular (Av) horizon. These soils have same structure and chemistry, and, therefore, the same hyperspectral signa-

ture, regardless of landform age, geomorphic process, or parent material. From a remote sensing perspective, this has a normalizing effect on reflectance across the landscape.

Spectral Mixture Analysis is a proven hyperspectral technique for mapping composition and abundance of surface materials characteristic of volcanic landforms that exhibit diagnostic absorption features. We found that desert pavement spectra are featureless in that they exhibit few distinct spectral features related to rock varnish, clast lithology, or soil. Image spectra of these surfaces are the result of intimate mixtures of heterogeneous materials, requiring non-linear spectral unmixing solutions.

The Chameleon Concept:
Modeling Quaternary Geomorphic Surfaces
Using Laboratory, Field, and Imaging Spectrometry
in the Lower Colorado Sonoran Desert

by
J. David Lashlee

A DISSERTATION

Submitted to

Oregon State University

in partial fulfillment of
the requirements for the
degree of

Doctor of Philosophy

Presented June 2, 2005
Commencement June 2005

ACKNOWLEDGEMENTS

CONTRIBUTIONS OF AUTHORS

Dr. Frederick Briuer was the first permanent professional archeologist hired by the Department of Defense research community. Working at the Engineer Research and Development Center, Waterways Experiment Station, he directed basic and applied research projects for improved cultural resource management at many U.S. military installations. He also served as Director of the Center for Cultural Site Preservation Technology from 1993 to 2003. The archaeological field work summarized in Chapter One was performed by Dr. Briuer and his team of contract archaeologists from the Chambers Group, Redlands, California, and Mr. Lorey Cachora, tribal elder and consultant for the Quechan Indian Tribe, Yuma, Arizona. Dr. Briuer mapped cultural resources, supervised statistical data analysis, and significantly contributed to the project technical report and subsequent publication in the refereed journal *Arid Land Research and Management*—Special Edition on Management and Mitigation of U.S. Department of Defense Arid Lands.

Thomas Harris is a remote sensing consultant and trainer with Research Systems Incorporated in Boulder, Colorado. He holds a Master of Science in Geology from the University of Colorado, Boulder, and a Bachelor of Science in Forest Management from Auburn University. His research interests include applying hyperspectral remote sensing to analyzing long-term vegetation change in arid ecosystems and GIS analysis of global scale processes related to livestock grazing. For this study, Mr. Harris contributed significantly to AVIRIS data processing and analysis. He authored the methods section and edited the remainder of Chapter Five of this dissertation.

Dr. A. Jon Kimerling is Professor of Geography in the Department of Geosciences at Oregon State University. For over 25 years, he has taught courses and conducted research in cartography and remote sensing. He is an author of several books including the *Elements of Cartography* and *Map Use* textbooks. As the Minor Professor of this dissertation research committee, Dr. Kimerling provided guidance in Earth Information Science and Technology, performed critical technical reviews of each chapter, and contributed to the technical relevance of this work.

David Lashlee is Associate Technical Director at the Topographic Engineering Center, U.S. Army Engineer Research and Development Center. He designs enterprise geographic databases, performs spatial analyses in support of military testing and training, builds digital terrain models for visual and computer generated forces databases, and is involved with remote sensing issues with the Army and Joint intelligence communities. Mr. Lashlee is a registered Professional Geologist and Certified Mapping Scientist in Remote Sensing and in GIS/LIS (ASPRS). As primary author of this dissertation, his current research interests include laboratory, field, and imaging spectrometry of arid environments for landscape model generation. Other research interests include development of Synthetic Environments for modeling and simulation applications.

Dr. Eric McDonald is Associate Research Professor in the Division of Earth and Ecosystem Sciences at the Desert Research Institute, Reno, Nevada. He is also Director of the Center for Arid Lands Environmental Management at DRI. Dr. McDonald's research expertise is in soil science, geomorphology, and Quaternary geology. He is the author of numerous articles on soil stratigraphy, Quaternary landscape history, soil landscape relations, and the geochemical and hydrological analyses of soils and sediments. Dr. McDonald contributed to this effort by performing soils geomorphology in the field, including soil pit excavations and soil profile descriptions, as well as subsequent laboratory analyses soil samples. He also helped correlate physical and chemical soil properties to hyperspectral reflectance characteristics of laboratory and field soil spectra.

William Murphy is a long-time professional geologist for the U.S. Army Engineer Research and Development Center's Geotechnical and Structures Laboratory. Now retired, Mr. Murphy contributed to the Chapter One of this dissertation in several ways. He interpreted stereoscopic aerial photography to delineate Quaternary geomorphic surfaces for a portion of the U.S. Army Yuma Proving Ground and assisted with verification and validation of these data in the field. He also contributed a regional geologic literature review and analysis to the final technical report from which the journal paper in Chapter One was derived.

CONTRIBUTIONS OF AUTHORS (Continued)

Dr. Charles L. Rosenfeld, Professor of Geosciences at Oregon State University, Cascades Campus, is a geomorphologist with specialties in remote sensing applications, natural hazards, and environmental management. He has served as Chair of the Commission on Natural Hazards of the International Council of Scientific Unions during the UN's International Decade for Natural Hazards Reduction (IDNDR). Dr. Rosenfeld is the author of numerous articles on remote sensing techniques and hazards mapping, and has served as an advisor on emergency management worldwide. He also serves as a Major General in the Army National Guard, currently assigned as the Wartime Chief of Staff, U.S. Forces, Korea. As major professor for this research effort, Dr. Rosenfeld worked directly with the primary author during all phases of the project, including geomorphic field reconnaissance, collection of fixed-wing airborne color videography, spectral analysis of surficial geologic materials, helicopter overflights to verify mapping results, and report generation.

Dr. Stefanie Tompkins holds degrees in geology from Princeton and Brown Universities. She served 4 years as a U.S. Army officer between her undergraduate and graduate degrees, and another 10 years in the Reserves. She is currently a Senior Staff Scientist at Science Applications International Corporation (SAIC) in Chantilly, Virginia, managing research and development projects for hyperspectral image exploitation, and conducting independent research as a NASA Principal Investigator. Her research efforts focus on reflectance spectroscopy as it applies to remote geochemical analysis of planetary surfaces, including the Earth's Moon and, of course, the Earth itself. Dr. Tompkins is the Chameleon Project Manager at SAIC, the primary project contractor and software developer, and this work is documented in Appendix D. As a Subject Matter Expert in spectral mixture analysis, Dr. Tompkins contributions to Chapter Six were significant.

TABLE OF CONTENTS

TABLE OF CONTENTS (Continued)

Page

TABLE OF CONTENTS (Continued)

LIST OF FIGURES

LIST OF FIGURES (Continued)

LIST OF FIGURES (Continued)

LIST OF FIGURES (Continued)

LIST OF TABLES

CHAPTER 1—INTRODUCTION

The Department of Defense (DoD) operates a network of test and evaluation centers located in variety of natural environments and extreme climatic conditions for the purposes of developmental and operational testing of equipment, training and doctrine support, and surveillance and security operations. To effectively accomplish these objectives, the physical and environmental geography, as well as cultural resources, of these sites must be understood, managed, and in some cases protected. This dissertation initially focused on the use of remote sensing technologies for installation environmental impact management and cultural resource evaluation. Successful application of aerial photograph and multispectral satellite imagery interpretation, integrated with a Geographic Information System (GIS), provided considerable improvements in survey archeology for a portion of the U.S. Army Yuma Proving Ground (YPG) in Arizona. This initial success provided a vision of quantitative analysis of hyperspectral data having potential for improved desert characterization.

Spatial Patterns of Cultural Resources and Alluvial Geomorphic Surfaces

Two-thirds of DoD land holdings are located in the arid southwestern United States (U.S.). This represents an enormously expensive cultural resource compliance requirement. Chapter one was published in the Special Edition on Management and Mitigation of U.S. Department of Defense Arid Lands in the *Arid Land Research and Management* journal (Lashlee et al., 2002). This paper describes procedures used to relate the occurrence of cultural artifacts to landscape position and age of geomorphic surfaces mapped from stereoscopic aerial photography and augmented with multispectral Landsat Thematic Mapper satellite data. Spatial analysis was performed using GIS algorithms and statistically verified using chi-square analysis.

Reliable cultural resource information was generated and provided to Army Conservation Managers and the Arizona State Historic Preservation Officer in a useful spatial context. Additionally, the interdisciplinary approach used was found to be a scientifically defensible technique that not only met, but also exceeded, requirements of the National Historic Preservation Act. Recommendations for development of predictive cultural landscape models were subsequently proved viable by an independent investigation in an adjacent study area and the methodology has since become the basis for a major cultural resource-mapping program at YPG. Based on these results, the laboratory spectrometry investigation summarized in chapter two,

and a priori knowledge that cultural resources in the region are surficial features, hyperspectral remote sensing data were hypothesized to have significant potential for improved arid land mapping and modeling and that quantitative analysis of these data might yield efficiencies leading to automated detection and recognition of natural and cultural features.

Laboratory Spectrometry of Rock and Soil Samples (Micro-Scale Measurements)

There are many ways to misinterpret the earth, including erroneous assumptions and extrapolations in space, time, and location; scale, direction, and magnitude; cause, process, and system response (Schumm, 1991); and positional and thematic mapping (Lashlee et al., 1993). There are as many ways, if not more, to incorrectly model the terrain. Problems inevitably arise when reducing the complexity of natural systems to a state that can be modeled efficiently and distributed effectively in simulations. To address these problems, we compared the physical properties of landforms to laboratory, field, and imaging spectrometry data to quantify the hyperspectral response of surficial geologic materials in the solar reflected spectrum. This involved not only the collection and analysis of large amounts of new spectroscopic data of different land covers, but also the systematic collection and analysis of detailed chemical and petrographic data for rocks, rock coatings, and soils. These data allowed correlation of mapped composition and abundance information to spectral signatures collected at three measurement scales.

Chapter two was published in the proceedings of the Army Test and Evaluation Command's Natural Environments Testing Workshop (Lashlee and Rosenfeld, 2000). This paper explores the relationship between chemistry and optical reflectance properties of a variety of common rock coatings, including weathering rinds, carbonate deposits, and rock varnishes, on lithologic reflectance of individual desert pavement clasts. Laboratory spectra were collected at a spatial scale of a few millimeters under controlled laboratory illumination and environmental conditions, then analyzed to measure shape and strength of spectral absorption features. These micro-scale measurements clearly show that reflectance of rock samples collected from geomorphic surfaces is significantly altered by the presence of a variety rock coatings. The most ubiquitous rock coating encountered in the Lower Colorado Sonoran Desert is manganese-rich rock varnish, which significantly alters laboratory spectra reflectance from 400 to 2000 nanometers (nm), but transmits lithologic information in the geologic bands from 2000- to 2500-nm wavelengths. However, as spatial scales shift toward the larger ground areas sampled with field

and imaging spectrometry, lithologic information is more difficult to establish owing to the heterogeneous nature of desert pavement clasts, increasing atmospheric attenuation of terrestrial signatures, and decreasing signal-to-noise ratios in the shortwave infrared wavelengths.

Field Spectrometry of Desert Landforms (Meso-Scale Measurements)

Alluvial geomorphic surfaces compose 70% of the YPG landscape. Chapter three summarizes our work toward defining geomorphic controls on hyperspectral reflectance of these surfaces (with emphasis on desert pavements) and the implications of these results for mapping and modeling arid landforms. Field spectra were collected using the same instrumentation, calibration techniques, and materials described in chapter two, so these data are directly comparable to laboratory spectra. However, field spectra differ by definition from laboratory signatures in that they were collected under natural solar illumination and weather conditions. In addition, spatial resolution of these data is about 1 m, which records an integrated average of groups of desert pavement clasts within the instruments field-of-view, as well as the soil matrix that holds them *in situ*, and minor fractions of non-photosynthetic vegetative matter. Comparing spectra collected along surveyed transects provided valuable meso-scale reflectance data on the variations within and between landforms.

Chapter three summarizes soils geomorphology performed in the field and laboratory, and then correlates physical and chemical soil properties, as well as pavements clast signatures, with hyperspectral reflectance. We learned that spectral signatures of surface soil from each landform are affected most by iron-bearing minerals in the visible and near-infrared wavelengths, and by calcium carbonate absorption features in the shortwave infrared wavelength region. The presence of both was confirmed by laboratory chemical analysis. We also gained an appreciation for the extensive effects of eolian dust as a geomorphic material and normalizing factor on arid land reflectance. Soil samples from each study site have similar texture and mineralogy, resulting in identical hyperspectral signatures, regardless of landform type, heterogeneity of parent materials, or differences in geologic age. On undisturbed terrain, it's not the composition of surface soils that changes, but the amount of soil matrix exposed that is recorded in remotely sensed imagery.

Imaging Spectrometry of Arid Landscapes (Macro-Scale Measurements)

The criteria most often used for mapping alluvial geomorphic surfaces in deserts are: 1) degree of desert pavement development, 2) amount and character of rock varnish, 3) soil type, 4) topographic position, and 5) drainage characteristics (Bull 1991). With the exception of subsurface soil profile development, each of these criteria can, with varying degrees of success, be assessed remotely. Chapter four continues the spectral analyses summarized in previous chapters using imaging spectrometry. Airborne Visible–Infrared Imaging Spectrometer (AVIRIS) data are used to characterize the spectral properties of the same three study sites at a landscape scale. These data differ from laboratory and field spectrometry in spatial and spectral resolution. The AVIRIS data have 220 bands of hyperspectral information sampled in 4-m pixels, while laboratory and field spectrometer data have over 1500 bands of ultraspectral information.

Results of this study show that most alluvial geomorphic surfaces can be differentiated and their boundaries mapped using hyperspectral data. However, accurate composition and abundance mapping of desert pavements remains problematic. A significant finding of our research is that the pavement surfaces studied lack significant diagnostic absorption features that hyperspectral data are designed to resolve as compared to multispectral data. While it would be advantageous if the world's geomorphic surfaces could be accurately mapped and quantitative information about them extracted remotely, heterogeneous lithologies typical of many pavements result in intimate mixtures requiring advanced non-linear unmixing analysis. Therefore, the high spectral and spatial resolution data required to model terrain, sensor systems, and perform target detection and recognition are not necessarily the most efficient remote sensing technology for mapping desert pavements. Topographic position and pavement development (image texture) interpreted by a terrain analyst (Lashlee et al., 2002) appear to be as important as the application of deterministic digital image processing algorithms for delineating heavily varnished desert pavements. We have demonstrated that Holocene geomorphic surfaces can be differentiated from Pleistocene surfaces. The next research question is if early, mid-, and late Holocene surfaces and also early, mid-, and late Pleistocene surfaces can be spectrally discriminated and accurately mapped in terms of composition *and* geomorphic age.

Together, the spectral analyses summarized in these chapters provide a comprehensive under-standing of hyperspectral reflectance of the natural desert environment at YPG. As the Army's desert analog for arid environments around the world, the science and software developed from this research have important implications and immediate application. We've also demonstrated that the Lower Colorado Sonoran Desert is a more compositionally diverse and spectrally com-plex landscape than is generally acknowledged by the remote sensing community. The knowl-edge gained through these studies is essential for accurate terrain mapping and modeling for both civilian and military applications.

The Chameleon Concept—Linear Remixing for Synthetic Landscape Generation

A primary objective of DoD training simulations is to immerse personnel in a synthetic envi-ronment that accurately models the terrain, environmental conditions, and threats to be en-countered in the real world. This is also true for Army developmental and operational testing, where the greatest application of Modeling and Simulation (M&S) is the ability to efficiently create the most realistic virtual environment possible for a system under test (Barr, 2002). Current simulation architectures for military testing and training applications consist of het-erogeneous, but interoperable, computer workstations that are distributed across the Internet. Recent improvements in these computer, server, and network technologies have supported the development of more sophisticated models and simulations needed to accurately depict the increasing complexity of modern weapon systems. However, traditional visual digital terrain databases developed to operate a single simulator have been replaced by rigorous require-ments for more complete synthetic natural environments (including ocean, atmosphere, near-space, and terrain data) that are correlated to assure parity among all distributed participants. As a critical precondition to successful simulation interoperability, synthetic natural environ-ments are costly in terms of both time and money to produce and maintain, and therefore rep-resent a programmatic risk for many M&S applications. Chameleon was designed to address some of these new and still evolving virtual terrain data requirements.

Chameleon is both an analytical methodology and software system for generating spectrally accurate, physics-based digital terrain hypercubes for civilian and military M&S applications. A Chameleon landscape is based on n-dimensional hyperspectral data, where n is the number of image bands. Image spectra can be modified on a neighborhood, per-pixel, or sub-pixel basis, or the entire hypercube can be affected at once. Hence, hypercubes are dynamic, rather than

static, imagery. Using Chameleon software, the terrain becomes a spectral chameleon, able to change color based on compositional variations in natural and cultural surface materials; multitemporal variations in vegetation cover, atmosphere, sun angle geometry; or other parameters required by specific test or simulation scenarios.

In the last decade, a great deal of research has focused on problems related to how spectra of more than one material mix mathematically. Chameleon exploits and then expands upon this work in Spectral Mixture Analysis (SMA). Typically, linear unmixing is performed to decompose each pixel in an image into spectral endmembers. An innovative toolset is provided for mathematically manipulating fractional abundances of materials and for introduceing new spectral information. One of the more innovative Chameleon technologies—linear remixing— is then used to regenerate synthetic, but spectrally accurate, landscape models. Chapter six gives examples of these procedures using environmental extremes in the sparsely vegetated Sonoran Desert and a double canopy tropical forest in the Republic of Panama.

The Chameleon Software User's Guide

Appendix A lists the *Chameleon Software User's Guide* in its entirety, which summarizes the functionality of Chameleon at the time of this publication. Over the previous 3 years of development, software has been released as "Gecko" versions 1.0 through 3.4, reflecting the initial development stages of the program. In December 2004, Gecko 4.0 became Chameleon Software release version 1.0. While not a complete implementation, Chameleon 1.0 meets Army requirements necessary to declare Chameleon at Initial Operating Capability (IOC1). It's a fully operational and documented software prototype.

References

Barr, B. (2002) USAOTC: The Role of Modeling and Simulation in Operational Testing. *Journal of the International Test and Evaluation Association: Modeling and Simulation Applications in T&E*, **23**(1): 21–25.

Bull, W.B. (1991) *Geomorphic Response to Climatic Change.* New York: Oxford Press.

Lashlee, D., Briuer, F., Murphy, M., and McDonald, E. (2002) Geomorphic mapping enhances cultural resource management at the U.S. Army Yuma Proving Ground, Arizona, USA. *Arid Land Research and Management: Special Edition on Management and Mitigation of U.S. Department of Defense Arid Lands,* **16**: 213–229.

Lashlee, J.D., and Rosenfeld, C. (2000) Laboratory spectrometry of rock coatings: Implications for land management activities in the arid Southwest. *Proceedings of the Natural Environments Testing Workshop, U.S. Army Test and Evaluation Command, Washington, D.C. 29–30 November 2000.*

Lashlee, J.D., McKinley, G.B., and Bishop, M.J. (1993) Quantitative land cover classification accuracy assessments derived from single pass and ISODATA unsupervised clustering algorithms. Technical Report GL-93-21, U.S. Army Corps of Engineers, Waterways Experiment Station, Geotechnical Laboratory.

Schumm, S.A. (1991) *To Interpret the Earth: Ten Ways to be Wrong.* New York: Cambridge University Press.

CHAPTER 2—GEOMORPHIC MAPPING ENHANCES CULTURAL RESOURCE MANAGEMENT AT THE U.S. ARMY YUMA PROVING GROUND, ARIZONA, USA

David Lashlee, Frederick Briuer, William Murphy, and Eric V. McDonald

Abstract

Provisions of the National Historical Preservation Act of 1966, particularly Section 106 of that Act, require the Yuma Proving Ground (YPG) to conduct archaeological surveys and assess cultural resources to evaluate potential effects of planned military testing activities on those cultural resources considered eligible or potentially eligible for inclusion in the National Register of Historic Places. Landscape reconstruction was performed using aerial photograph and satellite image interpretations, ground verification, including detailed soils geomorphology descriptions, and archaeological surveys. Geographic Information System overlay analyses were used to determine the preferential distribution of cultural resources in the study area. A vast majority of the 40 mapped cultural sites are located on Pleistocene age geomorphic surfaces. Few sites occurred on Holocene age surfaces. Spatial relationships between geomorphology and archaeology were supported by chi-square statistical tests rejecting the hypothesis that culture is evenly distributed across the landscape as a function of the size of geomorphic surfaces composing it. Of cultural resources designated eligible for the National Register of Historic Places, 92% occur on Pleistocene age geomorphic surfaces. Results of this interdisciplinary study suggest that both differential preservation of geomorphic surfaces and human behavior act together to explain the spatial distribution of cultural resources at YPG.
Keywords: Archaeology, Geographic Information Systems, geomorphic surfaces, remote sensing, soils geomorphology.

Introduction

The Department of Defense (DoD) is steward of vast land holdings in the arid southwestern U.S. This chapter presents an interdisciplinary study that merges traditional aerial photography interpretation, field verification, including desert pavement surface characteristics and soil profile analysis, cultural resource mapping, and Geographic Information System (GIS) overlay analysis to determine which landforms at the U.S. Army Yuma Proving Ground (YPG) have cultural significance. Evidence presented of the spatial distributions of archaeological sites with respect to the landscape may, if validated by future studies in the Lower Colorado Sonoran Desert, provide valuable information needed to develop predictive models of the location and condition of cultural sites and substantially reduce the cost of complying with cultural resource surveys and assessments on military lands.

Environmental Setting

YPG is a general-purpose testing facility within the U.S. Army Test and Evaluation Command, whose mission includes testing artillery, tank and automotive systems, aircraft armament and air delivery systems, and smart munitions. YPG also supports training operations and visiting military units. Located adjacent to the confluence of the Colorado and Gila Rivers (Fig. 1), YPG is larger in size than the state of Rhode Island, encompassing more than 3367 km^2 (1300 miles^2) of the hottest and driest area in the U.S. (Yuma Meteorological Team 1998).
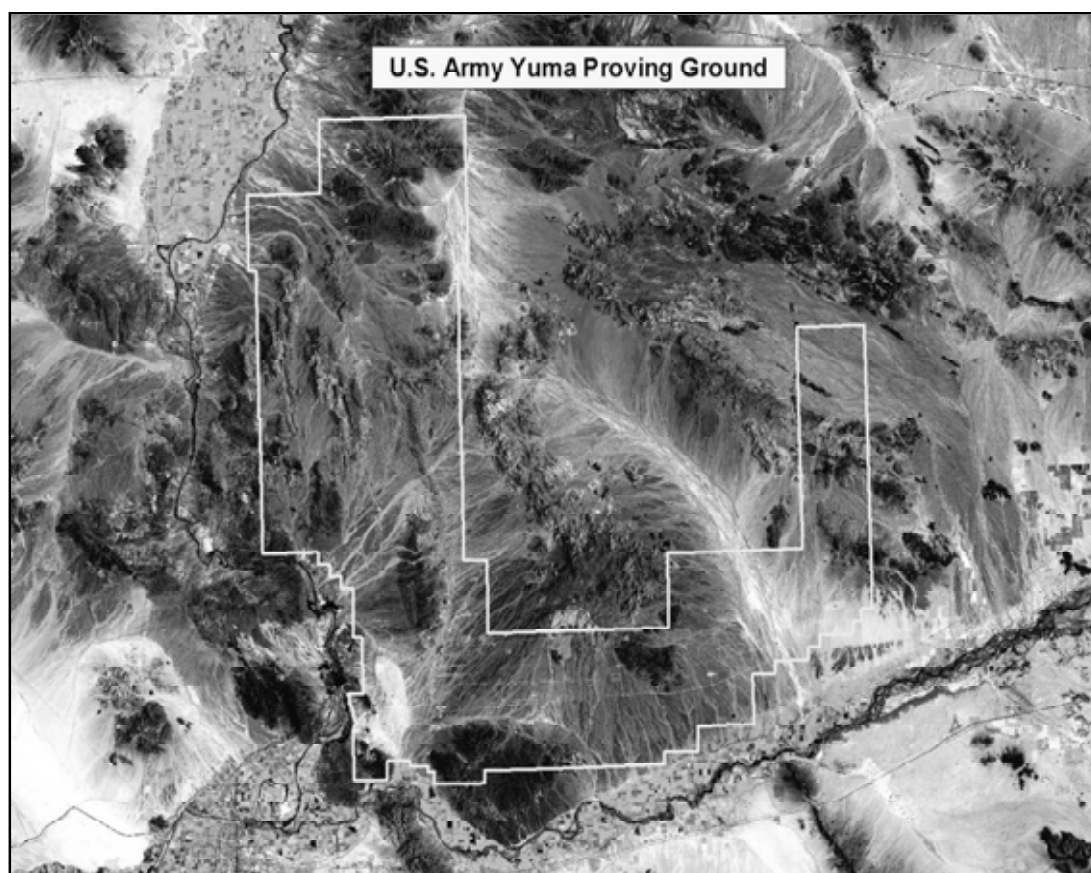
Figure 1. Landsat Thematic Mapper image of the Yuma Proving Ground. This image is centered on geographic coordinates N 33°11' 00", W 114°7' 32".

The most prominent geologic features of YPG's landscape are Tertiary volcanic and meta-morphic mountain ranges and broad intermontane alluvial basins, typical of the Basin and Range physiographic province of the southwestern U.S. (Dohrenwend 1987). Other land-forms include sand dunes and alluvial fans and bajadas, which often transition to extensive

alluvial plains drained by ephemeral stream washes. Fan terraces and alluvial plains make up almost 70% of YPG's landscape and are locations of extensive, well-developed desert pavements. Vegetation at YPG is sparse, estimated not to exceed 4% of the land surface area, and uniquely adapted to the hot, dry climate (Bern 1995).
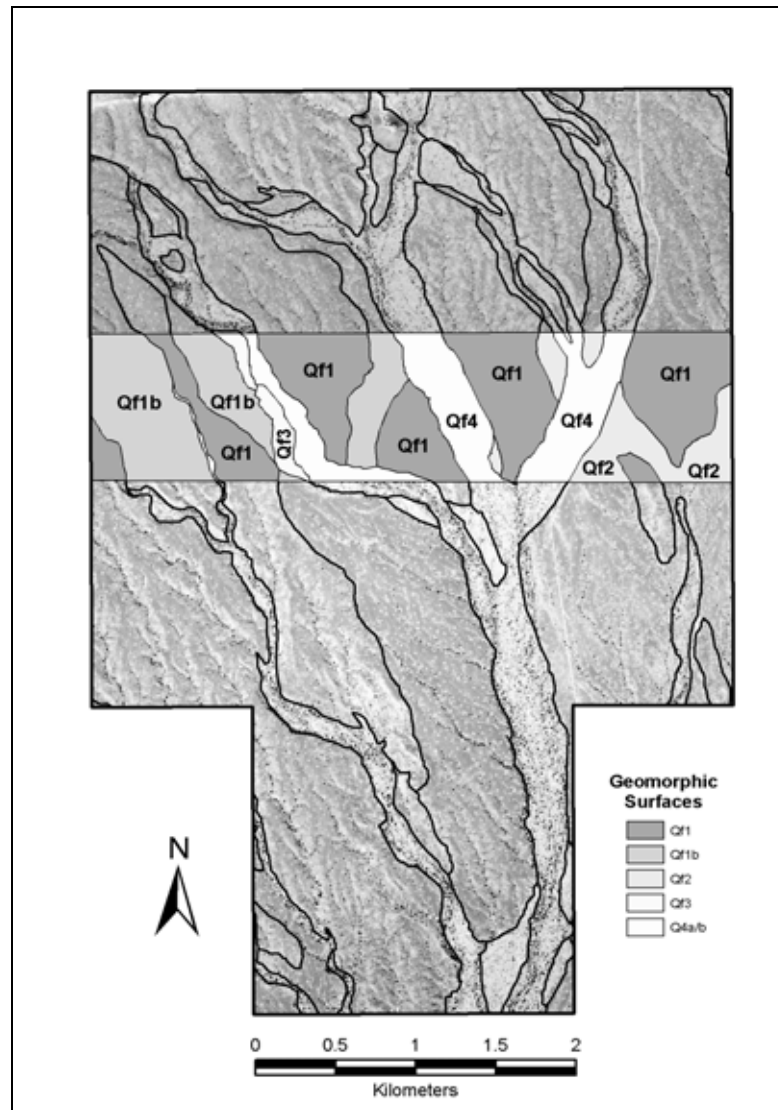
Figure 2. Aerial photograph of the Phase IIb study area and a portion of the landform interpretation.

The study area is a 15-km^2 area known as "Phase IIb" (Fig. 2) and is located within the Roll, Arizona, 7-½ minute topographic quadrangle. Part of the Castle Dome Plain, Phase IIb lies in the medial to distal portions of a gently sloping system of coalescing alluvial fans. Dark col-

ored desert pavement with well-developed manganese-rich rock varnish occurs over much of the study area. Major source areas of alluvial deposits include the Castle Dome Mountains immediately to the north and Red Bluff Mountain to the west. These mountains are composed of Quaternary, Tertiary, and older volcanic basalts and rhyolites, metamorphic schists and gneisses, Tertiary granitic rocks, and Tertiary and older sedimentary rocks. The drainage system is characterized as ephemeral tributaries and active channels that flow through alluvial valley fill draining south to the Gila River.

Procedures

Geomorphic surfaces are mappable landscape elements formed during discrete time periods. Geomorphic mapping, much like traditional geologic mapping, seeks to define surface units on the basis of distinctive surface and subsurface characteristics. The criteria most often used for identifying and mapping desert geomorphic surfaces in the field are: 1) degree of desert pavement development, 2) amount and character of rock varnish, 3) soil type, 4) topographic position, and 5) drainage characteristics (McFadden et al. 1989, Bull 1991). We used a combination of remote sensing techniques and ground verification data collected in the field to identify these characteristics and delineate geomorphic surfaces.

Mapping Geomorphic Surfaces

Color aerial photography of 1:24,000 scale flown in 1985 was acquired from YPG's Directorate of Command Technologies, Environmental Sciences Division. In addition, a Landsat Thematic Mapper (TM) image of YPG collected on 24 June 1995 was acquired and used to supplement photographic interpretations. Phase IIb was delineated into individual geomorphologic surfaces using stereoscopic interpretation of aerial photography. A TM 7, 4, 2 (RGB) color image composite was displayed on a computer monitor for enhanced spectral discrimination of geomorphic surfaces. Interpretations were transferred from photography to mylar overlays, raster scanned, georeferenced, and mosaicked using Geographic Information System (GIS) software. Ground reconnaissance was then performed to refine the landform classification and develop age estimates of significant surfaces. Compared to these qualitative field observations, the geomorphic map was found to be accurate and few modifications to the interpretation were required.

Within Phase IIb there are five geomorphic surfaces sufficiently distinct and widespread to be mapped as time-stratigraphic units, each formed during a particular geologic time span (Fig. 2). These surfaces were labeled, from oldest (and generally topographically highest) to youngest, as Qf1, Qf1b, Qf2, Qf3, and Qf4a and b (Qf for Quaternary fan). Soil profile descriptions identified one exception to this topographic position to relative surface age relationship. The Qf1 alluvial *deposits* are topographically higher and older than other deposits, but actually have a younger, re-worked *surface* and soil profile compared to the other Pleistocene age surfaces Qf1b (Fig. 3) and Qf2. Qf3 surfaces are poorly varnished, exhibit bar and swale topography, and are typically located adjacent to Qf4a ephemeral washes and Qf4b active channels that drain the area. These surfaces range in age from early (Qf3) to late (Qf4b) Holocene (Fig. 4). Soil profiles and desert pavement observations suggest that Qf1b is the oldest geomorphic surface in the study area.

A final landform present in Phase IIb was mapped as QTv (Quaternary–Tertiary volcanics). Relatively small, but topographically prominent, this landform is a cone-shaped volcanic extrusion that rises 30 m above the surrounding alluvial plain. Known at YPG as Contraves Station J, QTv is used as an instrumented tracking and observation site (Fig. 5).

Figure 3. Soil pit excavation on the Qf1b Pleistocene geomorphic surface. The volcanic cone in the background is outside (north of) the study area boundary.
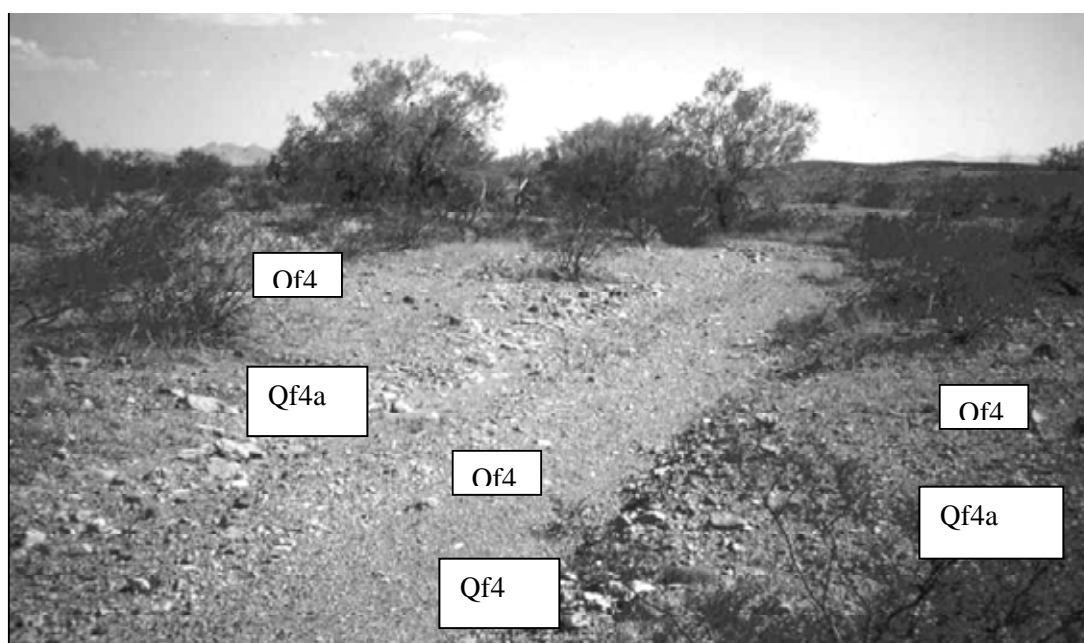
Figure 4. Holocene geomorphic surfaces Qf4a (abandoned) and Qf4b (active) channels.
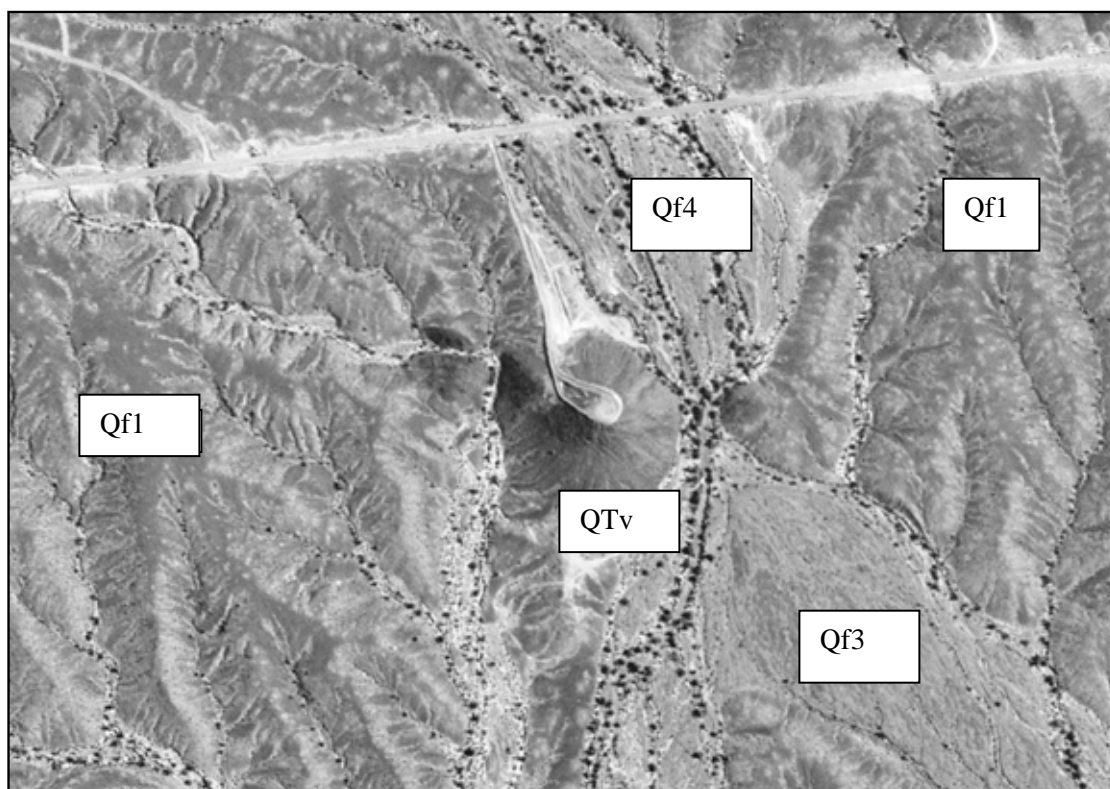
Figure 5. Digital orthophotograph at 1-m resolution of a portion of the Phase IIb study area.

Estimated Surface Age

Soils profile descriptions were collected as part of the site characterization effort. Because a limited number of dig permits were issued by YPG, only three soil pits were excavated and examined. Primary criteria for site selection were relative age and areal extent of geomorphic surfaces. Priority was given to Pleistocene surfaces with well-developed desert pavements and large areas (Qf1, Qf1b, and Qf2), thus maximizing our understanding of geomorphic processes and landform development on surfaces known to have significant cultural resources. Complete desert pavement surface and soil profile descriptions are given in Lashlee et al. (2000).

Soils profile data indicate that Qf1, Qf1b, Qf2 are indeed distinctly different Pleistocene surfaces as was delineated from the aerial photography. Soil formed on Qf1 has a moderately developed cambic horizon and is classified as Typic Haplocambids. Qf1b soils have moderately developed argillic and calcic horizons and are classified as Typic Calciargids. The soil on Qf2 has a moderately developed cambic and clacic horizon and is classified as Typic Haplocalcids.

General age of each surface was estimated based on the degree of soil profile development and correlation to soils and surfaces in the nearby Whipple Mountains, California (Bull 1991). The age of both Qf1 and Qf2 are estimated to be between 12,000 and 70,000 years old, while the Qf1b is between 70,000 and 200,000 years old. Qf1 surfaces generally have the highest elevation and should be the oldest deposit and with the best-developed soils. The degree of soil formation on this surface, however, is substantially weaker than soils on topographically lower, younger Qf1b and Qf2 surfaces. Further, the presence of scattered pavement clasts with coatings of carbonate, characteristic of subsurface pedogenic processes, indicates that this surface has undergone substantial surface erosion in the past. These relations strongly suggest that the current soil and desert pavement have most likely formed on a recently restabilized surface and the age of the soil reflects the amount of time since the last period of major fan degradation.

The Qf3 surfaces exhibit bar and swale topography, with poorly varnished desert pavement clasts, and are generally located adjacent to Qf4a ephemeral washes and Qf4b active channels

(Fig. 5). Soils formed on the Qf3 surfaces have weakly to moderately developed cambic hori-
zons classified as Typic Haplocambids. Qf4 soils are minimally developed Typic Torri-
orthents. Ages of the Qf3 and Qf4 Holocene surfaces are estimated to be about 8000 to 4000
years old and less than 4000 years old, respectively.

Mapping Cultural Resources

Surface-exposed cultural resources were recorded and mapped between 25 February and 31
March 1998 (Briuer et al. 1999). On-line sweeping and recording procedures were used to
survey the study area with a 15 to 30 meter interval. We recorded 40 cultural resource sites
and mapped them using 1:24,000-scale maps, color air photos, and Global Positioning System
(GPS) receivers. This inventory included prehistoric and historic sites with various combina-
tions of rock structures and features (Fig. 6) as well as ceramic, stone tool, and lithic assem-
blages. We also mapped 72 prehistoric trail segments (Fig. 7). In addition, 95 isolated occur-
rences of low density and diversity were also recorded and mapped. "Isolated Occurrences"
are defined as low priority cultural resources that contain a minimum of artifactual material
and are often small lithic scatters lacking both stone tool density and diversity. We judged 16
of the best-preserved Recorded Archeological Sites and trail segments to have significant re-
search potential and to be eligible for National Register Nomination.

Figure 6. Rock ring on Qf1b Pleistocene geomorphic surface.

Figure 7. Aboriginal trail and associated cleared circles on Qf2 Pleistocene geomorphic surface.

Results

Geomorphic surfaces and cultural resources data of Phase IIb were compiled into geospatial data, documented with geospatial metadata compliant with the Federal Geographic Data Committee, and compared using a GIS overlay analysis for each type of cultural resource mapped in the field. Results shown in Figure 8 and Table 1 indicate that, with the exception of Isolated Occurrences, culture features are not distributed evenly across the Phase IIb landscape.

Table 1. Percentage of cultural resources located within each geomorphic surface.

Geomorphic surface	Landform (m^2)	Isolated occurrences (number of sites)	Archeological sites (m^2)	Aboriginal trails (lineal meters)
Qf1	47.28	56.99	47.0	40.0
Qf1b	16.91	20.43	4.0	21.7
Qf2	13.01	13.98	21.0	24.6
Qf3	3.38	2.15	0.0	1.7
Qf4a/b	19.08	6.45	16.0	12.0
QTv	0.34	0.00	12.0	0.0
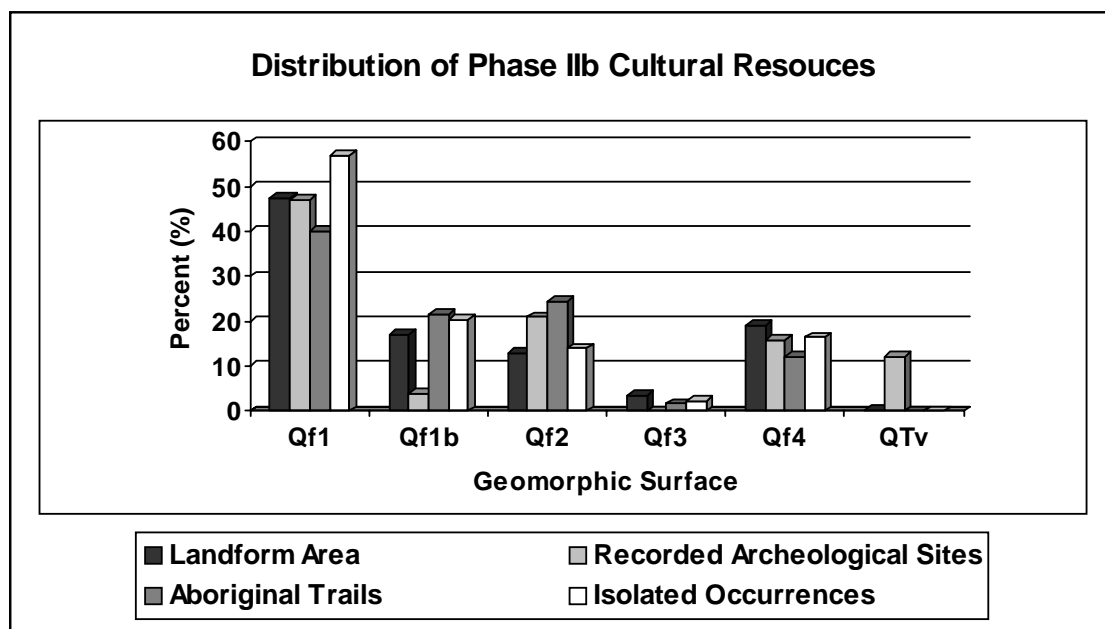
Figure 8. Cultural resource distribution in the Phase IIb study area. *Landform area* was calculated as square meters (percentage of the total study area), *recorded archaeological sites* as square meters (areas), trails as percent lineal meters (lines), and *isolated occurrences* as the percentage of the number of sites (points).

Recorded Archaeological Sites

Recorded Archeological Sites exhibit strong spatial patterns—72% of these sites are found on Pleistocene age geomorphic surfaces (Qf1, Qf1b and Qf2). Of this, 47% are located on Qf1, which is exactly proportional to the 47% areal extent of Qf1 surfaces in Phase IIb. This suggests no strong cultural preference for the oldest and topographically highest landform. Qf1b composes 17% of Phase IIb, but contains only 4% of Recorded Archeological Site area. Qf2 is 13% of Phase IIb, but contains 21% of the Archaeological Site area. To summarize, results for these Pleistocene surfaces vary. Based on size, Qf1 is proportional to culture, while Qf1b contains less culture, and Qf2 contains more culture than expected.

Holocene geomorphic surfaces (Qf3 and Qf4) accounted for a total of 16% of Archeological Site area, all of which was mapped within Qf4 washes. None of the 40 Recorded Archeological Sites occur on Qf3, which composes only 3.4% of Phase IIb. Though Qf4 results are higher than anticipated, washes are still under-represented with respect to size, as they represent 19% of the study area (Fig. 8). Moreover, as explained in the discussion section below, it

is possible, if not likely, that some of the culture attributed to Qf4 is the result of mapping error. This conjecture is supported by field observations that, with few exceptions, artifacts encountered on Qf4 surfaces were isolated occurrences or artifactual material that appeared to be secondarily deposited by floods.

Perhaps the most surprising result concerns the least prominent landform in Phase IIb. Of the Recorded Archaeological Site area, 12% is located in QTv, which consists of only 0.34% of the total landform area. These numbers represent an increase of more than two orders of magnitude in cultural features compared to landform size. Field data indicate that this landform was probably heavily used throughout the archaeological record as a stone tool procurement and manufacturing area owing to its desirable geologic material—a chert-like cryptocrystalline rhyolite exposed as a cone-shaped volcanic extrusion. QTv may also have served other prehistoric site functions, such as hunting and gathering encampments, because of its prominent elevation.

Aboriginal Trails

Aboriginal trails remain a fascinating, but relatively poorly understood, spatial and anthropological phenomenon in the region. Trails in Phase IIb also exhibit spatial patterns with respect to geomorphic surfaces. Pleistocene surfaces account for 86% of trails, while only 14% are located on the younger Holocene surfaces. There are slightly fewer trails on the Qf1 Pleistocene surface than expected, considering its areal extent (Fig. 8, Table 1). However, an increased percentage of lineal trails are associated with both intermediate age Qf1b and Qf2 Pleistocene desert pavements. Qf2, in particular, composes 13% of Phase IIb, but accounts for about 25% of mapped trails. Both Holocene age Qf3 and Qf4 surfaces are under-represented with respect to trails, which is attributed to the active erosional and depositional geomorphic processes common to these surfaces.

Isolated Occurrences

Isolated Occurrences have the least cultural significance of archaeological phenomena mapped in Phase IIb. There are more than twice the numbers of Isolated Occurrences (93) than Recorded Archeological Sites (40) in the study area. With the exception of Qf4 wash areas, iso-

lated occurrences are ubiquitously distributed across the landscape and lack differential spatial patterns exhibited in both trails and recorded archaeological sites data.

Condition of Recorded Archeological Sites

As part of the cultural resource evaluation, the relative condition of each site was classified on a scale of 1 (best condition, least disturbed) to 3 (worst condition, heavily disturbed). The physical condition of recorded cultural features and structures, such as rock rings and trails, were evaluated as well as the relative condition of the surrounding desert pavement. Although containing other well and moderately preserved sites, 94% of sites classified as worst condition are located on Qf1. The remaining 6% of worst condition sites occurred in Qf4 drainage areas. These results are perhaps not surprising given the enhanced hillslope and sheetwash processes characteristic of the ridge-and-ravine topography of Qf1 and the active erosional and depositional processes typical in wash areas. The oldest and youngest landforms, both of which are well-drained surfaces, contain all culture determined to be in a state of poor preservation.

Significant Cultural Sites

From a military arid land management perspective, the most critical results concern those sites that may require mitigation. Significant cultural sites also manifest strong patterns based on geomorphic age. In fact, 92% of the sites designated eligible or potentially eligible for the National Register of Historic Places occurred on Pleistocene age geomorphic surfaces (Table 2). Of the 17 Significant Sites, 10 are located on Qf1, more than twice as many as occurred on any other geomorphic surface. However, Qf1 is more than twice the size of the next largest landform. Only three significant sites were mapped on Qf2. However, their cumulative size (42,378 m^2) is significantly larger than the cumulative area of all other significant sites combined (29,983 m^2). Fewer sites of greater site size seem to correlate with greater trail length in the Pleistocene Qf2 landform.

Only 8% of significant cultural site area was found on Holocene geomorphic surfaces, all of which were located in Qf4 wash areas. No significant cultural sites occurred on Qf3. Finally, although QTv contained a preponderance of Recorded Archeological Sites relative to its size (12%), none of the Recorded Sites on QTv surfaces were determined to be significant.

Table 2. Number and Size of Significant Cultural Resources.

Geomorphic Surface	Number of Significant Sites	Total Area (m^2)
Qf1	10	22,485.244
Qf1b	4	1,954.545
Qf2	3	42,378.439
Qf4a/b	4	5,542.720

Statistical Results

To further quantify these results, a chi-square statistical test was performed to test the hypothesis that archaeological site locations, expressed as center point data collected with GPS, were evenly distributed within the five geomorphic surfaces as a function of the relative size of each landform. The hypothesis of no significant difference was rejected at the 99% confidence level (Lashlee et al. 2000). There is clear evidence that archaeological sites are distributed unevenly with respect to landform. That is, archaeological sites are preferentially located on older landforms (Qf1 and Qf2). Sites are under-represented on the youngest and least stable Qf4a/b active floodplain landforms. When site area and trail segment length are considered in the analysis, data indicate over-representation of archaeological sites and trails on the Qf2 landforms. This suggests that archaeological sites are likely to be most numerous and best preserved on the Qf2 landforms, which represent younger *deposits* but older and less disturbed *surfaces* than the Qf1.

Discussion

Map scale, positional accuracy, and precision of measurements are important issues in mapping applications like this one. For this study, we used 1:24,000 scale aerial photography to delineate geomorphic surface boundaries, 1:24,000 scale digital orthophotoquads as control to georeference and mosaic landform interpretations, and 1:24,000 scale topographic maps for delineating archaeological site boundaries. These maps have a 12-m circular error associated with positional accuracy, so we expect that a majority of boundaries drawn at this scale are to be within 24 m of the actual location on the ground.

For example, 1610 m^2 of Significant Archeological Site 41 were mapped in Pleistocene Qf2, while 27 m^2 were located in a Holocene Qf4 wash. Two other Significant Sites were also partially located in Qf4 when overlaid with geomorphology. We attribute these discrepancies to the map scale used. In addition, there is always potential introduction of error during the de-

lineation, digitization, and georeferencing procedures. We can reliably report that, of the 3,817,027 m^2 of Qf4 in Phase IIb, only one relatively small but significant site was mapped entirely within a wash. This site was found to be a small relict area of Pleistocene desert pavement located within active channels and abandoned washes. With this exception, artifacts encountered during the archaeological field survey on Qf4 surfaces were Isolated Occurrences or other artifactual material that appeared to be secondarily deposited by floods.

Cartographically, the closer cultural resource sites are in juxtaposition to geomorphic surface boundaries, the less confidence we have in their correct landform association. For future studies, we recommend using a GIS buffer procedure to produce a 24-m buffer zone around landform and archaeological site boundaries. Cultural sites that fall within this zone of questionable spatial accuracy should be more carefully examined to determine whether the entire site area is located on a single surface or on multiple landforms. Ultimately, the usefulness of these results is commensurate with verification of their reliability.

Conclusions

Two-thirds of Department of Defense (DoD) land holdings are located in the arid southwestern U.S. This represents an enormously expensive compliance requirement for cultural resource management. It is essential to develop more efficient survey, prediction, evaluation, and inventory techniques to meet explicit Federal legal requirements. Results of this study clearly have important implications for more efficient and cost-effective strategies for achieving future comprehensive cultural resource management in areas yet to be inventoried. Treatment of each landscape element with equal consideration (equal likelihood of having significant cultural resources) is both unnecessary and prohibitively expensive, not only at YPG, but in other vast DoD arid land holdings, particularly when it is clear that some landforms deserve more intensive consideration than others. In Phase IIb, Pleistocene landforms contain vast amounts of cultural remains, including significant archeological sites and aboriginal trails, compared to Holocene geomorphic surfaces. Indeed, there is evidence of spatial patterning among Pleistocene surfaces. For example, relatively large, complex, and obtrusive archaeological sites, such as stone circles, stone alignments, and cleared circles, are well preserved or very minimally disturbed on Qf2.

Ground verified, remotely sensed data is a time and cost-effective technique for regional geomorphic mapping. Stereoscopic aerial photography contains valuable spatial information for mapping geomorphic surfaces, such as topographic position and surface roughness, that are not typically available in commercially available satellite imagery. Landsat TM data were valuable for evaluating the study area in a regional context and provided enhanced spectral information of surficial geologic deposits compared to aerial photography. However, the 28.5-m spatial resolution of TM imagery is insufficient for large scale mapping and is more appropriate for medium scale mapping applications. High spectral resolution data, i.e., hyperspectral data, are available for geomorphic research (Lashlee and Rosenfeld 2001) but are generally neither available nor cost-effective for regional scale inventories.

The ability to map cultural resources remotely would also be advantageous, particularly for areas like YPG with a general lack of vegetative cover and preponderance of surficial archaeological features. With the possible exception of trail networks and certain high-contrast architectural structures, however, very high spatial and perhaps spectral resolution data are required to identify and delineate cultural resources at YPG. At present, these cultural features are best mapped using traditional field archaeological techniques.

The interdisciplinary approach used for this study is a scientifically defensible technique that not only met requirements of the National Historic Preservation Act, but also exceeded them. Reliable cultural resource information was generated and provided to YPG Conservation Managers and the Arizona State Historic Preservation Officer in a useful spatial context. Data derived were used to develop a new set of hypotheses that, if proven viable by future studies, may be used to develop predictive models of cultural resource distribution for improved management of arid military lands.

Acknowledgments

and consultant for the Quechan Indian Tribe. Approved for public release; distribution is unlimited.

References

Bern, C.M. (1995) Land condition—Trend analysis installation report, Yuma Proving Ground, Arizona, 1991–1994. Center for Ecological Management of Military Lands, Colorado State University, Fort Collins, Colorado.

Briuer, F.L., Lashlee, J.D., and Murphy, W.L. (1999) Survey and evaluation of cultural resources in the Phase I and Phase II areas of the proposed combat systems maneuver area, U.S. Army Yuma Proving Ground, Yuma County, Arizona. U.S. Army Waterways Experiment Station, Vicksburg, Mississippi.

Bull, W.B. (1991) *Geomorphic Response to Climatic Change.* New York: Oxford Press.

Dohrenwend, J.C. (1987) Basin and Range. In *Geomorphic Systems of North America* (W.L. Graf, Ed.). Geological Society of America Centennial Special Volume 2, pp. 303-342.

Lashlee, J.D., and Rosenfeld, C. (2000) Laboratory spectrometry of rock coatings: Implications for land management activities in the arid Southwest. In *Proceedings of the Natural Environments Testing Workshop, U.S. Army Test and Evaluation Command, Washington, D.C. 29–30 November 2000.*

Lashlee, J.D., Briuer, F.L., Murphy, W.L., and McDonald, E.V. (2000) Spatial distribution of cultural resources in the Combat Systems Maneuver Area. Technical Report No. 00-001. U.S. Army Yuma Proving Ground, Yuma, Arizona.

McFadden, L.D., Ritter, J.B., and Wells, S.G. (1989) Use of multiparameter relative-age methods for age estimations and correlation of alluvial fan surfaces on a desert piedmont, eastern Mojave Desert, California. *Quaternary Research*, 276–290.

Yuma Meteorological Team (1998) Climatological summary for the month of July. Yuma Proving Ground, Yuma, Arizona.

CHAPTER 3—LABORATORY SPECTROMETRY OF ROCK COATINGS: IMPLICATIONS FOR LAND MANAGEMENT ACTIVITIES IN THE ARID SOUTHWEST

J. David Lashlee, and Dr. Charles Rosenfeld

Abstract

Accurate knowledge of landforms, natural processes that form and modify them, and engineering characteristics of surface materials is fundamental knowledge for landscape managers. This is particularly true where military testing and training activities accelerate natural geomorphic processes or modify landforms that are associated with natural and cultural resources. Arid environments are often assumed by remote sensing specialists to be less complicated to analyze for earth science applications than humid, tropical, and arctic environments, as there is minimal vegetation to obscure surface features. While this may indeed be the case for many aerial photograph and image interpretation applications, the results of more quantitative multispectral and hyperspectral digital image processing techniques are complicated by a variety of environmental factors that are not always fully appreciated by the remote sensing community. Rock coatings, including rock varnish, weathering rinds, and carbonate deposits, have pronounced effects on hyperspectral reflectance in the reflected solar spectrum (400- to 2500-nm wavelengths). It is important for those who study arid environments remotely to understand geomorphic controls on spectral reflectance and the potential problems they may introduce to classification accuracy, landscape modeling, and target recognition algorithms.

Introduction

Yuma Proving Ground

Yuma Proving Ground (YPG) is a general-purpose testing facility within the U.S. Army Test and Evaluation Command. YPG's mission includes testing artillery, tank, and automotive systems, aircraft armament and air delivery systems, mines, and munitions. It also supports training operations and visiting military units. YPG is located adjacent to the confluence of the Colorado and Gila Rivers in the Sonoran Desert Section of the Basin and Range Physiographic Province (Fig. 9). Larger in size than the state of Rhode Island, YPG encompasses more than 3367 km^2 (1300 mi^2) of the hottest and driest area in the U.S. Extreme temperatures and low annual precipitation best characterize climatic conditions at YPG. The highest recorded temperature since 1954 was 51°C (124°F) in June 1990 (Yuma Meteorological Team 1998). Precipitation at YPG usually occurs in late summer months as brief, but intense, thun-

derstorms and in winter as less intense, longer duration rain showers. The area has been arid for the last 13,000 years with the present climatic regime and plant species established approximately 4000 years ago (Betancourt et al. 1990). Perennial plant cover averages from 1 to 5% across this region.
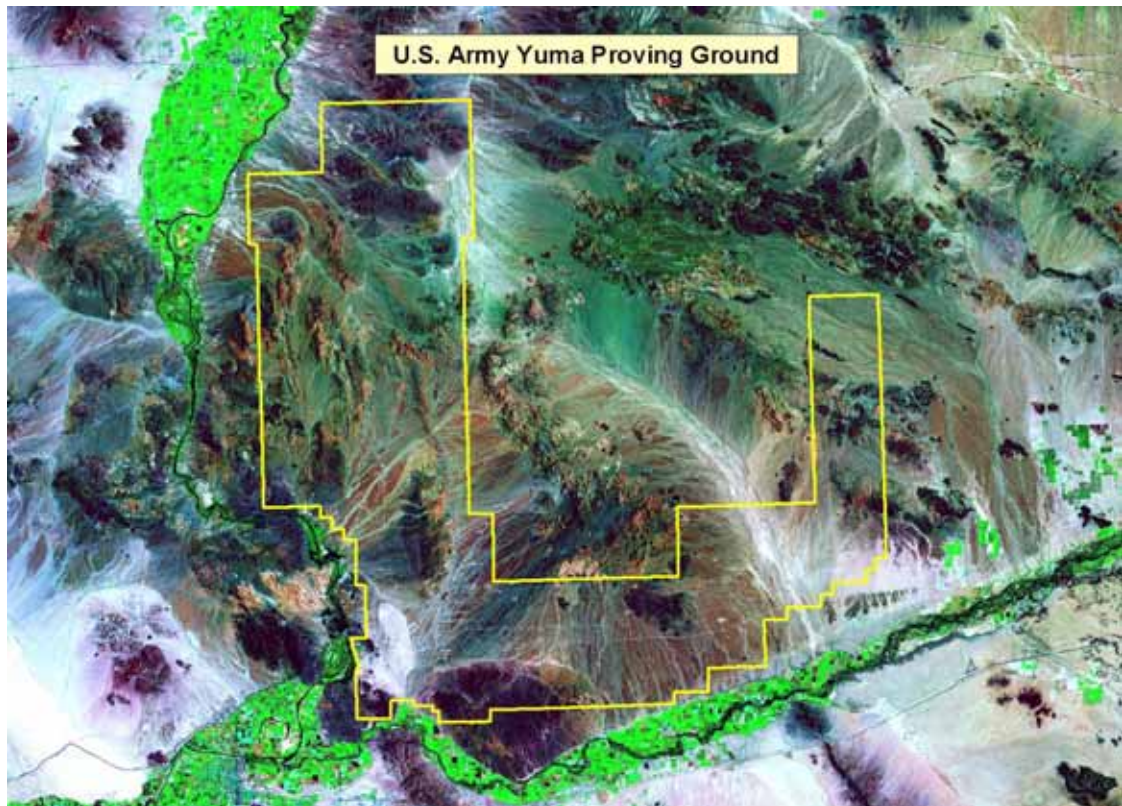
Figure 9. Landsat Thematic Mapper bands7, 4, 2, color composite image of the Yuma Proving Ground.

Geomorphology

YPG lies at the southern end of the Basin and Range physiographic province, a vast area extending as far north as Oregon, characterized by over 400 relatively regularly spaced, north–northwest trending subparallel mountain ranges, with intervening, broad and gently sloping alluviated basins formed by high angle extensional faulting (Dohrenwend 1987). The most notable features of the YPG landscape are the relief and bareness of these mountains and extensive desert pavements developed in broad intermontane alluvial basins. Other major landforms on the installation include alluvial fans and bajadas, which often transition to broad al-

luvial plains drained by ephemeral stream washes, and sand dunes. These Quaternary valley fill deposits make up almost 70% of the YPG landscape (Fig. 9).

Geologic maps are a primary source of information for a variety of applied earth science applications, including land use evaluation and planning, siting critical facilities, and the design and construction of infrastructure, such as utilities, transportation corridors, and surface-water impoundments (National Geologic Mapping Act of 1992, 2000). Unfortunately, geologic materials at YPG are relatively poorly understood. The only geologic maps covering the entire YPG area are State of Arizona maps at 1:1,000,000 (Reynolds 1988) and 1:500,000 (Wilson et al. 1969) map scales. Few large or medium scale maps needed for improved installation management have been published. This problem is compounded when those areas that are mapped at 1:24,000 scale have all alluvial deposits, an estimated 2331 km^2 (900 mi^2) of YPG, generalized into a single map category called "Quaternary Alluvium." It would be advantageous if these areas could be accurately mapped and quantitative information about them extracted using remote sensing techniques. Significant funding has been directed towards development of knowledge on remote sensing characteristics of geomorphic surfaces and their correlation with climatic change. However, limitations in the spectral and spatial resolutions of airborne and space-borne multispectral scanners have restricted the usefulness of these data for detailed, large-scale mapping (Lashlee et al. 1993). As a result, soils and geomorphic surfaces of large regions of semi-arid and arid land in North America remain unmapped and uncorrelated (Fischer 1991).

Geomorphic Mapping for Installation Management

Installation management methodologies at YPG based on a geomorphic framework provide managers with a scientific basis for making decisions related to planning, design, construction, implementation, operation, and maintenance of engineering projects, as well as a variety of resource management and compliance issues. These data are also critical for mitigating the effects of erosion and waste dispersal for environmental protection. An understanding of the landscape as an integrated process-response system, rather than a set of discrete and independent landforms, facilitates prediction of impacts of the geomorphic system on testing operations, and likewise, impacts of military testing and training on landscape stability.

Natural and cultural resource management at DoD installations is an increasingly important component of military planning and operations support. For example, Lashlee et al. (2000) mapped geomorphic surfaces in a 64-km^2 area of YPG using 1:24,000 scale stereoscopic color aerial photography and Landsat Thematic Mapper color composite images. Geomorphic surfaces were then compared to Native American cultural resources mapped in the field with differentially corrected Global Positioning System coordinates using Geographic Information System spatial overlays. A vast majority of cultural sites, including those eligible for the National Register of Historic Places, were located on Pleistocene age (10,000 to 2 million years old) geomorphic surfaces. Very few sites occur on Holocene age (< 10,000 year old) surfaces. Spatial patterns demonstrated between archaeology and geomorphology were supported by a chi square statistical test rejecting the hypothesis that sites are evenly distributed across the landscape as a function of the size of geomorphic surfaces. This research suggests that both geomorphic age of landforms and human behavior act in concert to explain the spatial distribution of cultural resources at YPG. Landform and geomorphic process maps such as these allow managers to develop predictive models concerning how resources are most likely distributed across landscape elements and how operations can be managed to minimize impacts and maintain landscapes for sustained mission use.

Geomorphic Controls on Hyperspectral Reflectance: Geomorphic Surfaces and Desert Pavements

The criteria most often used for field identification and mapping of alluvial geomorphic surfaces are: 1) degree of desert pavement development, 2) amount and character of rock varnish, 3) soil type, 4) topographic position, and 5) drainage characteristics (Bull 1991). With the exception of subsurface soil profile development, each of these mapping criteria can, with varying degrees of success, be assessed remotely in the reflected solar spectrum. It is also important to note that other recent studies that have demonstrated the application of thermal (Gillespie et al. 1984) and radar data (Kierein-Young 1995, Farr and Chadwick 1996) for mapping geomorphic surfaces.

Desert pavements are common landscape features in arid regions of the world and are known as hamada or reg in Arabic regions, sai in Asia, and gibber in Australia (Cooke et al. 1993). While formational geomorphic processes are generally understood, the magnitude and duration of processes responsible for formation of pavements vary with location. Desert pave-

ments consist of a surface layer of closely packed gravel, usually one particle thick, that over-lies a thin, gravel-poor vesicular A (Av) soil horizon. Pavements are important features in the Southwestern U.S., where they have been used in subdividing and correlating Quaternary al-luvial fans for studying neotectonics and Quaternary climatic change (Christenson and Purcell 1985, Bull 1991). Desert pavements are a fundamental part of the soil and landscape evolu-tion of volcanic landforms (Wells et al. 1985, McFadden et al. 1986) and are found on a vari-ety of landforms ranging from Holocene to Tertiary in age (Cooke and Warren 1973, Bull 1991). Well-developed pavements are common features of YPG and the Lower Colorado So-noran Desert.

Rock Coatings

Rock Varnish

One of the most striking features of arid landscapes is the nearly ubiquitous presence of rock varnish; a thin, dark, shiny film or coating, found on the surfaces of pebbles, boulders, and rock outcrops (Allen 1978). A typical rock varnish layer is less than half a millimeter deep on a rock's surface and is generally composed of about 60% clay minerals, 20 to 30% oxides of manganese and iron, and trace amounts of more than 30 other minor compounds (White 1990). The source of these materials is eolian (wind-blown) dust. The rarity of well-developed rock varnish on Holocene aged geomorphic surfaces suggests that the formation of continuous black varnish coatings requires at least 10,000 years and develops slowly, at a rate of a few micrometers per thousand years. Rock varnish developed on surfaces of pavement clasts has been used to provide calibrated age estimates of Quaternary landforms (Christenson and Purcell 1985, Bull 1991).

The upper surfaces of late Holocene and Pleistocene desert pavement clasts at YPG and else-where in the Sonoran Desert are covered with manganese-rich (Mn-rich) rock varnish (Fig. 10). The undersides of many clasts, particularly those on older, well-developed pavements, are covered with iron-rich (Fe-rich) rock varnish (Fig. 11). In Arizona's Lower Colorado So-noran Desert, Elvidge and Collet (1981) estimated that 75% of rock outcrops are coated or show significant traces of rock varnish, that alluvial and colluvial materials may or may not be varnished, and that the environmental conditions for varnish formation still likely exist. As is shown in Figure 12, the presence of well-developed Mn-rich rock varnish completely obscures

host rock lithology in the visible wavelengths from 400 to 700 nm. Laboratory spectrometry was performed for this study to quantify the spectral effects of rock coatings in the reflected solar spectrum (400 to 2500 nm wavelengths).

Figure 10. Manganese-rich (Mn-rich) rock varnish on desert pavement clast sample.
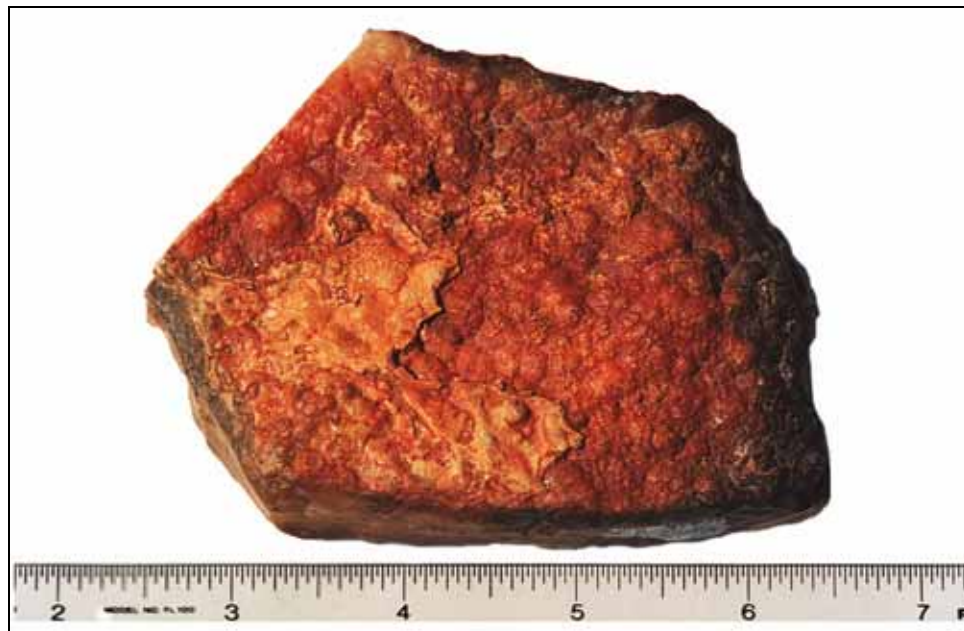
Figure 11. Iron-rich (Fe-rich) rock varnish on desert pavement clast sample.

Figure 12. Host rock lithology of desert pavement clast sample.

Spectral Effects of Rock Varnish

Laboratory spectrometry reported herein was performed with a FieldSpec FR Spectroradi-ometer (Analytical Spectral Devices 1995) and a tripod mounted, 14.5-V, 50-W Lowel Pro-lamp light source. Data were acquired by positioning the spectrometer optical probe 3 to 5 mm above each sample and collecting 10 different measurements across the surface of each clast. A spectralon panel was used as an ideal diffuse reference surface to calibrate clast measurements from raw digital numbers to spectral reflectance. Spectra were then compiled in a spectral library and individual measurements of each clast were averaged using Environ-ment for Visualizing Images (ENVI) software (Research Systems Incorporated 1999).

Figure 13 shows average hyperspectral reflectance signatures of the desert pavement clast shown in Figures 10 (sample top), 11 (sample bottom), and 12 (host rock interior). Three general observations are shown in these data. First, Mn and Fe-rich rock varnish have very different spectral reflectance characteristics. Second, Mn-rich varnish has a much more per-vasive effect on host rock reflectance than does Fe-rich varnish. Finally, the presence of either type rock varnish has serious implications for remote sensing studies in arid lands, particularly

geologic mapping that attempts to delineate the spatial distributions of rock type and condition, and geomorphic mapping, concerned primarily with landform delineation and identification of geomorphic processes.
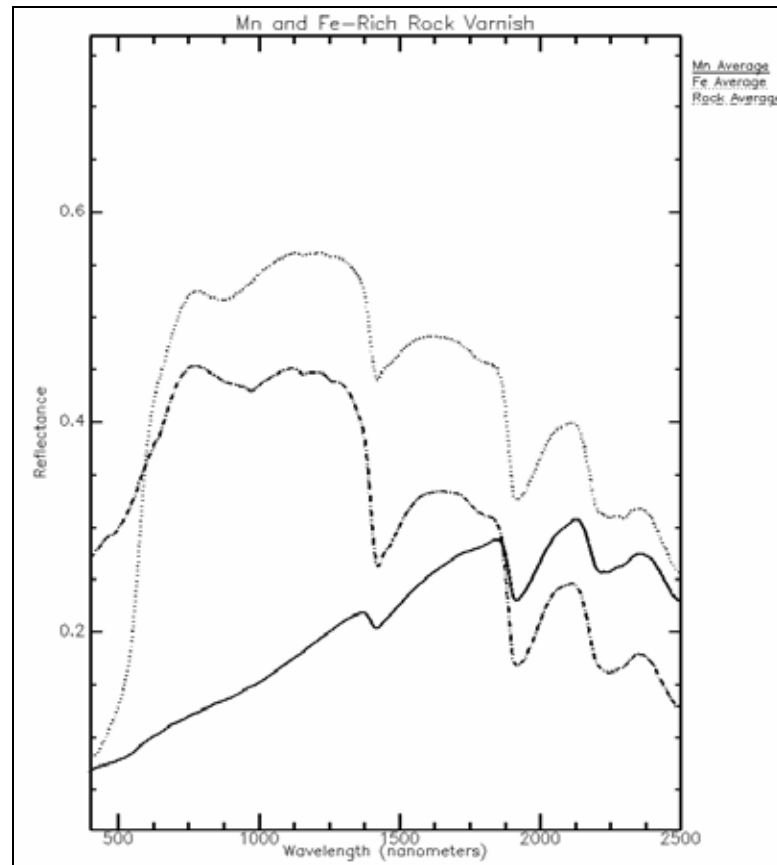
Figure 13. Hyperspectral signatures of Mn and Fe-rich rock varnish and host rock lithology.

The major effect of Fe-rich varnish is to increase the overall brightness of the clast signature in the 500- to 2500-nm wavelengths without significantly changing the shape of the original host rock signature. This suggests that clast lithology could be mapped using hyperspectral remote sensing techniques in areas where Fe-rich varnish dominates the landscape. Alternatively, spectral attenuation by the well-developed Mn-rich varnish typical of the Sonoran Desert is twofold. First, Mn varnish both decreases spectral reflectance and significantly modifies signature shape in the visible and infrared wavelengths from 400 to 1800 nm. Because incident radiation is completely absorbed by the Mn varnish, spectral information in the 400- to 1800-nm wavelengths is limited to the varnish. However, spectral information the mid-

infrared 2000- to 2500-nm wavelengths is brighter than, but similar to, host rock reflectance. Fortunately, this wavelength region is where many diagnostic spectral absorption features for geologic materials are located, which also shows potential for lithologic discrimination. For example, although both the shape and depth are modified, neither Mn nor Fe-rich rock varnish significantly obstructed the host rock absorption feature centered on 2250 nm. Spectral absorption features exhibited by all three signatures at 1.4 and 1.9 nm are attributable to water absorption bands.

Weathering Rinds

Weathering rinds are uniformly thick zones of chemical alteration that occur around the periphery of clasts when they are exposed to environmental conditions at or near the Earth's surface (Birkeland 1984). Rinds are common features in arid and semi-arid regions of the U.S., where they are typically several millimeters thick. However, weathering rinds are not limited to arid or even terrestrial environments, having also been observed on Mid-Ocean Ridge basalts (Seifert and Brunotte 1995) and basaltic flows on surface of Mars (Burns and Fischer 1993). Rates of chemical weathering vary with mineral composition and grain size of clasts as well as climatic regimes. For example, Birkeland (1984) notes that in the time it takes to completely weather granitic boulders to grus in a soil, dense volcanic rocks may show only thin weathering rinds. Data from an extensive study by Coleman and Pierce (1981) in which over 7000 weathering rinds were sampled at 150 sites in the western U.S. suggest that at least 4000 years are needed to form incipient weathering rinds.

Fine-grained volcanic rocks like basalts often exhibit distinct rinds because the sharp coloration differences produce a clear boundary (Fig. 14) compared to coarser grained volcanics and sedimentary rocks. A typical effect of chemical weathering on basalt is for feldspar and mica to be converted to clay and magnetite. Basalt weathering rind thicknesses increase at rates that are functions of the kinetics of chemical reactions at the inner edge of the advancing rind (Bull 1991). As such, the green-colored rind records an inward progression of chemical weathering, whose thickness corresponds to the duration of exposure of the sample. As is the case in Figure 14, weathering rinds may exhibit variable thicknesses because rinds are more friable than the underlying host rock and may separate from the clast surface because of spalling, exfoliation, biologic activity, or other physical weathering processes. Generally,

however, the arid, hyperthermic Sonoran climate and ubiquitous occurrence of rock varnish favor oxidizing conditions that promote rind growth as well as conditions for minimal rates of erosion of weathering rinds (Bull 1991).

Figure 14. Basalt cobble (black) and external weathering rind (yellow-green).

Spectral Effects of Weathering Rinds

Figure 15 shows spectral reflectance of the basalt sample shown in Figure 14. Basalt has a dark, flat, and featureless spectral signature. The weathering rind is both brighter, particularly in the green and red portions of the visible spectrum responsible for its light greenish-yellow color, and also exhibits a strong, wide absorption feature centered at 1000 nm, as well as the water absorption features at 1400 and 1900 nm. Differences in the reflectance of fresh and weathered surfaces are highly significant in the reflected solar spectrum. Only the outermost layer of rocks, a depth between 5000 and 10,000 nm, actually contributes to spectral reflectance (Amos and Greenbaum 1989). Because weathering rinds in the Sonoran Desert can form to a depth several millimeters, spectral signatures are derived completely from the weathered clast surface. In addition, because the products of chemical weathering are often chemically different from the original rock surface, classification and mapping errors can result owing to misleading interpretations of mineral constituent composition.
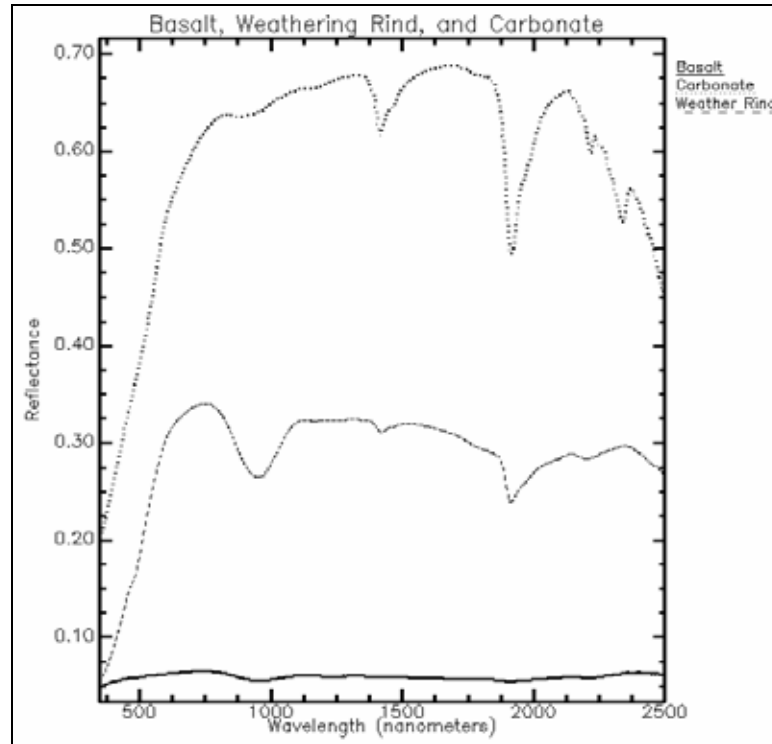
Figure 15.   Hyperspectral signatures of basalt rock sample,
weathering rind, and carbonate deposit.

Carbonate Deposits

Both Waters (1985) and Lashlee et al. (2000) discussed the geomorphology of different parts
of YPG and summarized field observations of calcic horizons, indurated layers formed as cal-
cium carbonate migrates in solution downward from A and B soil horizons and precipitates at
depth. Stage II calcic horizon development is characterized by continuous coatings on subsur-
face pebbles and some inter-pebble filling. Figure 16 shows a thick carbonate deposit overly-
ing the weathering rind of the basalt sample shown previously in Figure 14. Continued car-
bonate leaching and deposition over time leads to Stage III, characterized by greater inter-
pebble filling and plugging of soil pore space.

Figure 16.   Carbonate deposit (white) and weathering rind (yellow-green) on basalt clast sample from Figure 14.

Because carbonate deposition is a subsurface pedogenic process, coated rocks buried for some time in soil must be exposed at the surface to be a factor in remotely sensed data. The presence of desert pavement clasts containing significant amounts of carbonate indicate degraded surfaces that have been substantially reworked by surface erosion in the past, perhaps during less arid climatic conditions. Such geomorphic surfaces are not uncommon at YPG. It is also not unusual to find relatively young desert pavements, with immature soil profiles, that have formed on top of older, formerly degraded, then restabilized geomorphic surfaces, that have mature profiles at depth (Lashlee et al. 2000).

Carbonate can also form spatially extensive deposits of considerable thickness that, over time, may be exposed at the surface and visible in remotely sensed imagery. Figure 17 shows Stage IV carbonate deposits, the highest degree of development, characterized by an impermeable calcic horizon sometimes capped by pure laminate layers of calcium carbonate. Waters, citing Bull (1991), states that Stage IV calcic horizons, like that shown in Figure 17, might require

50,000 years to develop. Therefore, Pleistocene soils typically have a greater accumulated volume of calcic horizons at greater depth and than do Holocene soils.

Figure 17. Calcium carbonate cemented Gila River fluvial gravels at Yuma Proving Ground.

Spectral Reflectance of Carbonate Deposits

Figure 15 shows the average of spectra collected from the carbonate, weathering rind, and fresh basalt surface shown in Figures 14 and 16. Three observations can also be made from these data. First, carbonate reflectance is significantly brighter, not only in the visible wavelengths sensed by the human visual system (400- to 700-nm wavelengths), but across the entire reflected solar spectrum. Second, the carbonate signature lacks the strong absorption feature centered at 1000 nm exhibited by the weathering rind data. Finally, the carbonate data contain diagnostic absorption features at 2225 and 2350 nm that are absent from both the basalt and weathering rind spectra (Fig. 18). It is clear from these data that materials present in and on the basalt clast shown in Figures 14 and 16 are chemically and spectrally very different substances.
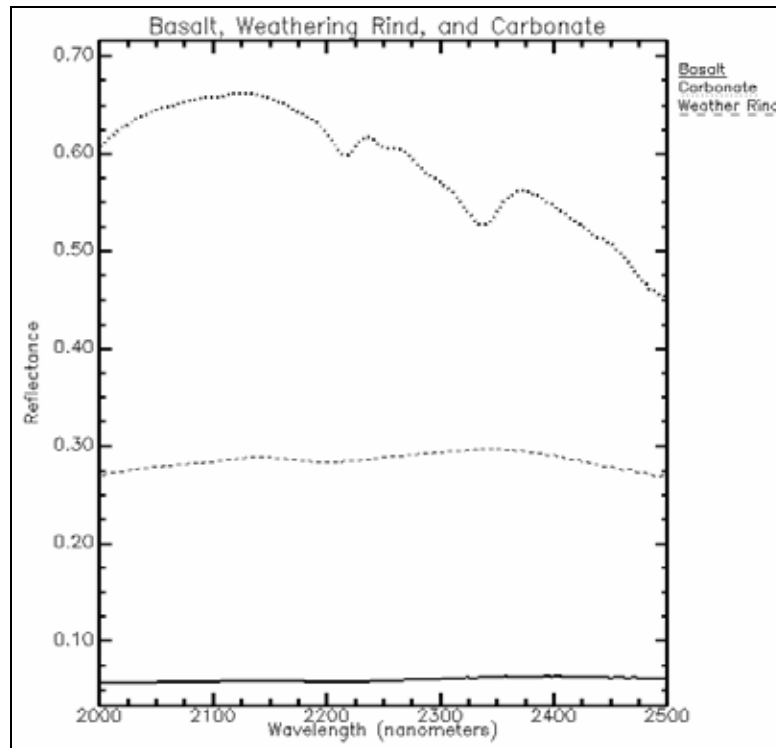
Figure 18. Spectral absorption features of carbonate deposit in
the 2000- to 2500-nm wavelengths.

Integrated Desert Pavement Spectral Reflectance

Mapping Quaternary geomorphic surfaces in arid and semi-arid environments requires an un-
derstanding of landforms, geomorphic processes, and the controls they exert on spectral re-
flectance. Geomorphic processes that dominate reflectance in the Sonoran Desert are desert
pavement and rock varnish formation, eolian silt deposition, and fluvial dissection. As re-
corded at spatial resolutions currently available, desert pavements are spectral mixtures in
which each pixel contains an integrated average reflectance of the surface materials present
within its bounds. The presence, chemistry, and condition of rock coatings are primary con-
siderations, particularly when applying new and emerging technologies like hyperspectral data
analysis. Data presented in this chapter clearly show that a single pavement clast sample can
have more than one type of rock coating, each with significantly different hyperspectral sig-
natures. The following discussion summarizes some important considerations related to spec-
tral reflectance of desert terrain in order of significance—rock varnish, lithology, soils, and
vegetation.

Rock Varnish

The degree to which lithologic information is obscured by rock coatings depends on the type of coating formed, its chemistry, morphology, and condition, which is, in turn, controlled by complex environmental factors (White 1990). In the Lower Colorado Sonoran Desert, well-developed Mn-rich rock varnish generally precludes lithologic mapping in the 400- to 1800-nm wavelength regions. Only the 2000- to 2500-nm wavelengths are available for lithologic discrimination. Fe-rich coatings clearly have a less significant effect on host rock spectral reflectance characteristics than do Mn-rich varnishes. Pleistocene age desert pavements in the Sonoran Desert typically are Mn-rich on clast tops and Fe-rich on clast bottoms. Most re-searchers agree that this type varnish significantly decreases overall spectral brightness and that shorter wavelengths are absorbed by rock varnish coatings to a greater extent than longer wavelengths. However, there is disagreement in the literature on whether heavily varnished and sediment-coated surfaces retain reflectance information of underlying rock types. Spatz et al. (1987) and Rivard et al. (1992) found that long wavelength radiation penetrated varnish coatings resulting in lithologic spectral dominance, so bedrock information could be derived. Elvidge and Collet (1981) and White (1990) found that Mn-rich varnishes precluded lithologic recognition by obscuring underlying host rocks.

Rock varnish often develops discontinuously on pavement clasts (Fig. 19), first filling in low spots in the rock surface. As a result, pits and groves are often more heavily varnished than smoother areas. Varnish may also adhere differently to the various minerals on a single clast. It is not uncommon for banded rocks such as gneiss to be varnished such that lithology is ob-scured in the visible wavelengths on all but the banded minerals, which show through. Differ-ent rates of erosion on heterogeneous desert pavement gravels also contribute to spectral variation. For example, granular rocks, like sandstone and granite, may disintegrate before a varnish coat can form. Carbonate-based rocks like limestone may be too soluble, even in the desert, to form varnish.

Figure 19. Desert pavement surface with variable clast size and shape, types, and amounts of rock varnish, heterogeneous clast lithology, and soil matrix.

Clast Lithology

Desert pavement clast lithology can be homogeneous or heterogeneous and it is common for pavements in proximity to have very different lithologic and morphologic characteristics. For example, the authors have studied in detail three pavements with different stages of development and formed on different landforms in the Yuma Wash watershed at YPG. The youngest is an alluvial fan developed from mudflow and other alluvial deposits from a single canyon whose surface was later covered by volcanic rhyolite deposited during a Holocene igneous extrusion event. This surface has homogeneous lithology, very consistent brownish-red rock varnish development, and exhibits a strong bar and swale topography, typical of young desert pavements. The middle age pavement is a truncated pediment whose clasts are composed of a heterogeneous mixture of banded gneisses, foliated schists, quartzites, and other metamorphic rock, each exhibiting different rock varnish characteristics. Directly across the channel is a Pleistocene stream terrace composed of alluvial fanglomerate, a mixture of potentially every rock type present in drainage basin. The clast shown in Figures 10 through 12 was collected on this surface and illustrates the well-developed Mn- and Fe-rich rock varnish present. Soil geomorphology suggests the ages of these pavements range from 8 to 12 ka, 12 to 70 ka, and 70 to 200 ka, respectively.

In addition to lithologic differences evident in the 2000- to 2500-nm wavelengths, differences in rock type and relative age also result in surface roughness variations (gravel and cobble size and shape), which may be observable in optical remote sensing data as variable amounts of shadow. One should reasonably expect more shadow on surfaces with bar and swale topography and terrain where boulder and cobble fields exist as compared to the older, flatter well-developed desert pavement surfaces. As shadow varies with sun angle, the amount of shadow in the reflected solar spectrum changes both seasonally and temporally throughout the day.

Soils

Laboratory and field data collected for this study, including soil texture classification, chemical composition analysis, and extensive field spectrometry data, support the accretionary desert pavement formation model (Wells et al. 1985) assumes that the underlying soil matrix is composed of eolian dust accumulating above a vesicular Av soil horizon. Soil samples from Av horizons at different locations at YPG have similar texture and mineralogy and, therefore, similar hyperspectral signatures, regardless of the geologic age, or available parent material of individual surfaces. These data not only suggest the dominant pedogenic process for pavement development is dust accumulation, but also that dust at YPG may originate from a single source area in the region. From a remote sensing perspective, this process has a normalizing effect on spectral contributions of soils, as it is likely the same for different aged pavements. This allows geomorphologists using remote sensing to concentrate on the more problematic interpretations of integrated rock varnish, clast lithology, and surface roughness. It is, however, common to have variable amounts of soil matrix exposed in different aged pavements as well as at different locations on the same surface. For example, the edges of some pavements at YPG are often lighter colored because runoff in the form of concentrated sheetflow over-turns and disperses pavement clasts to a greater extent than at the center of the surfaces. It is not the composition of the soil matrix that changes, but rather the amount of soil matrix exposed that is recorded in remotely sensed data.

Vegetation

Vegetation on desert pavement surfaces is generally sparse and typically restricted to washes that drain them. A study of pavement surfaces of Yuma, Arizona (Musick 1975) found that underlying soils had a higher silt, clay, and salinity content than non-pavement soils in the area. As a result, pavements have slower infiltration rates, with little precipitation entering the soils compared to non-pavement soils, and precipitation that does enter the soil is held near the surface and evaporates quickly. Temperature extremes may also contribute to bareness of these surfaces. While the average maximum daily temperature for July is 41°C (106°F), Cochran (1992) found that temperatures within 25 mm (1 in.) of the black, desert pavement gravels in Yuma often exceed 160°F during July and August. The authors also measured pavement soil temperatures of 150°F in July 1998 at YPG. The restriction of vegetation to drainage networks of desert pavements is a valuable indicator of drainage pattern and density, both in the field and in remotely sensed data.

Summary

Understanding natural environments and geomorphic processes at the Nation's test centers is essential to installation management and critical to mapping, modeling, and simulation efforts. Desert pavements at YPG and elsewhere in the Lower Colorado Sonoran Desert are dominated by Mn-rich rock varnish and are spectrally featureless in that they contain no diagnostic spectral absorption features. Relative degrees of varnish darkening, or patination, have long been used as a relative age indicator in the fields of archaeology and geomorphology. A research question currently being addressed at YPG is whether hyperspectral remote sensing is an effective tool for determining both relative geologic age (500- to 1800-nm wavelengths) and dominant rock lithology (2000- to 2500-nm wavelengths) for mapping Quaternary geomorphic surfaces in the Lower Colorado Sonoran Desert. Spectral data presented in this chapter demonstrate that, even under controlled laboratory conditions, remote sensing of terrains characterized by the presence of a variety of rock coatings may be more problematic than is generally acknowledged by the remote sensing community.

Acknowledgements

References

Allen, C.C. (1978) Rock varnish of the Sonoran Desert—Optical and electron probe microanalysis. *Journal of Geology*, **86**: 743–752.

Amos, B.J., and Greenbaum, D. (1989) Alteration detection using TM imagery: The effect of supergene weathering in an arid climate. *International Journal of Remote Sensing*, 10: 515–527.

Analytical Spectral Devices, Inc. (1995) *Environment For Visualization of Images Technical Guide*. Boulder, Colorado, pp. 24–28.

Betancourt, J.L., Van Devender, T.R., and Martin, P.S. (1990) *Packrat Middens, The Last 40,000 Years of Biotic Change*. Tucson, Arizona: University of Arizona Press.

Birkeland, P.W. (1984) *Soils and Geomorphology*. New York: Oxford Press.

Bull, W.B. (1991) *Geomorphic Response to Climatic Change*. New York: Oxford Press/

Burns, R.G., and Fisher, D.S. (1993) Rates of oxidation weathering on the surface of Mars. *Journal of Geophysical Research Planets,* **98**(E2): 3365–3372.

Christenson, G.E., and Purcell, C. (1985) Correlation and age of Quaternary-fan sequences, Basin and Range Province, Southwestern United States. In *Soils and Quaternary Geology of the Southwestern United States* (Weide, D.L., Ed.). Geological Society of America, Special Paper 203, pp. 115–122.

Cochran, C.C. (1992) Soil survey of the U. S. Army Yuma Proving Ground, Arizona—parts of LaPaz and Yuma Counties. USDA, Soil Conservation Service.

Coleman, S.M., and Pierce, K.L. (1981) Weathering rinds on andesitic and basaltic stones as a Quaternary age indicator, western United States. U.S. Geological Survey Professional Paper 1210.

Cooke, R.U., Warren, A., and Goudie, A. (1993) *Desert Geomorphology*. London: UCL Press.

Cooke, R.U., and Warren, A. (1973) *Geomorphology in Deserts.* London: Batsford, Ltd.

Dohrenwend, J.C. (1987) Basin and Range. In *Geomorphic Systems of North America* (W.L. Graf, Ed.)*,* Geological Society of America, Centennial Special Volume 2, pp. 303-342.

Elvidge, C.D., and Collet, C.J. (1981) Rock varnish in Arizona, distribution, and spectral characteristics. In *Technical Papers of the American Society of Photogrammetry, ASP-ACSM Fall Technical Meeting, San Francisco*, pp. 215–222.

Farr, T.G., and Chadwick, O.A. (1996) Geomorphic processes and remote sensing signatures of alluvial fans in the Kun Mountains, China. *Journal of Geophysical Research,* **101**(E10): 23,091–23,100.

Fischer, A.F. (1991) Mapping and correlating desert soils and surfaces with imaging spectrometry. In *Proceedings of the Third Airborne Visible/Infrared Imaging Spectrometer (AVIRIS) Workshop.* NASA/JPL Publication 91-28, pp. 23.

Gillespie, A.R., Kahle, A.B., and Palluconi, F.D. (1984) Mapping alluvial fans in Death Valley, California, using multi-channel thermal infrared images. *Geophysical Research Letters,* **11**(11): 1153–1156.

Kierein-Young, K. (1995) Integration of quantitative geophysical information from optical and RADAR remotely sensed data to characterize mineralogy and morphology of surfaces. PhD Dissertation, University of Colorado*,* Boulder.

Lashlee, J.D., Briuer, F.L., Murphy, W.L., and McDonald, E.V. (2000) Spatial distribution of cultural resources in the Combat Systems Maneuver Area. Technical Report No. 00-001, U.S. Army Yuma Proving Ground, Yuma, Arizona.

Lashlee, J.D., McKinley, G.B., and Bishop, M.J. (1993) Quantitative land cover classification accuracy assessments derived from single pass and ISODATA unsupervised clustering algorithms. Technical Report GL-93-21*,* U.S. Army Corps of Engineers, Waterways Experiment Station, Geotechnical Laboratory.

McFadden, L.D., Wells, S.G., and Dohrenwend, J.C. (1986) Influence of Quaternary climatic changes on processes of soil development on desert loess deposits of the Cima volcanic field, California. *Catena,* **13**: 361–389.

Musick, H.B. (1975) Barrenness of desert pavement in Yuma County, Arizona. *Arizona Academy of Science*, **10**: 135.

USGS (1992). *National Geologic Mapping Act of 1992*. United States Geological Survey web site. http://ncgmp.usgs.gov/ngmact.html

Research Systems Incorporated (1999). *ENVI User's Guide Version 3.2.* Boulder, Colorado.

Reynolds, S.J. (1988) Geologic map of Arizona. Arizona Geological Survey Map 26.

Rivard, B., Arvidson, R.E., Duncan, M.S., and Kaliouby, B.E. (1992) Varnish, sediment, and rock controls on spectral reflectance of outcrops in arid environments. *Geology,* **20**: 295–298.

Seifert, K., and Brunotte, D. (1995) Geochemistry of weathered mid-ocean ridge basalt and diabase clasts from hole 899B in the Iberia Abyssal Plain. ODP SR-149 Abstracts. http://www-odp.tamu.edu/publications/srv/abstr149/149-29.html.

Spatz, D.M., Taranik, J.V., and Hsu, I.C. (1987) Rock varnish on volcanic rocks of the basin and range province—Composition, morphology, distribution, origin, and influence on Landsat imagery. In *Proceedings of the Twenty-First Symposium on Remote Sensing of the Environment,* Vol. 2*,* pp. 843–852.

Waters, M.R. (1985) Geomorphic investigations on the Yuma Proving Ground, Arizona. Unpublished Report to Yuma Proving Ground.

Wells, S.G., Dohrenwend, J.C., McFadden, L.D., Turrin, B.D., and Mahrer, K. (1985) Late Cenozoic landscape evolution on lava flow surfaces of the Cima volcanic field, Mojave Desert, California. *Geologic Society of America Bulletin,* **96**: 1518–1529.

White, K. (1990) *Spectral Reflectance Characteristics of Rock Varnish in Arid Areas,* Special Paper 46. University of Oxford Press, pp. 1–31.

Wilson, E.D., Moore, R.T., and Cooper, J.R. (1969) Geologic Map of Arizona, 1:500,000 Scale. Arizona Bureau of Mines and United States Geological Survey. USGS Federal Center, Denver, Colorado.

Yuma Meteorological Team (1998) Climatological Summary for the Month of July. Yuma Proving Ground, Yuma*,* Arizona.

CHAPTER 4—GEOMORPHIC CONTROLS ON HYPERSPECTRAL REFLECTANCE OF DESERT PAVEMENTS: IMPLICATIONS FOR MAPPING AND MODELING ARID ENVIRONMENTS

J. David Lashlee, Dr. Eric McDonald, Dr. Charles Rosenfeld, and Dr. Jon Kimerling

Abstract

Hyperspectral reflectance of geomorphic surfaces is the result of complex interactions be-
tween electromagnetic energy and surficial geologic materials in the 400- to 2500-nm wave-
length regions. We analyzed laboratory and field spectra of three landforms with geomorphic
surfaces of different geologic age and composition located in the Lower Colorado Sonoran
Desert at the U.S. Army Yuma Proving Ground (YPG), Arizona. Spectral reflectance and ab-
sorption features were then compared to petrographic analyses of desert pavement clasts and
soil structure and geochemical data for each site. Results show quantitatively that a variety of
rock coatings, including rock varnish, weathering rinds, hydrothermal stains, and carbonate
deposits, dramatically alter lithologic reflectance of Pleistocene age surfaces. In contrast, the
eolian-derived soil matrix of each surface shares similar structure and chemistry, and therefore
hyperspectral reflectance. From a remote sensing perspective, this tends to have a normalizing
effect on spectral reflectance at a regional landscape scale. We found that desert pavement
surfaces at YPG can be accurately mapped using hyperspectral data, but are spectrally fea-
tureless in that they exhibit no diagnostic absorption features related to rock varnish or pave-
ment clast lithology. As the Army's Test and Evaluation desert analog for the world, results
obtained at YPG have implications for geomorphic mapping, change analysis and target de-
tection, and modeling and simulation applications for many other arid regions.
Keywords: Chameleon, Geomorphic Mapping, Hyperspectral, Remote Sensing

Introduction

Yuma Proving Ground

The U.S. Army Test and Evaluation Command (ATEC) is the premiere Test and Evaluation
(T&E) organization in the Department of Defense (DoD). Its mission is to plan, conduct, and
integrate developmental and operational tests of military equipment, as well as provide inde-
pendent evaluations of test results to decision makers, to ensure war-fighters are equipped
with effective weaponry and soldier systems (Armbruster 2003). The Developmental Test
Command (DTC), one of three subordinate Commands within ATEC, conducts rigorous per-
formance tests on weapons systems and materiel under controlled conditions on highly in-
strumented ranges and test courses. Products of Developmental Testing include impartial

technical data on system design, feasibility, performance, safety, and risks during system development (Williams 2002). Yuma Proving Ground (YPG) is a general-purpose test facility within DTC that assesses nearly every weapon in the ground combat arsenal, including artillery, tank and automotive systems, soldier systems, aircraft armament and air delivery systems, and smart munitions. It also supports training operations and visiting military units, like the Military Free Fall School and Special Forces groups. Located at the confluence of the Colorado and Gila Rivers, YPG encompasses more than 3367 km^2 (1300 mi^2) of the hottest and driest area in the United States—the Lower Colorado Sonoran Desert section of the Basin and Range Physiographic Province (Fig. 20).
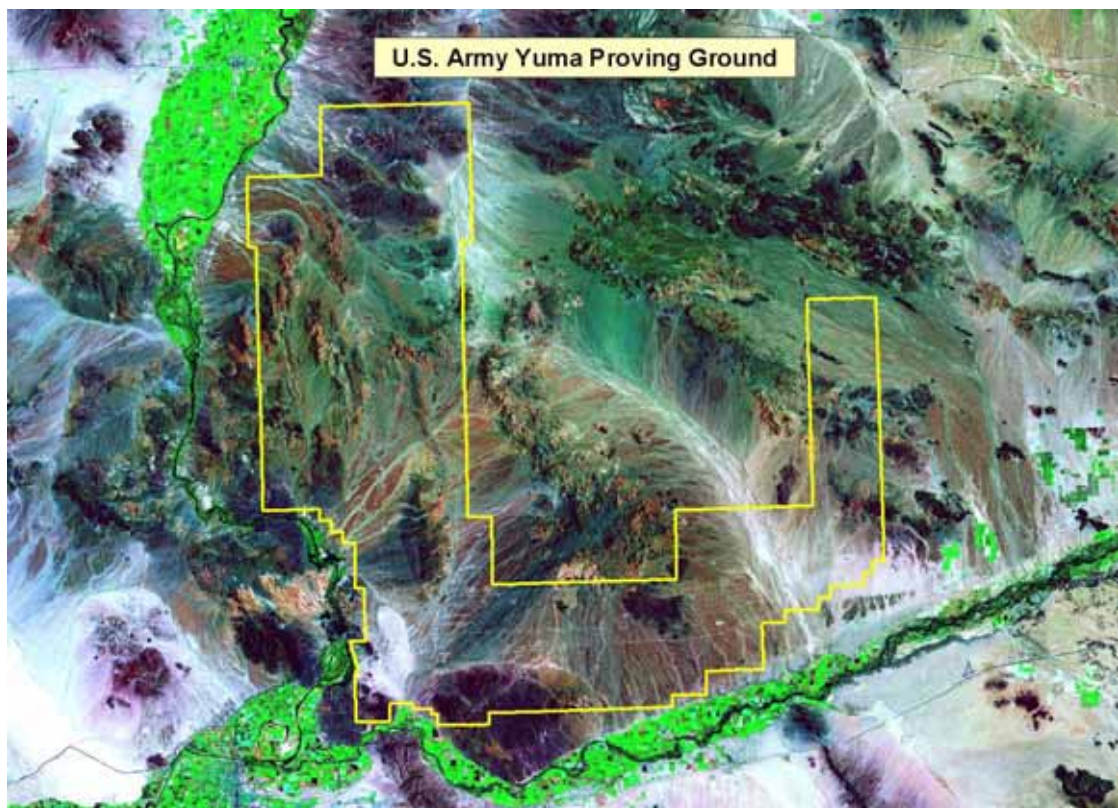
Figure 20. Landsat Thematic Mapper 7, 4, 2, color composite image of the Yuma Proving Ground.

Three of the four natural environments recognized as critical for testing military equipment are managed by YPG: 1) Yuma Test Center (YTC) performs arid land testing at YPG; 2) the Cold Regions Test Center (CRTC) plans and conducts winter, mountain, and near polar environment testing at Fort Greely, Alaska; and 3) the Tropic Regions Test Center (TRTC)

operates facilities in Hawaii and the Republic of Panama to accomplish its test mission. With 1700 military and civilian employees performing one million man-hours in climatic extremes, YPG is the Army's Natural Environments Tester.

Purpose and Scope

There are many reasons to collect spectral measurements in the field. For example, field spectra of ground targets that are homogeneous at the scale of the imaging sensor and collected using ambient solar illumination can be used to convert radiance images to reflectance (Conel et al. 1987a,b). Field spectra of target materials are also collected to allow for more precise image analysis and interpretation (Goetz and Srivastava 1985). Field spectroscopy is also a powerful tool for remote sensing feasibility studies to understand if and how a material or process can best be detected remotely. Indeed, YPG is interested in each of these and other applications. In general terms, the purpose of our research is to quantify spectral reflectance and absorption features of geomorphic surfaces at YPG using the three different scales of data obtained from laboratory, field, and imaging spectrometry and to apply this knowledge to installation management, landscape mapping, target detection and recognition applications, and Modeling and Simulation (M&S) for Army transformation efforts, including the Virtual Proving Ground (VPG) and Future Combat Systems (FCS) Programs.

This chapter discusses geomorphic controls on hyperspectral reflectance of desert pavements. Emphasis is placed on reflectance of pavement clast lithology, spectral attenuation by rock varnish, and the influence of the soil matrix that surrounds the clasts. Some consideration is also given to the effects of surface texture and spectral contributions of vegetation. Our analysis is limited in scope to the study of laboratory and field spectra and the correlation of these data to material composition and structure data collected from three geomorphic surfaces located within the Yuma Wash Drainage Basin at YPG. Our results address: 1) continuous hyperspectral field measurements in the 400- to 2500-nm wavelengths, 2) spectral reflectance of naturally occurring surficial geological materials, and 3) their relationship to temporal landscape modeling and simulation (M&S) applications.

Techniques

Spectral Data Collection. For each geomorphic surface, we identified transect locations on aerial photographs, then surveyed them in the field with real-time differentially corrected GPS coordinates. Small areas of desert pavement were cleared of clasts, exposing the underlying soil matrix, at regularly spaced stations located along each transect. The actual number of stations varied for each surface based on landform length. Field spectrometry was performed using a portable FieldSpecFR[1] spectroradiometer (Analytical Spectral Devices 1995), which collects 1512 contiguous spectral measurements in the solar reflective wavelengths from 350 to 2500 nm. Spectral resolutions are 3 and 10 nm for the 350- to 1000-nm and 1000- to 2500-nm wavelength regions, respectively. A 1.4-m fiber optic cable was used to transmit light reflected from targets to the instruments' three internal detectors, which were calibrated to reflectance using a portable spectralon white reference panel at each transect station. Spectra of undisturbed desert pavement and cleared areas of exposed surface soil were collected at each station, such that each spectrum was an average of 25 different measurements acquired in about 200 ms.

Laboratory spectrometry was also performed on individual desert pavement clast samples under controlled illumination conditions, again using a FieldSpecFR. The diffuse light source used was a Lowel Pro-lamp, a 14.5-V, 50-W, tripod mounted indoor laboratory light with its probe was positioned 3 to 5 mm above the sample surface. We obtained 15 spectra from each clast sample, including five measurements from varnished top, five from varnished bottom, and five from the unvarnished cut rock surface. These data gave quantitative measurements of the effects of Mn (top) and Fe-rich (bottom) rock varnish on spectral reflectance of host rock lithology for comparison to both field and imaging spectrometer data. Both laboratory and field spectra were compiled into spectral libraries and analyzed using Environment For Visualization of Images (ENVI) software (Analytical Spectral Devices 1995).

Geotechnical Data Collection. Geomorphic surface characteristics were also recorded in the field, including desert pavement development (clast size, shape, arrangement, and texture),

---

[1] YPG has since upgraded its instrumentation to the FieldSpec Pro spectroradiometer.

rock varnish type and condition, and relative surface topographic position. Samples of pavement clasts and the Av horizon soil were collected at each station for laboratory analyses. Soil tests included standard sieve and hydrometer analysis to determine grain size distributions (gravel, sand, silt, and clay) and Unified Soil Classification System category, as well as computer-assisted x-ray powder diffraction (XRD) to determine mineral composition. Additionally, a soil pit was excavated at each site and soil profile characteristics documented.

Desert pavement clasts were also subject to laboratory tests to identify physical and chemical properties of clasts and associated rock varnish. Petrographic analyses performed included scanning electron microscopy (SEM), energy-dispersive x-ray fluorescence (XRF), micro-image analysis, and optical microscopy techniques. These data provided information on rock type, minerology and bulk chemistry; thickness and chemical composition of rock varnish coatings on individual clasts; and elemental maps showing distinctions between composition of host rock and varnish coatings.

Background

Mapping Geomorphic Surfaces

The criteria most often used for identification and mapping of alluvial geomorphic surfaces in deserts are: 1) degree of desert pavement development, 2) amount and character of rock varnish, 3) soil type, 4) topographic position, and 5) drainage characteristics (Bull 1991). With the exception of subsurface soil profile development, each of these mapping criteria can, with varying degrees of success, be assessed remotely. Our current research focus is high spectral resolution measurements in the reflected solar spectrum; however, other studies have demonstrated the application of thermal (Gillespie et al. 1984) and radar data (Kierein-Young 1995, Farr and Chadwick 1996) for mapping geomorphic surfaces.

Site Characterization

YPG lies at the southern end of the Basin and Range physiographic province, a vast area extending as far north as Oregon, characterized by over 400 relatively regularly spaced, north-northwest trending subparallel mountain ranges, with intervening, broad and gently sloping alluviated basins formed by high angle extensional faulting (Dohrenwend 1987). The most

notable features of the YPG landscape are the relief and bareness of these mountains and extensive desert pavements developed in broad intermontaine alluvial basins. Desert pavements consist of a surface layer of closely packed gravel, usually one particle thick, that overlies a thin, gravel-poor vesicular A (Av) soil horizon. Other major landforms on the installation include alluvial fans and bajadas, which often transition to broad alluvial plains drained by ephemeral stream washes, and sand dunes. These Quaternary valley fill deposits make up about 70% of the YPG landscape (Fig. 20).

Surface I: Alluvial Fan. Surface I is an alluvial fan centrally located in the Yuma Wash drainage basin (33° 07' 25" N, 114° 30' 02" W). A striking feature of this geomorphic surface is its pronounced bar-and-swale topography (Fig. 21). Clasts range in size from boulders on the proximal fan area, to cobble bars and small gravel-sized clast fractions in swales that meander across the rest of the surface. Rock varnish is relatively poorly developed and has a reddish-brown, Fe-rich hue in the visible spectrum compared to the darker Mn-rich varnish typical of the other surfaces in Yuma Wash. Surface relief, rock varnish characteristics, and an immature soil profile (Fig. 22, Table 3), reflect the mode of origin and relative age. Our data suggest that clasts, which are almost entirely fine-grained igneous rhyolite, were deposited and have been reworked by ephemeral braided streams since the early to mid-Holocene period, between 8000 and 12,000 years ago (ka). Although a geologically young surface, the desert pavement is sufficiently well developed in both bars and swales to preclude significant exposure of the underlying soil matrix along our transect, which had 11 sample stations. The alluvial fan also has significantly more vegetation (located predominately in drainage channels) and a mottled texture on imagery (Fig. 23—A).

Table 3. Summary of key soil morphology and age estimates.

Soil Property	S1 - Alluvial Fan	S2 - Pediment	S3 - Stream Terrace
Horizon Sequence	Avk-ABvk-Ck1-Ck2-Ck3-Bkb-Ckb	Avk-ABvk-Bwk1-Bwk2-Bwk3-Ck1-Ck2-Ck3	Avk-Bwky1-Bwky2-Bky1-Bky2-Bky3-Bky4-CBk-Ck
Av thickness (cm)	3	4	4.5
Av texture	loam	Silt loam	Silt loam-silty clay
Av gravel content	15–25%	10–30%	<5%
B thickness (cm)	no B horizon	45	137
Strongest B horizon texture	no B horizon	sandy loam	silty clay loam
Carbonate stage	I–	II–	III–
C texture	sand	sand	loamy sand
C gravel content	50–85%	50–80%	40–80%
Estimated age	8–12 ka	12–70 ka	70–200 ka

Figure 21. Ground photographs of Holocene alluvial fan showing igneous geologic source area, vegetation, bar and swale topography, poorly developed rock varnish, and variable clast size (texture).
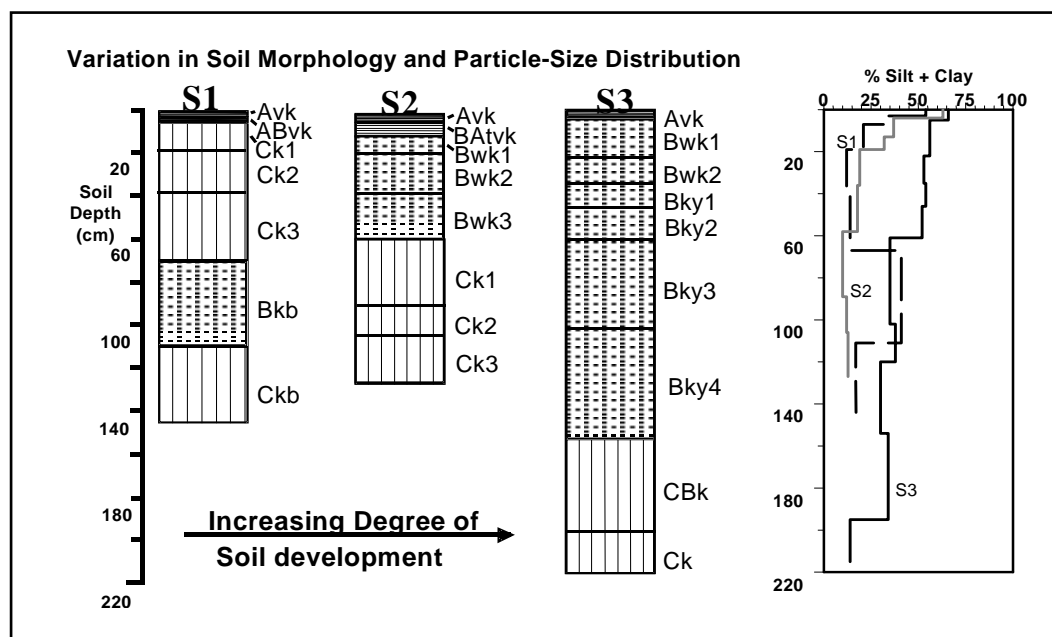
Figure 22. Soil profile summary for each geomorphic surface: S1—alluvial fan, S2—pediment, and S3—stream terrace.
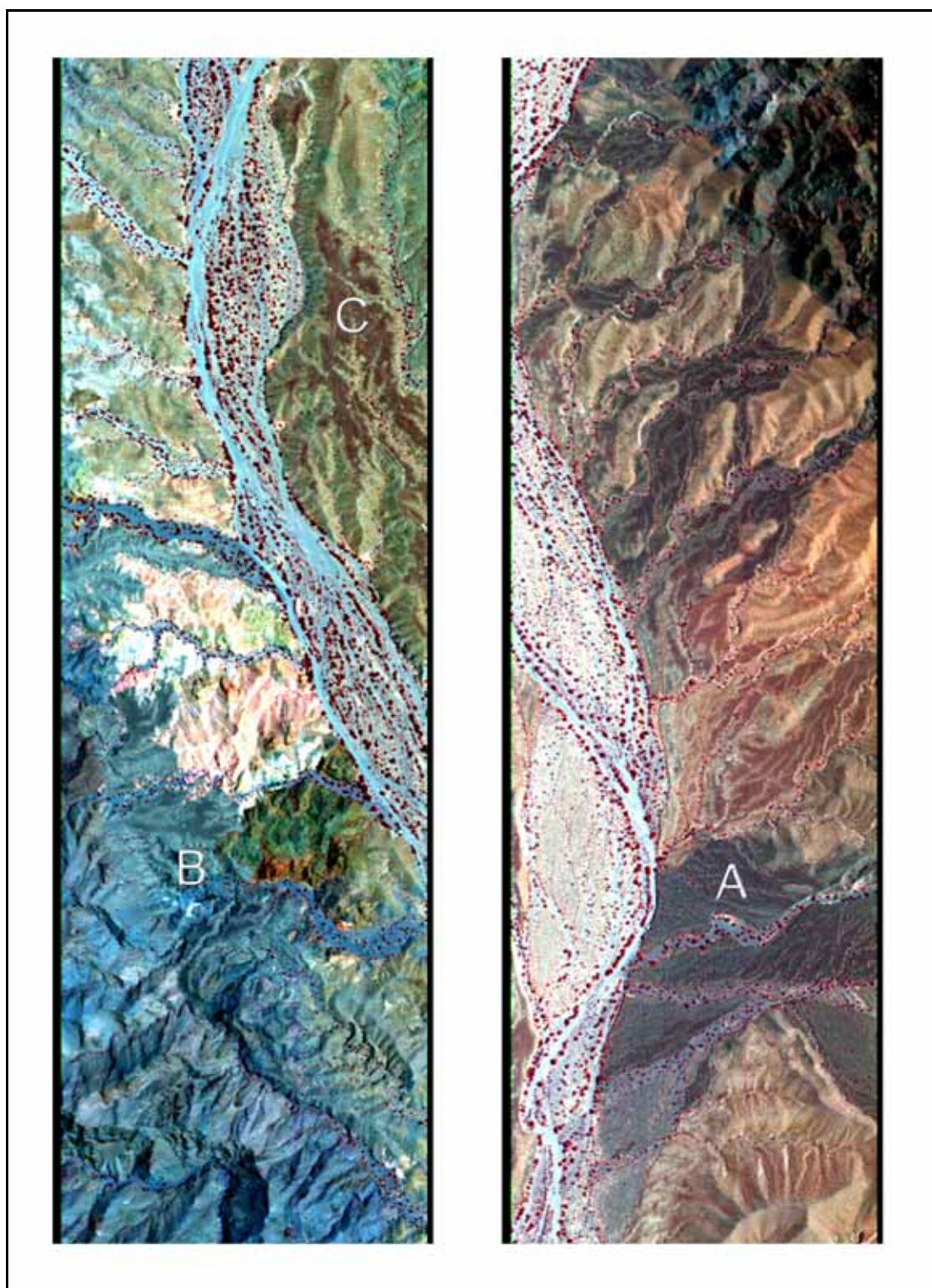
Figure 23. HYDICE band 100, 50, 25 color composite images showing three gemorphic surfaces: A—alluvial fan; B—truncated pediment; and C—stream terrace.

Surface II: Truncated Pediment. Surface II is a pediment remnant located in the lower reach of Yuma Wash (33° 03' 25" N, 114° 30' 2" W). This surface has the shortest transect of the three studied (three sample stations), owing to truncation by a normal fault at its proximal (western) edge and igneous intrusions on its distal (eastern) margin (Fig. 23—B). The pediment is characterized by a topographically smooth, well-developed pavement surface with well-sorted, uniform clast size (Fig. 24). Parent material is derived from the adjacent fault-bound Tertiary to Mesozoic metamorphic mountain (Sherod et al. 1997), resulting in heterogeneous clast lithology, including metamorphic schist, gneiss, and quartzite. The angular to subangular shaped clasts are more loosely packed, exposing more soil matrix than Surfaces I and III. There is also evidence of pavement damage by feral burros, suggesting natural biologic and geologic processes easily disturb the surface. Pavement clasts exhibit moderately developed rock varnish, which is more continuous and darker colored than Surface I in the visible spectrum. The pediment is poorly drained and generally devoid of vegetation. These observations indicate an older pavement whose original surface relief has been smoothed over a longer exposure time. Surface II is characterized by its short length, variable metamorphic lithology, and moderate rock varnish development. Based on soils geomorphology data (Fig. 22, Table 3), we estimate the age of Surface II at 12 to 70 ka.

Figure 24. Ground photographs of Surface II showing metamorphic source area, moderate desert pavement and rock varnish development, and well-sorted, but heterogeneous. clast lithology.

Surface III: Stream Terrace. Surface III (Fig. 23—C) is a stream terrace located in the lower reach of Yuma Wash (33° 03' 59" N, 114° 31' 36" W) across the main channel from the Surface II. The terrace is adjacent to and approximately 10 m above the main channel of Yuma Wash and, unlike most alluvial fans in the drainage basin that slope either to the east or west

away from mountain ranges, Surface III slopes gently southward, toward the Colorado River. Additionally, a U.S. Geological Survey (USGS) Open File Report (Sherod et al. 1997) shows this landform as composed of fanglomerate—potentially a collection of all possible lithologies present in Yuma Wash. The smooth, planar desert pavement that has formed on Surface III is well developed with angular to sub-angular clasts in a tightly packed mosaic. Sample data from five transect stations show clasts with a well-developed, continuous coating of dark Mn-rich rock varnish (Fig. 25). The surface is moderately drained with perennial vegetation located exclusively in medium density dendritic drainage channels that, like the landform slope, also trend in a southerly direction. These data indicate that the surface was deposited in a fluvial regime and long ago abandoned as a stable stream terrace. Surface III is distinguished from the other surfaces by its heterogeneous lithology; mature pavement with heavily varnished clasts; a well developed soil profile, including the deepest Av horizon and Stage III carbonate development (Table 3); and Pleistocene age ranging from 70 to 200 ka.

Figure 25. Ground photographs of Pleistocene stream terrace showing well-developed desert pavement and rock varnish. Mojave Peak, the northern drainage divide for Yuma Wash, is in background (left) and undisturbed soil matrix is shown (right). Note how the variable clast lithology (fanglomerate) is completely obscured by rock varnish in the visible wavelengths.

Site Summary

Several morphologic features of these soils indicate that the accumulation of dust is the primary mechanism driving development of soil and desert pavement. Silt and clay content is highest in the Av and progressively decreases downward below the Av horizon. For the three geomorphic surfaces described herein, Av horizon thickness also increased with age. Lack of significant chemical weathering of the clasts and matrix, other than a weak accumulation of

secondary iron oxides for each of the surfaces, as well as the accumulation of salt-shattered clasts for the older Surfaces II and III, indicate that the accumulation of silt, clay, carbonate, and salts is primarily from the addition of these constituents through the accumulation of eolian fines rather than in situ production related to chemical weathering. This conclusion is consistent with recent studies of the formation of soils on alluvial piedmonts in the Sonoran and Mojave Deserts (Wells et al. 1985, McFadden et al. 1987).

The geology of Yuma Wash is undocumented, as no large- or medium-scale geologic maps have been published and geomorphic surfaces are neither mapped nor regionally correlated. However, Yuma Wash is composed of erosional and depositional landforms typical to desert landscapes of the southwest U.S. and much of what is known about arid geomorphology applies to YPG. The three geomorphic surfaces chosen for this study would likely be generalized as Quaternary Alluvium on 1:24,000 scale geologic maps, if they existed for Yuma Wash. In fact, each is a different landform developed from different geologic materials and geomorphic processes. They differ in geologic age, clast lithology, soil profile maturity, and desert pavement development, including the amount and character of rock varnish, drainage, and vegetation characteristics. In summary, these three surfaces are sufficiently distinct, yet representative of geomorphic surfaces at YPG, to provide meaningful hyperspectral comparisons.

Hyperspectral Reflectance of Desert Pavements

Vegetation Distribution

Vegetation of the Sonoran Desert is sparse and uniquely adapted to the hot, dry climate. The region has been arid for the last 13,000 years and the present climatic regime and plant species were established about 4000 years ago (Betancourt et al. 1990). YPG is located in Lower Colorado River valley, the driest subdivision of the Sonoran Desert, where very high temperatures and very low, erratic precipitation support a desert scrub biome characterized by sparse stands of drought tolerant trees, shrubs, and cacti.

Plant communities of YPG are well characterized by 198 permanent monitoring plots established in 1991 for YPG's Land Condition Trend Analysis (LCTA) program. Ten of these plots are located within the Yuma Wash watershed. LCTA is part of the Army-wide Integrated Training Area Management program instituted to manage the Army's ranges for sus-

tained mission use. Dominant plant species at YPG include: *Larrea tridentata* (creosote bush), *Ambrosia dumosa* (white bursage), *Carnegiea gigantea* (saguaro), *Fouquieria splendens* (ocotillo), *Parkinsonia florida* (blue palo verde), *Parkinsonia microphylla* (foothill palo verde), *Olneya tesota* (ironwood), *Opuntia bigelovii* (teddybear cholla), *O. acanthocarpa* (deerhorn cactus), *O. echinocarpa* (thorny-fruit cactus), *O. basilaris* (beavertail pricklypear), and *Hilaria rigida* (galleta grass) (Bern 1995).

In Yuma Wash, vegetation distribution and channel geometry have been surveyed at 25 permanently monumented transects across the main channel and 10 more transects in the East Fork sub-basin to establish baseline conditions for future comparisons (Ayres Associates 1996). The ephemeral channels in Yuma Wash contain some of the densest and most diverse vegetation at YPG (Hermann Zillgens Associates 1992), suggesting a microclimate in which the limited amount of available water is quickly transported through shallow subsurface deposits to tributary channels before evaporation can occur, and accumulates in deep sand and gravel deposits of the main channel. As a result, vegetation location in Yuma Wash is correlated with proximity to primary and secondary channels, with the densest distributions occurring along wash margins. Density also increases in the lower reaches of the wash, particularly at the confluence with the Colorado River.

Vegetation Reflectance

Vegetation covers only 5% or less of the YPG landscape, but vegetation on desert pavement surfaces is even sparser. Soils underlying desert pavement in Yuma have a higher silt, clay, and salinity content than non-pavement soils in the area, resulting in slower infiltration rates, with little precipitation entering the soils compared to non-pavement soils, and precipitation that does enter the soil is held near the surface and evaporates quickly (Musick 1975). Temperature extremes may contribute to the bareness of these surfaces. While the average maximum daily temperature in July is 106°F, Cochran (1992) found that soil temperatures within 25 mm (1 in.) of desert pavement gravels at YPG often exceed 160°F during July and August and the authors have measured 150°F in July (1998) on the surfaces studied in this chapter. As a result, the impact of vegetation on pavement reflectance characteristics is minimal.

Unlike geologic minerals, all vegetation is composed of a limited set of spectrally active compounds (including water) and relative abundances indicate the condition of vegetation and surrounding environment. Reflectance in the visible and near infrared wavelengths (350 to 800 nm) is dominated by absorption from chlorophyll and other pigments. Reflectance in the shortwave infrared, or SWIR (800 to 2500 nm) is dominated by absorption caused by liquid water in plant tissue, modified by minor absorption features associated with compounds such as starches, proteins, oils, sugars, lignin, and cellulose (Curtiss 2003). Major water absorption features occur in spectra at the 1400-, 1900-, and 2200-nm wavelengths.

Spectral reflectance of some tree species change significantly at different times of the year (Fig. 26) and these reflectance characteristics are important for developing multitemporal landscape models; cover, concealment, and camouflage simulations; as well as for target detection and recognition applications.

Figure 26. Temporal differences in spectral reflectance of Palo Verde tree at Yuma Proving Ground in June (left) and November (right) 2003.

Pavement Clast Lithology

Absorption features in spectra of rocks and minerals are due to the presence of specific molecular groups and are often diagnostic of the minerals present in the sample (Hunt 1980). Mineralogy of clasts from the three YPG surfaces share some chemical similarities. All rocks are high in silica, represented universally by the presence of the mineral quartz (SiO_2) and by feldspars (silicate minerals that include other cations). Microcline and albite are the feldspars most commonly encountered, indicated consistently among evidence from XRD, minerals

identified in thin section, and chemical composition indicated by XRF. Other feldspars, such as sanidine and orthoclase, are present in some clasts.

Despite these mineralogical similarities, important differences exist in rock type (abundances of minerals) and relative age indicated by petrographic study of individual clasts. These differences are evident in the laboratory spectra of three individual pavement clasts shown in Figure 27, which suggest that clast lithology could easily be distinguished in both visible/near infrared (VNIR—400 to 1100 nm) and shortwave infrared (SWIR—1100 to 2500 nm) wavelengths. However, this would, of course, be an over simplification of the desert pavement remote sensing challenge. For example, both the pediment and stream terrace have heterogeneous clast lithologies not accounted for in Figure 27. Heterogeneous lithologies are averaged together in both field and image spectra scale measurements. Additionally, while the shape of spectral signatures of rock and soil tend to be invariant to differences in instrument and solar view angle geometry (Analytical Spectral Devices 2003), the overall brightness of the desert pavement field and image spectra may change because of differences in the amount of shadows within the instruments field of view. Surface roughness, or texture, of these surfaces (Fig. 21, 24, and 25) is related to rock type and geomorphic age and affects the relative proportion of the various sources of illumination. When compared to a smooth surface, a surface with a rough texture (like Surface 1) tends to have a higher overall proportion of illumination from diffuse and scattered sources relative to direct solar illumination (Curtiss and Ustin 1988).

Spectral Attenuation by Rock Varnish

One of the most prominent features of arid landscapes is the nearly ubiquitous presence of rock varnish; a thin, dark, shiny film or coating, found on the surfaces of pebbles, boulders, and rock outcrops (Allen 1978). The degree to which rock varnish obscures lithologic information depends on the type of coating formed, its chemistry, morphology, and condition, which are in turn controlled by complex environmental factors (White 1990). Lashlee and Rosenfeld (2001) used laboratory spectrometry to quantify spectral effects of rock varnish, weathering rinds, and carbonate deposits at YPG. Figure 28 shows average reflectance spectra of a single desert pavement clast (Fig. 29) collected from Surface III, including Mn-rich varnish (sample top), Fe-rich varnish (sample bottom), and host rock lithology (sample interior).
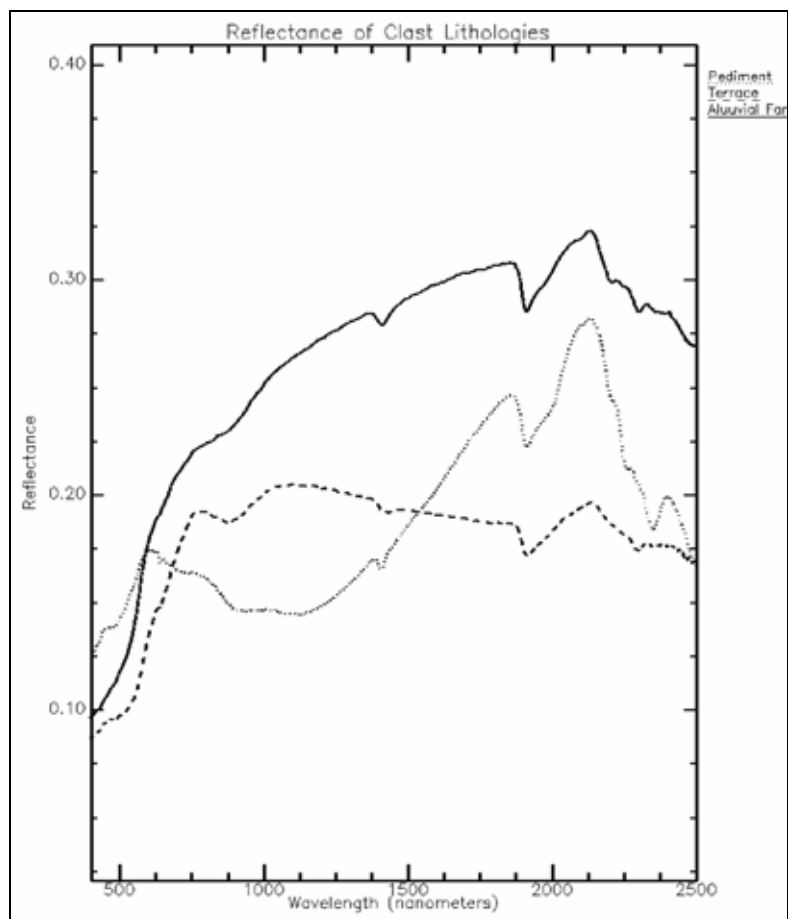
Figure 27. Laboratory spectra of desert pavement clast lithology of a single sample selected from each geomorphic surface.
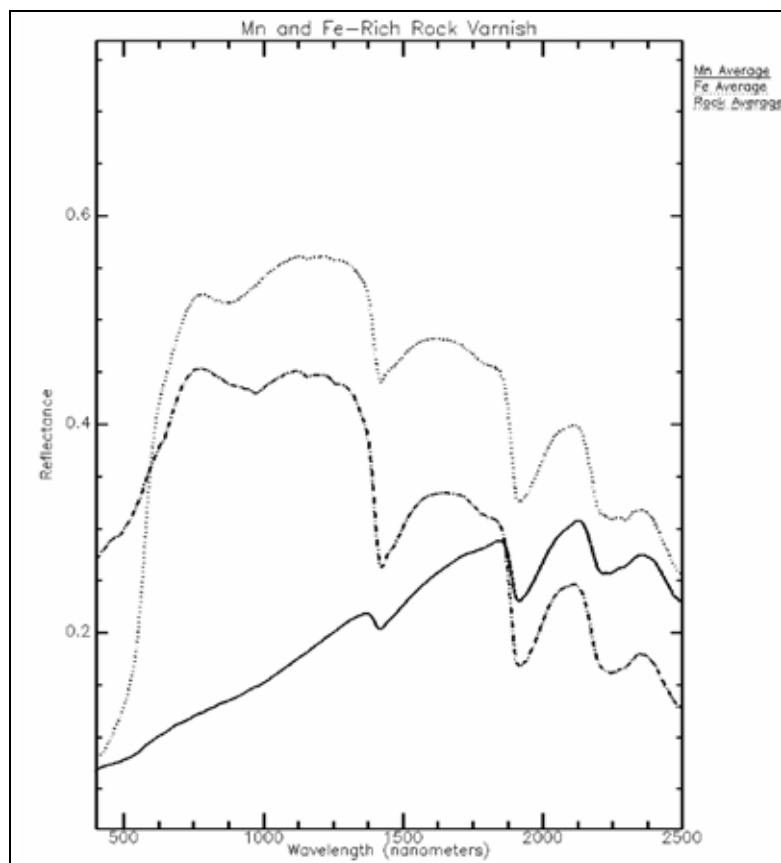
Figure 28. Laboratory spectra showing spectral attenuation of host rock lithology by Mn- and Fe-rich rock varnish. Spectral absorption features common to all three spectra at 1400 and 1900 nm are water absorption bands.

a. Mn-rich rock varnish (sample top)   b. Fe-rich rock varnish (sample bottom).

c. Clast lithology (sample interior).

Figure 29. Desert pavement clast from Surface III showing rock varnish and clast lithology.

Spectral Contributions of Soil

Moisture content, the amounts of organic matter and iron oxide, and soil texture all significantly influence spectral characteristics of soils (Swain and Davis 1976). As water content increases, soil reflectance decreases throughout the reflective portion of the spectrum. Organic matter and iron oxide are also inversely related to reflectance. Increases in either, or both, decreases soil spectral reflectance. Conversely, when other factors are held constant, soil reflectance increases as particle size (texture) decreases. As the soil surface becomes smoother, more radiation is reflected.

Because hyperspectral remote sensing techniques are limited to energy reflected by the thin uppermost surface of soils, we performed extensive laboratory tests to determine the physical and chemical properties of the accumulated dust and underlying Av soil horizons along each transect. In Yuma Wash, these soils are fine textured, composed primarily of silt and clay

sized particles (Fig. 22, Table 3). All soil samples show a strong influx of dust, probably making up 40 to 75% of the mass of the soil in the upper 4–5 cm and silt and clay contents are well above levels in the C-horizon. Musick (1975) also studied pavement surfaces of Yuma, Arizona, and found that underlying soils had a higher silt, clay, and salinity content than non-pavement soils in the area.
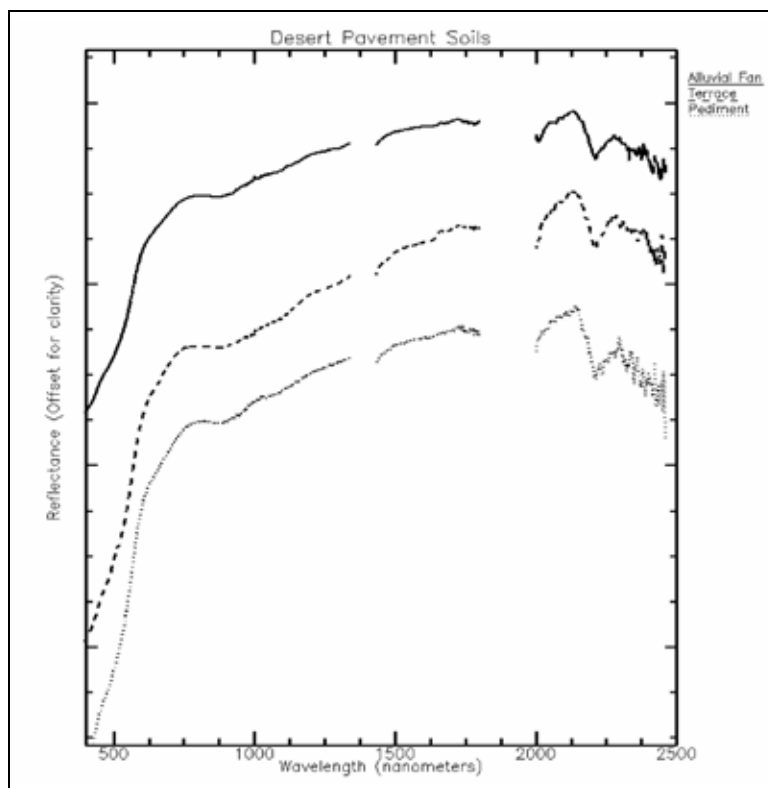
Figure 30. Field spectra of Av soil horizon for each surface, showing similar reflectance curves, particularly in the VNIR wavelengths. Reflectance (y-axis) is offset for clarity.

Chemically, XRD data showed these soils to be high in quartz and calcite, with less feldspar than the clast rock types that overlay them. In general, quartz is spectrally inactive in the VNIR–SWIR region and, therefore, tends to diminish other spectral features in the soil mixture (Ben-Dor 1999). While salt is also spectrally featureless, saline soils are relatively higher in albedo than non-saline soils. Pavement Av soils are low in oxides of iron and aluminum, low in carbonates, and very low in organic matter. With an average of about 8 cm (3 in.) of rain per year, soils at YPG are very dry, with low effective soil moisture. Finally, these soils are high in clay-sized particles, but not high in clay minerals. Figure 30 shows reflectance

curves for these soils. Spectra are quite similar in the VNIR region and part of the SWIR, but differ around 2200 to 2400 nm. In summary, surface soils along each transect are mineralogically similar to each other, rather than similar to the clasts located on the surfaces, and have similar signatures.

Discussion: Eolian Dust as a Geomorphic Agent

Laboratory and field spectrometry have yielded several interesting observations on hyperspectral characteristics of YPG terrain. One in particular, the spectral contribution of soil on alluvial geomorphic surface reflectance, has widespread implications for mapping and modeling arid landscapes. One might reasonably expect landforms of different geologic age and materials to develop different soil profiles and this is, in fact, what we observe in soil pits. For example, each site has different B-horizon and carbonate development characteristics (Fig. 22, Table 3). However, an aggrading Av horizon between 3 and 4.5 cm thick separates subsurface soil horizons from the pavement clasts that rise on accretionary dust layers. Because remote sensing using reflected solar wavelengths is a surficial data collection technique, subsurface soil characteristics of stable desert pavements are rarely imaged. Soil information collected at YPG is limited to a relatively thin layer of eolian dust.

Sources of Eolian Dust

Transportation of suspended sediment during storm events is common in arid and semi-arid environments and with negligible surface cover, low soil moisture, and low humidity; the Lower Colorado Sonoran Desert is no exception. Dust accumulation at YPG results from both natural and anthropogenic processes originating from local, regional, and even global source areas. Locally, the vast alluvial landforms and ephemeral washes located across the YPG are dust storage areas and YPG's military testing and training activities accelerate natural erosional and depositional geomorphic processes. On a regional scale, agricultural land use provides ample sources of dust. Yuma County is the state's third largest agricultural county with 18% of the Arizona's million-plus acres (Climate of Arizona 2003). Yuma is also located in the third fastest growing region of the country, so urbanization and construction activities are also major dust contributors.

Dust storms called "haboobs," an Arabic term for violent winds (Idso 1976), are typical of southern Arizona, where they accompany squall lines generated by the summer monsoonal flow of moist tropical air from the Gulf of Mexico, and Pacific tropical storms from the Gulf of California (Fig. 31). Brazel (1986) found that 50% of all dust storms in Arizona during a 15-year period (1965–1980) were the result of convective thunder cell activity. The remainder were attributed to the passage of fronts and, rarely, tropical disturbances. Surface winds at YPG are generally light throughout the year, with an average of 4–5 kt. Average peak winds during fall and winter are 14.3 kt and for the spring and summer are 18.7 kt. Prevailing wind direction is from the north–northwest from November through February and from the west to southwest the remainder of the year (Devine 1988). The storm of April 2002 is a regional example where several tens of millions of metric tons of dust were emitted from the central Mojave Desert of California alone (Chavez et al. 2002). Another significant event occurred April 1998 (Husar 2001) when dust generated in the Gobi Desert, China, reached the west coast of North America and penetrated the interior.

Figure 31. Dust storm over Phoenix, Arizona on July 6, 1999 produced rain, hail, and a tornado. Source **http://www.azcentral.com**.

Laboratory Spectra of Av Horizons

Av soil samples from each field site were air dried, then sifted to remove gravel. An ASD FieldSpec Pro was used with a Turntable Sampling Accessory (Analytical Spectral Devices 2003) to collect spectra under controlled illumination conditions (Table 4). After calibrating the instrument to a spectralon white reference standard, soil samples placed in a Petri dish

were rotated under a fixed halogen light source while the FieldSpec collected signatures. The turntable has a 150-mm viewing area, a 53.2-mm spot size, and rotates at 22 rpm. For this study, the spectrometer was set up to record and average 25 spectra before saving each signature and to perform 10 concurrent measurements while the soil sample rotated beneath the instrument. These data were collected in the YPG Laser Laboratory to assure that no secondary light sources influenced the measurements (Fig. 32).

Table 4. Eolian dust and Av soil horizon chemistry data for three Yuma wash surfaces.

Test	Alkalinity, bicarbonate (as $CaCO_3$)	Alkalinity, carbonate (as $CaCO_3$)	Calcium, CA	Magnesium, Mg	Iron, Fe
EPA method	(mg/kg)	(mg/kg)	(mg/kg)	(mg/kg)	(mg/kg)
SI—Dust	1886	84	20100	6470	10600
SI—Av	7254	86	29200	8410	12600
SII—Dust	1176	84	22000	5240	7440
SII—Av	9032	508	60300	7190	11900
SIII—Dust	8476	124	37400	3950	5670
SIII—Av	36288	212	49100	6580	9530
Test	Silicon, Si	Sodium, Na	Carbon, total organic	PH, Lab	Alkalinity, Total
EPA method	200.8	6010B	9060	150.1/9040	160.3
SI—Dust	102	206	<1010	9.24	1970
SI—Av	254	265	3190	9.20	7340
SII—Dust	89.3	268	<1010	9.35	1260
SII—Av	240	758	5180	9.67	9540
SIII—Dust	73.0	1030	<1000	9.17	8600
SIII—Av	136	2500	4840	8.37	36500
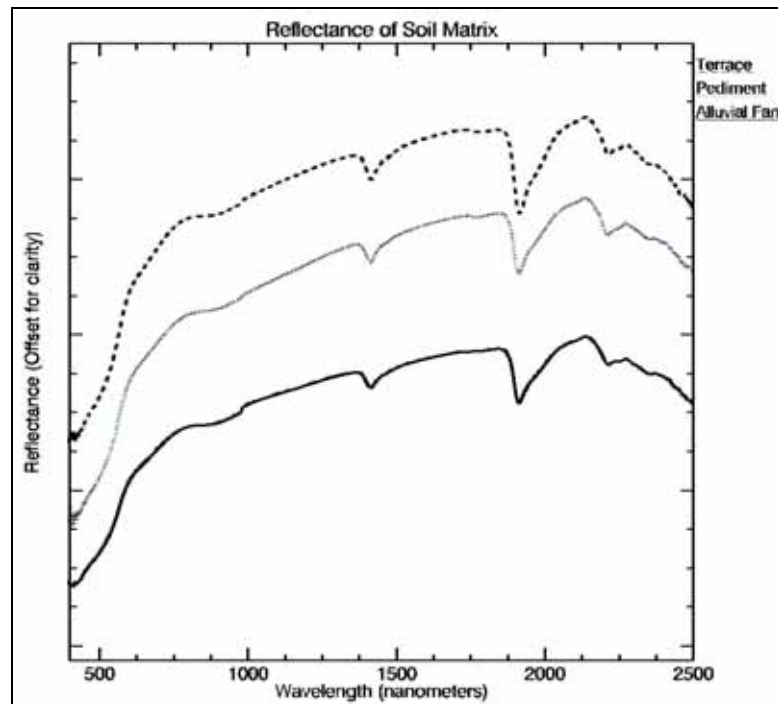
Figure 32. Laboratory Spectra of desert pavement wind-blown eolian dust matrix show identical signatures in the solar reflected spectrum. Reflectance (y-axis) is offset for clarity.

Conclusions

Mapping Quaternary geomorphic surfaces in arid and semi-arid environments requires an understanding of landforms and the geomorphic processes that form them, as well as surficial geologic materials and the controls they exert on spectral reflectance. Geomorphic processes that dominate reflectance in the Sonoran Desert are desert pavement and rock varnish formation, eolian silt and clay deposition, and fluvial dissection. Desert pavement signatures are spectral mixtures of the geologic materials found within the instruments field of view. The following discussion summarizes some important considerations related to spectral reflectance of desert terrain in order of significance—rock varnish, lithology, soils, and vegetation.

Rock Varnish

The degree to which rock coatings obscure lithologic information depends on the type of coating formed, its chemistry, morphology, and condition, which is in turn controlled by com-

plex environmental factors (White 1990). Rock varnish often develops discontinuously on pavement clasts, first filling in low spots in the rock surface. As a result, pits and grooves are often more heavily varnished than smoother areas. Varnish may also adhere differently to the various minerals on a single clast. It's not uncommon for banded rocks, such as gneiss, to be varnished such that lithology is obscured in the visible wavelengths on all but the banded minerals, which show through. Differential rates of erosion on heterogeneous desert pavement gravels also contribute to spectral variation. For example, granular rocks, like sandstone and granite, may disintegrate before a varnish coat can form.

Lashlee and Rosenfeld (2001) showed that a single desert pavement clast could have multiple rock coatings, like weathering rinds and carbonate deposits, and multiple rock varnishes, resulting in radically different hyperspectral signatures. Fe-rich coatings have a less significant effect on host rock spectral reflectance characteristics than do Mn-rich varnishes. In the Lower Colorado Sonoran Desert, Pleistocene age desert pavements sort typically with Mn-rich on clast tops and Fe-rich on clast bottoms. Well-developed Mn-rich rock varnish precludes lithologic mapping in the 400- to 1800-nm wavelength regions. Only the 2000- to 2500-nm wavelengths are useful for lithologic discrimination.

Clast Lithology

Desert pavement clast lithology can be homogeneous or heterogeneous and it's common for pavements at YPG to be close, but have very different lithologic and morphologic characteristics. We studied three pavements in detail that were formed on different landforms, composed of different lithologies, with different stages of pavement development. The youngest is an alluvial fan developed from mudflow and other alluvial deposits from a single canyon whose surface was later covered by volcanic rhyolite deposited during a Holocene igneous extrusion event. This surface has homogeneous lithology, consistent brownish-red rock varnish development, and exhibits a strong bar and swale topography typically of young desert pavements. The middle age pavement is a truncated pediment whose clasts are composed of a heterogeneous mixture of banded gneisses, foliated schists, quartzites, and other metamorphic rock, each exhibiting different rock varnish characteristics. Directly across the channel is a Pleistocene stream terrace composed of alluvial fanglomerate, a mixture of potentially every rock type

present in drainage basin. Soils geomorphology suggests the ages of these pavements range from 8 to 12 ka, 12 to 70 ka, and 70 to 200 ka, respectively.

Desert pavement clasts studied are spectrally distinct throughout the solar reflected wavelengths in laboratory spectra. However, field spectra confirm that only the 2000- to 2500-nm wavelengths are useful for lithologic discrimination (Fig. 33) owing to the pervasive effects of Mn-rich rock varnish. Pavement signatures are also modulated by soil matrix contributions and the presence of variable amounts of wind-blown dust present on clasts.
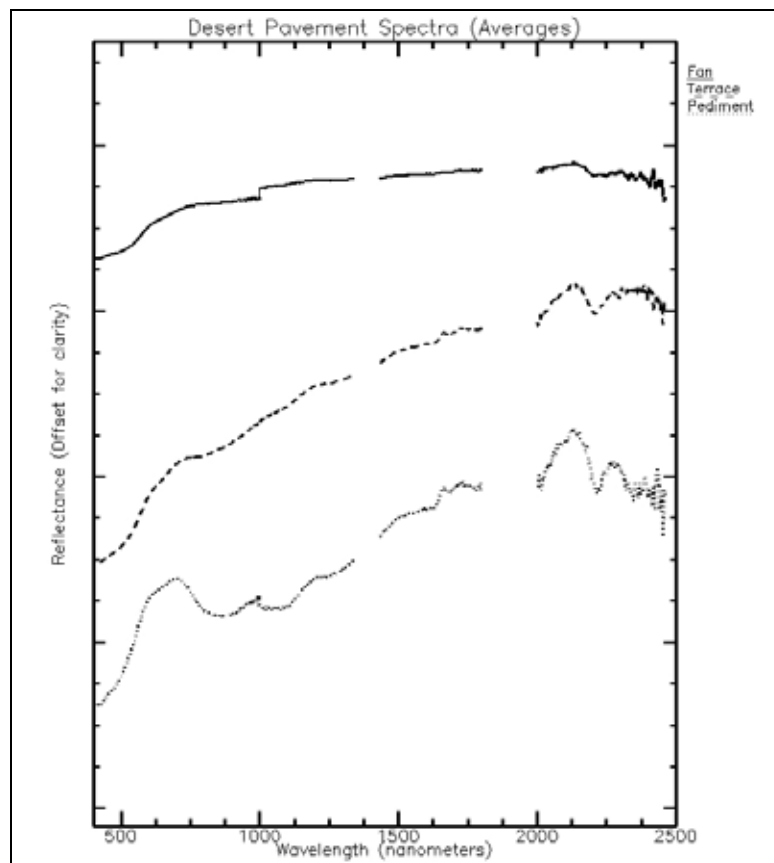
Figure 33. Field Spectra of desert pavement surfaces. With spectral contributions of eolian dust a constant, spectral variations in the 2000- to 25000-nm region show lithologic information. Reflectance (y-axis) is offset for clarity.

Differences in rock type and relative age also result in surface roughness variations (gravel and cobble size and shape) that may cause variable amounts of shadow in remotely sensed data. One should reasonably expect more shadow on surfaces with bar and swale topography

and terrain where boulder and cobble fields exist as compared to the older, flatter well-developed desert pavement surfaces. As shadow varies with sun angle, the amount of shadow in the reflected solar spectrum changes both seasonally and temporally throughout the day.

Soils

Laboratory and field data collected for this study, including soil texture classification, chemical composition analysis, and extensive field spectrometry data, support the accretionary desert pavement formation model (Wells et al. 1985) that holds that the underlying soil matrix is composed of eolian dust accumulating below desert pavement clasts and above a vesicular Av soil horizon. Soil samples from Av horizons at different locations at YPG have similar texture and mineralogy and, therefore, similar hyperspectral signatures, regardless of the geologic age or available parent material of individual surfaces. From a remote sensing perspective, spectral contributions of soils have a normalizing effect on pavement reflectance, since it's likely the same for different aged pavements. Once quantified with laboratory or field spectra, remote sensing geomorphologists can concentrate on the more problematic interpretations of integrated rock varnish, clast lithology, and surface roughness.

It's common for variable amounts of soil matrix to be exposed on different aged pavements as well as different locations of the same surface. For example, the edges of some pavements at YPG are often lighter colored because runoff in the form of concentrated sheetflow overturns and disperses pavement clasts to a greater extent than at the center of the surfaces. To summarize, it's not the composition of soils that change, but rather the amount of soil matrix exposed that is recorded in remotely sensed data.

Vegetation

Perennial plant cover across the YPG landscape averages 1 to 5%, but vegetation on desert pavements is even sparser and typically restricted to washes that drain them. Soils underlying pavement clasts have a high silt, clay, and salinity content, resulting in lower available soil moisture than non-pavement soils in the area. Temperature extremes measured at 160°F in summer months also contribute to bareness of these surfaces. The lack of significant vegetation on pavement surfaces simplifies quantitative geomorphic hyperspectral analyses of the Sonoran Desert. The restriction of vegetation to drainage networks of desert pavements is a

valuable indicator of drainage pattern and density, both in the field and in remotely sensed data.

Summary

Understanding natural environments, including the geomorphic and biologic systems, at the Nation's test centers is important for installation management and critical to accurate mapping, modeling, and simulation efforts. Desert pavements at YPG are dominated by Mn-rich rock varnish and are spectrally featureless in that they contain no diagnostic spectral absorption features. Relative degrees of varnish darkening, or patination, have long been used as a relative age indicator in the fields of archaeology and geomorphology. A research question currently being addressed at YPG is whether hyperspectral remote sensing is an effective tool for determining both relative geologic age (500- to 1800-nm wavelengths) and dominant rock lithology (2000- to 2500-nm wavelengths) for mapping Quaternary geomorphic surfaces in the Lower Colorado Sonoran Desert. Spectral data presented in this chapter demonstrate that remote sensing of arid terrains may be more problematic than is generally acknowledged by the remote sensing community.

Acknowledgements

References

Allen, C.C. (1978) Rock varnish of the Sonoran Desert—Optical and electron probe microanalysis. *Journal of Geology*, **86**: 743–752.

Analytical Spectral Devices (1995) Environment For Visualization of Images, Technical Guide. Boulder, Colorado, pp. 24–28.

Armbruster, R.E. (2003) Testing and Evaluation: Positioned to support the 21st century Army. ATEC Magazine. USATEC, CSTE-PA, Alexandria, Virginia, pp. 1.

Ayres Associates (1996) Geomorphic, hydrologic, and vegetation characterization and base-line conditions of Yuma Wash, Yuma Proving Ground, Arizona. Contract No. DACA39-93-C-0009.

Ben-Dor, E., Irons, J. R., and Epema, G.F. (1999) Soil reflectance. In *Remote Sensing for the Earth Sciences: Manual of Remote Sensing* (A.N. Rencz and R.A. Ryerson, Eds.), 3rd ed., Volume 3, New York: John Wiley and Sons, Inc.

Bern, C.M. (1995) Land condition—Trend analysis installation report, Yuma Proving Ground, Arizona, 1991–1994. Center for Ecological Management of Military Lands, Colorado State University, Fort Collins, Colorado.

Bull, W.B. (1991) *Geomorphic Response to Climatic Change*. New York: Oxford Press.

Betancourt, J.L., Van Devender, T.R., and Martin, P.S. (1990) *Packrat Middens, The Last 40,000 Years of Biotic Change*. Tucson, Arizona: University of Arizona Press.

Brazel, A.J., and Nickling, W.G. (1986) The relationship of weather types to dust storm generation in Arizona (1965–1980). *Journal of Climatology*, **6**: 255–275.

Chavez, P.S. Jr, Mackinnon, D., Clow, G., Tigges, R., Urban, F., Fulton, R., Reheis, M., Miller, D.K., Bultman, M., and Reynolds, R.L (2002) Monitoring dust emission in the Southwest U.S.—Interannual differences related to climatic variability. In *Geological Society of America Annual Meeting in Denver, 27–30 October*. Paper No. 109-10.

Climate of Arizona (2003) http://geography.asu.edu/azclimate/narrative.htm

Cochran, C.C. (1992) Soil survey of the U. S. Army Yuma Proving Ground, Arizona—parts of LaPaz and Yuma Counties. USDA, Soil Conservation Service.

Conel, J.E., Bruegge, C.J., and Curtiss, B. (1987a) Correcting airborne imaging spectrometer measurements for the atmosphere: A comparison of methods. In *Proceeding of the 31st S.P.I.E. International Technical Symposium on Optical and Optoelectronic Applied Science and Engineering*.

Conel, J.E., Green, R.O., Vane, G., Bruegge, C.J., Alley, R.E. and Curtiss, B. (1987b) AIS-2 radiometry and a comparison of methods for the recovery of ground reflectance. In *Proceeding of the of the Third Airborne Imaging Spectrometer Data Analysis Workshop*.

Curtiss, B., and Ustin, S.L. (1988) Spectral changes in Ponderosa Pine associated with natural ozone exposure. In *Proceedings of the U.S. Forest Service Forest Response Program Annual Meeting, Corpus Christi, Texas, 23–26 February*.

Devine, J.C. (1988) The U.S. Army Yuma Proving Ground, Arizona: 33-Year climate calendar and tables on associated weather elements 1954–1986, pp. 17.

Dohrenwend, J.C. (1987) Basin and Range. In *Geomorphic Systems of North America* (W.L. Graf, Ed.)*, Geological Society of America, Centennial Special Volume 2, pp. 303-342.

Goetz, A.F.H., and Srivastava, V. (1985) Mineralogical mapping in the Cuprite mining district, Nevada. In *Proceedings of the Airborne Imaging Spectrometer Data Analysis Workshop, April 1985*, JPL Publication, no. 85-41.

Farr, T.G., and Chadwick, O.A. (1996) Geomorphic processes and remote sensing signatures of alluvial fans in the Kun Mountains, China. *Journal of Geophysical Research*, **101**(E10): 23,091–23,100.

Gillespie, A.R., Kahle, A.B., and Palluconi, F.D. (1984) Mapping alluvial fans in Death Valley, California, using multichannel thermal infrared images. *Geophysical Research Letters*, **11**(11): 1153–1156.

Hermann Zillgens Associates (1992) Environmental assessment report, Target Recognition Range, Yuma Proving Ground, Arizona. Report prepared for U.S. Army Engineer District, Sacramento.

Hunt, G.R. (1980) Electromagnetic radiation: The communications link in remote sensing. In *Remote Sensing in Geology* (B.S. Siegal and A.R. Gillespie, Eds.). New York: Wiley, pp 5–45.

Husar, R.B., Tratt, D.M., Schichtel, B.A., Falke, S.R., Li, F., Jaffe, D., S., Gassó, Gill, T., Laulainen, N.S., Lu, F., Reheis, M.C., Chun, Y., Westphal, D., Holben, B.N., Gueymard, C., McKendry, I., Kuring, N., Feldman, G.C., McClain, C., Frouin, R.J., Merrill, J., Du-Bois, D., Vignola, F., Murayama, T., Nickovic, S., Wilson, W.E., Sassen, K., Sugimoto, N., and Malm, W.C (2001) Asian dust events of April 1998. *Journal of Geophysical Research*, 106: 18,317.

Idso, S.B. (1976) Dust storms. *Scientific American*, **235**(4): 108–114.

Kierein-Young, K. (1995) Integration of Quantitative Geophysical Information From Optical and RADAR Remotely Sensed Data to Characterize Mineralogy and Morphology of Surfaces, PhD Dissertation, University of Colorado, Boulder.

Lashlee, J.D., and Rosenfeld, C. (2001) Laboratory spectrometry of rock coatings: Implications for land management activities in the arid southwest. In *Proceedings of the Environmental Testing Workshop, 29–30 November 2000.* U.S. Army Test and Evaluation Command, Washington, D.C.

Lashlee, D., Briuer, F, Murphy, W., and McDonald, E. (2002) Geomorphic mapping enhances cultural resource management at the U.S. Army Yuma Proving Ground, Arizona, USA. *Arid Land Management* **16**: 213–229.

McFadden, L.D., Wells, S.G., and Jercinovich, M.J. (1987) Influence of eolian and pedogenic processes on the origin and evolution of desert pavements. *Geology*, **15**: 504–508.

Musick, H.B. (1975) Barrenness of desert pavement in Yuma County, Arizona. *Arizona Academy of Science,* **10**: 135.

Sherod, D.R., Tosdal, R.M., and Haxel, G.B. (1997) Geologic map of the Picacho, Picacho NW, Picacho SW, and Hidden Valley 7.5' Quadrangles, Arizona and California. United States Geologic Survey. Menlo Park, California.

Swain, P.H., and Davis, S.M. (Eds.) (1978) *Remote Sensing: The Quantitative Approach.* New York: McGraw-Hill.

Wells, S.G., Dohrenwend, J.C., McFadden, L.D., Turrin, B.D., and Mahrer, K. (1985) Late Cenozoic landscape evolution on lava flow surfaces of the Cima volcanic field, Mojave Desert, California. *Geologic Society of America Bulletin*, **96**: 1518–1529.

Williams, M.L. (2002) AFOTEC: Operational test and evaluation challenges: modeling and simulation. *Journal of the International Test and Evaluation Association: Modeling and Simulation Applications in T&E*, **23**(1): 17–20.

CHAPTER 5— IMAGING SPECTROMETRY ANALYSIS OF AN ARID LANDSCAPE AT YUMA PROVING GROUND: THE ARMY'S NATURAL ENVIRONMENT ANALOG FOR MODELING DESERT TERRAINS

David Lashlee, Thomas Harris, Charles Rosenfeld, and Jon Kimerling

Abstract

Hyperspectral reflectance of desert landscapes is the result of complex interactions between electromagnetic energy and surficial geologic materials in the solar reflected spectrum. We analyzed laboratory, field, and imaging spectrometer data of landforms with different composition, geologic age, and desert pavement development in the Lower Colorado Sonoran Desert at the U.S. Army Yuma Proving Ground (YPG), Arizona. Spectral reflectance and absorption features were compared to petrographic analyses of desert pavement clasts and soil structure and chemistry for each site. Results show quantitatively that a variety of rock coatings, including rock varnish, weathering rinds, and carbonate deposits, significantly modify lithologic reflectance of late Holocene and Pleistocene age geomorphic surfaces. In contrast, eolian-derived soils at each site have similar structure and chemistry, and, therefore, the same hyperspectral signature, which has a normalizing effect on spectral reflectance at landform and landscape scales. Spectral contributions of vegetation are minimal as density is estimated at 5% or less across the region, was calculated to be 1% density in our study area, and is spatially confined to ephemeral washes that drain landforms. Mixture Tuned Matched Filtering of Airborne Visible Infrared Imaging Spectrometer (AVIRIS) data were used to map composition and abundance of a variety of minerals typical of Tertiary and Quaternary volcanic landscapes, as well as to delineate desert pavements. However, we found that desert pavements are spectrally featureless in that they exhibit no diagnostic absorption features related to rock varnish or clast lithology. As a non-linear unmixing problem, deterministic extraction of quantitative geomorphic age and geologic composition information of pavement surfaces remains both an arid terrain mapping requirement and research challenge.
Keywords: Geomorphic Mapping, Hyperspectral, Matched Filtering, Remote Sensing

Introduction

Accurate knowledge of landforms, the geomorphic processes that occur on them, and the engineering characteristics of surface materials are critical to many facets of military planning, operations, and installation management. This is particularly true where military developmental and operational testing and training activities accelerate natural geomorphic processes and modify arid landforms. Unfortunately, soils and geomorphic surfaces of large regions of arid and semi-arid land in North America (Fischer 1991), as well as the rest of the world, are

unmapped and uncorrelated, resulting in an incomplete understanding of how these land uses affect natural environments and how to adequately model them as synthetic environments. It would be advantageous if the world's alluvial geomorphic surfaces accurately mapped and quantitative information about their composition could be extracted remotely. Until recently, limitations in the spectral, spatial, and radiometric resolutions of airborne and space-borne sensors have restricted the usefulness of these data for large-scale, detailed mapping. However, new and emerging sensor technologies hold significant potential for improved spectral mapping. This chapter summarizes our research on extraction of such information using airborne imaging spectrometer (hyperspectral) data collected of an arid landscape at the U.S. Army Yuma Proving Ground (YPG).

Imaging Spectrometry

Imaging spectrometry is defined as the acquisition of images in hundreds of registered, contiguous spectral bands such that for every picture element (pixel) it is possible to derive a complete reflectance spectrum (Goetz 1992). Also widely known as hyperspectral remote sensing, many early investigations demonstrated that mineralogical information could be automatically extracted from imaging spectrometer data (Hunt 1987) and that classification techniques could be extended to other terrestrial surface materials (Kruse and Lefkof 1993). These initial successes in geological applications were possible because many minerals have diagnostic absorption features at specific wavelengths and maintain them regardless of changes in seasonality and illumination conditions. Over the last decade, improvements in both sensor technology and spectral processing algorithms have significantly improved our ability to identify surface materials remotely (Mustard and Sunshine 1999), including progress toward quantifying the contributions of different materials to spectrally mixed pixels and the extraction of sub-pixel composition and relative abundance information.

Purpose and Scope

This chapter summarizes a spectral analysis of a complex arid landscape at YPG. Emphasis is placed on extraction of compositional information and mapping alluvial geomorphic surfaces using high spatial and spectral resolution imaging spectrometer data. Results are compared to laboratory and field spectrometry measurements and correlated to optical, chemical, and petrographic ground verification information collected from three geomorphic surfaces in the

study area. Specifically, our results address: 1) airborne hyperspectral imaging measurements in the 400- to 2500-nm wavelength range, 2) reflectance characteristics of naturally occurring surficial geological materials, and 3) the relationship of our results to Digital Terrain Modeling applications.

Spatially, our analysis is limited in scope to a portion of the Yuma Wash drainage basin. However, knowledge gained is certainly applicable to the rest of YPG and is also likely to apply to other locations in the Lower Colorado Sonoran Desert where similar geomorphic processes and geologic materials dominate the landscape. No attempt at signature extension to other arid regions was made in this chapter. However, YPG is the Army's natural environments desert analog for hot weather environments around the world. As such, some results presented herein may have immediate application and important implications for mapping and modeling other desert terrain.

Study Area

Yuma Proving Ground

The U.S. Army Test and Evaluation Command (ATEC) is the premiere Test and Evaluation (T&E) organization in the Department of Defense (DoD). Its mission is to plan, conduct, and integrate developmental and operational tests of military equipment, as well as provide independent evaluations of test results to decision makers, to ensure war-fighters are equipped with effective weaponry and soldier systems (Armbruster 2003). The Developmental Test Command (DTC), one of three subordinate Commands within ATEC, conducts rigorous performance tests on weapons systems and materiel under controlled conditions on highly instrumented ranges and test courses. Products of Developmental Testing include impartial technical data on system design, feasibility, performance, safety, and risks during system development (Williams 2002). YPG is a general-purpose test facility within DTC that assesses nearly every weapon in the ground combat arsenal, including artillery, tank and automotive systems, soldier systems, aircraft armament and air delivery systems, and smart munitions. It also supports training operations and visiting military units, like the Military Free Fall School and Special Forces groups. Located at the confluence of the Colorado and Gila Rivers, YPG encompasses more than 3367 km^2 (1300 mi^2) of the hottest and driest area in the U.S.—the

Lower Colorado Sonoran Desert section of the Basin and Range Physiographic Province (Fig. 34).
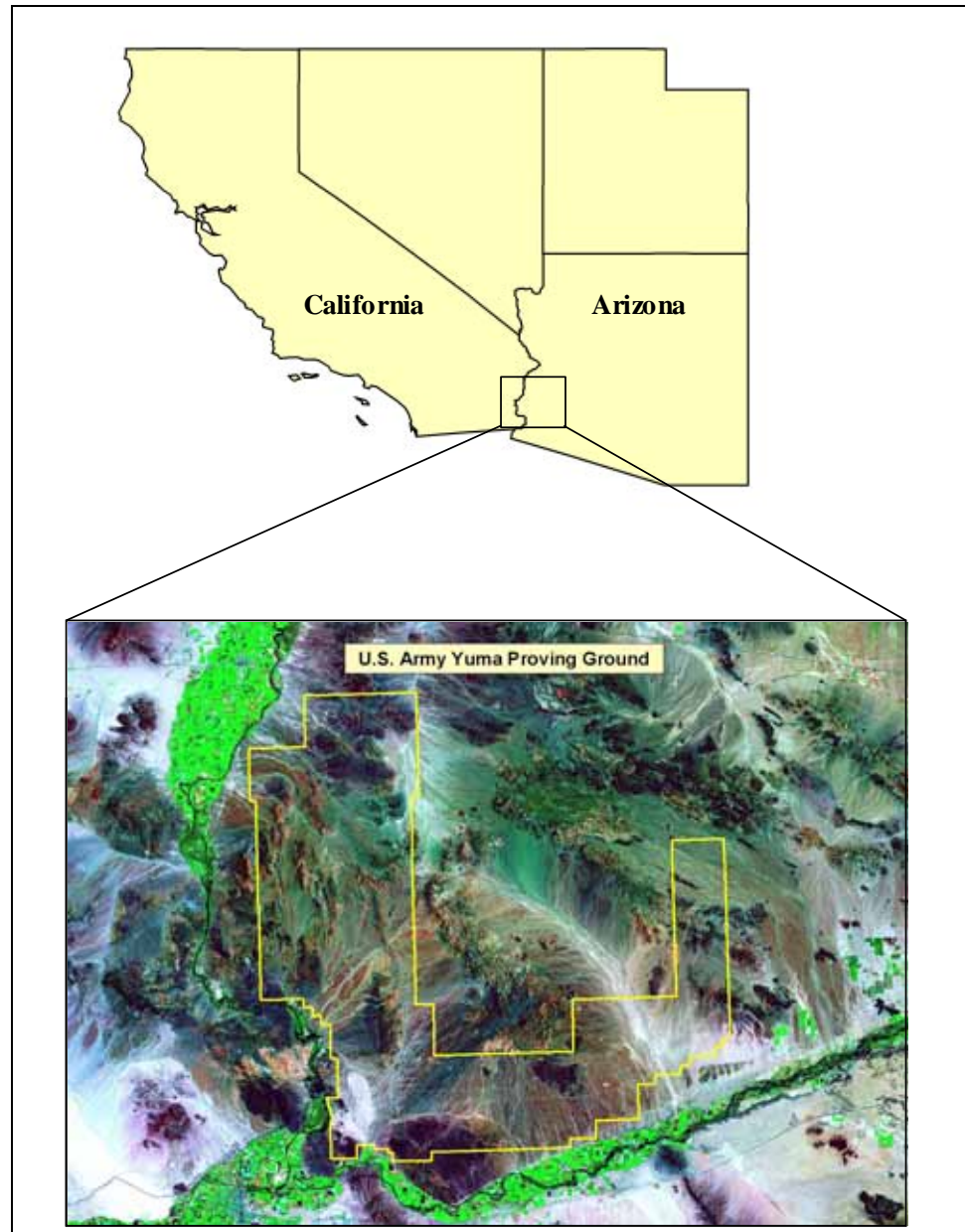
Figure 34. Landsat Thematic Mapper image showing YPG location.

Geomorphic Surfaces

The most prominent geologic features of the Lower Colorado Sonoran Desert are the rugged and barren Tertiary volcanic and metamorphic mountain ranges, which compose 30% of terrain at YPG, and broad intermontane alluvial basins typical of the Basin and Range in the southwestern U.S. (Dohrenwend 1987). Other landforms include sand dunes and alluvial fans and bajadas, which often transition to extensive alluvial plains drained by ephemeral stream washes (Fig. 35). Fan terraces and alluvial plains make up the remaining 70% of YPG's landscape (about 2350 km^2) and are locations of extensive, well-developed desert pavements. Vegetation at YPG is sparse, estimated not to exceed 4% of the land surface area, and uniquely adapted to the hot, dry climate (Bern 1995).

Geomorphic surfaces are mappable landscape elements formed during discrete time periods. Geomorphic mapping, much like traditional geologic mapping, seeks to define surface units on the basis of distinctive surface and subsurface characteristics. The criteria most often used for identification and mapping of alluvial geomorphic surfaces in deserts are: 1) degree of desert pavement development, 2) amount and character of rock varnish, 3) soil type, 4) topographic position, and 5) drainage characteristics (Bull 1991). With the exception of subsurface soil profile development, each of these mapping criteria can, with varying degrees of success, be assessed remotely. Our research focus is high spectral resolution measurements in the reflected solar spectrum; however, other studies have demonstrated the application of thermal (Gillespie et al. 1984) and radar data (Kierein-Young 1995, Farr and Chadwick 1996) for mapping geomorphic surfaces.
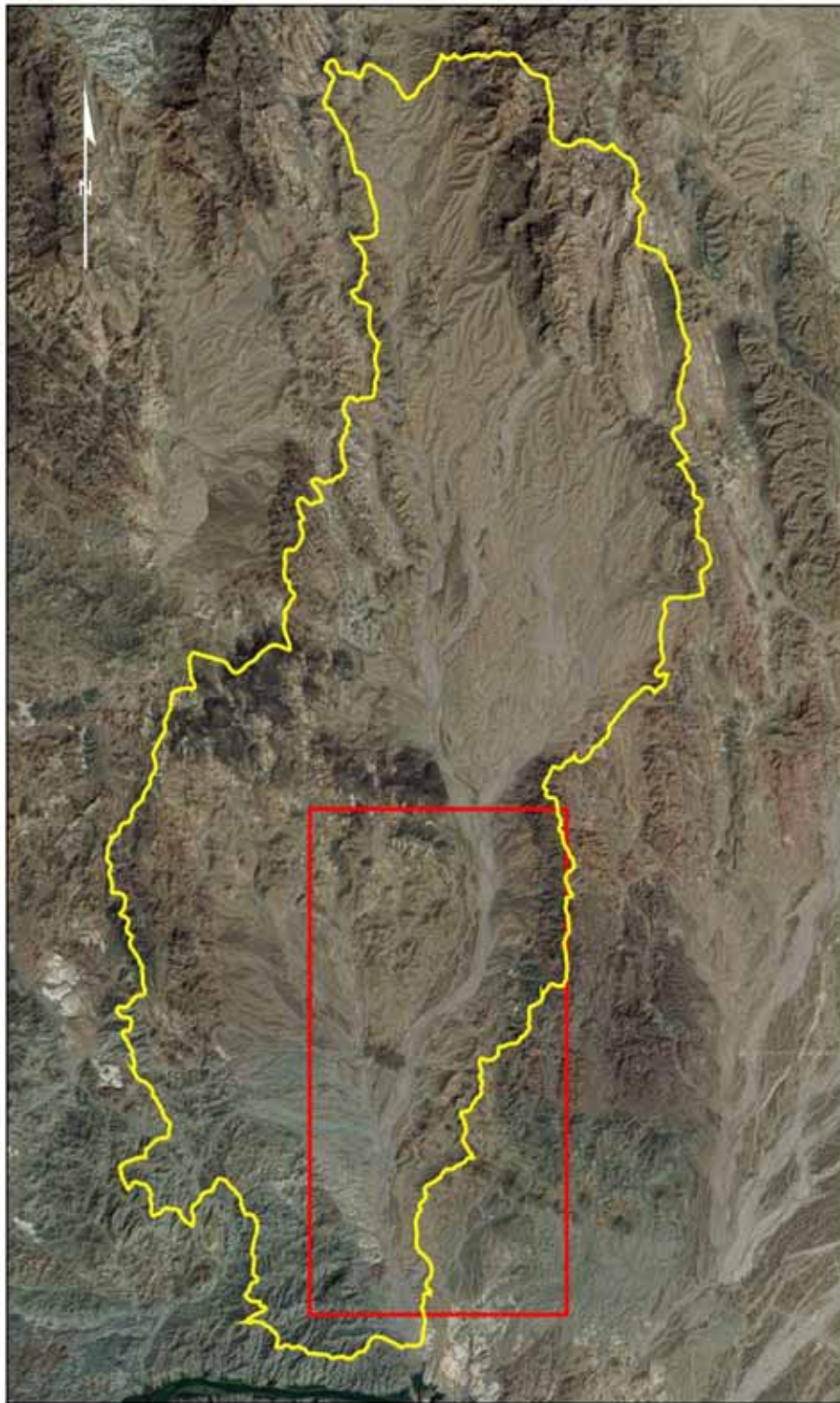
Figure 35. Yuma Wash drainage basin (defined in yellow) and imaging spectrometry study area boundary (highlighted in red) as depicted in an Indian Remote Sensing color composite satellite image.

Desert Pavements

Desert pavements are common features in arid regions of the world and are known as hamada or reg in Arabic regions, sai in Asia, and gibber in Australia (Cooke et al. 1993). While formational geomorphic processes are generally understood, the magnitude and duration of processes responsible for formation of pavements vary with location. Desert pavements consist of a surface layer of closely packed gravel, usually one particle thick, that overlies a thin, gravel-poor vesicular A (Av) soil horizon. Desert pavements are a fundamental part of soil and landscape evolution of volcanic landforms (Wells et al. 1985, McFadden et al. 1986) and are found on a variety of landforms ranging from Holocene to Tertiary in age (Cooke and Warren 1973, Bull 1991). Pavements are important features in the southwestern U.S., where they have been used in subdividing and correlating Quaternary alluvial fans for studying neotectonics and Quaternary climatic change (Christenson and Purcell 1985, Bull 1991). Well-developed desert pavements are widespread features at YPG and the Lower Colorado Sonoran Desert (Lashlee et al. 2001).

Rock Varnish

One of the most striking features of arid landscapes is the nearly ubiquitous presence of rock varnish; a thin, dark, shiny film or coating, found on the surfaces of pebbles, boulders, and rock outcrops (Allen 1978). A typical rock varnish layer is less than half a millimeter deep on a rock's surface and is generally composed of about 60% clay minerals, 20 to 30% oxides of manganese and iron, and trace amounts of more than 30 other minor compounds (White 1990). The source of these materials is eolian (wind-blown) dust. The rarity of well-developed rock varnish on Holocene aged geomorphic surfaces suggests that the formation of continuous black varnish coatings requires at least 10,000 years and develops slowly, at a rate of a few micrometers per thousand years.

The upper surfaces of late Holocene and Pleistocene desert pavement clasts in the Sonoran Desert are covered with Mn-rich rock varnish (Lashlee and Rosenfeld 2001). The undersides of many clasts, particularly those on older, well-developed pavements, are covered with Fe-rich rock varnish. In Arizona's Lower Colorado Sonoran Desert, Elvidge and Collet (1981) estimated that 75% of rock outcrops are coated or show significant traces of rock var-

nish, that alluvial and colluvial materials may or may not be varnished, and that the environmental conditions for varnish formation still likely exist.

Study Area Control Sites

Surface I: Alluvial Fan. Three land surfaces, representing geomorphic processes typical in the overall study area, were studied in detail for ground verification (Fig. 36). Surface I is an alluvial fan centrally located in the Yuma Wash drainage basin (33° 07' 25" N, 114° 30' 02" W). A prominent feature of this geomorphic surface is its pronounced bar-and-swale topography (Fig. 37a). Clasts, which are almost entirely fine-grained igneous rhyolite, range in size from boulders on the proximal fan area, to cobble bars and small gravel-sized clast fractions in swales that meander across the rest of the surface. Rock varnish is comparatively immature, with clasts exhibiting a continuous coating of varnish with reddish-brown hue in the visible spectrum compared to the darker Mn-rich varnish typical of older pavements in Yuma Wash. Surface relief, rock varnish characteristics, and a young soil profile suggest that clasts were deposited and have been reworked by ephemeral braided streams since the early to mid-Holocene period, between 8000 and 12,000 years ago (ka).

Although a geologically young surface, desert pavement is sufficiently well developed in both bars and swales to preclude significant exposure of the underlying soil matrix. The alluvial fan also has significantly more vegetation (located predominately in drainage channels) relative to the other field sites.
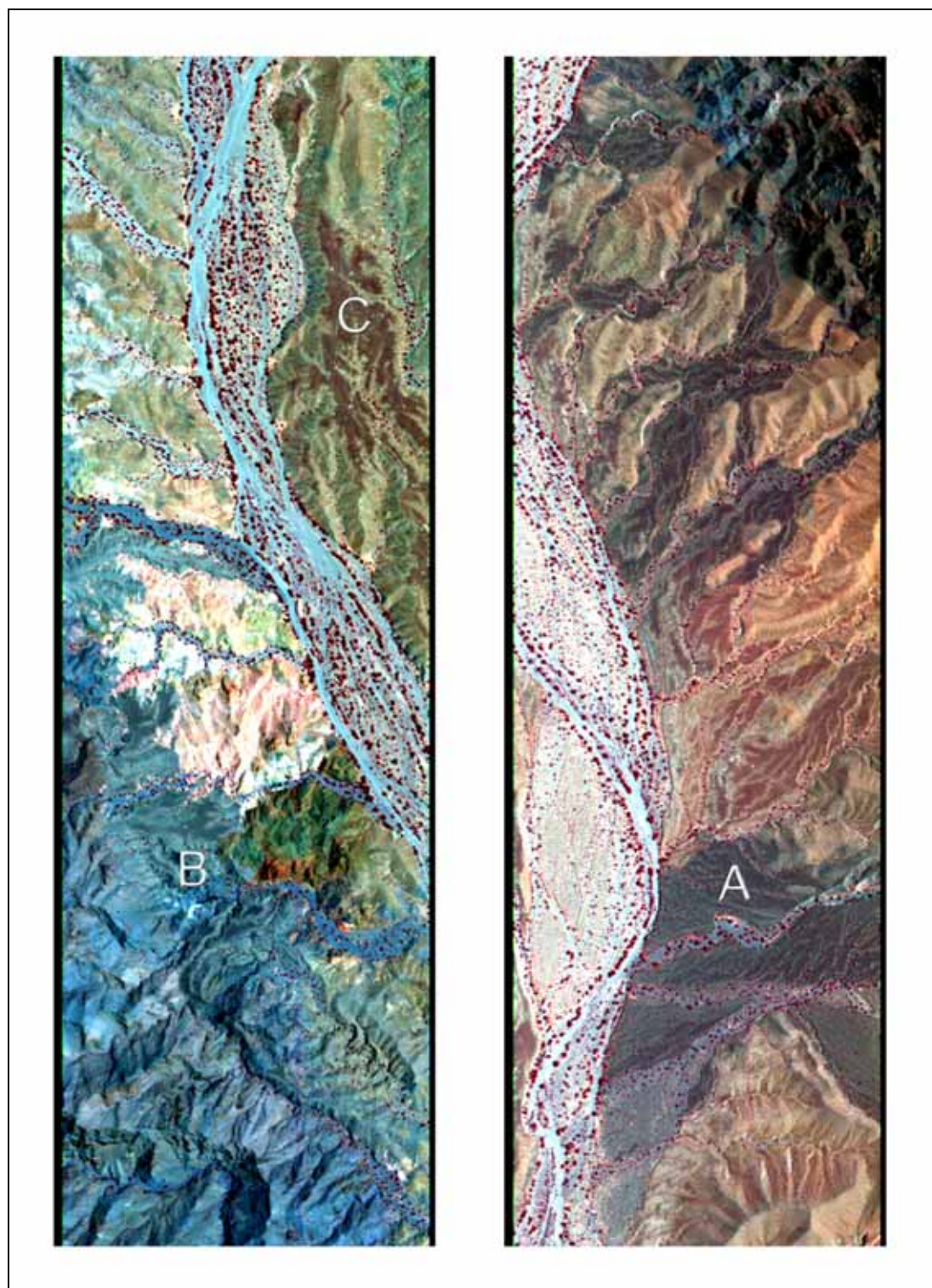
Figure 36.   HYDICE band 100, 50, 25 color composite images showing three gemorphic surfaces: A—alluvial fan; B—truncated pediment; and C—stream terrace.

a. Surface I: Holocene alluvial fan composed of igneous rhyolite.

b. Surface II: Mid Pleistocene pediment composed of a metamorphic mixture.

c. Surface III: Late Pleistocene stream terrace composed of fanglomerate.
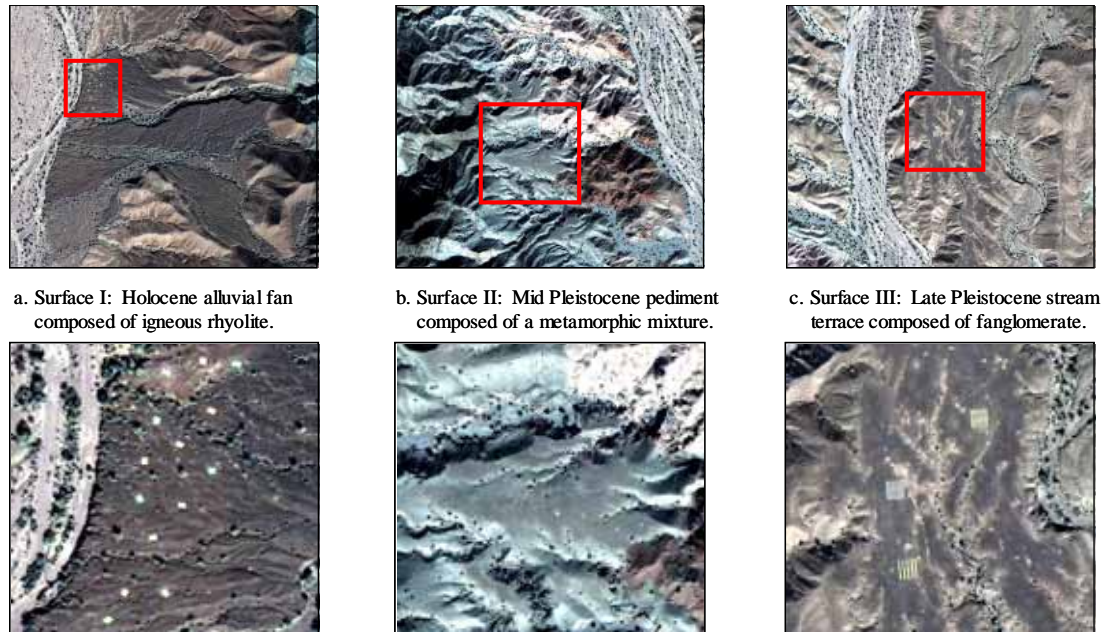
Figure 37. One-meter resolution IKONOS images of the three study sites in Yuma Wash. Surface I is young pavement exhibiting bar and swale topography. Surface II is intermediate in age, smooth, and poorly drained. Surface III has a well-developed desert pavement with a smooth, but dissected surface typical of older geomorphic surfaces in the Lower Colorado Sonoran Desert. Enlarged images are highlighted in red boxes. Figures 37a and 37c show calibration panels and stripe arrays, respectively, deployed for remote sensing studies.

Surface II: Pediment. Surface II is a pediment remnant located in the lower reach of Yuma Wash (33° 03' 25" N, 114° 30' 2" W). This surface has a topographically smooth, well-developed pavement, with a well-sorted, uniform clast size (Fig. 36b and 37b). Parent material is derived from the adjacent fault-bound Tertiary to Mesozoic metamorphic mountain (Sherod et al. 1997), resulting in heterogeneous clast lithology that includes metamorphic schist, gneiss, and quartzite. The angular to subangular shaped clasts are more loosely packed, exposing more soil matrix than the other control sites. There is also evidence of pavement damage by feral burros, suggesting natural biologic and geologic processes easily disturb the surface. Pavement clasts exhibit moderately developed, Mn-rich colored rock varnish compared to Surface I. However, varnish coatings on many clasts are discontinuous owing to foliation (schist), physical weathering by granular spalling (gneiss), and a general resistance to varnish development (quartzite). The pediment is poorly drained and generally devoid of vegetation. These observations indicate an older pavement whose original surface relief has

been smoothed over a longer exposure time. Estimated age of Surface II is from 12 to 70 ka, based on soils geomorphology data.

Surface III: Stream Terrace. Surface III (Fig. 36c and 37c) is a stream terrace located in the lower reach of Yuma Wash (33° 03' 59" N, 114 31' 36" W) across the main channel from the Surface II. The terrace is adjacent to and approximately 10 m above the main channel of Yuma Wash and, unlike most alluvial fans in the drainage basin that slope either to the east or west away from mountain ranges, Surface III slopes gently southward, toward the Colorado River. Additionally, the USGS has mapped this landform as composed of fanglomerate—potentially a collection of all possible lithologies present in Yuma Wash (Sherod et al. 1997). The smooth, planar desert pavement formed on Surface III is well-developed with angular to sub-angular clasts in a tightly packed mosaic. The surface is moderately drained with perennial vegetation located exclusively in medium density dendritic drainage channels that, like the landform slope, also trend in a southerly direction. These data indicate that the surface was deposited in a fluvial regime and long ago abandoned as a stable stream terrace. Surface III is distinguished from the other surfaces by its heterogeneous lithology; mature pavement with heavily varnished clasts; a well developed soil profile, including the deepest Av horizon and Stage III carbonate development; and Pleistocene age ranging from 70 to 200 ka.

Yuma Wash is composed of erosional and depositional landforms typical to desert landscapes of the southwest U.S. and much of what is known about arid geomorphology in general also applies to YPG. The three geomorphic surfaces chosen for this study would likely be generalized as Quaternary Alluvium on USGS 1:24,000 scale geologic maps, if they existed for Yuma Wash, when in fact each is a different landform developed from different geologic materials and geomorphic processes. They differ in age, clast lithology, soil profile maturity, and desert pavement development, including the amount and character of rock varnish, drainage, and vegetation characteristics. In summary, these surfaces are sufficiently distinct, yet representative of other regional geomorphic surfaces, to provide meaningful hyperspectral comparisons.

Methodology

A combination of laboratory, field, and imaging spectrometry techniques were performed to characterize surficial geologic materials and quantify hyperspectral reflectance at the three

ground control sites in Yuma Wash. Laboratory spectrometry (micro-scale measurements) was performed to quantify the spectral effects of rock coatings on desert pavement clast lithology. Field spectra (meso-scale measurements) were collected along transects to determine reflectance of each landform. These empirical ground verification spectral data are required for many quantitative remote sensing studies, such as mission-critical landscape modeling and simulation applications, and are certainly desirable for accurately mapping Quaternary geomorphic surfaces. Finally, imaging spectrometry data (macro-scale spectra) were collected and analyzed to measure reflectance and absorption features of the landscape.

Laboratory and Field Techniques

Geotechnical Data Collection. For each geomorphic surface, we identified transect locations on aerial photographs, then surveyed them in the field with a real-time differentially corrected Global Positioning System (GPS) system. Test data collected of monumented benchmarks in the area suggest that spatial accuracies acquired were about 0.2 m for x and y coordinates and about 0.4 m for elevations. Geomorphic surface characteristics were also recorded at each transect station, including desert pavement development (clast size, shape, arrangement, and texture), rock varnish type and condition, and relative surface topographic position.

Small areas of desert pavement were cleared of clasts, exposing the underlying soil matrix, at regularly spaced stations located along each transect. The number of stations varied for each surface, based on landform length. Samples of pavement clasts and the Av horizon soil were collected for laboratory analyses. Desert pavement clasts were subject to a variety of tests to identify physical and chemical properties of clast lithology and associated rock varnish. Petrographic analyses performed included scanning electron microscopy (SEM), energy-dispersive x-ray fluorescence (XRF), micro-image analysis, and optical microscopy techniques. These data provided information on rock type, mineralogy, and bulk chemistry; thickness and chemical composition of rock varnish coatings on individual clasts; and elemental maps showing distinctions between composition of host rock and varnish coatings. Soil tests included standard sieve and hydrometer analysis to determine grain size distributions (gravel, sand, silt, and clay) and Unified Soil Classification System category, as well as computer-assisted x-ray powder diffraction (XRD) to determine mineral composition. Additionally, a soil pit was excavated at each site and soil profile characteristics documented.

Laboratory and Field Spectra Collection. Laboratory and field spectrometry were collected using an Analytical Spectral Devices (ASD) FieldSpecFR spectroradiometer, which collects 1512 contiguous spectral measurements in the solar reflective wavelengths from 350 to 2500 nm (Analytical Spectral Devices 1995). Spectral resolutions are 3 and 10 nm for the 350- to 1000-nm and 1000- to 2500-nm wavelength regions, respectively. A 1.4-m fiber optic cable was used to transmit light reflected from targets to the instruments' three internal detectors, which were calibrated to reflectance using a portable spectralon white reference panel at each transect station.

Compared to vegetation reflectance, the shape of rock and mineral spectra tend to be invariant with respect to viewing geometry. However, the overall brightness of signatures varies with the amount of shadow present within the instruments field of view (Analytical Spectral Devices 2001). For geomorphic surfaces, the amount of shadow is proportional to desert pavement development in terms of surface roughness, as well as sun-angle geometry. Spectra of undisturbed desert pavement and cleared areas of exposed surface soil were collected such that each spectrum was an average of 25 different measurements. The FieldSpec FR acquired these spectra in about 200 milliseconds, which minimized atmospheric variations caused by wind. Data of each ground control site were collected during hours of direct solar illumination to minimize temporal effects of shadows.

Laboratory spectrometry was performed on individual desert pavement clast samples under controlled illumination conditions. The diffuse light source used was a Lowel Pro-lamp, a 14.5-V, 50-W, tripod mounted indoor laboratory light with its probe positioned 3 to 5 mm above each sample surface. We obtained 15 spectra from each clast sample, including five measurements from the varnished top, five from the varnished bottom, and five from the unvarnished cut rock surface. These data quantify the effects of manganese (top) and iron-rich (bottom) rock varnish on spectral reflectance of host rock lithology for comparison to both field and imaging spectrometer data (Fig. 38).
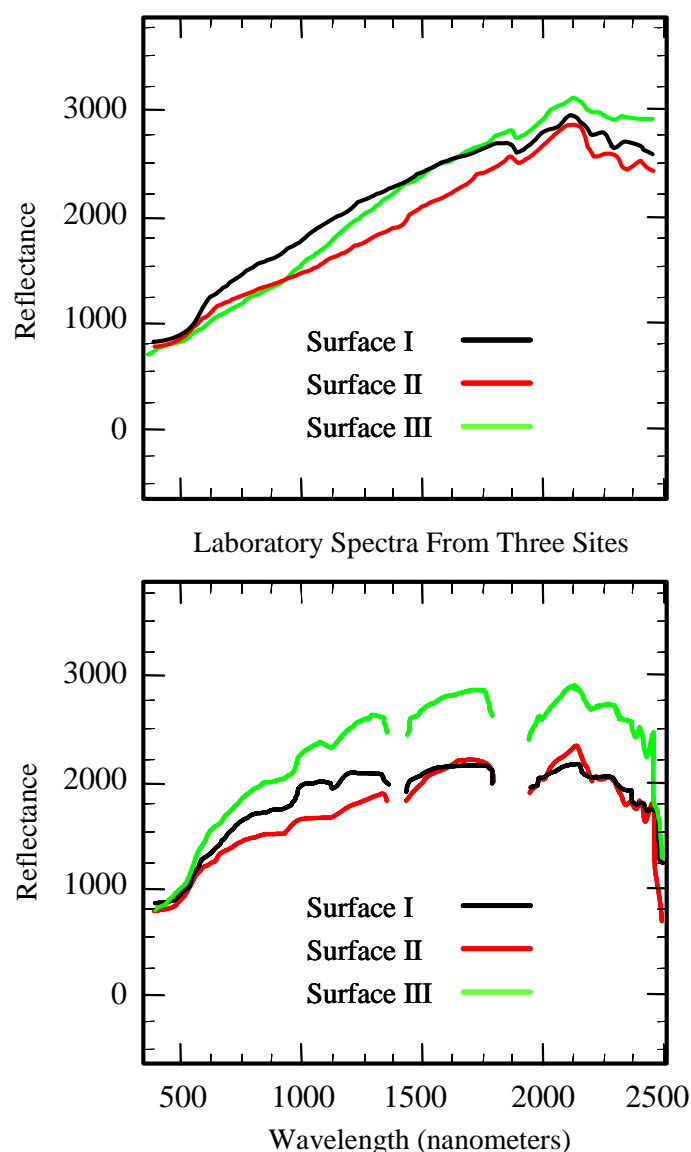
Figure 38. Average laboratory and AVIRIS image spectra of the three ground control sites

Av soil samples collected from each transect station were air dried, then sifted to remove the gravel fraction. An ASD FieldSpec Pro was used to collect spectra with a turntable-sampling accessory, again under controlled illumination conditions. After calibrating the instrument to a spectralon white reference standard, soil samples placed in Petri dishes were rotated under the fixed halogen light source while the FieldSpec collected signatures. The turntable has a 150-mm viewing area, a 53.2-mm spot size, and rotates at 22 rpm. For this study, 25 spectra were collected and averaged for each measurement saved as a signature and 10 concurrent measurements were acquired while the soil sample rotated beneath the instrument. These data

were collected in the YPG Laser Laboratory to ensure that no secondary light source adversely affected spectral measurements. Both laboratory and field spectra were compiled into spectral libraries and analyzed using Environment For Visualization of Images (ENVI) software (Research Systems Incorporated 2005).

a. Surface I: desert pavement.   b. Surface II: desert pavement.   c. Surface III: desert pavement and soil.
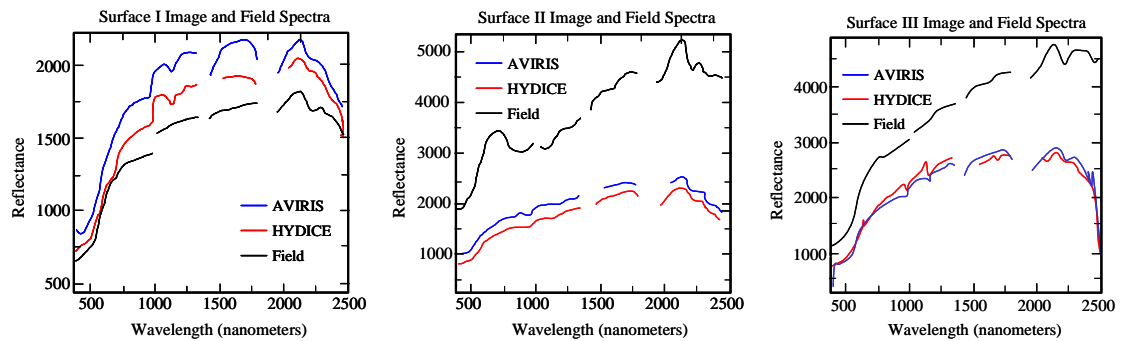
Figure 39. Ground photographs of desert pavements surfaces with field and image spectra for the three Yuma Wash ground verification sites.

Imaging Spectrometry Techniques

AVIRIS Data Collection. Airborne Visible Infrared Imaging Spectrometer (AVIRIS) data were acquired for a portion of the Yuma Wash drainage basin (Fig. 35) to record molecular absorption and particle scattering signatures of the landscape. AVIRIS is a push-broom sensor that measures upwelling radiance in the visible and near-infrared portions of the solar reflective spectrum from 400 to 2500 nm in 224 continuous spectral bands that have a nominal band spacing of 10 nm (Green et al. 1998). AVIRIS has been collecting data for diverse applications since becoming operational in 1989. The AVIRIS data used for this study were collected on 14 April 2002 from a Twin Otter turboprop fixed wing aircraft. The aircraft flew 4 km above ground level at 130 km/hour, resulting in an image pixel size of 3.8 m.

Data Calibration and Conversion to Apparent Surface Reflectance. Prior to delivery, the National Atmospheric and Space Administration (NASA) Jet Propulsion Laboratory (JPL) calibrated the AVIRIS data from raw digital numbers to radiance. These radiance values were converted to apparent surface reflectance using ACORN (Analytical Imaging and Geophysics 1995). ACORN is commercially available software that uses licensed MODTRAN4 technology to model the atmosphere (Berk et al. 1999) and calculate apparent surface reflectance without requiring ground measurements as input. However, ACORN's radiative transfer correction does require some user defined parameters to derive and model atmospheric absorption and scattering effects, which are then are used to invert radiance to apparent surface reflectance based on equations in Chandrasekhar (1960). AVIRIS data from three flight lines were required to cover the study area. ACORN was first run on each individual flight line without artifact suppression, and then a second time on each AVIRIS image using field spectra for single spectrum enhancement.

Data Correction. Numerical data quality inspection revealed that data from one flight line were spectrally shifted compared to the other datasets. Measurements from 10-× 10-pixel neighborhoods collected from adjacent, overlapping images were extracted and averaged to determine the amount of spectral shift and correction factors. The correction provided a closer match between AVIRIS runs. Each flight line was then spatially referenced and mosaicked using 1-m Digital Orthophoto Quads acquired from the USGS for positional control.

Image bands associated with water absorption features centered on 1400, 1900, and 2500 nm were identified by visual examination of reflectance spectra derived from image pixels and omitted from the analysis. The mosaicked image was also subset from its original dimensions to exclude image borders containing pixel values of zero to prevent those areas from skewing image statistics. Finally, dropped lines and pixels observed in the AVIRIS data were excluded from the analysis by applying a mask file identifying them as bad data values.

Data Reduction. An initial goal of many quantitative remote sensing investigations is to re-duce data dimensionality to a meaningful subset of image bands prior to applying computer-intensive processing algorithms. This is particularly true of the large data volumes associated with hyperspectral datasets. Because many minerals have diagnostic absorption features in the

SWIR wavelengths, the AVIRIS data were spectrally subset to 45 bands ranging from 2000–2439 nm.

These data were transformed using a Minimum Noise Fraction (MNF) algorithm. MNF determines the true dimensionality of a hyperspectral dataset through segregation of signal from noise, which allows a reduced number of bands containing most of the original variance of the input dataset to be used in subsequent processing (Boardman and Kruse 1994). As implemented in ENVI, MNF is modified from Green et al. (1988) as a two-cascaded Principal Components transformation. The first transformation, based on an estimated noise covariance matrix, decorrelated and rescaled noise in the data such that it had unit variance and no band-to-band correlation. The second iteration was a standard Principal Components transformation of these noise-whitened data.

Image Endmember Extraction. The resulting MNF bands were subject to Pixel Purity Index (PPI) analysis to identify spectrally extreme pixels that might represent image endmembers. Endmembers are reflectance spectra of well-characterized materials that mix to produce spectra equivalent to those pixels of interest in an image (Adams et al. 1995). The PPI projected data into *n*-dimensional spectral space and iteratively flagged those pixels positioned at the edges of the multidimensional data cloud (Green et al. 1988), resulting in a single band output image in which pixel values recorded the number of times each pixel was flagged as extreme. Most pixels in the PPI output image had values close to zero. However, spectrally extreme pixels were flagged many times and had substantially higher values. A total of 339 pixels with values of 80 or greater were identified as potential image endmembers.

The *n*-Dimensional Visualizer was then used to clump extreme pixels into groups with similar reflectance characteristics (Boardman 1993; Boardman and Kruse, 1994). Once grouped, these pixels were exported as discrete spectral endmembers. Initially, 38 endmembers were identified. Upon inspection, many of these endmembers were excessive, possessing similar reflectance characteristics. To decrease redundancy in the final endmember set, all endmembers were analyzed for similarity using the Spectral Angle Mapper (SAM) algorithm (CSES 1992, Kruse et al. 1993). Each spectrum in the original set of 38 was compared to all others. Spectra that had SAM similarity scores of 0.9 or greater *and* similar spectral shapes were

deemed to represent the same material. In this way, the original endmember set of 38 spectra was reduced to a final set of 18.

Mixture Tuned Matched Filtering. The Mixture Tuned Matched Filter (MTMF) algorithm (Chen and Reed 1987, Stocker et al. 1990, Yu et al. 1991, Harsanyi and Chang 1994, Board-man et al. 1995) was used to map the endmembers located in the study area. Because MTMF required an MNF transformed input file (with isotropic, unit variance noise), the 18 spectral endmembers were first transformed into MNF space. Matched filtering score results provide a means of estimating the relative degree of match to each endmember reference spectrum and approximate sub-pixel abundance. The infeasibility results (in noise sigma units) indicated the feasibility of the matched filter result. Correctly mapped pixels had a matched filter score above the background distribution (centered on zero) and a low infeasibility value. To flag positive matches, the score image was divided by the infeasibility image for each endmember, resulting in output images where higher values indicated closer matches to endmember spec-tra. These results were treated as endmember rule images and imported to the rule image clas-sifier tool, which allowed interactive adjustment of threshold factors for assignment of pixels to endmember classes. For consistency, a single threshold value of 0.012 was applied to all endmember score/infeasibility images, resulting in the classification image shown in Figure 40 and summarized in Table 5.

Table 5. Mixture tuned matched filter classification results.

Material	Number of pixels	Square kilometers	Percentage of area
Basalt	470,270	6.791	12.110
Lepidolite	135	0.002	0.003
Unknown	153,573	2.218	3.955
Holmquis	134,349	1.940	3.460
Montmorillonite	47,952	0.692	1.235
Muscovia	138,019	1.993	3.554
Muscovite 5	118,029	1.704	3.039
Soil	1,228,086	17.734	31.624
Illite	163,652	2.363	4.214
Montmorillonite	44,738	0.646	1.152
Chlorite	34,229	0.494	0.881
Soil	725,010	10.469	18.669
Kaosmectite	39,829	0.575	1.026
Vegetation	41,488	0.599	1.068
Rock Varnish	433,744	6.263	11.169
Unknown	110,327	1.593	2.841
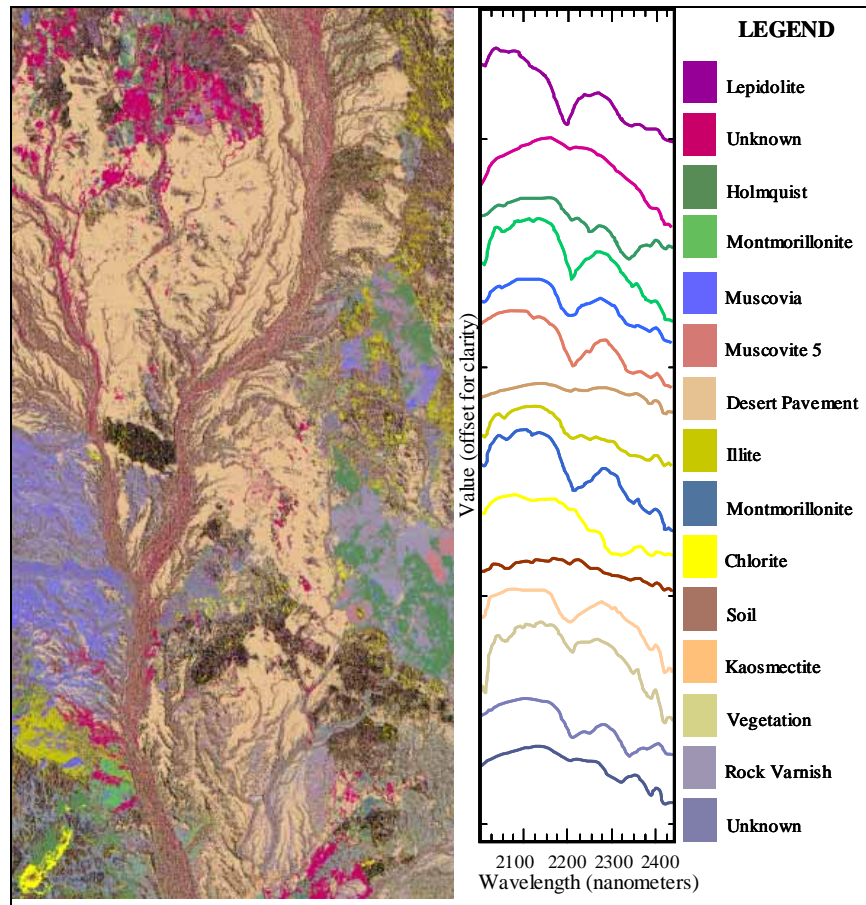
Figure 40. Mixture Tuned Matched Filter classification results and image endmember spectra.

Discussion

Results from MTMF and Spectral Feature Fitting techniques successfully identified many materials common to desert landscapes from the AVIRIS data. For the purpose of this discussion, landforms in the Yuma Wash study area are summarized as belonging to one of three major categories: 1) Tertiary bedrock uplands, 2) Quaternary alluvial geomorphic surfaces, and 3) the late Holocene ephemeral washes that drain them.

Bedrock Uplands

Three rock units are of primary concern to this study. Black areas in Figure 40 are highly correlated to zones mapped as basaltic andesite and rhyolite by Sherod et al. (1997). A majority

of Surface I, the alluvial fan, has also been classified with these materials, which matches geotechnical data showing that Surface I is composed almost entirely of rhyolite.

Another area of interest is the igneous extrusions in the northern portion of the study area. Mixed with basaltic andesite and olivine basalt is a red-colored class of unknown origin. Note that the secondary washes that drain this area to the south are clearly transporting large amounts of this material. This class also accounts for a significant portion of the main channel of Yuma Wash. Both observations suggest that this material is relatively unconsolidated and easily mobilized by intense, infrequent rainstorms of short duration. In fact, these areas corre-spond to areas mapped as volcanic ash-flow tuff and tuffaceous sedimentary rock units with varying degrees of imbrication (Sherod et al. 1997). Other geologic units include poorly indu-rated fanglomerate and sedimentary breccia, as well as air-fall tuff.

The third mountainous area of importance is the Mesozoic fault-bound metamorphic block located in southwest corner of the study area. This unit serves as a source area for desert pavement clasts located on Surface II. Clasts on the pediment surface are a metamorphic mixture consisting predominately of metamorphic gneiss, schist, and metaquartzite. This sur-face is bounded to the east by volcanic intrusions fine-grained rhyolite, andesite, and tuff (Fig. 36B). Other surficial materials identified in this area include the minerals chlorite, illite, montmorrilonite, and holquist. Chlorites are widely distributed in low-grade metamorphic rocks and as alteration products of ferromagnesian minerals (Bates and Jackson 1980). They are associated with and resemble mica minerals, including the two classes of muscovite identi-fied in the classification. In this study area, chlorite is a main component of chlorite schist and imparts the schistosity, or parallel arrangement, of its flakes, common to this upland unit.

Desert Pavement Surfaces

By far the largest class, covering almost 32% of the study area, is the "Desert Pavement" class. Based solely on spectral reflectance, this endmember was initially labeled as "Soil" when comparing its spectrum to the USGS spectral library of known materials. As shown in Figure 40, there is very little difference between the image endmember spectra of "Desert Pavement" and "Soil" classes in the 2000- to 2500-nm wavelengths. This observation in and of itself suggests a potential classification difficulty. Only after inspecting its spatial distribu-

tion in the study area was this class designated "Desert Pavement." So many different desert pavements having been combined into this single class is also problematic, given the known differences in geomorphic age and clast lithologies. This seems to confirm the hypothesis that many desert pavements are spectrally featureless; having no diagnostic absorption features recorded in the AVIRIS data. Together, the "Desert Pavement" and "Rock Varnish" classes combine to account for 43% of the study area, including Surfaces I and II and most other Pleistocene aged geomorphic surfaces.

Ephemeral Washes

The "Soil" class, concentrated in the ephemeral washes and was spatially and spectrally distinct as channel deposits, make up about 19% of the area. However, the "Desert Pavement" class is also present in drainage channels. While eolian soil and dust do contribute to pavement reflectance, the similarity between spectral signatures for desert pavements and channel materials and their co-occurrence in washes indicates a potential classification accuracy problem. As previously discussed, the volcanic tuff class is also abundant in throughout the washes, particularly adjacent to the ash flow source areas. Finally, vegetation, estimated to compose 5% or less of the region, covers only 1% of our study area, most of which is concentrated in drainage channels and along valley floors where sufficient residual soil moisture exists to support them.

Additional Data Analysis

The classification results for ground control sites warranted further analysis. AVIRIS data were revisited to determine if the three desert pavements surfaces used for ground verification could be more accurately delineated. The same spectral range was used (2000- to 2500-nm). However, the endmembers were averages of AVIRIS image spectra extracted from the surveyed transect stations at each ground control site. Image spectra were chosen rather than field spectra after a comparison to HYDICE image spectra of transects stations revealed a closer match between AVIRIS and HYDICE data (Fig. 39), and therefore greater confidence in the image-derived endmembers.

Although the HYDICE data in Figure 36 were available, they not used for quantitative spectral analysis because the datasets had both systematic and arbitrary horizontal and vertical striping

in many bands. Some of these bad bands were close to absorption features that might have proved useful in distinguishing some surficial materials. Detectors in pushbroom (or area array) sensors like HYDICE must be well-calibrated to each other or datasets can have spatially correlated noise components that are generally not handled well by noise estimations, such as shift difference or dark current procedures. If each line has different noise characteristics, striping often remains after the MNF noise-whitening iteration and could become a dominant part of the low MNF bands. This variance makes calculated endmember fractional abundances less precise and, if variance attributable to striping is large compared to the variance based on spectral classes, correct assignment of information classes may be more difficult and less accurate.

AVIRIS pixels with very distinct spectral features in the 2000- to 2500-nm range were masked such that only those pixels previously classed as "Desert Pavement" or "Rock Varnish" were used as input data. MTMF was applied again to map the three desert pavement endmembers across the study area. As before, the rule classifier tool was used to produce a ratio output image by dividing the MTMF output score image by the infeasibility image for each endmember. The same threshold value of 0.012 was then applied to identify pixels that closely matched the ground control sites in terms of high score and relatively low infeasibility. Figure 41 shows the resulting classification in which the ground control sites have been differentiated using image spectra.

Once again, Surface I was mapped with basaltic andesite igneous extrusions located throughout the study area. The critical difference; however, is that Surfaces II and III have been differentiated compared to the original classification and Figure 42 shows why. The continuum removed spectra of image endmembers used in this analysis show a close match in reflectance for Surfaces I and III. Continuum removal normalizes spectra between a range of 0.0 and 1.0 and accentuates absorption feature depth and position. Surface II has an important doublet absorption feature centered on 2350 nm that differentiates it from the others.
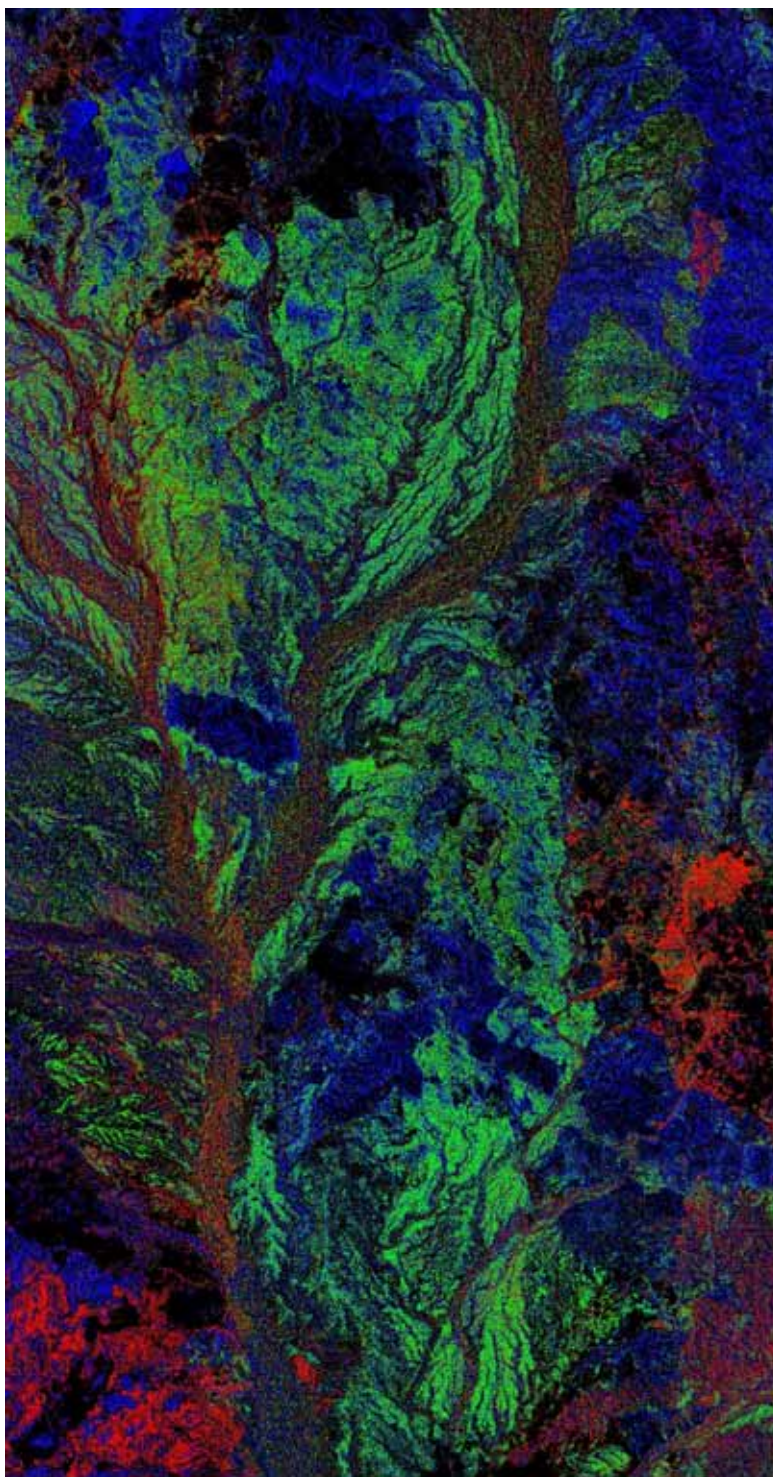
Figure 41. Mixture Tuned Matched Filter classification of desert pavements based on AVIRIS image endmembers extracted from each ground control site. Surface I matches are shown in blue, Surface II in red, and Surface III in green.
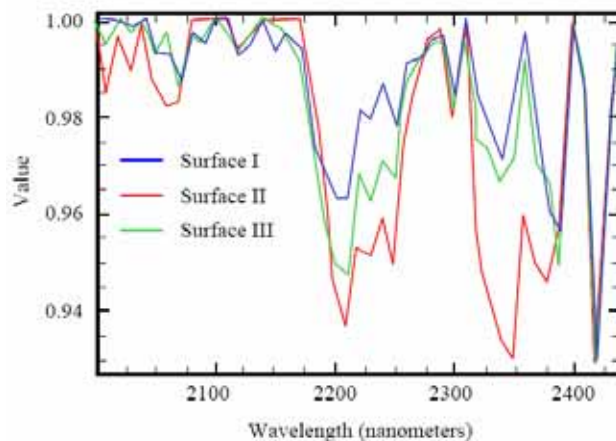
Figure 42.   Continuum removed, image-derived
endmembers for three ground control sites in Yuma
Wash.   Surface II exhibits an important absorption
feature at 2350 nm that helps differentiate it from the
other sites.

Conclusions

Mapping Quaternary geomorphic surfaces in arid and semi-arid environments requires an un-
derstanding of landforms, geomorphic processes, and the controls they exert on spectral re-
flectance. Geomorphic processes that dominate reflectance in the Sonoran Desert are desert
pavement and rock varnish formation, eolian silt deposition, and fluvial dissection. As re-
corded at spatial resolutions currently available, desert pavements are spectral mixtures in
which each pixel contains an integrated average reflectance of the surface materials present
within its bounds. The presence, chemistry, and condition of rock coatings are primary con-
siderations, particularly when applying new and emerging technologies such as hyperspectral
data analysis. The following discussion summarizes some important considerations related to
spectral reflectance of desert terrain in order of significance—rock varnish, lithology, soils,
and vegetation.

Rock Varnish

The degree to which rock coatings obscure lithologic information depends on the type of
coating formed, its chemistry, morphology, and condition, which is in turn controlled by com-

plex environmental factors (White 1990). In the Lower Colorado Sonoran Desert, well-developed Mn-rich rock varnish precludes lithologic mapping in the 400- to 1800-nm wavelength regions. Only the 2000- to 2500-nm wavelengths are available for lithologic discrimination. However, rock varnish often develops discontinuously on pavement clasts, first filling in low spots in the rock surface. As a result, pits and groves are often more heavily varnished than smoother areas. Varnish may also adhere differently to the various minerals on a single clast. It is not uncommon for banded rocks such as gneiss to be varnished such that lithology is obscured in the visible wavelengths on all but the banded minerals, which show through. Differential rates of erosion on heterogeneous desert pavement gravels also contribute to spectral variation. For example, granular rocks, such as sandstone and granite, may disintegrate before a varnish coat can form.

Clast Lithology

Desert pavement clast lithology can be homogeneous or heterogeneous and it is common for pavements in proximity to have very different lithologic and morphologic characteristics. The authors studied in detail three pavements with different stages of development that formed on different landforms in the Yuma Wash watershed at YPG. The youngest is an alluvial fan developed from mudflow and other alluvial deposits from a single canyon, whose surface was later covered by volcanic rhyolite deposited during a Holocene igneous extrusion event. This surface has homogeneous lithology, very consistent brownish-red rock varnish development, and exhibits a strong bar and swale topography typical of young desert pavements. The middle age pavement is a truncated pediment whose clasts are composed of a heterogeneous mixture of banded gneisses, foliated schists, quartzites, and other metamorphic rock, each exhibiting different rock varnish characteristics. Directly across the channel is a Pleistocene stream terrace composed of alluvial fanglomerate, a mixture of potentially every rock type present in drainage basin. Soils geomorphology suggests the ages of these pavements range from 8 to 12 ka, 12 to 70 ka, and 70 to 200 ka, respectively.

In addition to lithologic differences evident in the 2000- to 2500-nm wavelengths, differences in rock type and relative age also result in surface roughness variations (gravel and cobble size and shape) that may be observable in optical remote sensing data as variable amounts of shadow. One should reasonably expect more shadow on surfaces with bar and swale topogra-

phy, and terrain where boulder and cobble fields exist as compared to the older, flatter well-developed desert pavement surfaces. Because shadow varies with sun angle, the amount of shadow in the reflected solar spectrum changes both seasonally and temporally throughout the day.

Soils

Laboratory and field data collected for this study, including soil texture classification, chemical composition analysis, and extensive field spectrometry data, support the accretionary desert pavement formation model (Wells et al. 1985) that holds that the underlying soil matrix is composed of eolian dust accumulating above a vesicular Av soil horizon. Soil samples from Av horizons at different locations at YPG have similar texture and mineralogy and therefore similar hyperspectral signatures, regardless of the geologic age, or available parent material of individual surfaces. These data not only suggest that the dominant pedogenic process for pavement development is dust accumulation, but also that dust at YPG may originate from a single source area in the region. From a remote sensing perspective, this has a normalizing effect on spectral contributions of soils, as it is likely the same for different aged pavements. This allows remote sensing geomorphologists to concentrate on the more problematic interpretations of integrated rock varnish, clast lithology, and surface roughness. It is, however, common to have variable amounts of soil matrix exposed in different aged pavements as well as different locations of the same surface. For example, the edges of some pavements at YPG are often lighter colored because runoff in the form of concentrated sheetflow overturns and disperses pavement clasts to a greater extent than at the center of the surfaces. It is not the composition of soil matrix that changes, but rather the amount of soil matrix exposed that is recorded in remotely sensed data.

Vegetation

Vegetation on desert pavement surfaces is generally sparse and typically restricted to washes that drain them. A study of pavement surfaces of Yuma, Arizona (Musick 1975), found that underlying soils had a higher silt, clay, and salinity content than non-pavement soils in the area. As a result, pavements have slower infiltration rates, with little precipitation entering the soils compared to non-pavement soils, and precipitation that does enter the soil is held near the surface and evaporates quickly. Temperature extremes may also contribute to bareness of

these surfaces. While the average maximum daily temperature for July is 41°C (106°F), Cochran (1992) found that temperatures within 2.5 cm (1 in.) of the black, desert pavement gravels in Yuma often exceed 160°F during July and August. The authors also measured pavement soil temperatures of 150°F in July 1998 at YPG. The restriction of vegetation to drainage networks of desert pavements is a valuable indicator of drainage pattern and density, both in the field and in remotely sensed data.

Scale Dependency

Our analysis clearly shows that spectral reflectance of desert pavement surfaces is scale dependent. We analyzed three sites using laboratory, field, and imaging spectrometer data and found three distinct and increasing levels of spectral complexity. As the field of view from which spectra were calculated increased, atmospheric attenuation also increased, spectral sensitivity of the instruments decreased, and accurate classification of geomorphic surfaces became increasingly more problematic.

Natural surfaces are rarely composed of a single homogeneous material and desert pavements are no exception. Spectra from each image pixel are intimate mixtures of rock varnish, wavelength-dependent clast lithology reflectance, exposed soil and dust, and minor amounts of vegetation in various states of health. This spatial mixing of materials within areas represented by pixels is compounded by the addition of variable amounts of shade and shadow caused by differences in solar illumination owing to topographic effects and surface roughness. Linear spectral unmixing models assume no such interaction among materials, but appear to work well in many circumstances (Boardman and Kruse 1994). Our results indicate that geomorphic surfaces are often spectrally featureless because they generally do not exhibit diagnostic absorption features. Absorption features in laboratory spectra of individual components of these landforms (soil–rock) are often have diminished size or have modified shapes in field and imaging spectrometer data. The application of non-linear spectral mixing models may improve mapping composition and abundance of Quaternary geomorphic surfaces and are recommended for future studies.

Acknowledgements

References

Allen, C.C. (1978) Rock varnish of the Sonoran Desert—Optical and electron probe microanalysis. *Journal of Geology*, **86**: 743–752.

Analytical Imaging and Geophysics (2002) ACORN 4.0 user's guide. ImSpec LLC.

Analytical Spectral Devices, Inc. (1995) *Environment For Visualization of Images Technical Guide*. Boulder, Colorado, pp. 24–28.

Armbruster, R.E. (2003) Testing and Evaluation: Positioned to support the 21st century Army. ATEC Magazine. USATEC, CSTE-PA, Alexandria, Virginia, pp. 1.

Berk, A., Anderson, G.P., Bernstein, L.S., Acharya, P.K., Dothe, H., Mathew, M.W., Adler-Golden, S. M., Chetwynd, J.H., Richtmeier, S.C., Pukall, B., Allred, C.L., Jeong, L.S., and Hoke, M.L. (1999) MODTRAN4 radiative transfer modeling for atmospheric correction. In *SPIE Proceedings, Optical Stereoscopic Techniques and Instrumentation for Atmospheric and Space Research III,* Volume 3756.

Bern, C.M. (1995) Land condition—Trend analysis installation report, Yuma Proving Ground, Arizona, 1991–1994. Center for Ecological Management of Military Lands, Colorado State University, Fort Collins, Colorado.

Boardman, J.W. (1993) Automated spectral unmixing of AVIRIS data using convex geometry concepts. In *Summaries, Fourth JPL Airborne Geoscience Workshop*, JPL Publication 93-26, Volume 1, pp. 11–14.

Boardman J.W., and Kruse, F.A. (1994) Automated spectral analysis: A geologic example using AVIRIS data, north Grapevine Mountains, Nevada. In *Proceedings, Tenth Thematic Conference on Geologic Remote Sensing*. Ann Arbor: Environmental Research Institute of Michigan, pp. I-407–I-418.

Boardman, J.W., Kruse, F.A., and Green, R.O. (1995) Mapping target signatures via partial unmixing of AVIRIS data. In *Summaries, Fifth JPL Airborne Earth Science Workshop*, JPL Publication 95-1, Volume 1, pp. 23–26.

Bull, W.B. (1991) *Geomorphic Response to Climatic Change.* New York: Oxford Press.

CSES (1992) SIPS user's guide, spectral image processing system, version 1.2. Boulder, Colorado: Center for the Study of Earth from Space, p. 88.

Chandrasekhar, S. (1960) *Radiative Transfer*. New York: Dover, pp. 1–393.

Chen, J.Y., and Reed, I.S. (1987) A detection algorithm for optical targets in clutter. *IEEE Transactions on Aerospace Electronic Systems*, **AES-23**(1).

Christenson, G.E., and Purcell, C. (1985) Correlation and age of Quaternary-fan sequences, Basin and Range Province, Southwestern United States. In *Soils and Quaternary Geology of the Southwestern United States* (Weide, D.L., Ed.). Geological Society of America, Special Paper 203, pp. 115–122.

Cooke, R.U., Warren, A., and Goudie, A. (1993) *Desert Geomorphology.* London: UCL Press.

Cooke, R.U., and Warren, A. (1973) *Geomorphology in Deserts.* London: Batsford, Ltd.

Dohrenwend, J.C. (1987) Basin and Range. In *Geomorphic Systems of North America* (W.L. Graf, Ed.). Geological Society of America Centennial Special Volume 2, pp. 303-342.

Elvidge, C.D., and Collet, C.J. (1981) Rock varnish in Arizona, distribution, and spectral characteristics. In *Technical Papers of the American Society of Photogrammetry, ASP-ACSM Fall Technical Meeting, San Francisco*, pp. 215–222.

Farr, T.G., and Chadwick, O.A. (1996) Geomorphic processes and remote sensing signatures of alluvial fans in the Kun Mountains, China. *Journal of Geophysical Research,* **101**(E10): 23,091–23,100.

Fischer, A.F. (1991) Mapping and Correlating Desert Soils and Surfaces With Imaging Spectrometry. In *Proceedings of the Third Airborne Visible / Infrared Imaging Spectrometer (AVIRIS) Workshop.* NASA/JPL Publication 91-28, pp. 23.

Gillespie, A.R., Kahle, A.B., and Palluconi, F.D. (1984) Mapping alluvial fans in Death Valley, California, using multi-channel thermal infrared images. *Geophysical Research Letters,* **11**(11): 1153–1156.

Goetz, F.H. (1992) Imaging spectrometry for Earth observations," *Episodes*, **15**(1): 7.

Green, A.A., Berman, M., Switzer, P., and Craig, M.D. (1988) A transformation for ordering multispectral data in terms of image quality with implications for noise removal. *IEEE Transactions on Geoscience and Remote Sensing*, **26**(1): 65-74.

Green, R.O., Eastwood ,M.L., Sarture, C.M., Chrien, T.G., Aronsson, M., Chippendale, J.A., Pavri, B.E., Chovit, C.J., Solis, M., Olah, M.R., and others (1998) Imaging spectroscopy and the Airborne Visible/Infrared Imaging Spectrometer (AVIRIS). *Remote Sensing of the Environment*, **65**:227–248.

Harsanyi, J.C., and Chang, C.I. (1994) Hyperspectral image classification and dimensionality reduction: An orthogonal subspace projection approach. *IEEE Transactions on Geoscience and Remote Sensing*, **32**: 779–785.

Hoffbeck, J.P., and Landgrebe, D.A. (1996) Classification of remote sensing images having high spectral resolution. *Remote Sensing of Environment*, **57**: 119–126.

Kierein-Young, K. (1995) Integration of quantitative geophysical information from optical and RADAR remotely sensed data to characterize mineralogy and morphology of surfaces. PhD Dissertation, University of Colorado, Boulder.

Kruse, F.A., and Lefkoff, A.B. (1993) Knowledge-based geologic mapping with imaging spectrometers. *Remote Sensing Reviews*, **8**: 3–28.

Kruse, F.A. (2005) Comparison of ATREM, ACORN, and FLAASH atmospheric, corrections using low-altitude AVIRIS data of Boulder, Colorado. Boulder, Colorado: Horizon Geo-Imaging, LC.

Kruse, F.A., Lefkoff, A.B., Boardman, J.B., Heidebrecht, K.B., Shapiro, A.T., Barloon, P.J., and Goetz, A.F.H. (1993) The Spectral Image Processing System (SIPS)—Interactive visualization and analysis of imaging spectrometer data. *Remote Sensing of Environment*, *Special issue on AVIRIS*, **44**: 145–163.

Lashlee, J.D., and Rosenfeld, C. (2001) Laboratory spectrometry of rock coatings: Implications for land management activities in the arid Southwest. In *Proceedings of the Environmental Testing Workshop, 29–30 November 2000*. U.S. Army Test and Evaluation Command, Washington, D.C.

Lashlee, D., Briuer, F, Murphy, W., and McDonald, E. (2002) Geomorphic mapping enhances cultural resource management at the U.S. Army Yuma Proving Ground, Arizona, USA. *Arid Land Management,* **16**: 213–229.

McFadden, L.D., Ritter, J.B., and Wells, S.G. (1989) Use of multiparameter relative-age methods for age estimations and correlation of alluvial fan surfaces on a desert piedmont, eastern Mojave Desert, California. *Quaternary Research*, 276–290.

Mustard, J.F., and Sunshine, J.M. (1999) *Remote Sensing for the Earth Sciences: Manual of Remote Sensing*, 3rd ed., Volume 3. New York: John Wiley and Sons, Inc.

Sherod, D.R., Tosdal, R.M., and Haxel, G.B. (1997) Geologic map of the Picacho, Picacho NW, Picacho SW, and Hidden Valley 7.5' quadrangles, Arizona and California. Menlo Park, California: U.S. Geological Survey.

Stocker, A., Reed, I.S., and Yu, X. (1990) Multidimensional signal processing for electrooptical target detection. In *Proceedings, SPIE International Society of Optical Engineering*, Volume 1305.

Wells, S.G., Dohrenwend, J.C., McFadden, L.D., Turrin, B.D., and Mahrer, K. (1985) Late Cenozoic landscape evolution on lava flow surfaces of the Cima volcanic field, Mojave Desert, California. *Geologic Society of America Bulletin,* **96**: 1518–1529.

White, K. (1990) *Spectral Reflectance Characteristics of Rock Varnish in Arid Areas,* Special Paper 46. University of Oxford Press, pp. 1–31.

Williams, M.L. (2002) AFOTEC: Operational test and evaluation challenges: modeling and simulation. *Journal of the International Test and Evaluation Association: Modeling and Simulation Applications in T&E*, **23**(1): 17–20.

Yu, X., Reed, I.S., and Stocker, A.D. (1991) Comparative performance analysis of adaptive multispectral detectors. *IEEE Transactions on Signal Processing*, **41**(8).

CHAPTER 6—THE CHAMELEON CONCEPT: HYPERSPECTRAL REMIXING FOR SYNTHETIC LANDSCAPE MODEL GENERATION

David Lashlee, Stefanie Tompkins, Charles Rosenfeld, and Jon Kimerling

Abstract

Chameleon is an analytical methodology and software system designed to generate spectrally accurate digital terrain models for simulation applications. Using laboratory, field, and imaging spectrometer measurements as foundation data, terrain analysts can simulate environmental change by embedding spectrally accurate representations of targets and other real and virtual objects from hyperchip libraries; simulate use of pre-visual and visual vegetation stress as calculated from spectral signature libraries; and drape camouflage or apply obscurants. Spectra of background materials can be modified on a neighborhood, per-pixel, or sub-pixel basis, or conversely the entire hypercube can be affected at once. Chameleon uses linear spectral unmixing to decompose each pixel in an image into spectral endmembers. Tools are provided for mathematically manipulating these fractional abundances and introducing new spectral information. Sub-pixel percentages of spectral endmembers (including vegetation, soils and surficial geologic materials, targets, shade, and shadow) can be altered and camouflage, cover, and concealment materials added. Chameleon then uses remixing algorithms to regenerate synthetic, but spectrally accurate, terrain models. By incorporating high-resolution elevation, sun angle geometry, and historical weather data, the landscape becomes a hyperspectral "Chameleon"—able to change spectral properties based on multitemporal empirical measurements, requirements identified for developmental and operational tests, or defined by specific simulation scenarios. In addition to the solar reflected spectrum, Chameleon can be extended to thermal infrared and RADAR signatures. The ability to generate temporally dynamic arctic, desert, temperate, and tropic digital terrain models for any time of day, any day of the year, supports terrain data requirements for improvements in database reuse, dynamic landscape generation, and hypothesis testing. Applications include virtual simulations of environments, detection of environmental change, disaster assessment, and mitigation planning.

Keywords: Hyperspectral, Imaging Spectrometry, Synthetic Environments, Terrain Modeling

Introduction

Army Test and Evaluation Command

The Army Test and Evaluation Command (ATEC) is the U.S. Army's premiere Test and Evaluation (T&E) organization. Its mission is to plan, conduct, and integrate developmental and operational tests of military equipment, as well as provide independent evaluations of test results to decision makers, to ensure Warfighters are equipped with effective weaponry and soldier systems. On average, ATEC conducts 1100 tests and evaluations daily—on everything from boots to ballistic missiles—in the coldest, hottest, driest, and most humid natural environments on earth (Armbruster 2003).

ATEC consists of three subordinate Commands. Developmental Test Command (DTC) conducts rigorous performance tests on weapons systems and materiel under controlled conditions on highly instrumented ranges and test courses. Products of DTC include unbiased technical data on system design, feasibility, performance, safety, and risks collected the during system development stage. The Operational Test Command (OTC) performs tests to confirm system performance in realistic battle conditions, including real systems, soldiers, and threats. Finally, the Army Evaluation Center (AEC) evaluates technical data obtained from DTC and OTC Testing to determine system effectiveness, suitability, and survivability.

Given current economic trends, the T&E process may be pressured to shorten tests in the future, either by testing more quickly or by not testing as much (Seiglie 2002). In turn, this will force Test Centers to develop infrastructures that meet the needs of their customers and implement acquisition strategies that allow for efficient and effective support of new and emerging programs. In both the near and far term, ATEC will need to adapt to technological changes in instrumentation, data processing, and data analysis. Modeling and Simulation (M&S) may be used more in the future, not only to enhance operational realism of the test environment, but also to support more economical, timely, and controlled test execution (ATEC 2002).

Modeling and Simulation

Guidance for using M&S in T&E is given in USATEC Memorandum 73-21, *Simulation Technologies Supporting Test and Evaluation* (December 2002) and Army Regulation AR 5-11, *Management of Army Models and Simulations* (July 1997). Accredited models and simulations are most applicable when used to gain insight on system performance in situations where we cannot, or should not, test because of resource, range, security, or safety limitations (ATEC 2002). Nuclear, biological, and chemical weapons are some obvious examples. Another classic example of M&S—long used and considered valid for T&E applications—is constructing synthetic environments to simulate performance of a real system, such as electronic warfare systems (Williams 2002).

DoD Simulation, Test, and Evaluation Process guidelines state, "Simulation and test are not competing functions. They are complementary and mutually supportive approaches to understanding weapon system performance". Figure 43 illustrates how simulation and physical testing are related to evaluation. Both are influenced by evaluation requirements and provide information for the evaluation–decision–action process (Waite 2002). In addition, they are both clients to one another's information-server functions: simulation supports test planning and analysis; testing supports simulation validation.
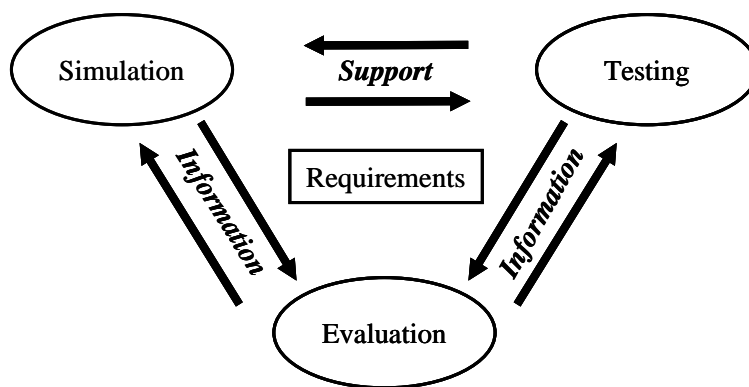

Figure 43. Simulation supports both testing and evaluation.

Distributed Testing and Training Applications

A primary objective of virtual simulation is to immerse the observer in a synthetic environment that accurately depicts the terrain, environmental conditions, and processes of interest. Today's simulation architecture consists of sets of heterogeneous, but interoperable, training systems that are distributed across computer networks. As a result, traditional visual representations of the landscape needed to operate a single environment simulator have been replaced by requirements for more complete and correlated synthetic environments that include seamless space, atmosphere, terrain, and ocean data. In addition, distributed computer systems allow for more sophisticated computer models and landscape simulations needed to match increasing complexity of environmental change and impacts. As a critical precondition to simulation interoperability, correlated synthetic natural environments are costly in terms of both time and money to produce and often represent a programmatic risk for distributed testing and virtual training applications.

Perhaps the greatest application of virtual models is the ability to efficiently create the most realistic operational environment possible for a system under evaluation (Barr 2002). Synthetic Environment (SE) is defined as "simulated representations of the expected physical environmental influences, both natural and man-made, on a system or procedure. Virtual models can be any combination of (virtual) simulations or (physical) stimulators, including the input and output data description, as well as analytic models and time ordered archived data." While dynamic simulations will never completely eliminate the need for physical testing, they can extend the range of test conditions into virtual environments and conditions that cannot be accessed "on demand."

The Army is leading an effort to develop a common synthetic environment for simulation, Hardware-In-The-Loop testing, and distributed testing of multiple systems, or families of systems, such as the Future Combat System (FCS). This common environment consists of high fidelity, high resolution synthetic scenes of test and training ranges, including digital terrain models, digital surface models, two-Dimensional (2-D) and three-Dimensional (3-D) surface objects, atmospherics, soil properties, and other geospatial data necessary to accurately replicate the of a test site. These databases are intended to be accessible to developers, testers,

trainers, and third party application developers—Government, private sector, and academia—through an open architecture information technology network that possesses high data throughput and well-defined interfaces to the synthetic scene databases. When established, this common simulation and test environment will be used to fully develop and test systems before, during, and after fabricating hardware. A few of the anticipated applications include virtual testing of manned and unmanned vehicles over digital terrain; virtual testing of chemical and biological agent sensors through the introduction of metrology and fluid dynamics into the scene; evaluation of ground sensors; testing of mine detection systems and improvised explosive devices; and testing of thermal imagers (Snyder et al. 2005).

Expanded Applications

The role of synthetic environments may be extended to a host of civilian applications of National and global importance. Obvious extensions of military virtual simulations are direct applications to Homeland Security, such as disaster simulations, impact assessments, and mitigation planning. Security planning applications could use high resolution LIDAR terrain mapping with hyperspectral image data to visualize possible surface-to-air missile launch sites along runway approaches, to identify the cover and concealment areas that must be monitored. Striking examples of change detection applications include the destruction of the World Trade Center by deliberate attack in 2001, and the disaster impacts of the Indian Ocean tsunami of 2005. Mitigation efforts are substantially enhanced by rapid assessment of changes, near real-time detection of priority targets, and simulations of planned recovery efforts. Post-disaster response operations often focus on search, rescue, and recovery, which may be substantially obscured by "debris fields" acting as an upper canopy. Composition and abundance maps of building materials within such a debris field, and sub-pixel influences of specific target signatures, might be used to identify high probability search areas. Damage assessment and insurance adjustments could be expedited through the combined terrain and spectral changes observed in high spatial and spectral libraries of urban areas, where, as an example, merged hyperspectral and LIDAR data are available.

Long-term environmental change may be evaluated through early detection of natural and man-made "precursor" targets, whether they be geomorphic (such as an increase in rockfalls and glacial crevasses in alpine terrain), biological (such as shifting ecosystem boundaries or

oceanic photo-plankton distributions), or anthropomorphic (crop type adjustments, land cover, or water resource changes). Virtual simulation technology will play a prominent role in planning global adaptation to changing environmental conditions. Regional applications conceivably might include the use of hyperspectral red edge/blue shift detection of pre-visual vegetation stress to monitor the effects of groundwater withdrawal or water conservation efforts.

Purpose and Scope

The purpose of this chapter is to summarize new hyperspectral data analysis techniques developed to produce high spectral resolution multi-temporal synthetic landscape models for modeling and simulation applications. The general procedure is based on linear spectral unmixing. Custom software tools are used to mathematically manipulate spectral reflectance signatures in the solar reflected spectrum to customize surface material composition and abundance at the sub-pixel level. Innovative linear spectral remixing algorithms are then used to rebuild synthetic, but spectrally accurate, terrain models. These image processing techniques are illustrated with hyperspectral image cubes of two environmental extremes of current interest to the military: 1) a relatively complex arid landscape in the Lower Colorado Sonoran Desert in southwest Arizona, and 2) a double canopy tropical forest in the Republic of Panama. Although the examples reported herein are limited in scope to airborne field and imaging spectrometer measurements in the 400- to 2500-nm wavelength range, Chameleon software works equally well with multispectral data, and the Chameleon concept can be extended to ultraviolet, thermal, and even radar wavelength regions.

Imaging Spectrometry

Hyperspectral Data

Imaging spectrometry (IS), also known as hyperspectral remote sensing, is defined as the acquisition of images in hundreds of registered, contiguous spectral bands, such that for every picture element (pixel) it is possible to derive a complete reflectance spectrum (Goetz 1992). Initial investigations demonstrated that mineralogical information could be automatically extracted from imaging spectrometer data (Hunt 1987) and that those classification techniques could be extended to other terrestrial surface materials (Kruse and Lefkof 1993). These early

successes in geological applications were possible because minerals maintain absorption features at specific wavelengths, regardless of changes in seasonality and illumination conditions. Over the last decade, improvements in both sensor technology and spectral processing algorithms have significantly improved our ability to identify surface materials remotely (Mustard and Sunshine 1999). Also during this time, progress has been made toward discriminating the spectral contributions of different materials in mixed pixels, resulting in the ability to quantitatively extract sub-pixel composition and relative abundance information.

Hyperspectral image data (HSI) are unique in that they are both a set of spatially contiguous spectra and a set of spectrally contiguous images (Fig. 44). As a result of this enhanced data dimensionality, hyperspectral data analysis techniques are fundamentally different than other remote sensing methods. Thematic mapping from aerial photography has traditionally relied on subjective interpretations by human analysts. Digital image processing of multispectral imagery (MSI) has typically involved computer processing and statistical data treatments, resulting in probability-based classification results. In contrast, imaging spectrometry is deterministic, in many cases allowing direct identification of surface materials based on known material laboratory or field measured spectra. Information extraction techniques algorithms developed for MSI are not particularly well-suited for HSI.
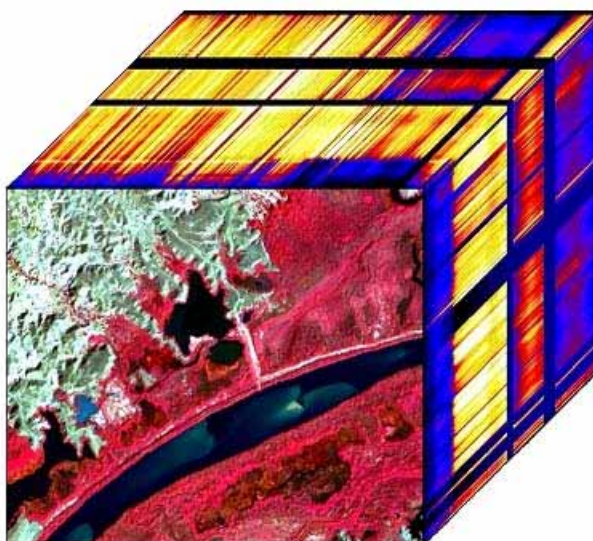

Figure 44. HYDICE hyperspectral image cube (hypercube) of a portion of the Colorado River.

Spectral Mixture Analysis

Spectral Mixture Analysis (SMA) is an approach to modeling and deconvolving the mixed signatures of multiple materials within a given pixel in a spectral image. Over the past 15 years, three demonstrated strengths of SMA have led to its popularity as a tool for analyzing spectral image data. First, SMA is a physically based model that transforms spectral data (radiance or reflectance) into physical variables, namely the sub-pixel abundances of endmember components within each pixel in a scene. Second, it provides a means to detect materials that are present entirely at sub-pixel levels, such as sparse vegetation in an arid environment (e.g., Smith et al. 1990a, b). And third, it provides as output quantitative information that can in turn be incorporated into models of surface processes (e.g., Blount et al. 1990, Elmore et al. 2000, Mustard 1993).

The underlying assumption of SMA, given linear mixing systematics, is that each pixel on the surface is a physical mixture of multiple components weighted by surface abundance, and the spectrum of the mixture is a linear combination of the endmember reflectance spectra. As illustrated in Figure 45, in the most general approach to SMA, a set of endmembers is selected from an image cube ("image endmembers") that best accounts for the cube's spectral variance within a constrained, least-squares mixing model (Adams et al. 1993, Gillespie et al. 1990). Ideally, these image endmembers can then be compared to "reference endmembers," which are field or laboratory spectra, for calibration and interpretation of the image data. The abundance of the endmembers within the image (represented by material abundance maps) can be used to investigate physical processes that are related to surface abundance, such as ecosystem models and change detection studies. Because these abundance maps are quantitative and physically meaningful, they are more easily incorporated into such studies than the results of simple classification models or purely statistical analytical methods (such as PCA).
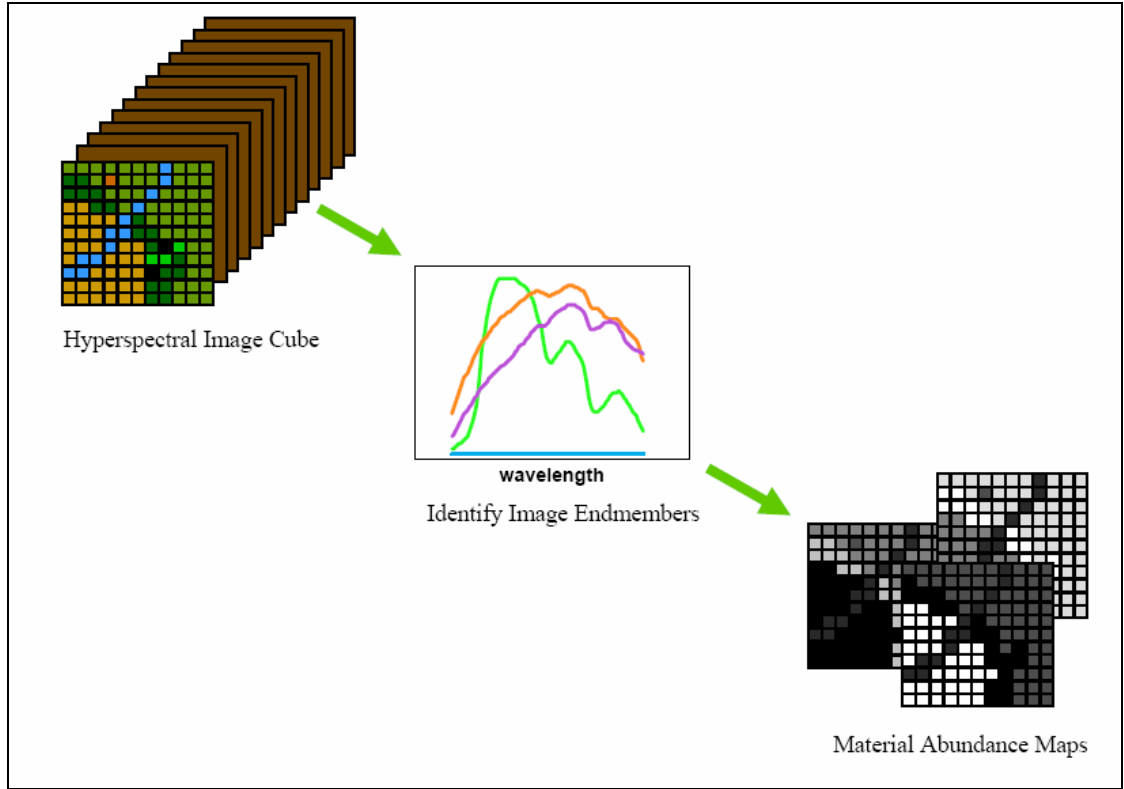
Figure 45. Schematic illustration of mixed pixel environment and linear mixing of endmember spectra. Material abundance maps are the building blocks for Chameleon.

The equations controlling SMA are:

$$R_b = \sum_{i=1}^{m} f_i r_{ib} + E_b \tag{1}$$

$$\sum_{i=1}^{m} f_i = 1.0 \tag{2}$$

where R_b is the reflectance of a pixel at band b, f_i is the fractional abundance of endmember i (from a total of m endmembers), r_{ib} is the reflectance at band b of endmember i, and E_b is the residual error in band b of the model fit. In addition to E_b, the root-mean-square (RMS) error is calculated for each pixel over all bands, as given by:

$$E_{RMS} = \sqrt{\frac{\sum\limits_{b=1}^{n} E_b{}^2}{b}} \hspace{3cm} (3)$$

where n = the number of bands. Further background and details on SMA applications are given in Adams et al. (1993) and Mustard and Sunshine (1999). The endmember spectra (r_{ib}) are typically determined from the image, and the fractions (f_i) are calculated using one of a variety of solution methods (commonly simple least squares or singular value decomposition). Parameters such as error to the model fit (E_b and E_{RMS}), pixels with unrealistic fractional abundances ($f_i < 0$ or $f_i > 1$), and spatial coherency of endmember materials provide critical limits on the validity of the endmembers.

Endmember Selection

Although many past studies have used reference endmembers (e.g., Adams et al. 1995) from a spectral library or from field measurements, they are generally more effective in multispectral imagery (MSI) data, whereas image endmembers have been found to be more robust in HSI. The broad bands of MSI data mask a great deal of subtle spectral variability, as HSI data do not. For reference endmembers to effectively model HSI data, removal of sensor and atmospheric effects must be nearly perfect—a condition that rarely occurs outside the laboratory. Thus, image endmembers are preferred and for this study, selected using an algorithm called Abacus®[2]. Within Abacus are successfully implemented many key decision making steps that an analyst makes in SMA. However, Abacus orders these steps in a way that leads to far fewer false steps and fewer refinements of endmember selection. The approach has been compared favorably to manual endmember selection by highly experienced analysts (Sunshine et al. 1999), and is particularly well suited for modeling background materials (Fig. 46).
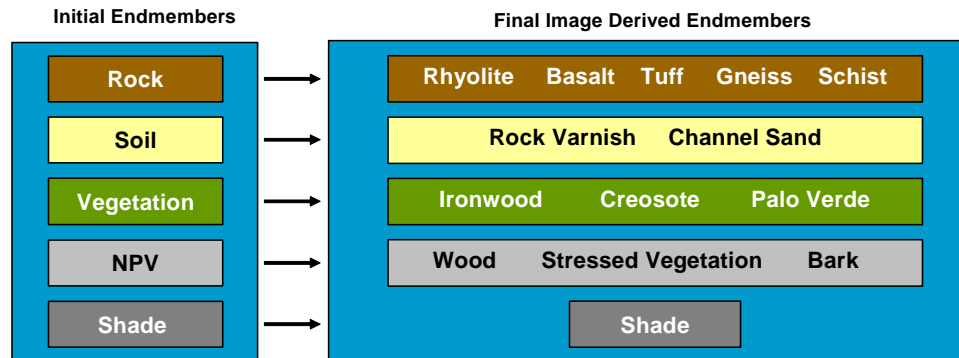
---

[2] U.S. Patent number 6,608,931

Figure 46. Initial and final image endmember extraction process.

Linear Remixing of Hypercubes

In the Chameleon approach, the component parts of an unmixed hyperspectral image—that is, the endmember spectra and the material abundance maps—can be used to make changes to the scene at either subpixel or superpixel levels. For subpixel changes, there are two basic methods for modifying the data:

1. The abundance of a given material may be changed, either in a localized area (a "region of interest," or ROI) or across the entire scene. (If the amount of one endmember is increased, the others are decreased proportionately.)

2. The type of material represented by the endmember itself can be changed. In this case, the spectrum of a different material can replace one of the endmembers.

In either or both options 1 and 2, after changes are made, the scene is remixed (i.e., the SMA equations are run in a forward mode, rather than inverted as in linear spectral unmixing) and a new hyperspectral scene is created (Fig. 47). This scene has most of the natural clutter and sensor noise of the original, because it is derived from real data, and the changes blend into the scene because they were made within the mixing model, rather than to the data itself.

Superpixel changes involve wholesale movement of pixels or groups of pixels (copying or moving terrain features to different parts of the scene, inserting military vehicles or other targets, etc.). These are also accomplished within the abundance maps, because the SMA process effectively normalizes one data set to another. Examples of both sub- and superpixel

scene manipulations are discussed below, as applied to two datasets from environmental extremes—arid and tropical.
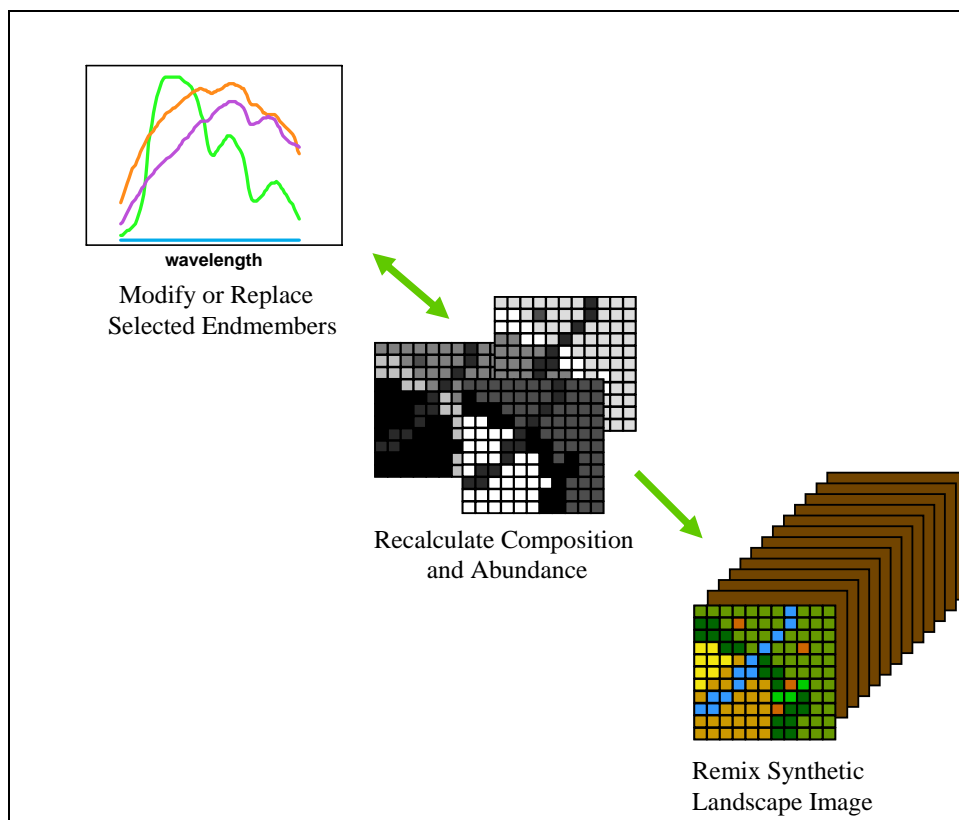

Figure 47. An illustration of linear remixing for synthetic landscape model generation.

Synthetic Landscape Generation: The Desert Chameleon

Two thirds of Department of Defense (DoD) land holdings are located in the arid southwestern U.S. The Yuma Wash drainage basin, located on the U.S. Army Yuma Proving Ground (YPG), is an outdoor natural environment laboratory and site of extensive research on mapping desert landscapes for both civilian and military applications. Recent work involved quantifying geomorphic controls on hyperspectral reflectance of Quaternary Geomorphic surfaces. As the Army's natural environments desert analog for hot weather regions, results obtained at YPG may have important implications and immediate application for mapping and modeling terrain in other arid terrain around the world.

One ground truth control site used in this research is shown in Figure 48. This alluvial fan is centrally located in the Yuma Wash (33° 07' 25" N, 114° 30' 02" W). A prominent feature of this geomorphic surface is a prominent desert pavement with pronounced bar-and-swale topography (Fig. 49). Clasts, which are almost entirely fine-grained igneous rhyolite, range in size from boulders on the proximal fan area, to cobble bars and small gravel-sized clast fractions in swales that meander across the rest of the surface. Rock varnish is moderately developed, with clasts exhibiting a continuous coating of dark reddish-brown varnish in the visible spectrum as compared to the darker manganese-rich varnish typical of older Pleistocene desert pavements in Yuma Wash. Surface relief, rock varnish characteristics, and a young soil profile suggest that clasts were deposited and have been reworked by ephemeral braided streams since the early to mid-Holocene period, between 8000 and 12000 years ago.

Figure 48. One-meter resolution IKONOS satellite image of an alluvial fan in Yuma Wash.

Figure 49. Ground photograph of the alluvial fan in Yuma Wash, Arizona. In the forefront is one of several calibration panels deployed for remote sensing studies.

Airborne Visible Infrared Imaging Spectrometer (AVIRIS) data were acquired of a portion of the Yuma Wash drainage basin, including the alluvial fan control site, to record molecular absorption and particle scattering signatures of the landscape. AVIRIS is a push-broom sensor that measures upwelling radiance in the visible and near-infrared portions of the solar reflective spectrum from 400 to 2500 nm in 224 continuous spectral bands that have a nominal band spacing of 10 nm (Green et al. 1998). AVIRIS has been collecting data for diverse applications since becoming operational in 1989. The AVIRIS data used for this study were collected on 14 April 14 2002 from a Twin Otter turboprop fixed wing aircraft flying 4 km above ground level, resulting in an image pixel size of 3.8 m.

Prior to delivery, the National Atmospheric and Space Administration (NASA) Jet Propulsion Laboratory (JPL) calibrated the AVIRIS data from raw digital numbers to radiance. These radiance values were converted to apparent surface reflectance using ACORN (Analytical Imaging and Geophysics 1995). ACORN is commercially available software that uses licensed MODTRAN4 technology to model the atmosphere (Berk et al. 1999) and calculate apparent

surface reflectance without requiring ground measurements as input. However, ACORN's radiative transfer correction does require some user defined parameters to derive and model atmospheric absorption and scattering effects, which are then are used to invert radiance to apparent surface reflectance based on equations in Chandrasekhar (1960). AVIRIS data from three flight lines were required to cover the study area. ACORN was first run on each individual flight line without artifact suppression, then a second time on each AVIRIS image using field spectra for single spectrum enhancement (polishing).

There is a wide range of scene modifications that the Chameleon software can perform, most of which fall into three general classes: 1) sub-pixel changes in material composition or abundance, or both, 2) super-pixel movement of material, and 3) insertion of objects from pre-existing hyperchip libraries. There are several ways to accomplish changes to the simulated landscape, however, and this section of the chapter describes some of these techniques.

Sub-pixel change to materials

Sub-pixel analyses require spectral unmixing. Figures 50 and 51 show the image endmember results of a spectral mixture analysis for the Yuma Wash study site. For simplicity, only five endmembers were selected (via Abacus) from the hyperspectral image, as plotted in the figure, and used to "unmix" the hyperspectral scene into a series of material abundance maps: one per endmember. Abacus begins by finding top level (i.e., MSI-equivalent) endmembers, such as "green vegetation" or "non-photosynthetic vegetation," or NPV. Each endmember is then broken down into more detailed subcomponents identifiable in hyperpspectral imagery (Fig. 46) using a hierarchical approach to endmember selection, beginning with a small set of material types ("Level 1"), and then finding more detailed subclasses of these endmembers ("Level 2"). These Level 2 endmembers do not need to occur in all pixels in the image, and may include plant species, soil classes, or subcomponents of such. Abundance maps in Figure 50 are displayed such that bright areas indicate high abundance of a given endmember, and dark areas indicate low abundances. For example, the abundance map associated with green vegetation clearly indicates the location of shrubs within the scene as areas abundant in vegetation.
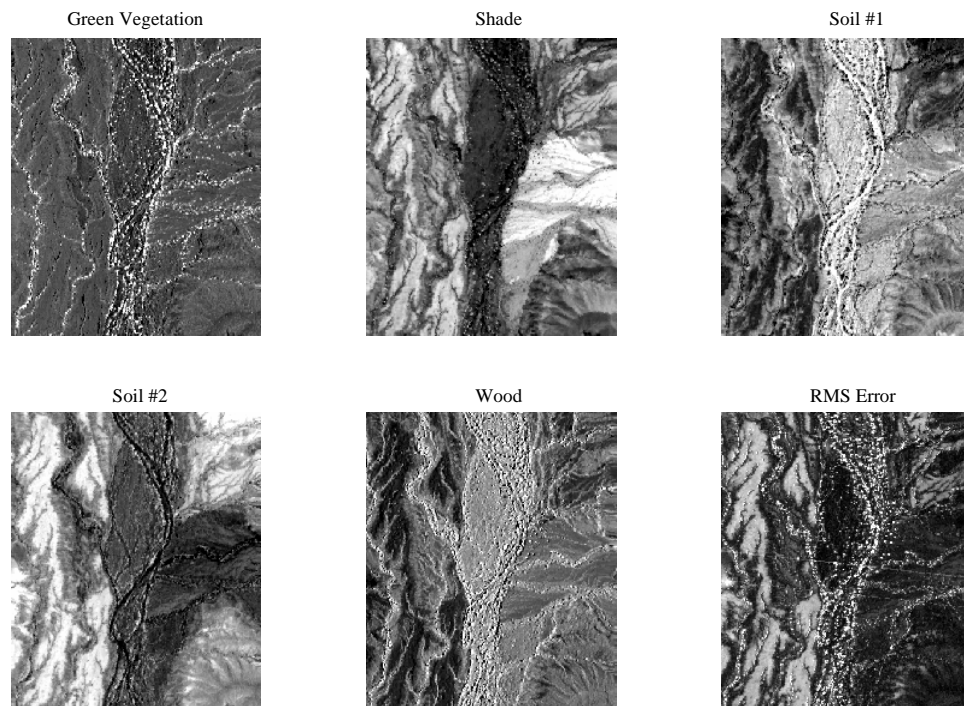
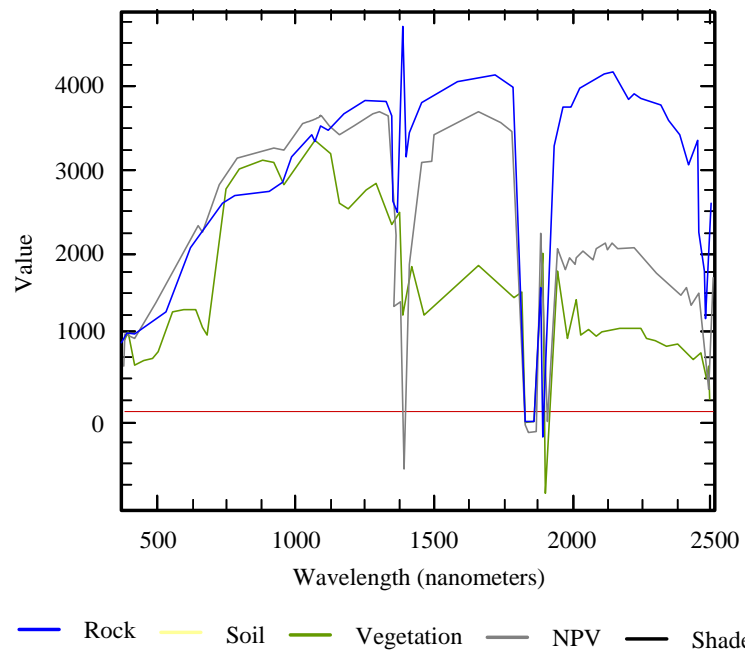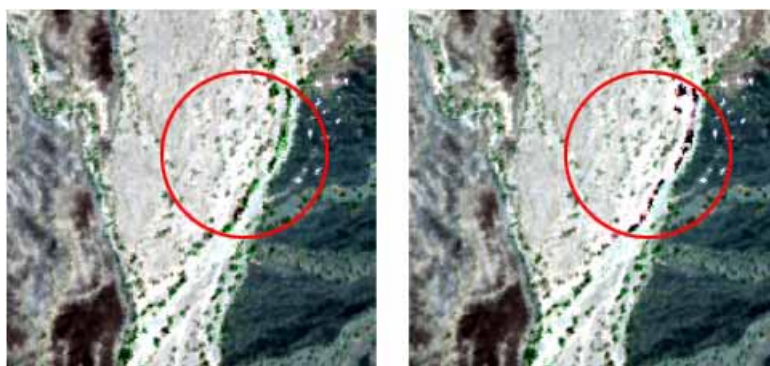Figure 50. Linear unmixing results for a portion of study area: material abundance and RMS images.

Figure 51. Endmember spectra derived from the Yuma Wash linear unmixing model.

a. Stressed vegetation within a user-defined Region of Interest.

b. Simulated change in seasonality across the entire landscape.

c. Increase in vegetation abundance within a Region of Interest.

Figure 52. Original (left) and virtual (right) landscape modifica-
tions to AVIRIS image.

Figure 52 (a and b) shows changes to existing vegetation within the AVIRIS scene. In this

example, a region of interest is identified and the abundance of endmembers is altered at the

sub-pixel level. The scene comprises five endmembers, including green vegetation and non-photosynthetic (senescent) vegetation (NPV). For the selected regions of interest only, the abundance of green vegetation is decreased, and NPV is increased, simulating a localized mortality of healthy green vegetation in the area adjacent to the main channel cut bank into the distal portion of the alluvial fan. Figure 52b shows a similar operation performed on the entire image cube to simulate a temporal change in seasonality. Because spectra of surficial geologic materials are generally invariant to changes in illumination based on sun angle, only the vegetation has been modified.

Super-pixel movement of materials

Movement within and addition of vegetation to the scene is illustrated in Figure 52c example; vegetation is selected from the scene as a region of interest, and then copied to other parts of the scene. Rotation of the vegetation, increase and decrease of size, and feathering around the edges allows these insertions to appear natural and non-repetitive. As illustrated in Figure 52c, the original scene contains numerous small shrubs dispersed across the wash. The modified scene contains a much more dense allocation of shrubs in the northern part of the wash, which were copied from other locations shown in the figure. The vegetation is moved within the fractional abundance maps, then remixed, resulting in a spectrally correct hypercube.

Inserting virtual objects from a hyperchip library

Figure 53 illustrates the concept of inserting of virtual objects a hyperchip library. On the right is a set of available objects extracted from other hyperspectral datasets, which have been inserted into the AVIRIS image in various locations, illustrating two potential problems. First, there are logical and illogical places to insert virtual objects across the landscape. One could expect to find a group of vehicles located in an active ephemeral channel, but not a permanent feature like a golf course, as is illustrated. Second, some of the objects seem to blend into the local background materials, while others do not. To create realistic virtual landscapes, Chameleon reconciles a number of inconsistencies between the host hypercube and virtual hyperchips. Differences in datasets derived from different sensors, such as number image bands, spectral and spatial resolutions, and full-width half maximum values, must be computed, compared, and matched. Each hyperchip is then unmixed using the same endmembers as the AVIRIS scene and the resulting fractional abundances of the objects are pasted into the appro-

priate scene fractional abundances in logical user defined locations, then remixed such that the resulting virtual scene appears natural (Fig. 54).
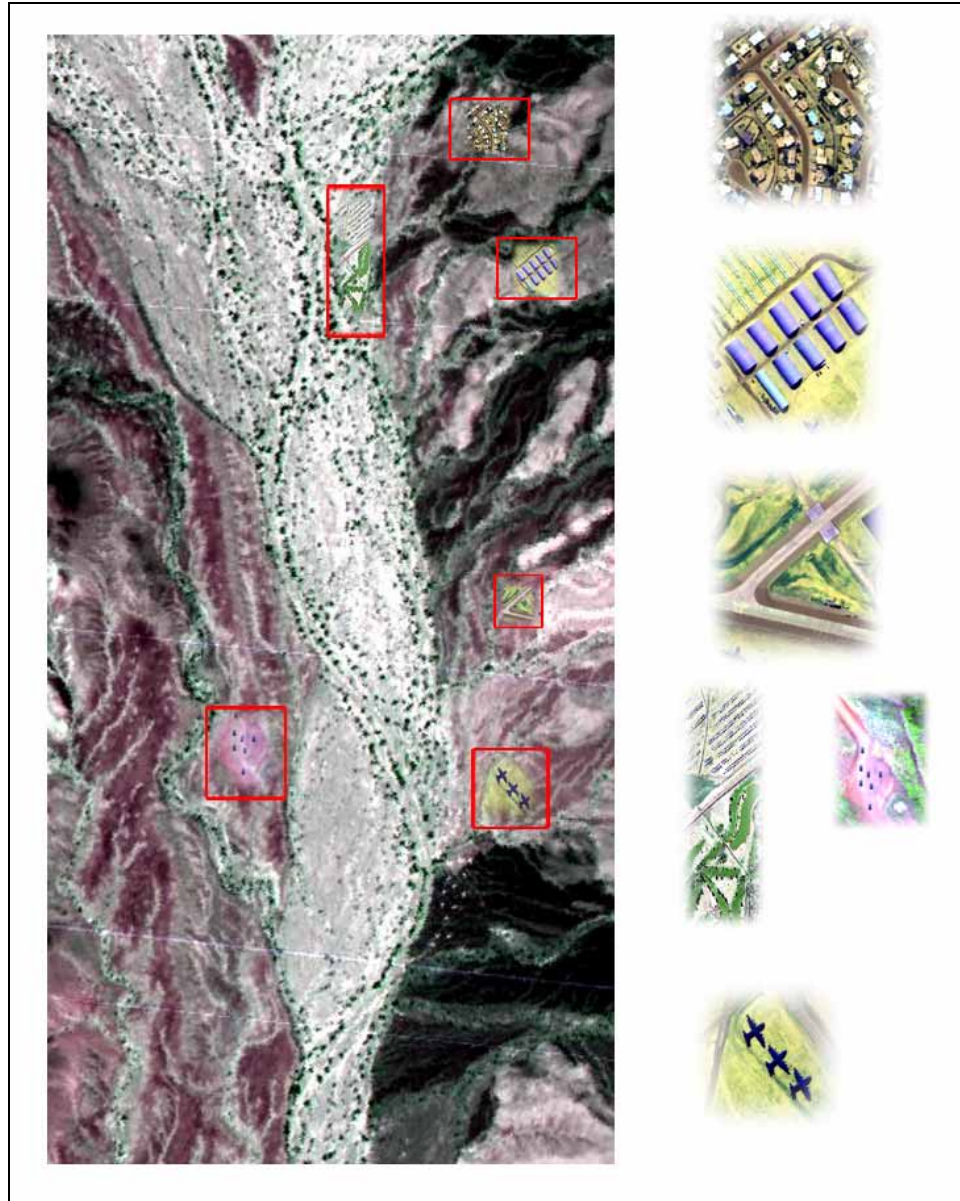

Figure 53. Conceptual examples of virtual landscape modification to an arid environment by inserting objects from an existing hyperchip library.
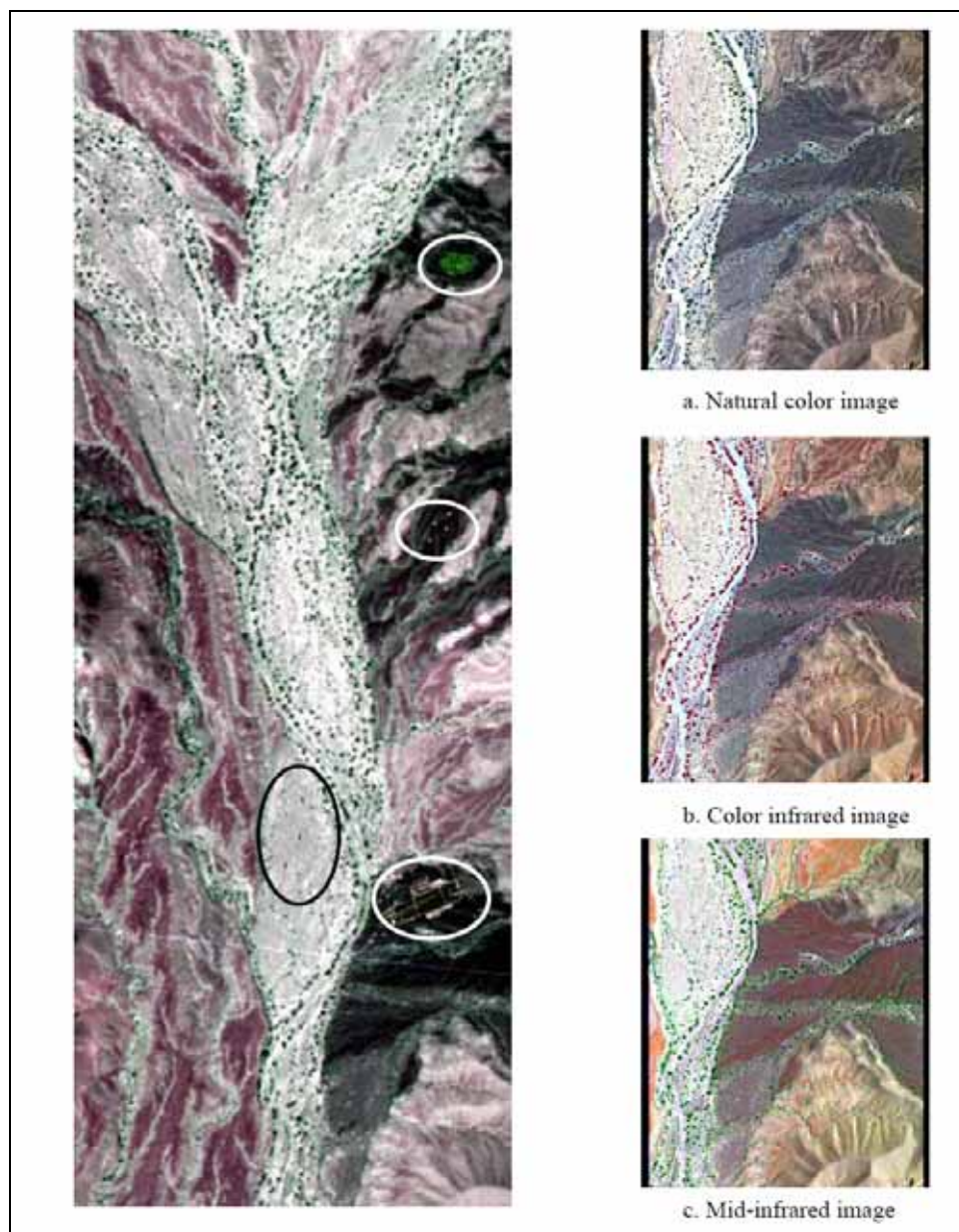
Figure 54. (Left) Examples of virtual landscape modification to an arid environment by inserting grass, vehicles, buildings, and an airstrip from a hyperchip library (top to bottom). Just as vegetation and geologic materials change color in different spectral regions (a) visible, (b) near infrared, and (c) middle infrared images, so to must objects inserted from Virtual Object Libraries.

Synthetic Landscape Generation: The Tropical Chameleon

The U.S. Army Tropic Regions Test Center is responsible for identifying advanced technologies to characterize tropical environments and understanding the effect tropical conditions have on equipment and system performance. In support of this mission, a HYDICE flight mission was performed in the Republic of Panama in March 1998. HYDICE data were collected throughout the former Panama Canal Zone, in areas where climatic differences result in diverse ecosystems ranging from double and triple canopy wet evergreen forest (Fig. 55), second growth tropical forests, to globally unique dry deciduous communities (Fig. 56) in the northern, central, and southern areas, respectively.

a. Natural color photograph of a triple canopy tropical forest in Panama.

Figure 55. Ground photographs of triple canopy tropical forest at Battery McKenzie, Fort Sherman, Republic of Panama (MTL 1998).

b. Color infrared photograph of a triple canopy tropical forest in Panama.

Figure 55 (cont'd). Ground photographs of triple canopy tropical forest at Battery McKenzie, Fort Sherman, Republic of Panama (MTL 1998).

a. Oblique aerial photograph of the STRI Dry Forest Research Canopy Crane

Figure 56. Oblique aerial photographs of dry deciduous tropical forest at the STRI Tropical Research Crane at the Parque Natural Metropolitano, Republic of Panama.

b. Double canopy tropical forest diversity as seen from the canopy crane gondola

Figure 56 (cont'd). Oblique aerial photographs of dry deciduous tropical forest at the STRI Tropical Research Crane at the Parque Natural Metropolitano, Republic of Panama.

The ground support mission included the deployment of multiple sets of calibration panels by two field teams during the HYDICE mission. Site-specific spectroradiometric, meteorological, and survey data were also acquired, including surface level and upper atmospheric meteorological parameters, and VNIR (visible and near-infrared, 350 to 1100 nm) and SWIR (short-wave infrared, 1100 to 2500 nm) spectral measurements of calibration panels and surrounding land cover (background) surfaces. It is seldom possible to have comprehensive ground verification data for tropical forest canopies to correlate with spectral signatures of individual trees. This study, however, offered a unique opportunity to characterize tropical ecosystems using field and imaging spectrometry.

The Smithsonian Tropical Research Institute (STRI) manages several land holdings in the Republic of Panama and HYDICE data were collected over several of them, including Barro Colorado Island and the wet and dry Tropical Forest Research Canopy Cranes, which together cover a distinct rainfall gradient from the Pacific Ocean to the Caribbean Sea. The dry forest canopy crane is located west of Panama City on the Pacific Coast of the Isthmus within the Parque Natural Metropolitano. The crane is 40 m tall, with a boom length of 50 m (Fig. 56a), giving access to 80 species of trees and lianas (Fig. 56b) in a 1-ha experimental plot of lowland semi-deciduous forest in which all trees with a minimum 10 cm trunk diameter have

been mapped, measured, and identified. The crane lifts scientists up above the trees by means of a metal gondola and, through radio communication with the crane operator, scientists directed the gondola movements above the canopy to collect field spectra of treetops at different spatial scales and times of the day (Fig. 57). As summarized in Figure 58, the HYDICE and field spectra data were used as foundation data for a Chameleon tropical landscape simulation proof-of-concept.
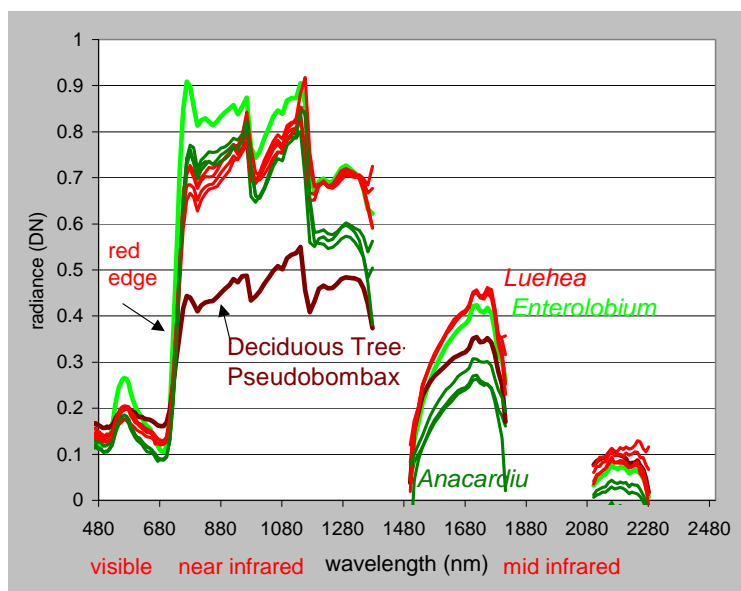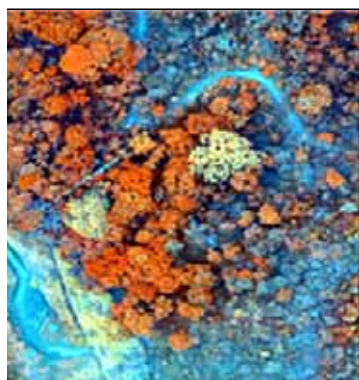

Figure 57. Spectral signatures of tropical tree and vine species collected from the STRI Tropical Research Crane at the Parque Natural Metropolitano, Republic of Panama.

a. Original color composite image.

Chameleon uses imaging, field, and laboratory spectrometry as an empirical foundation from which synthetic, but spectrally accurate landscape models are developed. Image endmembers are derived from the original hypercube using Spectral Mixture Analysis techniques. Composition and fractional abundances of pixels are modified as required for tests or simulation scenarios and a synthetic hypercube calculated by reversing the unmixing process. Temporal adjustments are modeled by incorporating high-resolution elevation datasets and sun angle geometry.

b. Stressed vegetation image.

Image spectra can be modified at the supra-pixel (neighbor), pixel, and sub-pixel levels. Here, vegetation stress has been induced to tree species falling within a user-defined spectral tolerance by reducing the fractional abundance of the healthy vegetation endmember, and increasing that of shade, shadow, and non-photosynthetic vegetation. Synthetic images permit simulation of naturally occurring phenomenon like drought, disease, or El Nino and anthropogenic effects like groundwater withdrawal, water conservation impacts, and urbanization.

c. Virtual object image.

Hyperchip libraries contain real and virtual hyperspectral objects that can be inserted in hypercubes. The yellow tree crown (left center) has been filled and enlarged compared to the original damaged tree (a) and is partially synthetic. A virtual tree has also been inserted in an area that was originally open canopy (lower right). This tree is entirely synthetic. It never existed in the real world. Every pixel used to create it was extracted from other trees of the same species from the same image, resulting in a spectrally and spatially accurate model.

Figure 58. Original (a) and synthetic (b and c) tropical landscapes produced by Chameleon.

Recommendations for Future Research

While the examples given indicate a potential for a number of applications areas, and the Chameleon software program has reached an Initial Operating Capability, a considerable research and development investment will be required before a truly operational capability will be achieved. Additionally, the Chameleon software would have to undergo formal verification and validation procedures before it could be used for modeling and simulation applications. This research utilized laboratory, field, and imaging spectrometry acquired over a limited area of desert and selva environments to investigate hyperspectral data collection and analysis procedures in contrasting, extremes of landscape conditions. Using the prototype Chameleon software to demonstrate hyperspectral manipulation for landscape modeling and feature extraction, this dissertation has stimulated research activity in dynamic terrain modeling and terrain database reuse for serving across distributed simulation networks.

In our applications discussion, it is apparent that a considerable effort must be expended in the collection and organization of hyperspectral libraries that depict the composition and material character of a broad spectrum of environments. These data are collected under controlled laboratory conditions, monitored field spectrometry studies, and by remote platforms, which generate concerns for atmospheric modeling (especially in wavelengths prone to scatter and absorption). In addition, hyperspectral technology has not progressed beyond prototype sensors from airborne platforms. Until long-term, reliable, large area datasets become available, there is little possibility that sufficient, multi-temporal examples will become available to develop functional hyperspectral libraries for areas of broad interest to the research community. However, future satellite systems, such as the NASA Earth Observation System, may address these requirements in the near future.

Dynamic terrain surrogates will require that multiple spectral, spatial, and process dynamics models be able to share, interrogate and re-use distributed datasets. This requires that "metadata-like" protocols with greatly expanded interoperability functions, scales, and dimensions be developed. Challenges exist for the geoscience community to measure and define surface and atmospheric parameters in ways potentially useful for modelers, and for planners, architects, and anthropologists to collaborate in the design of virtual features for inclusion in synthetic environments. There remains considerable interest in the further development of syn-

thetic environments for the modeling and simulation evaluation of vehicles, military systems, regional planning alternatives, and specter of global change.

Acknowledgments

References

Adams, J.B., D.E. Sabol, V. Kapos, R.A. Filho, D.A. Roberts, M.O. Smith, and A.R. Gillespie (1995) Classification of multispectral images based on fractions of endmembers: Application to land-cover in the Brazilian Amazon. *Remote Sensing of Environment*, **52**: 137–154.

Adams, J.B., M.O. Smith, and A.R. Gillespie (1993) Imaging spectroscopy: Interpretation based on spectral mixture analysis. In *Remote Geochemical Analyses: Elemental and Mineralogical Composition* (C.M. Pieters, and P. Englert, eds.). New York: Cambridge University Press, pp. 145–166.

Adams, J.B., M.O. Smith, and P.E. Johnson (1986) Spectral mixture modeling: A new analysis of rock and soil types at Viking Lander 1. *Journal of Geophysical Research*, **91**: 8113–8125.

Armbruster, R.E. (2003) Testing and evaluation: Positioned to support the 21st Century Army. *ATEC Magazine*. USATEC, CSTE-PA, Alexandria, Virginia, pp. 1.

Blount, G., M.O. Smith, J.B. Adams, R. Greeley, and P.R. Christensen (1990) Regional aeolian dynamics and sand mixing in the Gran Desierto: Evidence from Landsat Thematic Mapper images. *Journal of Geophysical Research*, **95**: 15463–15482.

Elmore, A., J.F. Mustard, S.J. Manning, and D.B. Lobell (2000) Quantifying vegetation change in semiarid environments: Precision and accuracy of spectral mixture analysis and the normalized difference vegetation index. *Remote Sensing of Environment*, **73**: 87–102.

Gillespie, A.R., M.O. Smith, J.B. Adams, S.C. Willis, A.F. Fischer, III, and D.E. Sabol (1990) Interpretation of residual images: Spectral mixture analysis of AVIRIS images, Owens Valley, California. In *Proceedings of the Airborne Science Workshop*, pp. 243–270.

Hapke, B. (1981) Bidirectional reflectance spectroscopy, 1. Theory. *Journal of Geophysical Research*, **86**: 3039–3054.

Bohlman, S., and Lashlee, D. (2005) High spatial and spectral resolution remote sensing of Panama Canal Zone Forests: An applied example mapping tropical tree species. In *The Rio Chagres: A Multidisciplinary Profile of a Tropical Watershed* (R.S. Harmon, ed.). Dordrecht, The Netherlands: Kluwer Academic Publishers, pp. 243–257.

Mustard, J.F. (1993) Relationships of soil, grass, and bedrock over the Kaweah Serpentinite Melange through spectral mixture analysis of AVIRIS data. *Remote Sensing of Environment*, **44**: 1–25.

Mustard, J.F., and J.M. Sunshine (1999) Spectral analysis for earth science investigations: Investigations using remote sensing data. in *Remote Sensing for the Earth Sciences: Manual of Remote Sensing*, edited by A.N. Rencz, pp. 251-206, John Wiley and Sons, Inc.,.

Seiglie, E.A. (2002) The future of test and evaluation. *Journal of the International Test and Evaluation Association: The Future of Testing*, **23**(3): 21–28.

Smith, M.O., S.L. Ustin, J.B. Adams, and A.R. Gillespie (1990a) Vegetation in deserts: I. A regional measure of abundance from multispectral images. *Remote Sensing of Environment*, **31**: 1–26.

Smith, M.O., S.L. Ustin, J.B. Adams, and A.R. Gillespie (1990b) Vegetation in deserts: II. Environmental influences on regional abundance. *Remote Sensing of Environment*, **31**: 27–52.

Snyder, J., Gorkavyi, N. Lorenzo. M., and Lashlee, D. (2005) High fidelity terrain models and geospatial datasets for use in distributed testing. In *SPIE's International Symposium on Defense and Security, 28 March–1 April 2005, Orlando, Florida*.

Sunshine, J.M., J.F. Mustard, M.A. Harlow, and A. Elmore (1999) Streamlining and automating spectral mixture analysis for use with hyperspectral imagery: Validation of SAIC's Abacus^{TM} software. Commercial Remote Sensing Program Office, NASA John C. Stennis Space Center, Michigan.

U.S. Army Test and Evaluation Command (2002) Simulation technologies supporting test and evaluation, USATEC Memorandum Number 73-21.

Waite, W.F. (2002) Using simulation—The past as a prologue… probably. *Journal of the International Test and Evaluation Association: Modeling and Simulation Applications in T&E*, **23**(1): 6–9.

Williams, M.L. (2002) AFOTEC: Operational test and evaluation challenges: Modeling and simulation. *Journal of the International Test and Evaluation Association: Modeling and Simulation Applications in T&E*, **23**(1): 17–20.

BIBLIOGRAPHY

Adams, J.B., Sabol, D.E., Kapos, V., Filho, R.A., Roberts, D.A., Smith, M.O., and Gillespie, A.R. (1995) Classification of multispectral images based on fractions of endmembers: Application to land-cover in the Brazilian Amazon. *Remote Sensing of Environment,* **52**: 137–154.

Adams, J.B., Smith, M.O., and Gillespie, A.R. (1993) Imaging spectroscopy: Interpretation based on spectral mixture analysis. In *Remote Geochemical Analyses: Elemental and Mineralogical Composition*(C.M. Pieters and P. Englert Eds.). Cambridge University Press, pp. 145–166.

Adams, J.B., Smith, M.O., and Johnson, P.E. (1986) Spectral mixture modeling: a new analysis of rock and soil types at Viking Lander 1. *Journal of Geophysical Research*, **91**: 8113–8125.

Allen, C.C. (1978) Rock varnish of the Sonoran Desert—Optical and electron probe microanalysis. *Journal of Geology*, **86**: 743–752.

Amos, B.J., and Greenbaum, D. (1989) Alteration detection using TM imagery: The effect of supergene weathering in an arid climate. *International Journal of Remote Sensing*, 10: 515–527.

Analytical Imaging and Geophysics (2002) ACORN 4.0 user's guide. ImSpec LLC. Analytical Imaging and Geophysics, LLC. (2002). *ACORN 4.0 User's Guide*. Boulder, Colorado

Analytical Spectral Devices, Inc. (1995) *Environment For Visualization of Images Technical Guide*. Boulder, Colorado, pp. 24–28.

Armbruster, R.E. (2003) Testing and Evaluation: Positioned to support the 21st century Army. ATEC Magazine. USATEC, CSTE-PA, Alexandria, Virginia, pp. 1.

Ayres Associates (1996) Geomorphic, hydrologic, and vegetation characterization and baseline conditions of Yuma Wash, Yuma Proving Ground, Arizona. Contract No. DACA39-93-C-0009.

Barr, B. (2002) USAOTC: The Role of Modeling and Simulation in Operational Testing. *Journal of the International Test and Evaluation Association: Modeling and Simulation Applications in T&E*, **23**(1): 21–25.

Bates, R.L., and Jackson, J.A. (1980) *Glossary of Geology*. Falls Church, Virginia: American Geological Institute.

Ben-Dor, E., Irons, J. R., and Epema, G.F. (1999) Soil reflectance. In *Remote Sensing for the Earth Sciences: Manual of Remote Sensing* (A.N. Rencz and R.A. Ryerson, Eds.), 3rd ed., Volume 3, New York: John Wiley and Sons, Inc.

Berk, A., Anderson, G.P., Bernstein, L.S., Acharya, P.K., Dothe, H., Mathew, M.W., Adler-Golden, S. M., Chetwynd, J.H., Richtmeier, S.C., Pukall, B., Allred, C.L., Jeong, L.S., and Hoke, M.L. (1999) MODTRAN4 radiative transfer modeling for atmospheric correction. In *SPIE Proceedings, Optical Stereoscopic Techniques and Instrumentation for Atmospheric and Space Research III,* Volume 3756.

Bern, C.M. (1995) Land condition—Trend analysis installation report, Yuma Proving Ground, Arizona, 1991–1994. Center for Ecological Management of Military Lands, Colorado State University, Fort Collins, Colorado.

Betancourt, J.L., Van Devender, T.R., and Martin, P.S. (1990) *Packrat Middens, The Last 40,000 Years of Biotic Change*. Tucson, Arizona: University of Arizona Press.

Birkeland, P.W. (1984) *Soils and Geomorphology.* New York: Oxford Press.

Blount, G., Smith, M.O., Adams, J.B., Greeley, R., and Christensen, P.R. (1990) Regional aeolian dynamics and sand mixing in the Gran Desierto: Evidence from Landsat Thematic Mapper images. *Journal of Geophysical Research*, **95**: 15463–15482.

Boardman J.W., and Kruse, F.A. (1994) Automated spectral analysis: A geologic example using AVIRIS data, north Grapevine Mountains, Nevada. In *Proceedings, Tenth Thematic Conference on Geologic Remote Sensing*. Ann Arbor: Environmental Research Institute of Michigan, pp. I-407–I-418.

Boardman, J.W. (1993) Automated spectral unmixing of AVIRIS data using convex geometry concepts. In *Summaries, Fourth JPL Airborne Geoscience Workshop*, JPL Publication 93-26, Volume 1, pp. 11–14.

Boardman, J.W., Kruse, F.A., and Green, R.O. (1995) Mapping target signatures via partial unmixing of AVIRIS data. In *Summaries, Fifth JPL Airborne Earth Science Workshop*, JPL Publication 95-1, Volume 1, pp. 23–26.

Bohlman, S., and Lashlee, D. (2005) High spatial and spectral resolution remote sensing of Panama Canal Zone forests: An applied example mapping tropical tree species. In *The Rio Chagres: A Multidisciplinary Profile of a Tropical Watershed* (R.S. Harmon, Ed.). Dordrecht, The Netherlands: Kluwer Academic Publishers, pp. 243–257.

Brazel, A.J., and Nickling, W.G. (1986) The relationship of weather types to dust storm generation in Arizona (1965–1980). *Journal of Climatology*, **6**: 255–275.

Briuer, F.L., Lashlee, J.D., and Murphy, W.L. (1999) Survey and evaluation of cultural resources in the Phase I and Phase II areas of the proposed combat systems maneuver area, U.S. Army Yuma Proving Ground, Yuma County, Arizona. U.S. Army Waterways Experiment Station, Vicksburg, Mississippi.

Bull, W.B. (1991) *Geomorphic Response to Climatic Change.* New York: Oxford Press.

Burns, R.G., and Fisher, D.S. (1993) Rates of oxidation weathering on the surface of Mars. *Journal of Geophysical Research Planets,* **98**(E2): 3365–3372.

Chandrasekhar, S. (1960) *Radiative Transfer*. New York: Dover, pp. 1–393.

Chavez, P.S. Jr, Mackinnon, D., Clow, G., Tigges, R., Urban, F., Fulton, R., Reheis, M., Miller, D.K., Bultman, M., and Reynolds, R.L (2002) Monitoring dust emission in the Southwest U.S.—Interannual differences related to climatic variability. In *Geological Society of America Annual Meeting in Denver, 27–30 October*. Paper No. 109-10.

Chen, J.Y., and Reed, I.S. (1987) A detection algorithm for optical targets in clutter. *IEEE Transactions on Aerospace Electronic Systems*, **AES-23**(1).

Christenson, G.E., and Purcell, C. (1985) Correlation and age of Quaternary-fan sequences, Basin and Range Province, Southwestern United States. In *Soils and Quaternary Geology of the Southwestern United States* (Weide, D.L., Ed.). Geological Society of America, Special Paper 203, pp. 115–122.

Climate of Arizona (2003) http://geography.asu.edu/azclimate/narrative.htm

Cochran, C.C. (1992) Soil survey of the U. S. Army Yuma Proving Ground, Arizona—parts of LaPaz and Yuma Counties. USDA, Soil Conservation Service.

Coleman, S.M., and Pierce, K.L. (1981) Weathering rinds on andesitic and basaltic stones as a Quaternary age indicator, western United States. U.S. Geological Survey Professional Paper 1210.

Conel, J.E., Bruegge, C.J., and Curtiss, B. (1987a) Correcting airborne imaging spectrometer measurements for the atmosphere: A comparison of methods. In *Proceeding of the 31st S.P.I.E. International Technical Symposium on Optical and Optoelectronic Applied Science and Engineering*.

Conel, J.E., Green, R.O., Vane, G., Bruegge, C.J., Alley, R.E. and Curtiss, B. (1987b) AIS-2 radiometry and a comparison of methods for the recovery of ground reflectance. In *Proceeding of the of the Third Airborne Imaging Spectrometer Data Analysis Workshop*.

Cooke, R.U., and Warren, A. (1973) *Geomorphology in Deserts*. London: Batsford, Ltd.

Cooke, R.U., Warren, A., and Goudie, A. (1993) *Desert Geomorphology*. London: UCL Press.

CSES (1992) SIPS user's guide, spectral image processing system, version 1.2. Boulder, Colorado: Center for the Study of Earth from Space, p. 88.

Curtiss, B., and Ustin, S.L. (1988) Spectral changes in Ponderosa Pine associated with natural ozone exposure. In *Proceedings of the U.S. Forest Service Forest Response Program Annual Meeting, Corpus Christi, Texas, 23–26 February*.

Devine, J.C. (1988) The U.S. Army Yuma Proving Ground, Arizona: 33-Year climate calendar and tables on associated weather elements 1954–1986, pp. 17.

Dohrenwend, J.C. (1987) Basin and Range. In *Geomorphic Systems of North America* (W.L. Graf, Ed.). Geological Society of America Centennial Special Volume 2, pp. 303-342.

Elmore, A., Mustard, J.F., Manning, S.J., and Lobell, D.B. (2000) Quantifying vegetation change in semi-arid environments: Precision and accuracy of spectral mixture analysis and the normalized difference vegetation index. *Remote Sensing of Environment*, **73**: 87–102.

Elvidge, C.D., and Collet, C.J. (1981) Rock varnish in Arizona, distribution, and spectral characteristics. In *Technical Papers of the American Society of Photogrammetry, ASP-ACSM Fall Technical Meeting, San Francisco*, pp. 215–222.

Farr, T.G., and Chadwick, O.A. (1996) Geomorphic processes and remote sensing signatures of alluvial fans in the Kun Mountains, China. *Journal of Geophysical Research,* **101**(E10): 23,091–23,100.

Fischer, A.F. (1991) Mapping and correlating desert soils and surfaces with imaging spectrometry. In *Proceedings of the Third Airborne Visible/Infrared Imaging Spectrometer (AVIRIS) Workshop.* NASA/JPL Publication 91-28, pp. 23.

Gillespie, A.R., Kahle, A.B., and Palluconi, F.D. (1984) Mapping alluvial fans in Death Valley, California, using multi-channel thermal infrared images. *Geophysical Research Letters,* **11**(11): 1153–1156.

Gillespie, A.R., Smith, M.O., Adams, J.B., Willis, S.C., Fischer, III, A.F., and Sabol, D.E. (1990) Interpretation of residual images: Spectral mixture analysis of AVIRIS images, Owens Valley, California. *Proceedings of the Airborne Science Workshop*, pp. 243–270.

Goetz, A.F.H., and Srivastava, V. (1985) Mineralogical mapping in the Cuprite mining district, Nevada. In *Proceedings of the Airborne Imaging Spectrometer Data Analysis Workshop, April 1985*, JPL Publication, no. 85-41.

Goetz, F.H. (1992) Imaging spectrometry for Earth observations, *Episodes*, **15**(1): 7.

Green, A.A., Berman, M., Switzer, P., and Craig, M.D. (1988) A transformation for ordering multispectral data in terms of image quality with implications for noise removal. *IEEE Transactions on Geoscience and Remote Sensing*, **26**(1): 65-74.

Green, R.O., Eastwood ,M.L., Sarture, C.M., Chrien, T.G., Aronsson, M., Chippendale, J.A., Pavri, B.E., Chovit, C.J., Solis, M., Olah, M.R., and others (1998) Imaging spectroscopy and the Airborne Visible/Infrared Imaging Spectrometer (AVIRIS). *Remote Sensing of the Environment*, **65**:227–248.

Hapke, B. (1981) Bidirectional reflectance spectroscopy—1. Theory. *Journal of Geophysical Research,* **86**: 3039–3054.

Harsanyi, J.C., and Chang, C.I. (1994) Hyperspectral image classification and dimensionality reduction: An orthogonal subspace projection approach. *IEEE Transactions on Geoscience and Remote Sensing*, **32**: 779–785.

Hermann Zillgens Associates (1992) Environmental assessment report, Target Recognition Range, Yuma Proving Ground, Arizona. Report prepared for U.S. Army Engineer District, Sacramento.

Hoffbeck, J.P., and Landgrebe, D.A. (1996) Classification of remote sensing images having high spectral resolution. *Remote Sensing of Environment*, **57**: 119–126.
Hunt, G.R. (1980). Electromagnetic radiation: The communications link in remote sensing. In B.S. Siegal & A.R. Gillespie (Ed.), *Remote Sensing in Geology (pp. 5-45).* New York: Wiley

Hunt, G.R. (1980) Electromagnetic radiation: The communications link in remote sensing. In *Remote Sensing in Geology* (B.S. Siegal and A.R. Gillespie, Eds.). New York: Wiley, pp 5–45.

Husar, R.B., Tratt, D.M., Schichtel, B.A., Falke, S.R., Li, F., Jaffe, D., S., Gassó, Gill, T., Laulainen, N.S., Lu, F., Reheis, M.C., Chun, Y., Westphal, D., Holben, B.N., Gueymard, C., McKendry, I., Kuring, N., Feldman, G.C., McClain, C., Frouin, R.J., Merrill, J., Du-Bois, D., Vignola, F., Murayama, T., Nickovic, S., Wilson, W.E., Sassen, K., Sugimoto, N., and Malm, W.C (2001) Asian dust events of April 1998. *Journal of Geophysical Research*, 106: 18,317.

Idso, S.B. (1976) Dust storms. *Scientific American*, **235**(4): 108–114.

Kierein-Young, K. (1995) Integration of quantitative geophysical information from optical and RADAR remotely sensed data to characterize mineralogy and morphology of surfaces. PhD Dissertation, University of Colorado, Boulder.

Kruse, F.A. (2005) Comparison of ATREM, ACORN, and FLAASH atmospheric, corrections using low-altitude AVIRIS data of Boulder, Colorado. Boulder, Colorado: Horizon Geo-Imaging, LC.

Kruse, F.A., and Lefkoff, A.B. (1993) Knowledge-based geologic mapping with imaging spectrometers. *Remote Sensing Reviews*, **8**: 3–28.

Kruse, F.A., Lefkoff, A.B., Boardman, J.B., Heidebrecht, K.B., Shapiro, A.T., Barloon, P.J., and Goetz, A.F.H. (1993) The Spectral Image Processing System (SIPS)—Interactive visualization and analysis of imaging spectrometer data. *Remote Sensing of Environment*, *Special issue on AVIRIS*, **44**: 145–163.

Lashlee, D., Briuer, F, Murphy, W., and McDonald, E. (2002) Geomorphic mapping enhances cultural resource management at the U.S. Army Yuma Proving Ground, Arizona, USA. *Arid Land Management* **16**: 213–229.

Lashlee, J.D., and Rosenfeld, C. (2000) Laboratory spectrometry of rock coatings: Implications for land management activities in the arid Southwest. *Proceedings of the Natural Environments Testing Workshop, U.S. Army Test and Evaluation Command, Washington, D.C. 29–30 November 2000.*

Lashlee, J.D., Briuer, F.L., Murphy, W.L., and McDonald, E.V. (2000) Spatial distribution of cultural resources in the Combat Systems Maneuver Area. Technical Report No. 00-001, U.S. Army Yuma Proving Ground, Yuma, Arizona.

Lashlee, J.D., McKinley, G.B., and Bishop, M.J. (1993) Quantitative land cover classification accuracy assessments derived from single pass and ISODATA unsupervised clustering algorithms. Technical Report GL-93-21, U.S. Army Corps of Engineers, Waterways Experiment Station, Geotechnical Laboratory.

Liebert, R., Astling, A., Clardy, T., Hernandez, R., Lashlee, D., and Valentine, D. (2003) Synthetic Environments Integrated Testbed (SEIT): Environmental representations to support distributed testing. *Simulation Interoperability Workshop.*

McFadden, L.D., Ritter, J.B., and Wells, S.G. (1989) Use of multiparameter relative-age methods for age estimations and correlation of alluvial fan surfaces on a desert piedmont, eastern Mojave Desert, California. *Quaternary Research*, 276–290.

McFadden, L.D., Wells, S.G., and Dohrenwend, J.C. (1986) Influence of Quaternary climatic changes on processes of soil development on desert loess deposits of the Cima volcanic field, California. *Catena,* **13**: 361–389.

McFadden, L.D., Wells, S.G., and Jercinovich, M.J. (1987) Influence of eolian and pedogenic processes on the origin and evolution of desert pavements. *Geology*, **15**: 504–508.

Musick, H.B. (1975) Barrenness of desert pavement in Yuma County, Arizona. *Arizona Academy of Science,* **10**: 135.

Mustard, J.F. (1993) Relationships of soil, grass, and bedrock over the Kaweah Serpentinite Melange through spectral mixture analysis of AVIRIS data. *Remote Sensing of Environment*, **44**: 1–25.

Mustard, J.F., and Sunshine, J.M. (1999) *Remote Sensing for the Earth Sciences: Manual of Remote Sensing*, 3rd ed., Volume 3. New York: John Wiley and Sons, Inc.

Research Systems Incorporated (1999). *ENVI User's Guide Version 3.2.* Boulder, Colorado.

Reynolds, S.J. (1988) Geologic map of Arizona. Arizona Geological Survey Map 26.

Rivard, B., Arvidson, R.E., Duncan, M.S., and Kaliouby, B.E. (1992) Varnish, sediment, and rock controls on spectral reflectance of outcrops in arid environments. *Geology,* **20**: 295–298.

Schumm, S.A. (1991) *To Interpret the Earth: Ten Ways to be Wrong*. New York: Cambridge University Press.

Seifert, K., and Brunotte, D. (1995) Geochemistry of weathered mid-ocean ridge basalt and diabase clasts from hole 899B in the Iberia Abyssal Plain. ODP SR-149 Abstracts. http://www-odp.tamu.edu/publications/srv/abstr149/149-29.html.

Sherod, D.R., Tosdal, R.M., and Haxel, G.B. (1997) Geologic map of the Picacho, Picacho NW, Picacho SW, and Hidden Valley 7.5' quadrangles, Arizona and California. Menlo Park, California: U.S. Geological Survey.

Smith, M.O., Ustin, S.L., Adams, J.B., and Gillespie, A.R. (1990) Vegetation in deserts I: A regional measure of abundance from multispectral images. *Remote Sensing of Environment*, **31**: 1–26.

Smith, M.O., Ustin, S.L., Adams, J.B., and Gillespie, A.R. (1990) Vegetation in deserts II: Environmental influences on regional abundance. *Remote Sensing of Environment*, **31**: 27–52.

Spatz, D.M., Taranik, J.V., and Hsu, I.C. (1987) Rock varnish on volcanic rocks of the basin and range province—Composition, morphology, distribution, origin, and influence on Landsat imagery. In *Proceedings of the Twenty-First Symposium on Remote Sensing of the Environment,* Volume 2*, pp. 843–852.

Stocker, A., Reed, I.S., and Yu, X. (1990) Multidimensional signal processing for electrooptical target detection. In *Proceedings, SPIE International Society of Optical Engineering*, Volume 1305.

Sunshine, J.M., Mustard, J.F., Harlow, M.A., and Elmore, A. (1999) Streamlining and automating spectral mixture analysis for use with hyperspectral imagery: Validation of SAIC's Abacus[TM] software. Bay Saint Louis, Mississippi: NASA John C. Stennis Space Center, Commercial Remote Sensing Program Office.

Swain, P.H., and Davis, S.M. (Eds.) (1978) *Remote Sensing: The Quantitative Approach*. New York: McGraw-Hill.

USGS (1992). *National Geologic Mapping Act of 1992*. United States Geological Survey web site. http://ncgmp.usgs.gov/ngmact.html

Waters, M.R. (1985) Geomorphic investigations on the Yuma Proving Ground, Arizona. Unpublished Report to Yuma Proving Ground.

Wells, S.G., Dohrenwend, J.C., McFadden, L.D., Turrin, B.D., and Mahrer, K. (1985) Late Cenozoic landscape evolution on lava flow surfaces of the Cima volcanic field, Mojave Desert, California. *Geologic Society of America Bulletin,* **96**: 1518–1529.

White, K. (1990) *Spectral Reflectance Characteristics of Rock Varnish in Arid Areas,* Special Paper 46. University of Oxford Press, pp. 1–31.

Williams, M.L. (2002) AFOTEC: Operational test and evaluation challenges: modeling and simulation. *Journal of the International Test and Evaluation Association: Modeling and Simulation Applications in T&E*, **23**(1): 17–20.

Wilson, E.D., Moore, R.T., and Cooper, J.R. (1969) Geologic Map of Arizona, 1:500,000 Scale. Arizona Bureau of Mines and United States Geological Survey. USGS Federal Center, Denver, Colorado.

Yu, X., Reed, I.S., and Stocker, A.D. (1991) Comparative performance analysis of adaptive multispectral detectors. *IEEE Transactions on Signal Processing*, **41**(8).

Yuma Meteorological Team (1998) Climatological summary for the month of July. Yuma Proving Ground, Yuma, Arizona.

APPENDICES

Appendix A: List of Acronyms

Appendix B: Glossary of Geomorphic Terms[*]

accretion—The gradual or imperceptible increase or extension of land by natural forces acting over a long period of time, as on a beach by the washing-up of sand from the sea or on a flood plain by the accumulation of sediment deposited by a stream.

alluvial—Pertaining to or composed of alluvium, or deposited by a stream or running water.

alluvial fan—A low, outspread, relatively flat to gently sloping mass of loose rock material, shaped like an open fan or a segment of a cone, deposited by a stream (especially in a semiarid region) at the place where it issues from a narrow mountain valley upon a plain or broad valley, or where a tributary stream is near or at its junction with the main stream, or wherever a constriction in a valley abruptly ceases or the gradient of the stream suddenly decreases; it is steepest near the mouth of the valley where its apex points upstream, and it slopes gently and convexly outward with gradually decreasing gradient.

anastomosing stream—A product of braiding; esp. an interlacing network of branching and reuniting channels.

basin-and-range—Said of a topography, landscape, or physiographic province characterized by a series of tilted fault blocks forming longitudinal, asymmetric ridges or mountains and broad, intervening basins; specifically, the Basin and Range physiographic province in Southwest U.S.

channel (streams)—(a) The bed where a natural body of surface water flows or may flow; a natural passageway or depression of perceptible extent containing continuously or periodically flowing water, or forming a connecting link between two bodies of water; a watercourse; (b) The deepest or central part of the bed of a stream, containing the main current, and occupied more or less continuously by water; the thalweg.

creep—The slow, more or less continuous downslope movement of mineral, rock, or soil particles under gravitational stresses.

deflation—The sorting out, lifting, and removal of loose dry fine grained particles (clay and silt sizes) by the turbulent eddy action of the wind, as along a sand-dune coast or in a desert; a form of wind erosion.

degradation—The wearing down or away, and the general lowering or reduction, of the Earth's surface by the natural processes of weathering and erosion.

desert—A region with a mean annual precipitation of 10 in. or less, and so devoid of vegetation as to be incapable of supporting any considerable population. Four kinds of deserts may be distinguished: (1) polar or high-latitude deserts, marked by perpetual snow cover and intense cold; (2) middle-latitude deserts, in the basin like interiors of the continents, such as the Gobi, characterized by scant rainfall and high summer temperatures; (3) trade-wind deserts,

---

[*] The definitions in Appendix B were obtained from Bates and Jackson (1980).

notably the Sahara, with negligible precipitation and a large daily temperature range; and (4) coastal deserts, as in Peru, where there is a cold current on the western coast of a large land mass.

desert armor—A desert pavement whose surface of stony fragments protects the underlying finer-grained material from further wind erosion; a common feature of stony deserts.

desert pavement—A natural residual concentration of wind-polished, closely packed pebbles, boulders, and other rock fragments, mantling a desert surface (such as an area of reg) where wind action and sheetwash have removed all smaller particles, and usually protecting the underlying finer-grained material from further deflation. The fragments commonly are cemented by mineral matter.

drainage basin—A region or area bounded by a drainage divide and occupied by a drainage system; specifically, the tract of country that gathers water originating as precipitation and contributes it to a particular stream channel or system of channels, or to a lake, reservoir, or other body of water.

eolian—Pertaining to the wind; especially said of such deposits as loess and dune sand, of sedimentary structures such as wind-formed ripple marks, or erosion and deposition accomplished by the wind.

ephemeral stream—A stream or reach of a stream that flows briefly only hi direct response to precipitation hi the immediate locality and whose channel is at all times above the water table.

geomorphology—The science that treats the general configuration of the Earth's surface; specifically, the study of the classification, description, nature, origin, and development of present landforms and their relationships to underlying structures, and of the history of geologic changes as recorded by these surface features.

Holocene—An epoch of the Quaternary period, from the end of the Pleistocene, approximately 10.000 years ago, to the present time.

landform—Any physical, recognizable form or feature of the Earth's surface, having a characteristic shape, and produced by natural causes; it includes major forms such as plain, plateau, and mountain, and minor forms such as hill, valley, slope, esker, and dune. Taken together, the landforms make up the surface configuration of the Earth.

landscape—The distinct association of landforms, especially as modified by geologic forces, that can be seen in a single view, e.g. glacial landscape.

pediment—A broad gently sloping rock-floored erosion surface or plain of low relief, typically developed by subaerial agents (including running water) in an arid or semi-arid region at the base of an abrupt and receding mountain front or plateau escarpment, and underlain by bedrock (occasionally by older alluvium deposits) that may be bare, but are more often partly mantled with a thin discontinuous veneer of alluvium derived from the upland masses and in transit across the surface.

Pleistocene—An epoche of the Quaternary period which began two to three million years ago and lasted until the start of the Holocene some 8000 years ago.

Quaternary—The second period of the Cenozoic era, following the Tertiary, which began 2 to 3 million years ago and extends to the present. It consists of two grossly unequal epoches: the Pleistocene, up to about 8000 years ago, and the Holocene since that time.

rock varnish—A thin dark shiny film or coating, composed of iron oxide accompanied by traces of manganese oxide and silica, formed on the surfaces of pebbles, boulders, and other rock fragments in desert regions after long exposure, as well as on ledges and other rock outcrops. It is believed to be caused by exudation of mineralized solutions from within and deposition by evaporation on the surface. A similar appearance produced by wind abrasion is properly known as desert polish.

sheet flow—An overland flow or downslope movement of water taking the form of a thin, continuous film over relatively smooth soil or rock surfaces and not concentrated into channels larger than rills.

stream terrace—One of a series of level surfaces in a stream valley, flanking and more or less parallel to the stream channel, originally occurring at or below, but now above, the level of the stream, and representing the dissected remnants of an abandoned flood plain, stream bed, or valley floor produced during a former stage of erosion or deposition.

Tertiary—The first period of the Cenozoic era, thought to have covered the span of time between 65 and three to 2 million years ago.

wash (streams)—(a) A term applied in the western U.S. (especially in the arid and semiarid regions of the Southwest) to the broad, gravelly, normally dry bed of an intermittent stream, often situated at the bottom of a canyon; it is occasionally filled by a torrent of water.

watershed management—Administration and regulation of the aggregate resources of a drainage basin for the production of water and the control of erosion, streamflow, and floods. Also includes the operational functions.

Appendix C: Glossary of Remote Sensing and Mapping Terms[*]

accuracy—The closeness of results of observations, computations, or estimates to the true values or to values which are accepted as being true.

band—A selection of wavelengths.

byte—Group of consecutive binary digits operated upon as a unit and in general shorter man a computer word; in electronics, a group of eight bits used to encode a single letter, number, or a symbol.

classification—The process of assigning individual pixels to categories on the basis of spectral-reflectance characteristics.

color composite—A color picture produced by assigning a color to a particular spectral band.

delineation—The visual selection and distinguishing of mapworthy features on various possible source materials by outlining the features on the source material, or on a map manuscript (as when operating a stereoscopic plotting instrument); also, a preliminary step in compilation. The delineation of features on a photograph.

electromagnetic radiation (EMR)—Energy propagated through space or through material media in the form of an advancing interaction between electric and magnetic fields. The term radiation, alone, is used commonly for this type of energy, although it actually has a broader meaning. Also call electromagnetic energy.

ground control—Control obtained by ground surveys as distinguished from control obtained by photogrammetric methods; may be for horizontal or vertical control, or both. Ground (in-situ) observations to aid in interpretation of remote sensor data.

ground information—Information derived from ground data and surveys to support interpretation of remotely sensed data.

image—The counterpart of an object produced by the reflection or refraction of light when focused by a lens or mirror. The recorded representation of an object produced by optical, electro-optical, optical mechanical, or electronic means. It is generally used when the EMR emitted or reflected from a scene is not directly recorded on film.

image enhancement - The manipulation of image density to more easily see certain features of the image.

image processing—Encompasses all the various operations which can be applied to photographic or image format data. These include, but are not limited to, image compression, image

---

[*] Unless otherwise noted, the definitions in Appendix C were reprinted from the Multilingual Dictionary of Remote Sensing and Photogrammetry (1984).

restoration, image enhancement, preprocessing, quantization, spatial filtering, and other image pattern recognition techniques.

imaging spectrometry—The collection of image data such that for each pixel a complete reflectance spectrum can be extracted.[*]

large-scale—Aerial photographs with a representative fraction of 1:500 to 1:10,000. Maps with a representative fraction (scale) greater than 1:100,000.

map—A representation in a plane surface, at an established scale, of the physical features of (natural, artificial, or both) a part or all of the earth's surface with the means of orientation indicated. Also, similar representation of certain features to satisfy specific requirements. Frequently the word "map" is preceded by an adjective which explains what type of information the map is designed primarily to present. Many types and scales of maps are made to serve numerous purposes.

map (verb)–To prepare a map or engage in a mapping operation.

medium-scale–Aerial photographs with a representative fraction of 1:12,000 to 1:36,000. Maps with a representative fraction (scale) of 1:100,000 to 1:1,000,000.

micrometer (µm)–A unit of length equal to one-millionth (10^{-6}) of a millimeter.

multispectral—Generally used for acquisition of remote sensing data in two or more spectral bands.

nanometer (nm)—A unit of length equal to one-billionth (10^{-9}) of a millimeter.

photographic interpretation—The act of examining photographic images for the purpose of identifying objects and judging their significance.

pixel—A contraction of a picture element. In Landsat, an integrated radiance mapping unit.

precision - A quality associated with the refinement of instruments and measurements, indicated by the degree of uniformity or identity of repeated measurements.

reconnaissance—A general examination or survey of the main features, or certain specific features, of a region, usually as a preliminary to a more detailed survey.

reflection—EMR neither absorbed nor transmitted is reflected. Reflection may be diffuse, when the incident radiation is scattered upon being reflected from the surface, or specular, when all or most angles of reflection equal the angle of incidence.

remote sensing—In the broadest sense, the measurement or acquisition of information of some property of an object or phenomenon, by a recording device that is not in physical or intimate contact with the object or phenomenon under study; e.g., the utilization at a distance (as from aircraft, spacecraft, or ship) of any device and its attendant display for gathering in-

---

[*] Goetz (1992).

formation pertinent to the environment, such as measurements of force fields, electromagnetic radiation, or acoustic energy.

resolution—The ability of an entire remote sensor system, including lens, antennae, display, exposure, processing, and other factors, to render a sharply defined image.

scale—The full range of tones of which a photographic paper is capable of reproducing is called the scale of the paper, it is also termed dynamic range. The ratio of a distance on a photograph or map to its corresponding distance on the ground. Scale may be expressed as a ratio, 1:24,000; a representative fraction, 1/24,000; or an equivalence, 1 in. = 2000 ft.

sensor—Any device which gathers EMR or other energy and presents it in a form suitable for obtaining information about the environment. Passive sensors, such as thermal infrared and microwave, utilize EMR produced by the surface or object being sensed. Active sensors, such as radar, supply their own energy source. Aerial cameras use natural or artificially produced EMR external to the object or surface being sensed.

signature analysis techniques—Techniques which use the variation in the spectral reflectance or emittance of objects as a method of identifying the objects.

small-scale—Aerial photographs with a representative fraction smaller than 1:40,000. Maps with a representative fraction (scale) less than 1:1,000,000.

spectral signature—Quantitative measurement of the properties of an object at one or several wavelength intervals. Radiant energy is subject to dispersion. A rainbow-colored band of light is formed when white light is passed through a prism or a diffraction grating. This band of colors results from the fact that the different wavelengths of light are bent in varying degrees by the dispersing medium and is evidence of the fact that white light is composed of colored light of various wavelengths.

texture—In a photo image, the frequency of change and arrangement of tones. Some descriptive adjectives for textures are fine, medium or coarse; and stippled or mottled.

wavelength—Wavelength = velocity/frequency. In general, the mean distance between maximums (or minimums) of a roughly periodic pattern. Specifically, the least distance between particles moving hi the same phase of oscillation in a wave disturbance.

APPENDIX D
Chameleon User's Guide, Version 1.0

IDL®
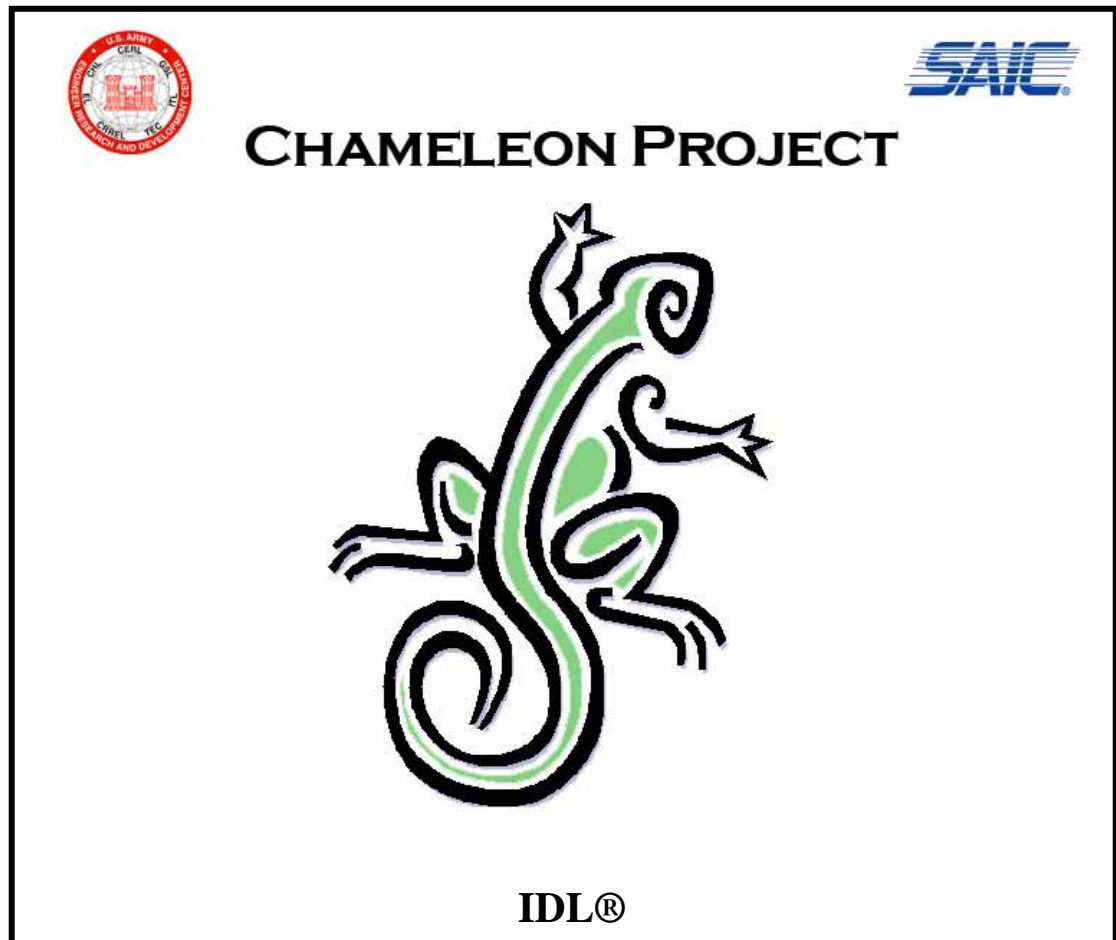
Chameleon Contact Information:

J. David Lashlee
U.S. Army Engineer Research and Development Center
Topographic Engineering Center
Office of Technical Directors
CEERD-TV-T
Alexandria, VA 22315-3864

Chameleon User's Guide

1   Introduction

Chameleon is a software system designed to generate spectrally accurate digital terrain models for modeling and simulation applications. Example applications include:

- Feature extraction,
- Target detection and identification,
- Change detection,
- Battle damage assessment,
- Search and rescue

Chameleon creates "virtual" hyperspectral image (HSI) cubes. Instead of creating a simulated HSI cube from scratch, Chameleon uses the data from a "real" HSI cube and transforms that data into information layers using SAIC's Abacus® tool. Those information layers are then used to re-create a "virtual" HSI cube that can then be manipulated by the user. For example, if the original HSI cube was collected in the spring during the rainy season in a desert environment, Chameleon can "adjust" the vegetation in the scene to make it look more stressed during the dry summertime. In addition, manmade materials can be introduced into the scene to test the feasibility of target detection.

2   System Requirements

Chameleon will operate on either Windows or UNIX systems and requires a run-time license for IDL® (Interactive Data Language) from Research Systems, Inc. (version 5.5 or higher). For license purchasing information, please contact RSI directly at www.rsinc.com.

3   Installation

3.1 Installing the Program Files

This document assumes that the user will create a subdirectory named *Chameleon* and will put the contents of the CD provided with this document there. Often the *Chameleon* subdirectory is a subdirectory of the main IDL® directory (*i.e.*, the directory pointed to by the !Dir system variable inside of IDL®), but it does not have to be in this directory; it can be created anywhere. The IDL® *home directory* is another good place to put it. To find the IDL® home directory, start IDL® and type these commands as the first commands in the IDL® session:

IDL> CD, Current = homeDirectory
IDL> Print, homeDirectory

3.2 Making Sure the Chameleon Directory is on the IDL® Path

No matter where the *Chameleon* subdirectory is created, the user will want to make sure that the directory is on the IDL® path. The path is given by the *!Path* system variable in IDL®. To permanently add the *Chameleon* directory to the path requires a system administrator to edit the IDL® file configuration. See the IDL® on-line help for information on setting the *!Path* system variable. When using the IDL® Development Environment (IDLDE), one can permanently set the *!Path* system variable from the *File → Preferences → Path* tab.

To temporarily add the *Chameleon* directory to the IDL® path, use the command AddPath, provided on the Chameleon CD within the *Chameleon* directory. Use the CD command in IDL® to change to the appropriate *Chameleon* directory. For example, if the *Chameleon* directory is a subdirectory of the IDL® home directory and the home directory is where the user is currently working, the *Chameleon* directory can be added to the IDL® path by typing these commands:

IDL> CD, 'Chameleon'
IDL> AddPath

The user will want to move into the *Chameleon* directory and use the AddPath program each time IDL® is run.

4   Data Requirements

Chameleon uses hyperspectral data calibrated to apparent reflectance with the following file parameters:

- Image files must be in Band Interleaved by Line (BIL) format or Band Interleaved by Pixel (BIP) format with accompanying ENVI®-format external header files.

- Header files should contain the file size information and any available wavelength and bad band information (see the ENVI® User's Guide for a description of the header file format).

- Image data must be unaffected by geometric processing, registration or other processing that influences the value of the image pixels.

- Geographic coordinate information, if available, should be in a separate file in Band Sequential (BSQ) format and should contain two image planes with spatial dimensions identical to those of the hyperspectral image. Pixel values should be expressed in units of latitude and longitude or UTM northing and easting.

- Each dataset (a hyperspectral image and its associated metadata) must be in its own folder, since Chameleon is folder-based in its functionality. Chameleon will create a new sub-folder within that data folder to store its output files. For an example of the folder-based system used by Chameleon, see Figure 1.
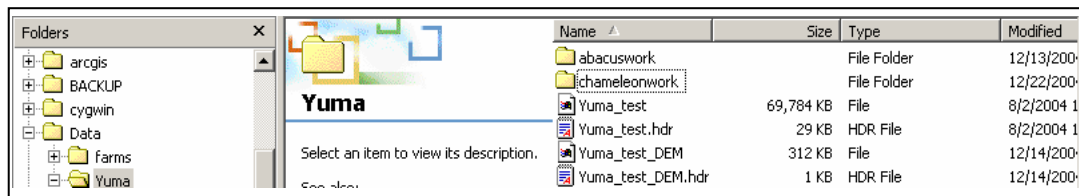

Figure 1: Example of how data sets should be stored as a folder-based system when used by Chameleon.

4.1 Chameleon Output Files

Chameleon creates a working sub-folder, called *chameleonwork*, in the same directory as the image file being analyzed. During the Chameleon session, a number of files will be written to the *chameleonwork* folder, so it is very important that the user has write permission for the original data folder. These files may be used to restore and continue any previous Chameleon session.

The following is a list of some of the more important files that will be created in the *chameleonwork* sub-folder:

1. Simulated Hyperspectral Cube

The output HSI cube from Chameleon will be in BIL format and will have the same file name as the input HSI data, but with an added "_remix" extended to the name. For example, if the input HSI data file had the name "myhsi.cub", then the output simulated Chameleon cube would be "myhsi_remix.cub". This HSI data cube has an accompanying ENVI®-compatible header file (extension ".hdr").

2. Simulated Background Abundance Cube

This file is a BIL image file, which contains the pixel-by-pixel fractional abundance values for each compositional component, or endmember, of the simulated HSI data. It will have the same file name as the input abundance data, but with an added "_remix" extended to the name. For example, if the input abundance data file had the name "myhsi_frac.sma", then the output simulated abundance cube would be "myhsi_frac _remix.sma". Each "band" in this file is an abundance image of an individual endmember, where brighter pixels represent higher concentrations of that particular endmember. This

abundance data cube has an accompanying ENVI-compatible header file (extension ".hdr").

3. Spectral Background, or Endmember, ASCII File

This file is an ASCII file with the extension "_remix.em" containing the spectral information of the image's compositional components or endmembers. The wavelength data is the first column, followed by columns for the spectrum of each endmember.   This file can be imported into ENVI® for further analysis.

4. Metadata SAV File

This file, called ROIINFO.SAV, is in a binary format and stores essential metadata associated with the current Chameleon session. An example of the type of metadata stored in this file includes all information associated with defined Regions-Of-Interest (ROI).

5   Launching Chameleon

The user can make a Chameleon icon on the desktop (for Windows machines) by creating a shortcut to the Chameleon.sav file found in the installation directory. If a Chameleon icon is not available on the workstation desktop, begin by launching IDL® or IDLDE (the IDL® Development Environment). In the IDL® command window, type "Chameleon". The Chameleon setup window will appear (Figure 2).
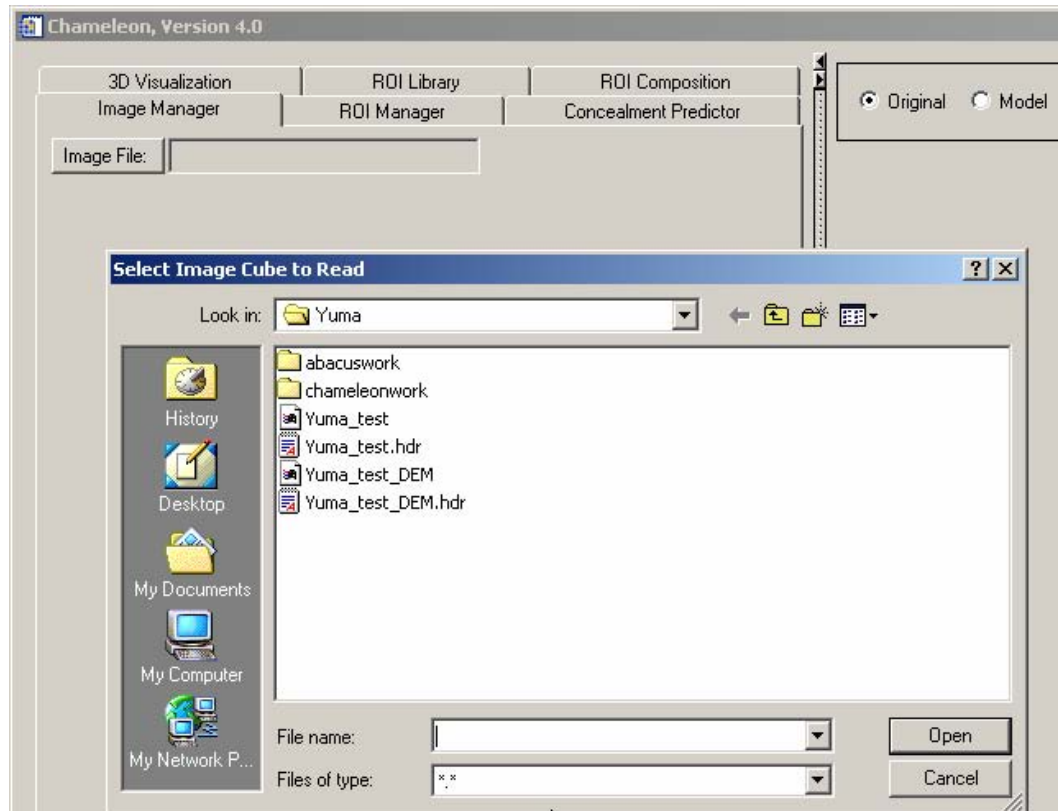
Figure 2: Chameleon Setup Window

5.1 Getting Started

Chameleon requires two input files: 1) the file name for the "real" HSI data to use in the simulation, and 2) the file name for the background abundance cube for that HSI image. This abundance cube is the product of running Abacus® to find the spectral background components, or endmembers, of the given hyperspectral data (for more information about Abacus®, please contact SAIC, Division 1360).

5.1.1   Selecting a Hyperspectral Image to use in the Simulation

All image data files are accessed and read into Chameleon by clicking the "Image File" button (please see Section 4 for the proper data formats used by Chameleon). When the "Select Image Cube To Read" window appears, browse through the directories, select the image to be processed, and then click "Open."

5.1.2   Selecting the Accompanying Abundance Data

Chameleon requires background abundance data to start the initial simulation process. This data is the product of running Abacus® to find the spectral

background components, or endmembers, of the given hyperspectral data. There are three ways to provide abundance data for Chameleon: 1) by clicking the "Restore Previous Work" button and resuming a previous session; 2) by clicking the "Generate Scene Components Via Abacus®" button and starting a new Abacus® session to create the fractional abundance cube, then entering that file's name by 3) clicking the "Select Existing Abundance Data" button (the user can go directly to this button if an abundance data file is already available). How to use Abacus® is beyond the scope of this document; however, information may be obtained by contacting SAIC, Division 1360. These abundance files from Abacus® will have the file extension ".*sma*" and will be stored in a sub-folder called "abacuswork". When the "Enter the Fraction Cube File Name" window appears, browse through the directories where the Abacus® products are located, select the SMA data to be processed, and then click "Open."

5.1.3   Restoring Previous Work

The "Restore Previous Work" button allows previously saved Chameleon work to be opened and displayed without rebuilding the simulated data. By default, data from a previous Chameleon session will be saved into a sub-folder called "chameleonwork" of the working directory (see Section 4.1 for a description of output products from Chameleon). A new window will pop up asking the user for the names of the saved simulated files (Figure 3).
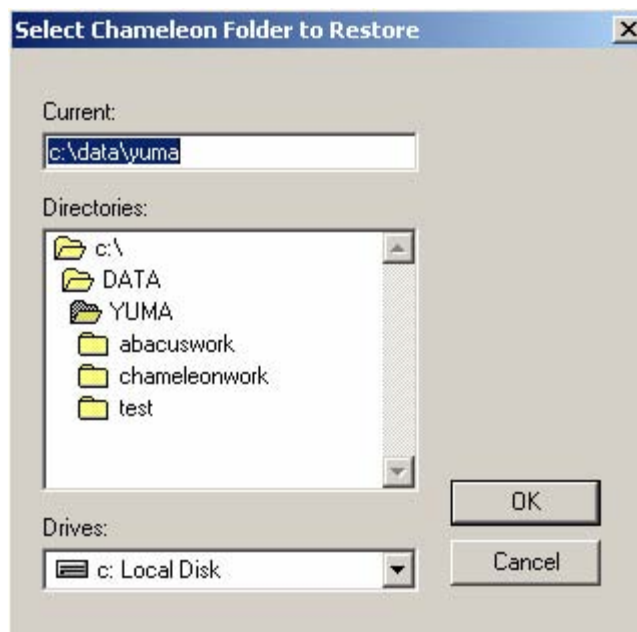
Figure 3: Restore Chameleon Session Dialog Window

1. Browse to the proper sub-folder in the working directory.

2. Click "OK".

5.1.4 Processing the Data

Clicking the "Process" button will:

1. Build the initial simulation cube on which to work. The spectra for each pixel of this simulation cube is calculated by linearly combining a particular amount of each of the endmember spectra found by Abacus® (and which has been provided as input to Chameleon). The amount of each endmember spectrum to add together is based on the fractional abundance data for that pixel, which is found in the input SMA file.

2. Open the Chameleon Image Display and Chameleon Toolkit windows (see Section 6). By default, the data processing output files will be written to a sub-folder called "chameleonwork" within the folder where the image data is located. If this folder does not exist, it will be created automatically; if it does already exist, then a subsequent folder will be created (*e.g.*, chameleonwork1, chameleonwork2, etc.). This is to ensure previous work is not overwritten and can be compared with current work. If a bad bands list is not provided in the associated ENVI® header file for the image data, then another window will pop up asking whether the user wants the software to build a default bad bands list.

6 Chameleon Overview

Chameleon consists of one main window with three panes: 1) the Chameleon Image Display, 2) the Fractional Abundance Display (which appears once the mouse is clicked on the image) and 3) the Chameleon Toolkit.

6.1 Chameleon Image Display

The Chameleon Image Display window (right pane Figure 4) shows either the original hyperspectral imagery or the corresponding simulated imagery depending on which radio button is selected. Initially, the simulated image will look exactly like the original HSI image. The two images are linked so that any functions applied to one image (*e.g.*, zooming, etc.) are automatically applied to the other. A variety of color-composite or black-and-white images can be displayed in the image window (see Section 7).
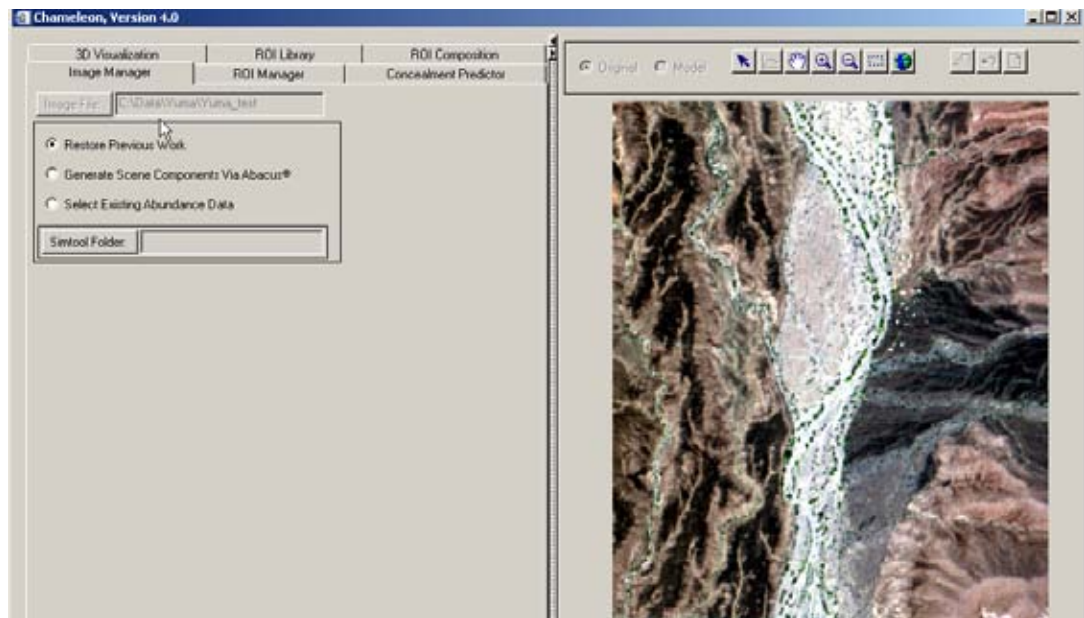
Figure 4: Chameleon Image Display Window (right pane) and Chameleon Toolkit (left pane)

6.1.1 Functions of the Image Display

6.1.1.1 Retrieving Spectra

When the cursor is moved over the image, zoom factor, pixel and geographic coordinates are updated in the text box below the Chameleon Toolbox. If geographic coordinates are not provided to Chameleon at the start of the session

(*i.e.*, choosing the proper sensor type), then only the current zoom factor and pixel coordinates will be displayed.

The user can retrieve spectral or background abundance information by choosing the spectra button above the image display. A bar chart of the background abundances of that pixel for both the original HSI data and the simulated data will be displayed in the Fractional Abundance Display window (Figure 5).

6.1.1.2 Original vs. Model Data Display

The user can toggle between displaying the Original data and the modeled data by using the radio buttons at the top of the Image Display Window (Figure 4).

6.1.1.3 Zooming

The toolbar above the image allows the user to zoom into and pan to a specific area of the image. To activate the 'zoom in' feature, click the button with the positive magnifying glass (⊕) on it. To activate the 'zoom out' feature, click the button with the negative magnifying glass (⊖) on it. To activate the 'box zoom' feature, click the button with the dashed box (⬚) on it. To reposition an image while zoomed in, click the pan button (✋) to activate a click and drag function. The active zoom button will remain depressed to signify that zoom mode is active. While in zoom mode, the pixel coordinates and geographic information in the text box above the image will not update as the cursor moves over the image.

The images can be quickly reset to their full spatial extent by clicking the 'zoom to full image' button (🌐).

6.1.1.4 Show/Hide ROIs (⬡)

The toolbar above the image allows the user to show or hide the ROIs that they have created. If the Show/Hide ROI button is selected (appears to be "pushed down"), the ROIs will be displayed. If the button is unselected, the ROIs will NOT be displayed.

6.1.1.5 Start New Chameleon Session (🗋)

The toolbar above the image allows the user to start a new Chameleon session. Pushing this button will produce a pop up window that asks the user if they want to start a new session. Selecting *YES* will clear the current data and allow the user to begin a new session by selecting another image file. Selecting *NO* will take the user back to the current Chameleon session.

6.2 Fractional Abundance

The Fractional Abundance window (in Figure 5) displays a plot of the original spectrum for that pixel (plotted in red) and the simulated spectrum for that pixel (plotted in yellow). This simulated pixel spectrum is based on a linear combination of the input endmember spectra, multiplied by the fractional abundance of each endmember for that pixel coordinate. The Fractional Abundance window also shows bar charts of the fractional abundances of both the original HSI data for that pixel coordinate (solid colored boxes) as well as the simulated abundances (striped boxes).

(a)   (b)
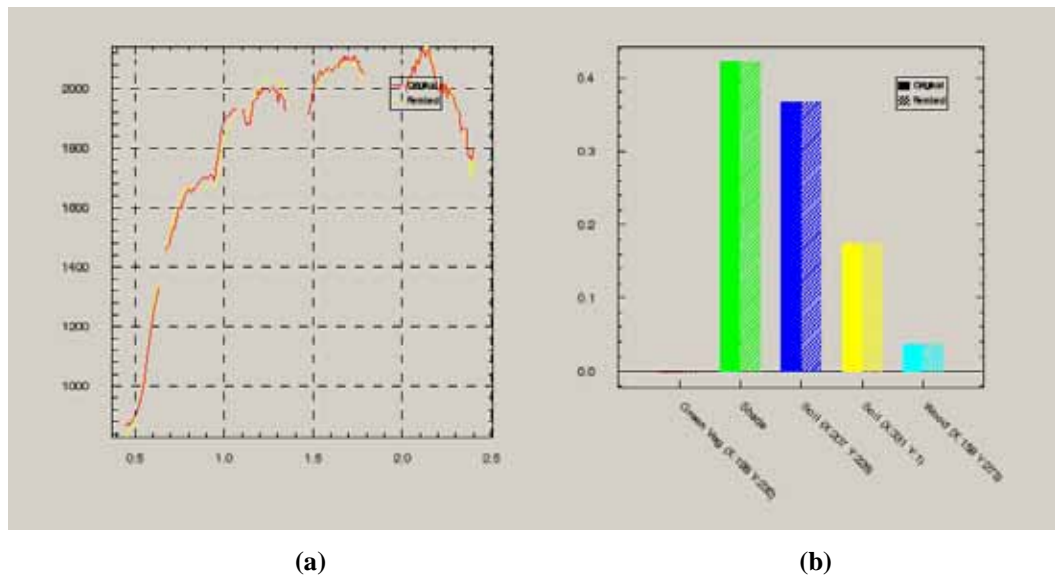
Figure 5: Fractional Abundance Display showing: a) HSI spectra for the input pixel coordinate, where the red spectrum is from the original HSI data and the yellow spectrum is the simulated spectrum from the updated endmember information for that pixel; b) a bar chart of relative abundances of endmember components for the input pixel coordinate. The solid boxes represent the abundances from the original HSI data and the striped boxes represent the remixed abundances in the simulated HSI data.

6.3 Chameleon Toolkit

The Chameleon Toolkit is a collection of tools. Each tool performs a different function in the creation of a simulated HSI cube and is selected using the tabs as shown in Figure 6. Currently, there are six tool collections: 1) Image Manager, 2) ROI Manager, 3) ROI Library, 4) ROI Composition, 5) Concealment Predictor, and 6) 3D Visualization. Each one of these tools is described in detail in Sections 7 through 12.
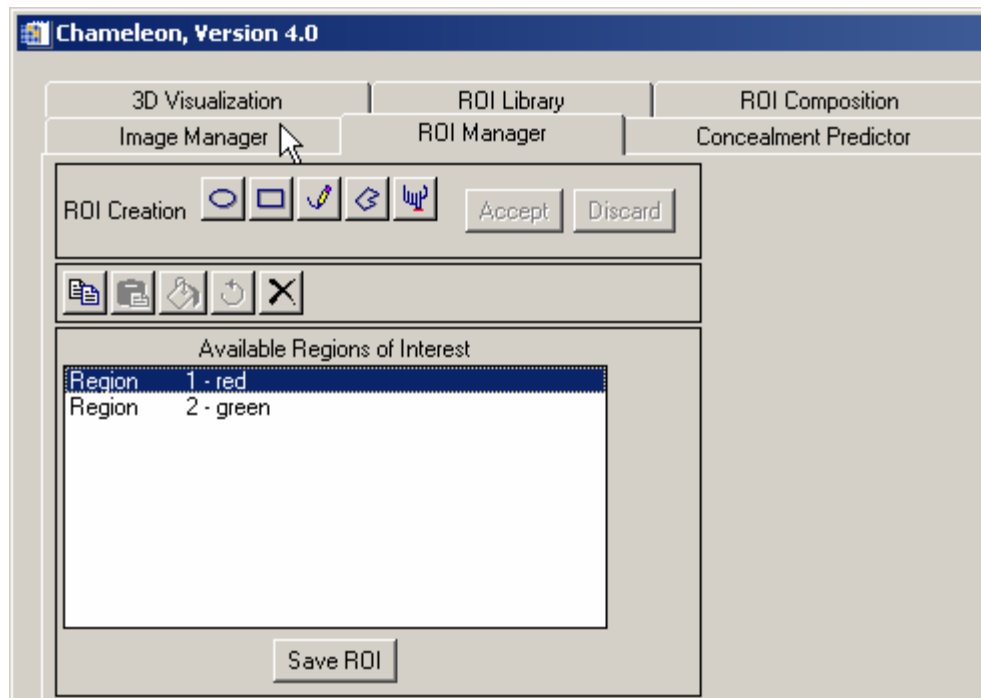
Figure 6: The tab shows which simulation tool is currently active (ROI Manager in this example).

7 Image Manager

There are many options to change the display through band combinations and contrast stretching.

7.1 RGB Color Composite

Select this option to view different color composites for the image windows. Preprogrammed and user-specified options for various color composites are described in Table 1.

| Color Composite	Description
True Color	This is the default. This composite uses the wavelengths 650 nm, 550 nm, and 470 nm in the red, green, and blue bands, respectively.
Vegetation Map 1	This composite uses the wavelengths 800 nm, 650 nm, and 550 nm in the red, green, and blue bands, respectively.
Vegetation Map 2	This composite uses the wavelengths 2300 nm, 800 nm, and 650 nm in the red, green, and blue bands, respectively.
Soil Map	This composite uses the wavelengths 2300 nm, 1650 nm, and 800 nm in the red, green, and blue bands, respectively.
SWIR Map	This composite uses the wavelengths 2300 nm, 1650 nm, and 1200 nm in the red, green, and blue bands, respectively.
Panchromatic	This is a simple black and white image. It defaults to 550 nm for a VNIR/SWIR image.
Fraction Combination	This option allows the user to place three background endmembers in the red, green, and blue bands of the image display windows in order to build a colored terrain map. A new window will appear which contains a list of the terrain endmembers found for the current image file. Using the pull-down menus, choose an endmember for the red, green, and blue color bands. This type of display will show areas within the image where these endmembers dominate by coloring them the specified color. It is also possible to choose the same endmember for all bands and display a black-and-white abundance map of that terrain endmember.
User-Defined	This option allows the user to choose any available band in the hyperspectral image. A new window will appear which contains a list of all image bands within the image file (see Figure 7). The Available Bands List allows one to display grayscale and color image composites.

Table 1: Color Composite Descriptions
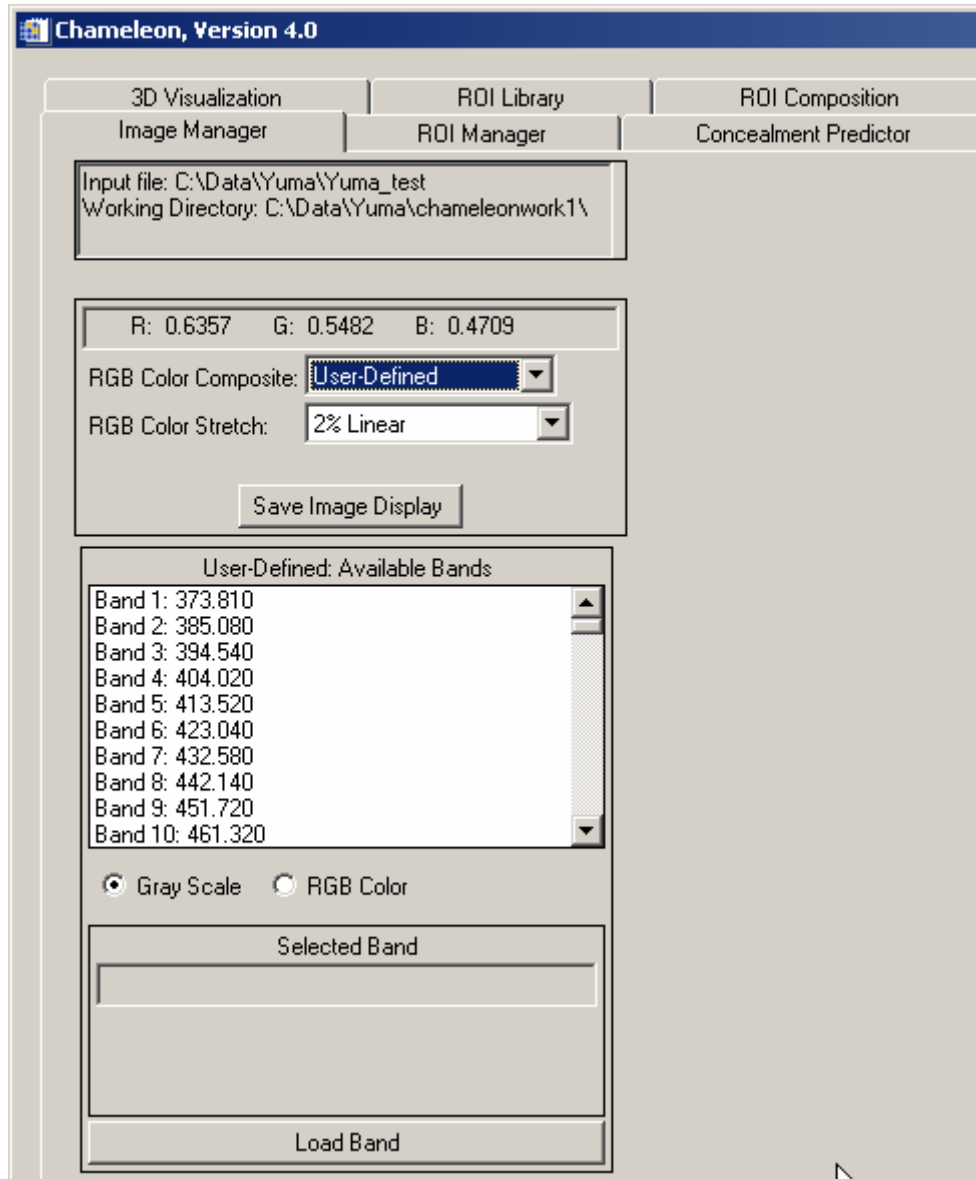
Figure 7: The Available Bands List

7.2 RGB Color Stretch

Select this option to apply different contrast stretching techniques to the image window. The available stretching options are:

- 2% Linear Stretch (This is the default)
- 5 % Linear Stretch
- Linear
- Optimal
- Histogram Equalization

8   ROI Manager

The user can draw ROIs, which are graphically-selected image subsets. The regions can be irregularly-shaped and are typically used by Chameleon to change the background information associated with a particular area in the HSI data. Chameleon allows selection of any combination of polygons or vectors as a region of interest. Multiple regions of interest can be defined and drawn in the Image Display window.

ROIs can be copied and pasted to other areas of the simulated scene, rotated and pasted, or simply saved out to Chameleon's ROI library to be used as part of another data set.

Figure 8 shows the layout of the ROI Manager tool and the controls associated with it. This tool controls the creation and spatial extent of all ROIs used by the other tools of the Chameleon Toolkit.
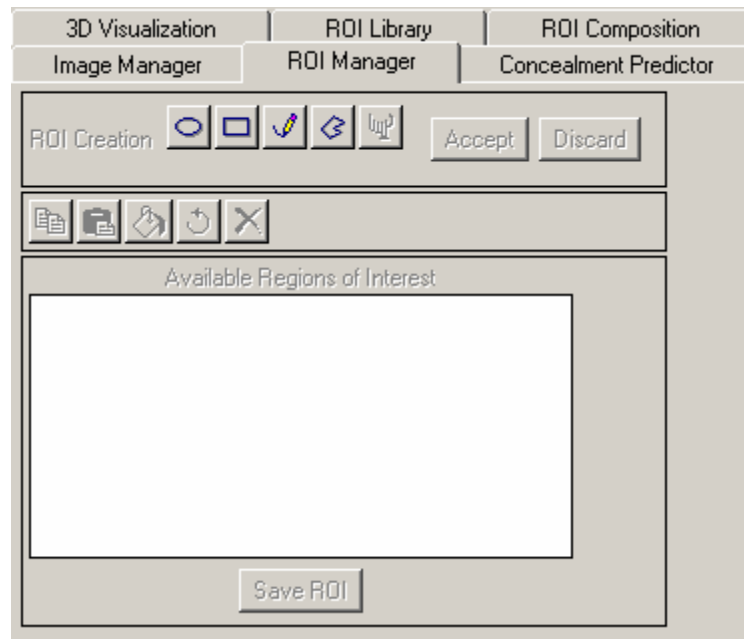
Figure 8: ROI Manager Toolbox

8.1 Creating Regions of Interest

There are four types of regions of interest: Circle, Rectangle, Polyline, and Polygon. Each type has a different set of mouse assignments and drawing options that are explained below.

8.1.1   Circle

The Circle mode allows circles and/or ovals to be drawn as ROIs.

1. In the ROI Creation toolbox, select *Circle*.

2. Click the left mouse button and drag the cursor to the desired size of the circle then release the mouse button.

3. Select either *Accept* or *Discard* in the ROI Creation Toolbox. If the user *accepts* the ROI, the region will display in the Available Regions of Interest list. If the user d*iscards* the ROI, the ROI will be cleared from the image display.

8.1.2   Rectangle

The Rectangle mode allows rectangles and/or squares to be drawn as ROIs.

1. In the ROI Creation toolbox, select *Rectangle*.

2. Click the left mouse button and drag the cursor to the desired size of the rectangle then release the mouse button.

3. Select either *Accept* or *Discard* in the ROI Creation Toolbox. If the user *accepts* the ROI, the region will display in the Available Regions of Interest list. If the user d*iscards* the ROI, the ROI will be cleared from the image display.

8.1.3   Polyline

The Polyline mode is similar to the polygon mode except that a multi-segment vector is drawn rather than a closed polygon. This is particularly useful for drawing riverbeds. The regions enclosed by the defined line segments are not a part of the ROI, only the pixels comprising the line segments themselves are selected.

1. In the ROI Creation toolbox, select *Polyline*.

2. Click the left mouse button in the image window and proceed to draw your polyline. When you are finished with the line, release the mouse button.

3. Select either *Accept* or *Discard* in the ROI Creation Toolbox. If the user *accepts* the ROI, the region will display in the Available Regions of

Interest list. If the user d*iscards* the ROI, the ROI will be cleared from the image display.

8.1.4 Polygon

The Polygon mode allows the user to outline a region of interest with connected line segments.

1. In the ROI Creation toolbox, select *Polygon*.

2. Click the left mouse button in the image to establish an initial endpoint for an outlining segment.

3. Click the left mouse button at each place in the image that you wish to have a vertex on the polygon.

4. To close the polygon, double click with the mouse. The polygon will automatically close by adding the last segment to the position of the first segment.

4. Select either *Accept* or *Discard* in the ROI Creation Toolbox. If the user *accepts* the ROI, the region will display in the Available Regions of Interest list. If the user d*iscards* the ROI, the ROI will be cleared from the image display.

8.1.5 Reset ROIs

The "Reset ROIs" button allows the user to reset all of the ROI buttons on the toolbar. If the user has any buttons currently active, pressing this button will "reset" them so that NONE of the ROI buttons are pushed.

8.2 Copy/Paste

Regions of Interest can be copied and pasted to other areas of the simulated image scene. To copy and paste an ROI, the user must first select the ROI to copy from the Available Regions of Interest list and then choose the "Copy" button on the toolbar. Two different techniques for pasting have been provided: "Paste As Is" and "Fill Selected ROI".

8.2.1 Paste As Is

To copy and paste an ROI using this method:

1. Click the radio button to choose "Paste As Is". Note that a copy of the ROI is displayed in the Image Window on top of the original ROI that was copied.

2. Move the cursor to the location in the image where the chosen ROI is to be pasted. Click the right mouse button at the selected image coordinate.

3. Once this has been done, the Blur-Blend Settings window will appear (Figure 9). This feature allows the user to "blend" the edges of the pasted ROI into the background area of the image using the slider bars provided. The ROI Transparency value ranges from 0 to 255, where zero denotes no blending and 255 returns only the background area. The value 128 is the default. The Rotation Angle allows the user to rotate the ROI to a desired angle between -180 degrees and 180 degrees, with zero being the default. Please note that positive values are counterclockwise in degrees. The Gaussian Edge Blur setting allows the user to smooth the edge of the pasted ROI via convolution. The "Gaussian Edge Blur" allows the user to select the size of the smoothing kernel used by the operation. The user may select no blur or kernels of size 3 by 3, 5 by 5, or 7 by 7 from the pull down list.
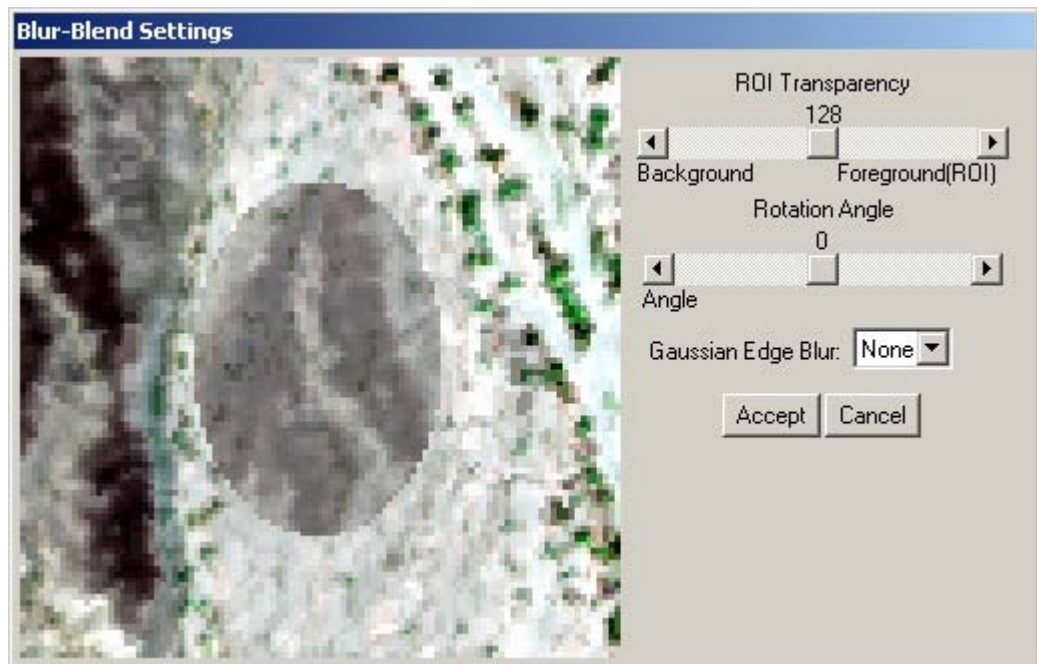
Figure 9: Blur-Blend Settings Window for "Paste As Is" type pasting

4. Click *Accept* to paste this ROI into the selected area of the simulated scene, or *Cancel* to cancel the copy/paste operation.

8.2.2 Fill Selected ROI

To copy and paste an ROI using this method:

1. Click the radio button to choose "*Fill Selected ROI*".

2. A pop up box will inform the user to "Select an existing ROI in which to paste the copied data". Click *OK*.

3. In the Image Display window, left click the mouse on top of the ROI in which you wish to paste the copied ROI. If the chosen ROI to paste is smaller than the area in which it is being pasted and is the Polygon draw type, multiple copies of the ROI will be randomly pasted throughout the area being filled. This is a good method if, for example, the user wants to change a plowed field to a forest grove.

4. Again, once the user has finished drawing the region of interest to be filled, a blending window will appear (Figure 10). This blending window is similar to the one that the user will see while "Pasting As Is", except the user will not have a choice to rotate the ROI.

Figure 10: Blur-Blend Settings Window for "Fill Selected ROI" type pasting

5. Click *Accept* to paste this ROI into the selected area of the simulated scene, or *Cancel* to cancel the copy/paste operation.

8.3 Rotate ROI ⟳

Regions of Interest can be rotated before being pasted to other areas of the simulated image scene. To rotate and paste an ROI:

1. Select the ROI to rotate from the Available Regions of Interest list.

2. Choose "Copy/Paste", and then choose "Paste As Is". A copy of the chosen ROI will be displayed in the Image window for reference. The ROI Rotation slide bar will appear under the Available Regions of Interest list (Figure 11).
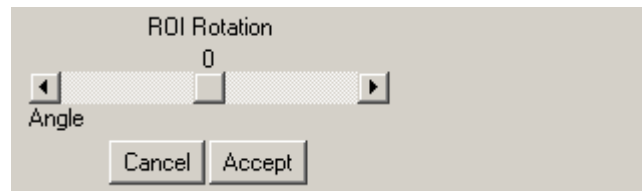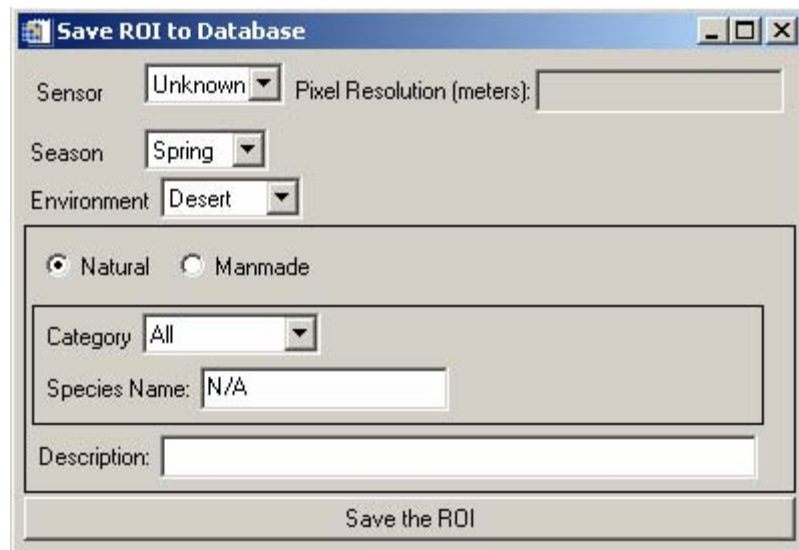

Figure 11: ROI rotation slide bar

3. Enter the Rotation Angle (positive values are counterclockwise in degrees).

4. If you wish to cancel the rotation, click *Cancel*. When satisfied with the look of the rotated ROI, click *Accept*. The ROI outline in the Image Window will now show the rotated ROI. Place according to instructions in "Paste As Is" (Section 8.2.1).

8.4 Save ROI

ROIs can be saved for future use via the Save ROI tool (Figure 12). Enter the sensor name, pixel resolution, season, environment, natural/manmade, category, species name and description and save the ROI into an ROI Database Library (see Section 9).

Figure 12: Save ROI Tool Box

9   ROI Library

The user can add a region of interest to the simulated HSI data from the collection of ROI images stored in the image database library provided with Chameleon.
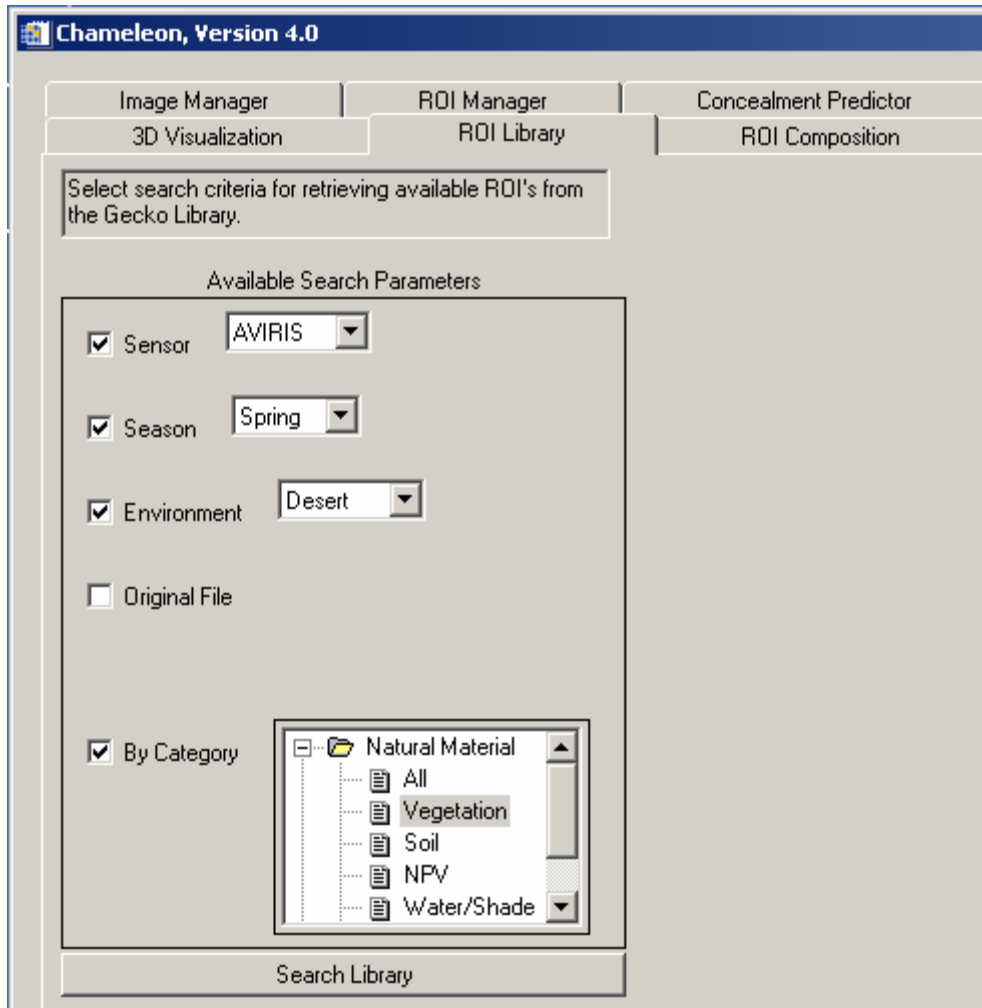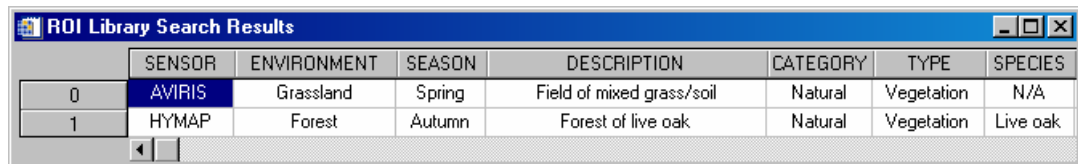

Figure 13: ROI Library Tool

9.1   Searching for an ROI Image in the ROI Database Library

Select the "Search ROI Library" tab (Figure 13) to search the Chameleon ROI library for a new region of interest to add to the simulated HSI scene.

1. Click on the checkbox of any of the available attributes on which to search the Chameleon ROI library. When the user clicks "on" an attribute checkbox, a pull-down menu of the available search parameters for that attribute will become available. Choose the appropriate search attributes.

2. Once one or more attributes have been selected for the query, click the "Search Library" button. In order to search by category, double click on either the Natural Material or Manmade Material folder and select a material type. Chameleon will then search the ROI library for appropriate entries and return a table listing all of the available ROI images in its database that meet the search criteria (see Figure 14).

	SENSOR	ENVIRONMENT	SEASON	DESCRIPTION	CATEGORY	TYPE	SPECIES
0	AVIRIS	Grassland	Spring	Field of mixed grass/soil	Natural	Vegetation	N/A
1	HYMAP	Forest	Autumn	Forest of live oak	Natural	Vegetation	Live oak

Figure 14: Example of ROI Library search results given the provided input search attributes.

Clicking on a row in the result table will pop up a new window showing the user what that ROI image looks like (Figure 15).

Figure 15: Example of one of the ROI images stored in the Chameleon ROI library. This display window will pop up when the user clicks one of the entries listed in the library search result table (see Figure 14).

9.2   Adding an ROI Library Image to the Simulated HSI Image

To add the ROI library image to the simulated HSI scene:

1. If the library image is a fabric, the user is given the choice of changing the image's target signature. If this is not applicable, proceed to step 2. If the user wishes to change the target signature using the spatial characteristics from the ROI library, select "Change Target Signature." Press the "Get New Target" button, navigate to a spectral library, and select a spectrum.

2. Click on the "Copy This ROI Into Image" button in the display window for that ROI image. Note that a message is provided letting the user know that ROI copy/paste mode is active. The cursor will also change to crosshairs.

3. Move the cursor to the location in the image where this ROI is to be pasted in the Chameleon Image Display window. Click the mouse at the selected image coordinate.

4. An IDL® window will pop up asking the user to provide the HSI pixel resolution in meters of the image into which it will be pasted. This will only occur the first time an ROI is pasted into the image during a Chameleon session. If the ROI library image is of higher spatial resolution than the image it is being pasted into, the ROI image will be degraded to match the resolution of the current image. Figure 16 shows an example of pasting a tree from the ROI library into the simulated HSI image.
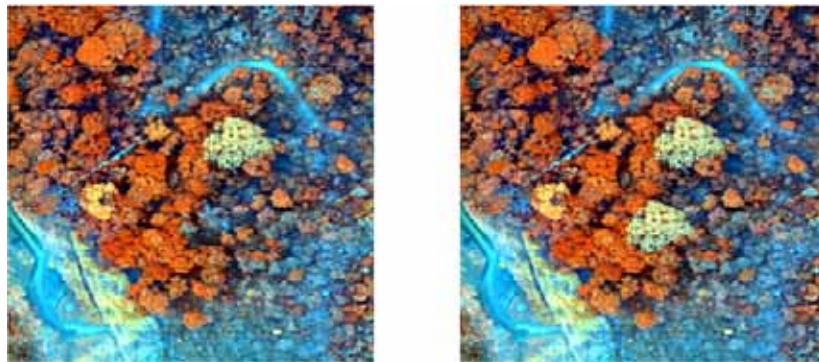

Figure 16: Example of pasting an ROI image (a tree) from the Chameleon library into the simulated HSI image.

10 ROI Composition

The user can change the fractional abundance of any or all of the background components, called endmembers, in the simulated HSI data. Figure 17 shows the layout of the ROI Composition tab and the controls associated with it. The user has the option of changing the fractional abundance of a particular endmember over the entire simulated scene, or just within a particular region of interest. If the "Within ROI" radio button is selected, the Available Regions of Interest list will become visible. Keep in mind that the regions of interest must first be created with the Define Region of Interest tools (see Section 8.1)

User cans also change, or swap out, the spectral information of any or all of the background components, called endmembers, in the simulated HSI data. The user has the option of swapping out a particular endmember over the entire simulated scene, or just within a particular region of interest. If the "Within ROI" radio button is selected, the Available Regions of Interest list will become visible. Once again, keep in mind that the regions of interest must first be created with the Define Region of Interest tools (see Section 8.1).

With either region option (entire scene or just within an ROI), the available endmembers for that particular region will be provided in the Current Endmember List.
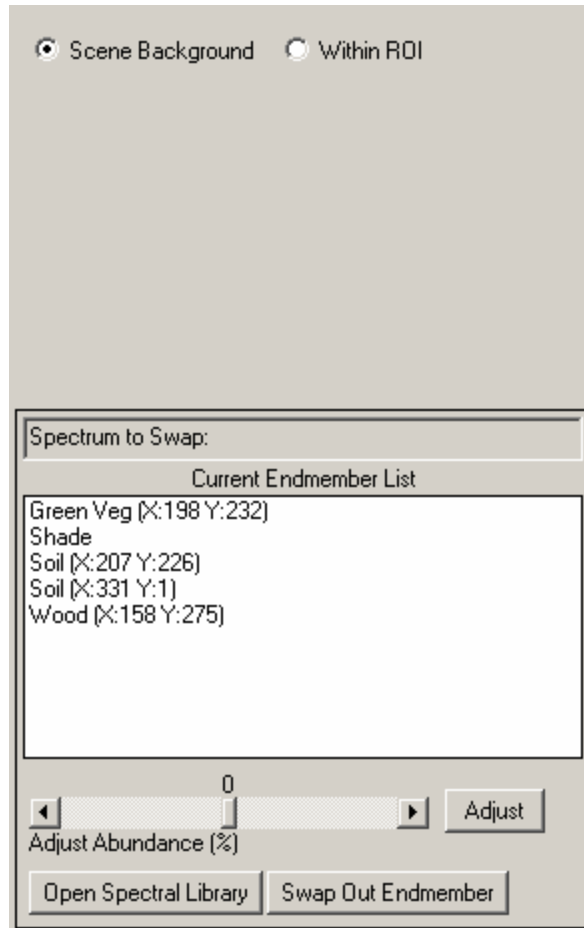
Figure 17: Chameleon Toolkit with ROI Composition tab selected.

10.1 Adjusting the Abundance of an Endmember

To change the fractional abundance of an endmember:

1. Click on the name of the endmember in the Current Endmember list.

2. Use the slider bar below the list to either increase or decrease the current fractional abundance of this endmember (units are in percentage of current value).

3. Click the "*Adjust*" button.

Chameleon will then adjust the abundances of all endmembers within the specified region – the chosen endmember will be modified according to the percentage value supplied, and the other endmembers will be re-normalized so that the total abundance of all background components remains at 100%.

The remixed image in the Chameleon Image Display window will then re-display the updated simulated HSI data. If the user wishes to adjust endmembers within

an ROI, it is sometimes helpful to go back to the Define ROI tool to plot the mean fractional abundances for that ROI. An example of adjusting endmembers within an ROI is given in Figure 18.
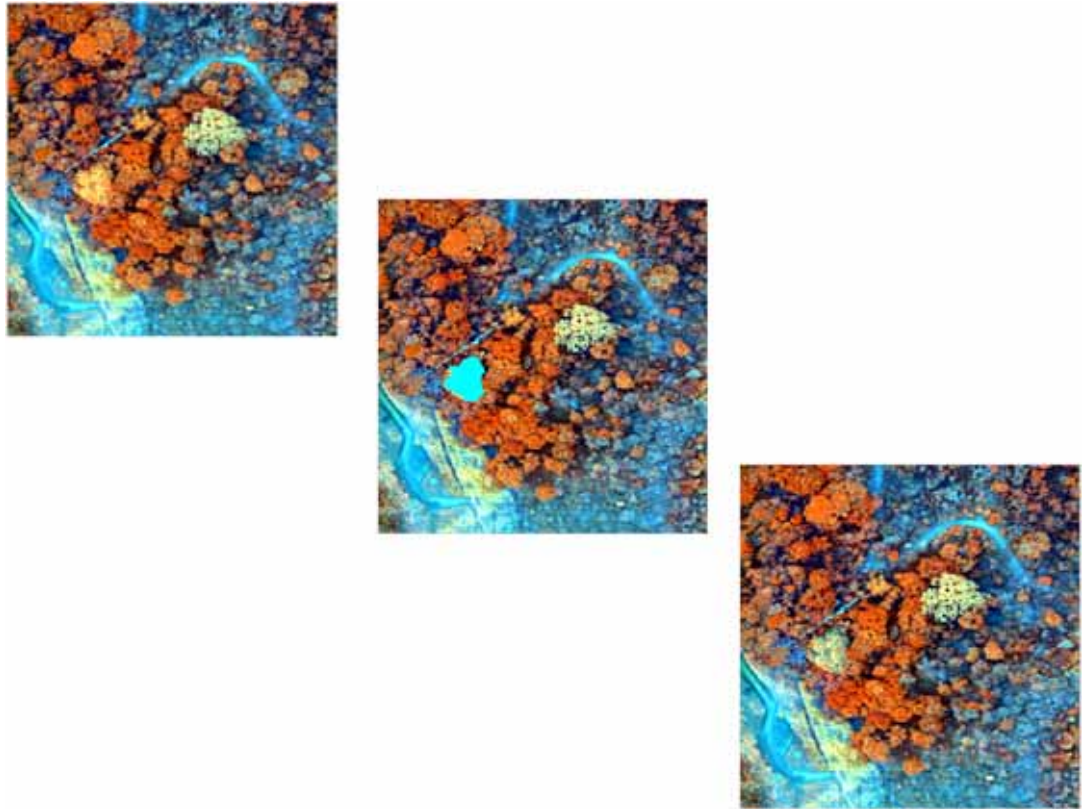

Figure 18: Example of "stressing" a tree by changing the abundance of a vegetation endmember that makes up the HSI spectrum for that tree.

10.2 Swap Endmembers

To swap out the spectrum of an endmember:

1. Click on the name of the endmember to swap out in the Current Endmember list.

2. Click the "Open Spectral Library" button. When the file selection dialog appears, select a spectral library filename.

   Spectral library data can come from a variety of sources including ground truth spectra, standard ENVI® spectral libraries, or even spectra from the image data itself that have been previously saved using ENVI®. Data

formats supported by Chameleon for spectral library information consist of the following:

- Any space-delimited ASCII file, where the first data column is the associated wavelengths.

- ENVI® ASCII file (see the ENVI® User's Guide for correct format).

- ENVI® SLI file, which stores the spectral library in ENVI® binary image format with the number of samples equal to the number of bands and the number of lines equal to the number of spectra in the library. The file type is set to spectral library in the header and there are associated wavelengths (see the ENVI® User's Guide for a more detailed description).

- *The preferred format is the ENVI® spectral library file with a .sli file extension*

3. When the list of library spectra is supplied to the Spectral Library Viewer, choose the library spectrum to be used in the endmember swap. Once the original endmember and a library spectrum have both been selected, the user can press the "Plot Spectra" button to bring up a window comparing the two spectra.

4. Click the "Swap Out Endmember" button.

Chameleon will then swap out the spectrum of the current endmember within the specified region of interest and replaces the area with the newly selected library spectrum. It will use the fractional abundance values of the previous endmember within the affected region to calculate the abundance of the new endmember.

The remixed image in the Chameleon Image Display window will then re-display the updated simulated HSI data for review.

11 Concealment Predictor

The best locations to hide a target can be found via the Concealment Predictor tab. As seasonal and weather effects may change the best spectral matches for the target being concealed, it is suggested that any results found are implemented at the same time of year as the collection of the image data.

Start by activating the Concealment Predictor tab (see Figure 20a) and selecting the target spectrum. Navigate to the spectral library that contains the desired target spectrum. Open the library and select a target spectrum, which will be plotted in

the "Select Target Spectrum" window (see Figure 19). If the target spectrum is not in the current library, select the "New Library" button, which will allow a new library to be loaded. Press the "Accept Spectrum" button once the desired target spectrum is found.

Select one of the two prediction methods: Matched Filter or Spectral Matching. Select the "Do Prediction" button to run the selected algorithm. The result will automatically be displayed in the Chameleon Image Display window (see Figure 20b). Select the "Clear Display" button to turn off the prediction, the "Display Prediction" button to display the prediction again, or alternately toggle back and forth with the "Toggle Mask" button (located at the top of the Chameleon Image Display window).
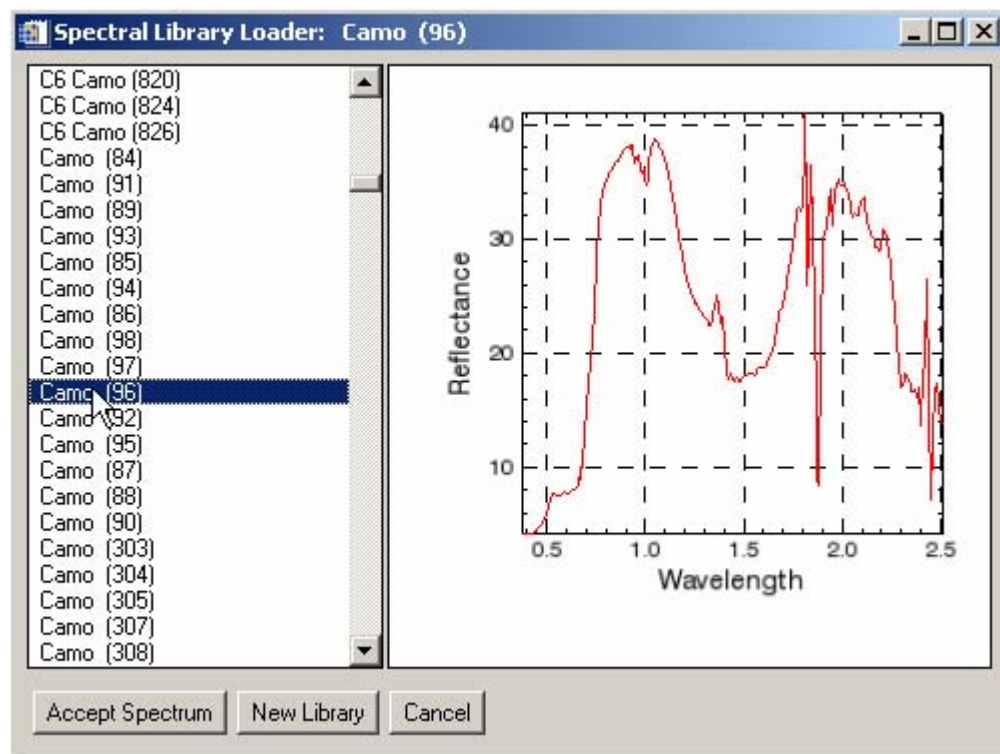

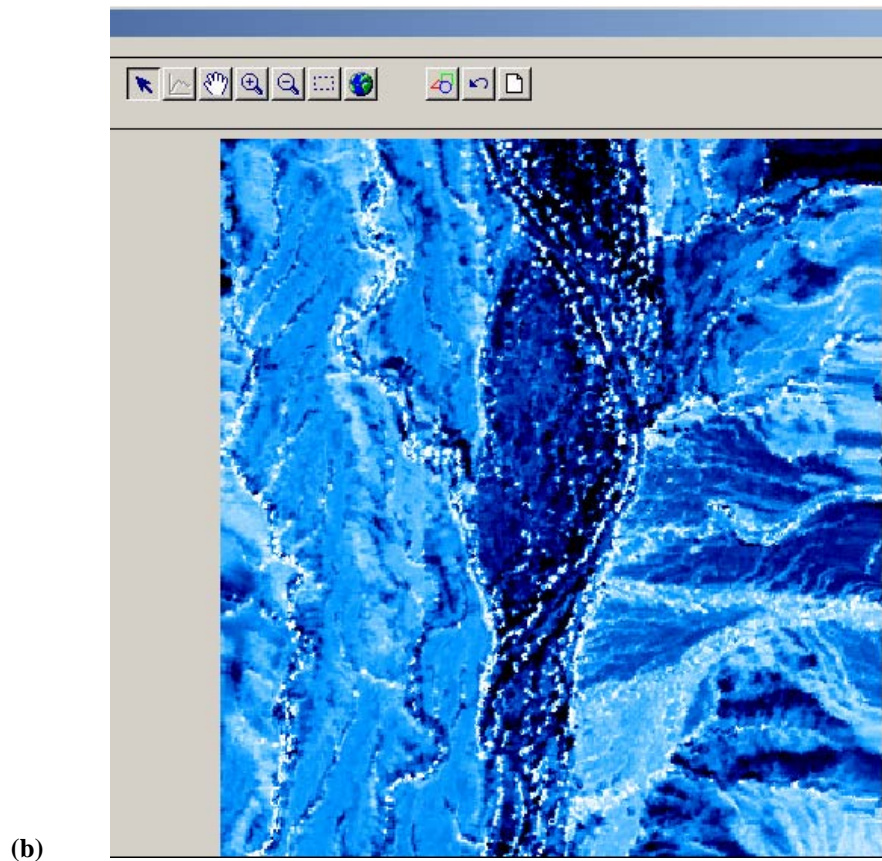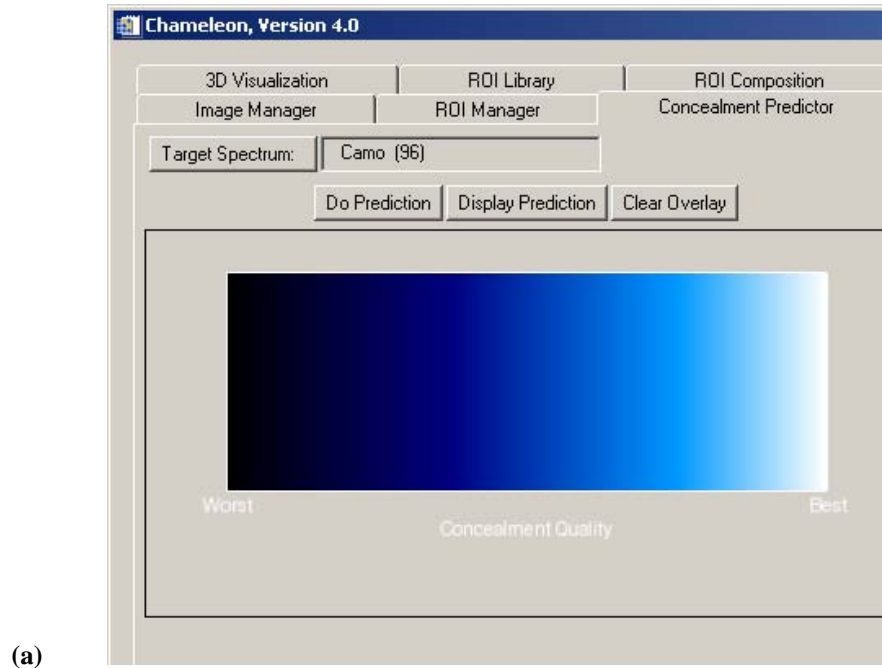**Figure 19: Target selection list and selected target spectrum.**

(a)

(b)

Figure 20: a) The Concealment Predictor tab and b) the Concealment Prediction results.

12 3D Visualization

If coincident elevation data (*e.g.*, DEM, LIDAR) is available, the user may visualize the HSI data in three dimensions. To accurately portray the image in 3D, the elevation data must spatially coincide with the hyperspectral data (*i.e.*, cover the exact area as the hyperspectral data). The elevation file must be in one of the following formats: (1) an ENVI-formatted one-band image cube or (2) a grid file exported as an ASCII text file from ESRI's ArcView software. In addition to the data in the elevation file, the 3D View also incorporates height data associated with building ROIs (see Figure 21b) that have been added by way of the ROI Library (Section 9.2).

12.1 Opening the 3D View

Select the 3D Visualization tab in the Chameleon Toolkit (Figure 22), and load the elevation file. The resulting 3D image will be displayed in the "3D View" window (Figure 21a). Holding the mouse button down in the window and dragging it allows the image to be viewed from various perspectives. The "Reset" button restores the 3D image to its original orientation.
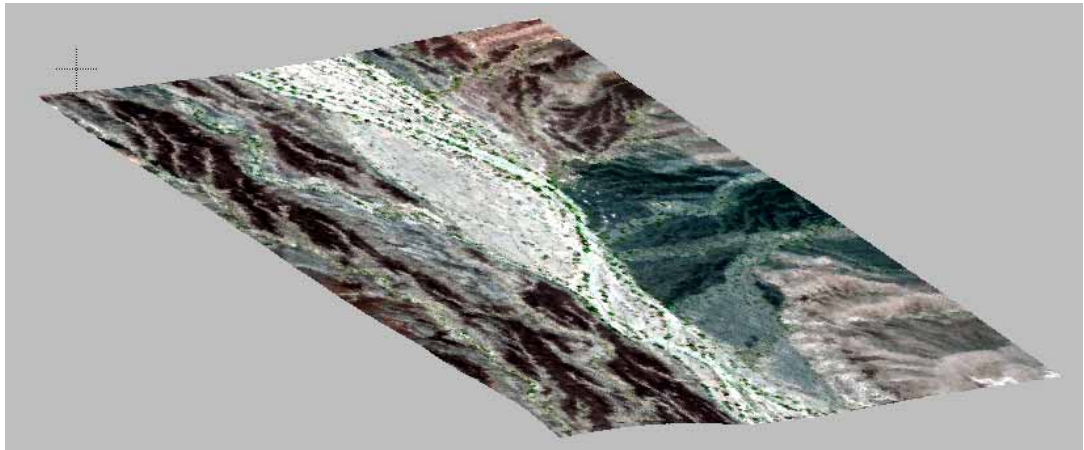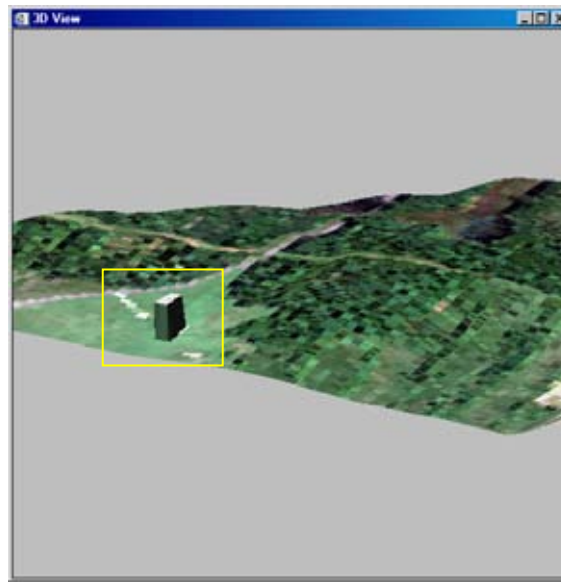
(a)   (b)

Figure 21: a) A full HSI image displayed in 3D and b) a building ROI (outlined in yellow) that was previously added to the same image from the ROI Library (details in Section 9.2).

12.2 3D View Properties

Three settings (Transformations, Contours, and Illumination) can be changed via the Properties pull-down menu on the 3D Visualization tab, as seen in Figure 22.
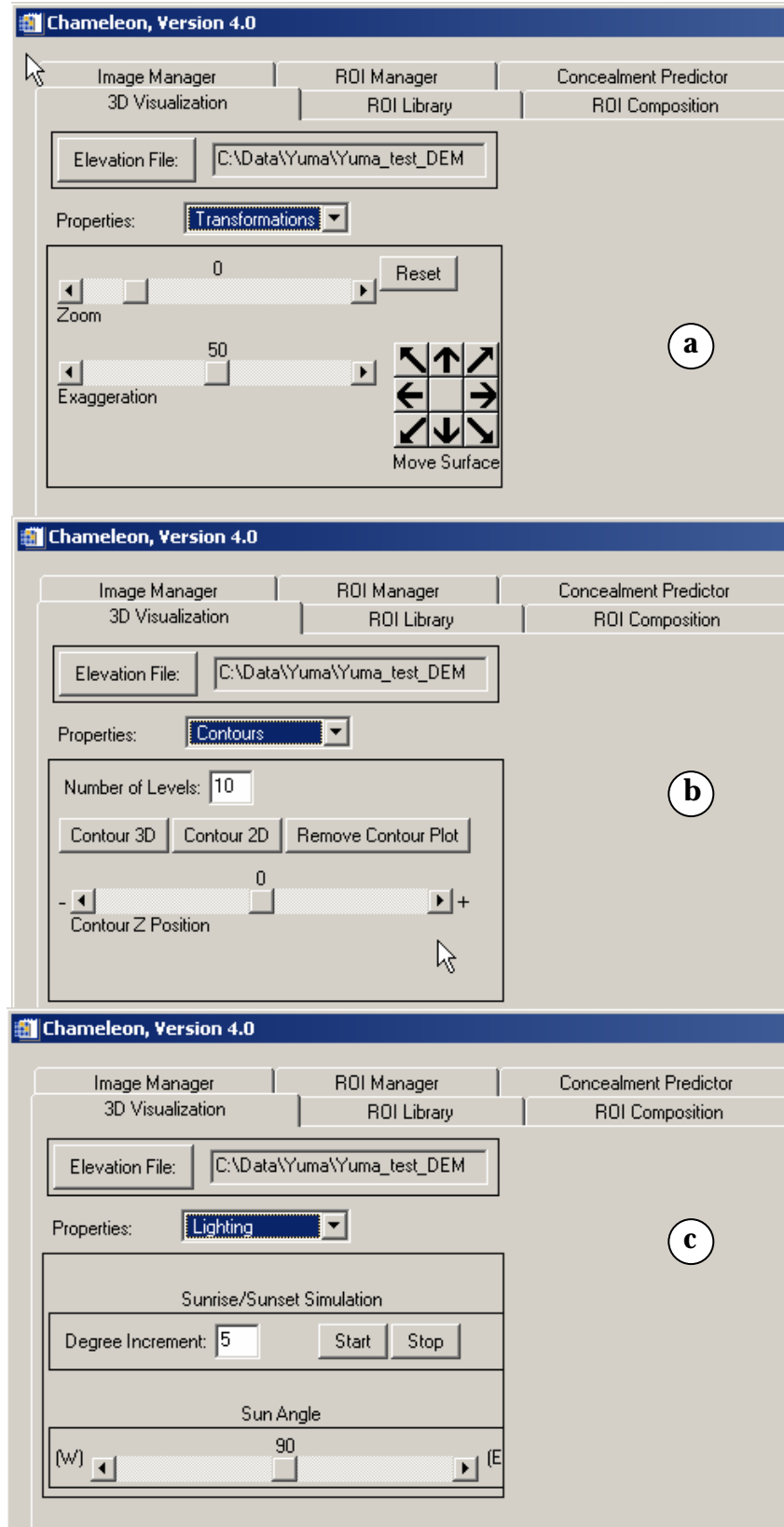
Figure 22: Chameleon Toolkit with 3D Visualization tab options activated: (a) Transformations, (b) Contours, and (c) Illumination.

12.2.1 Transformations

When "Transformations" is selected from the pull-down menu (Figure 22a), the user can zoom into the image or exaggerate features by dragging the associated slider bars. The "Move Surface" arrow keys allow the image to be positioned at various locations within the viewing window.

12.2.2   Contours

By selecting the "Contours" option (Figure 22b), the user has the choice of overlaying 2D or 3D contours on the image. The number of contour levels to be displayed may be specified, as well. The "Remove Contour Plot" button clears the image of all contours. Additionally, the contour plot can be positioned directly on the image or offset above or below the image via the Contour Z-Position slider bar.

12.2.3   Illumination

This option, as seen in Figure 22c, enables the user to see how different areas in the image would be affected by shadow/sun illumination at various sun angles. An animated sunrise/sunset simulation can be run based on a specific sun angle increment.   Type in the sun angle increment to be used in the simulation, and press the "Start" button to see how the image changes as the sun passes back and forth between 0 and 180 degrees. The animation will continue until the "Stop" button is pressed.

13 Message-Passing Interface

This version of Chameleon provides a message interface that allows a remote user to send commands to the application via the network. Currently, the only supported remote operation is to insert an ROI image from the image database library provided with Chameleon.

The sections that follow provide an overview of the Message Interface Architecture and the User Interfaces. Please see Section 14 for installation instructions.

13.1   Message-Passing Interface Architecture

Figure 23 shows the system architecture of the Chameleon Message Interface. Two new components were created for this interface: the Chameleon Message Interface Client and Server Applications. The client application provides the graphical user interface for the user on the remote system. The server is a utility application that receives networked commands from the client and passes these to the Chameleon Application. The server functions without direct user interaction. The user interfaces and network communications for this new feature are implemented in Sun's Java language. This was done since RSI's IDL language

does not support multiple threads, a feature needed for the required TCP/IP socket server. RSI's IDL/Java Bridge software is utilized to move information from the Java environment into the IDL environment.

Figure 24 shows the Chameleon Message Interface Client Application GUI. This application allows the remote user to select ROI images, specify the X and Y locations to paste it within the scene, and transmit this command to the remote Chameleon Message Interface Server Application over the network via a TCP/IP socket.

The main area of the client application user interface is a table showing details about each of the ROI images. The first row is a list of column headers. Every other row in this table represents a different ROI image from the library. The columns present different attributes about the ROI images. Please see the section on the Chameleon ROI Library for a description of these fields.
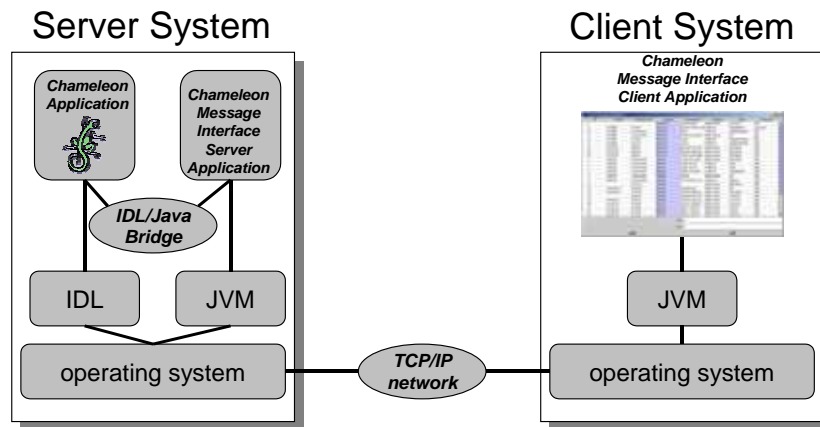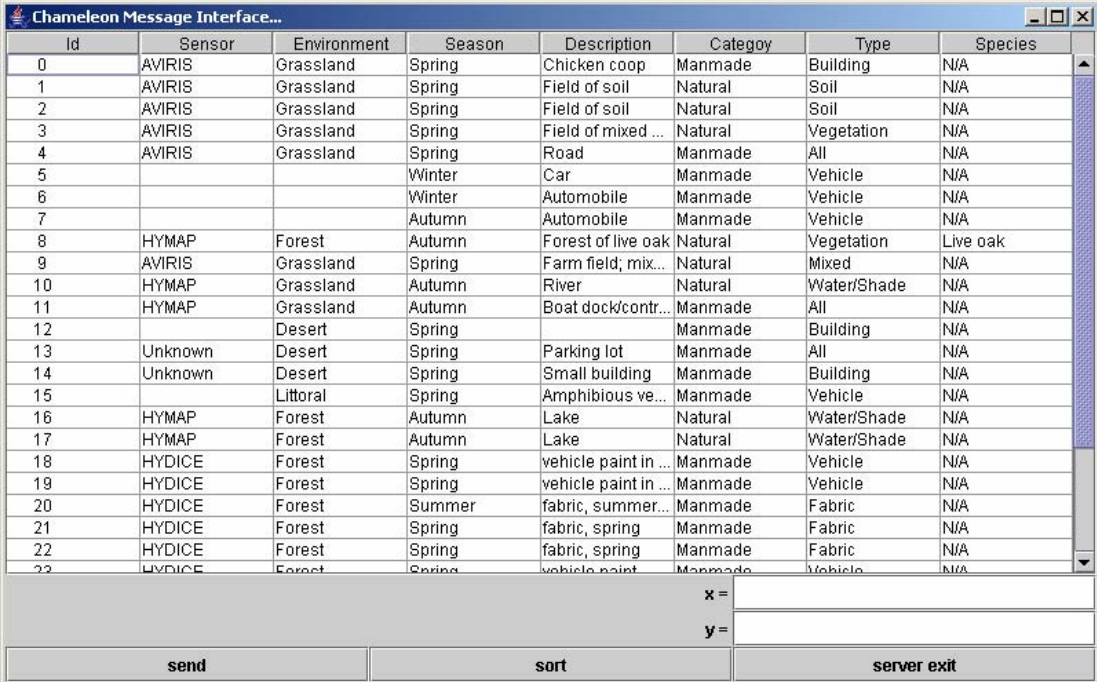

Figure 23: Message-Passing Interface Architecture

Id	Sensor	Environment	Season	Description	Categoy	Type	Species
0	AVIRIS	Grassland	Spring	Chicken coop	Manmade	Building	N/A
1	AVIRIS	Grassland	Spring	Field of soil	Natural	Soil	N/A
2	AVIRIS	Grassland	Spring	Field of soil	Natural	Soil	N/A
3	AVIRIS	Grassland	Spring	Field of mixed ...	Natural	Vegetation	N/A
4	AVIRIS	Grassland	Spring	Road	Manmade	All	N/A
5			Winter	Car	Manmade	Vehicle	N/A
6			Winter	Automobile	Manmade	Vehicle	N/A
7			Autumn	Automobile	Manmade	Vehicle	N/A
8	HYMAP	Forest	Autumn	Forest of live oak	Natural	Vegetation	Live oak
9	AVIRIS	Grassland	Spring	Farm field; mix...	Natural	Mixed	N/A
10	HYMAP	Grassland	Autumn	River	Natural	Water/Shade	N/A
11	HYMAP	Grassland	Autumn	Boat dock/contr...	Manmade	All	N/A
12		Desert	Spring		Manmade	Building	N/A
13	Unknown	Desert	Spring	Parking lot	Manmade	All	N/A
14	Unknown	Desert	Spring	Small building	Manmade	Building	N/A
15		Littoral	Spring	Amphibious ve...	Manmade	Vehicle	N/A
16	HYMAP	Forest	Autumn	Lake	Natural	Water/Shade	N/A
17	HYMAP	Forest	Autumn	Lake	Natural	Water/Shade	N/A
18	HYDICE	Forest	Spring	vehicle paint in ...	Manmade	Vehicle	N/A
19	HYDICE	Forest	Spring	vehicle paint in ...	Manmade	Vehicle	N/A
20	HYDICE	Forest	Summer	fabric, summer...	Manmade	Fabric	N/A
21	HYDICE	Forest	Spring	fabric, spring	Manmade	Fabric	N/A
22	HYDICE	Forest	Spring	fabric, spring	Manmade	Fabric	N/A
23	HYDICE	Forest	Spring	vehicle paint	Manmade	Vehicle	N/A

x =

y =

| send | sort | server exit |

Figure 24: Message-Passing Interface Client GUI

If the application is unable to display all the rows of the data table within the current window, a scroll bar will automatically appear along the right side of the table.

To select a data cell of the table, the user simply clicks within it. The outline of this cell changes color to blue to indicate selection. Please note that if multiple cells are selected, the operation is performed based on the contents of the upper leftmost cell only.

The user can sort the contents of the data table by each of the columns. To do this, the user selects a cell and clicks on the sort button. The contents of the data table are then sorted in alphabetical order by this column. In addition, the sort column is changed to a light blue color to indicate sort criteria until the user selects another cell.

The user can select an ROI to send by selecting a cell within the data table. The user may select a cell in any column of the desired row. After selecting the cell, the user can click on the send button to transmit this ROI to the Chameleon Server. In addition, the transmitted row is changed to a light blue color to show the user which data was sent. This highlighting lasts until the user selects another cell within the data table.

If the remote Chameleon application is not set to receive mode, the send operation will fail and an error message similar to "remote connection refused" will be displayed.

The X and Y text boxes allow the user to specify the coordinates within the currently displayed scene to place the ROI. These values are for the upper leftmost corner of the ROI image. When the user clicks on the send button, the application attempts to convert the contents of the two text boxes into non-negative integers. If this conversion fails, the text box is highlighted in red and the message is not sent. If the user presses the send button before specifying values for the X and Y, these are both automatically set to zero.

Please note there are no upper bound checks for X and Y values within the Message Interface Client Application. Values larger than the dimensions of the current scene are transmitted to Chameleon. Chameleon ignores these commands if it can't position the entire ROI within the scene using the X and Y values selected by the remote user.

The server exit button is used to put the Chameleon server out of message-interface mode. Within the Chameleon Application, message passing server mode is started by clicking on the "start message passing" of the ROI Library tab as shown in Figure 25.
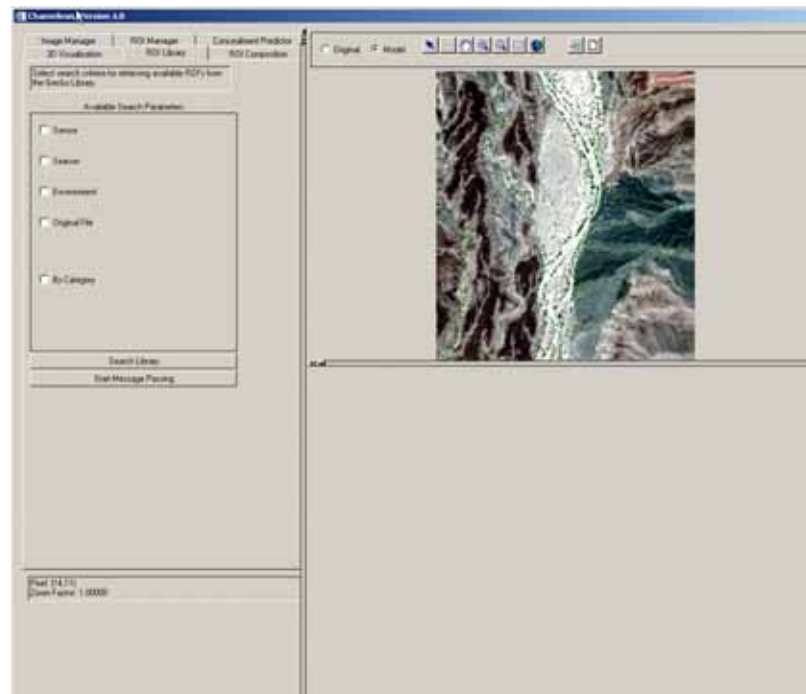

Figure 25: Start Message Passing Button on ROI Library Tab

14 Chameleon Message Interface Installation

Please perform the following steps on the remote system to install and configure the Chameleon Message Interface Client Application:

- Download and install the Java 2 Platform, Standard Edition (J2SE) Java Runtime Environment (JRE). The version used to create these applications is version 1.4.2_06. This software is freely available at the following URL: http://java.sun.com/j2se/1.4.2/download.html. Please note the directory created (typically c:\Program Files\java\j2re1.4.2_06)
- Insert the Chameleon Message Interface CD-ROM into the remote PC
- Create the directory "C:\ChameleonMsgClient" and copy the following files from the CD:
    1 javaChameleonMsg.class: Java class file for the application
    2 runClient.bat: A PC bat file that configures and runs the application
    3 test.xml: An XML file containing the ROI information
- Using Notepad, open up the file "runClient.bat". Edit the two set lines to match your configuration:

1. Modify the line starting with "set JAVA_HOME" to point to the subdirectory of the directory created by step one. For example, if you installed the JRE to the directory "c:\Program Files\java\j2re1.4.2_06" in step one please make this line read "set JAVA_HOME= c:\Program Files\java\j2re1.4.2_06"
2. Modify the line starting with "set DEST_IP" to have the IP address of the Chameleon Server. For example, if you determine that the server's IP address is "10.41.132.224" you would want to modify the line to read "set DEST_IP=10.41.132.224". If you are installing the client on the same system as the server, please use the address "127.0.0.1". Otherwise, the IP address of the server can be determined by issuing the command "ping <host name>" where <host name> is the name of the server system from a Windows Command Prompt. The four numbers separated by periods between the two brackets after the host's name is the IP address of that system.
    - Run the Chameleon Message Interface Client Application by opening a Windows Command Prompt, changing to the directory created in step 3, and typing "runClient".
    - Verify that the Chameleon Message Interface Client Application starts.

Please perform the following steps on the server system to install and configure the Chameleon Message Interface Server Application.
- Download and install the Java 2 Platform, Standard Edition (J2SE) Java Runtime Environment (JRE). The version used to create these applications is version 1.4.2_06. This software is freely available at the following URL: http://java.sun.com/j2se/1.4.2/download.html. Please note the directory created (typically c:\j2jre1.4.2_06\)
- Insert the Chameleon Message Interface CD-ROM into the server PC.

- Create the directory "C:\ChameleonMsgServer" and copy the following files from the CD into it:
    1. OTHserver.class
    2. SrvSock.class
    3. TmpSock.class
- Copy the file "C:\RSI\IDL61\external\objbridge\java\idljavabrc" to "C:\RSI\IDL61\external\objbridge\java\idljavabrc.ORIG" The actual location of this file may vary based on the installed drive and the IDL version number.
- Using notepad, edit the file "C:\RSI\IDL61\external\objbridge\java\idljavabrc". Add the string ";C:\ChameleonMsgServer" to the end of the line that begins with "JVM Classpath=".

15 Examples of Chameleon Working in Different Environments

The Chameleon software has been tested against a variety of environments. Most of the example screen shots throughout the document have been taken displaying data from an arid environment.   The following figures illustrate Chameleon displaying data from temperate and tropical environments.
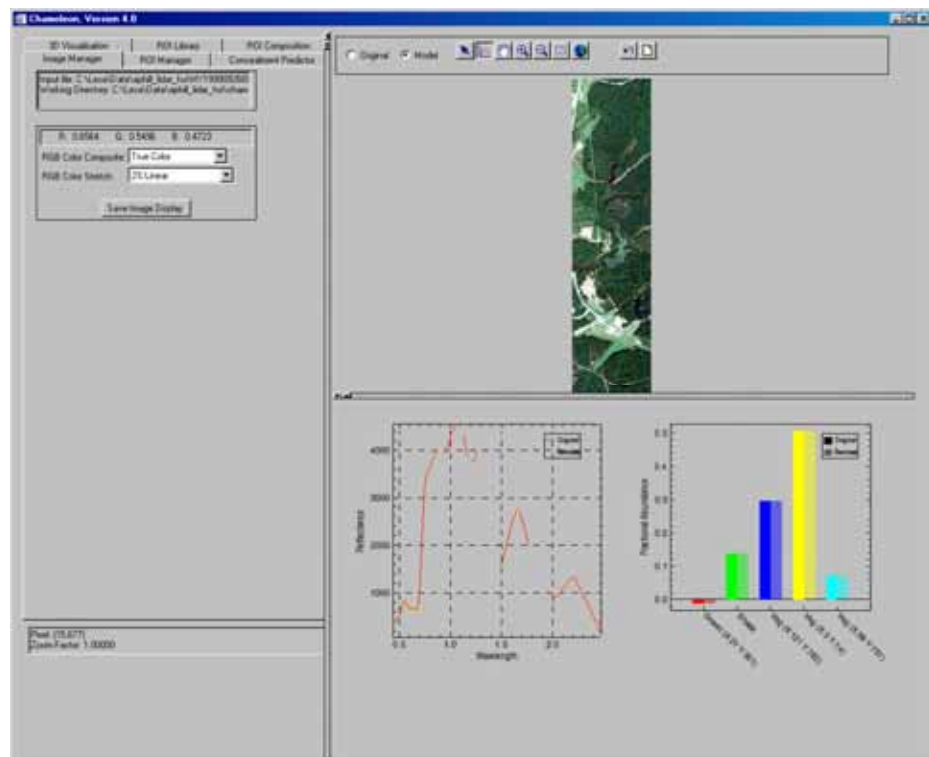

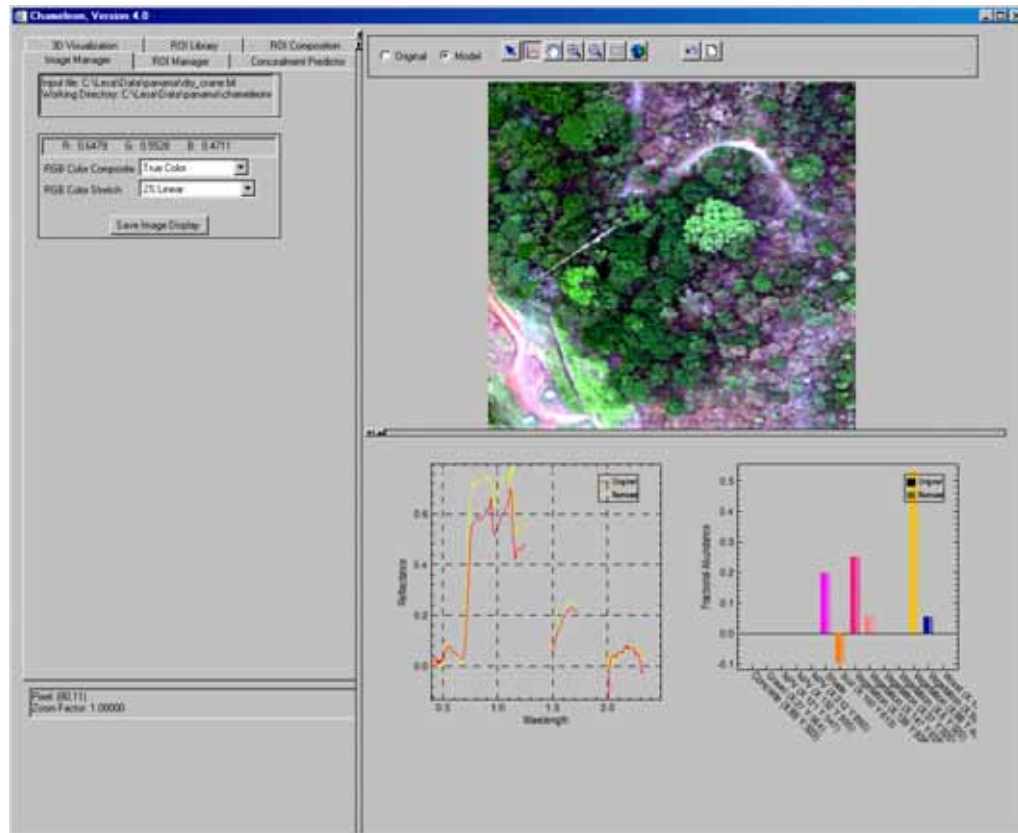**Figure 26: Chameleon Displaying Temperate HyMap Data**

Figure 27: Chameleon Displaying Tropical Data from HYDICE

16 Examples of Chameleon Working with Different Sensors

In addition to working fine with a variety of environments, Chameleon has also been tested with different sensors. The majority of the screenshots in this document illustrate Chameleon working with the AVIRIS sensor. Figure 26 shows Chameleon working with HyMap data. Figure 27 shows Chameleon working with HYDICE data.

Since all of these sensors are hyperspectral, we're also including an image that shows a commercial multispectral scene. Figure 28 shows an example of Chameleon displaying data from IKONOS.
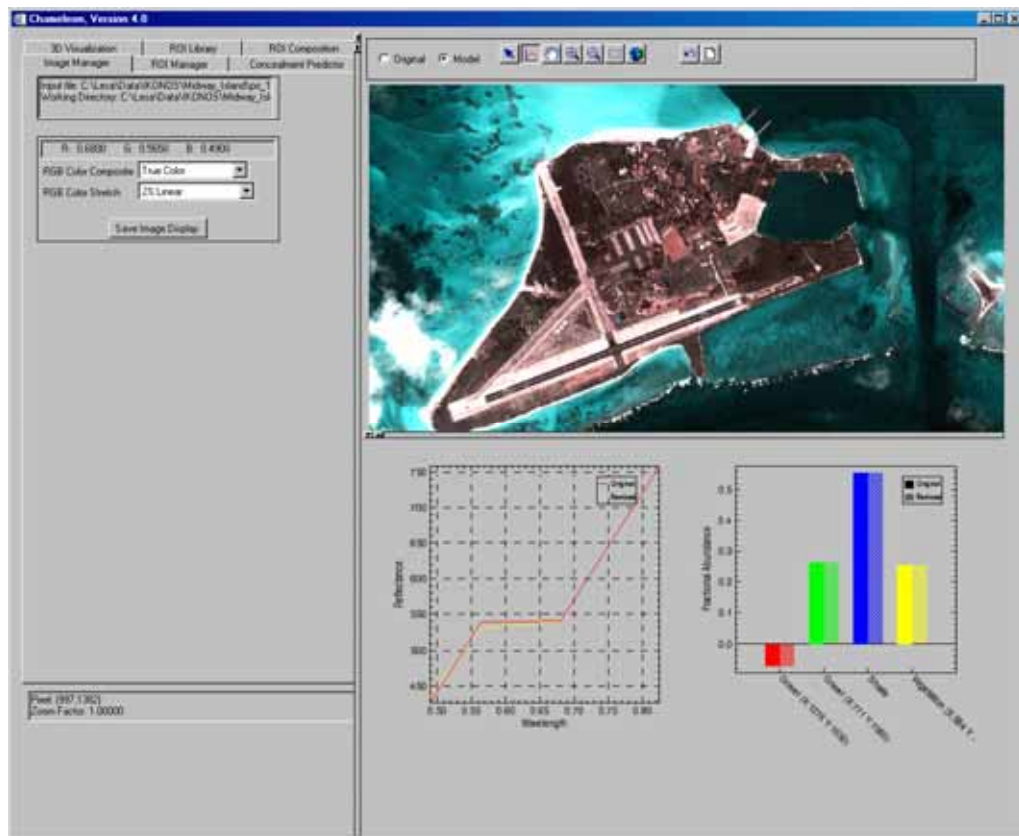
Figure 28: Chameleon Displaying IKONOS Commercial MSI data

REPORT DOCUMENTATION PAGE

1. REPORT DATE *(DD-MM-YYYY)*	2. REPORT TYPE	3. DATES COVERED *(From - To)*
November 2005		

4. TITLE AND SUBTITLE

The Chameleon Concept: Modeling Quaternary Geomorphic Surfaces Using Laboratory, Field, and Imaging Spectrometry in the Lower Colorado Sonoran Desert

5a. CONTRACT NUMBER

5b. GRANT NUMBER

5c. PROGRAM ELEMENT NUMBER

6. AUTHOR(S)

J. David Lashlee

5d. PROJECT NUMBER

5e. TASK NUMBER

5f. WORK UNIT NUMBER

7. PERFORMING ORGANIZATION NAME(S) AND ADDRESS(ES)

Topographic Engineering Center
U.S. Army Engineer Research and Development Center
7701 Telegraph Road
Alexandria, VA 22315-3864

8. PERFORMING ORGANIZATION REPORT NUMBER

ERDC/TEC TR-05-1

9. SPONSORING / MONITORING AGENCY NAME(S) AND ADDRESS(ES)

10. SPONSOR/MONITOR'S ACRONYM(S)

11. SPONSOR/MONITOR'S REPORT NUMBER(S)

12. DISTRIBUTION / AVAILABILITY STATEMENT

Approved for public release; distribution is unlimited

13. SUPPLEMENTARY NOTES

14. ABSTRACT

Chameleon is a physics-based landscape modeling software system designed for modeling and simulations. Hyperspectral laboratory, field, and imaging spectrometer measurements are collected as empirical foundation data. Linear spectral unmixing decomposes each image pixel into spectral endmembers. Spectral editing tools allow mathematical manipulation of these fractional abundances and introduction of new spectral information. Image spectra are modified on a sub-pixel, per-pixel, or neighborhood basis, or the entire hypercube can be customized at once. Chameleon then regenerates synthetic, but spectrally accurate, terrain models using linear spectral remixing algorithms. By incorporating elevation, sun angle, and weather data, the landscape becomes a "Chameleon"—able to change hyperspectral properties based on multitemporal spectral measurements, requirements for developmental tests and operational training, or as required by specific simulation scenarios. Advanced knowledge of natural environments to be modeled is prerequisite to generating useful synthetic terrains. Our spectral research on arid Quaternary geomorphic surfaces suggests that deserts (often assumed to be less difficult to study remotely than humid, temperate, and cold environments) are more complex than is generally accepted. A variety of rock coatings can significantly alter reflectance in the solar reflected spectrum. Weathering rinds and carbonate deposits inhibit lithologic reflectance altogether. However, manganese-rich rock varnish obscures rock reflectance in the visible and near infrared wavelengths, but transmits lithologic information in the 2000 to 2500 nanometer wavelengths. Surface soils on desert pavements consist of a layer of eolian dust that overlies an accreting vesicular (Av) horizon. These soils have same structure and chemistry and, therefore, the same hyperspectral signature, regardless of landform age, geomorphic process, or parent material. From a remote sensing perspective, this has a normalizing effect on reflectance across the landscape. Spectral Mixture Analysis is a proven hyperspectral technique for mapping composition and abundance of surface materials characteristic of volcanic landforms that exhibit diagnostic absorption features. We found that desert pavement spectra are featureless in that they exhibit few distinct spectral features related to rock varnish, clast lithology, or soil. Image spectra of these surfaces are the result of intimate mixtures of heterogeneous materials, requiring non-linear spectral unmixing solutions.

15. SUBJECT TERMS

Chameleon	Hyperspectral measurements	Terrain models
Deserts	Landscape modeling	
	Quaternary geomorphic surfaces	

16. SECURITY CLASSIFICATION OF:

a. REPORT	b. ABSTRACT	c. THIS PAGE	17. LIMITATION OF ABSTRACT	18. NUMBER OF PAGES	19a. NAME OF RESPONSIBLE PERSON
U	U	U			

19b. TELEPHONE NUMBER *(include area code)*